A theoretical framework for analysis of immune tolerance induction in thymus and periphery

Von der Fakultät für Lebenswissenschaften
der Technischen Universität Carolo-Wilhelmina zu Braunschweig
zur Erlangung des Grades
eines Doktors der Naturwissenschaften
(Dr. rer. nat.)
genehmigte
D i s s e r t a t i o n

von Sahamoddin Khailaie
aus Esfahan / Iran

1. Referent:	Prof. Dr. Michael Meyer-Hermann
2. Referent:	Prof. Dr. Stefan Dübel
3. Referent:	Prof. Dr. Markus Löffler
eingereicht am:	29.02.2016
mündliche Prüfung (Disputation) am:	08.08.2016

Druckjahr 2017

Vorveröffentlichungen der Dissertation

Teilergebnisse aus dieser Arbeit wurden mit Genehmigung der Fakultät für Lebenswissenschaften, vertreten durch den Mentor der Arbeit, in folgenden Beiträgen vorab veröffentlicht:

Publikationen

- Milanez-Almeida, P.; Meyer-Hermann, M.; Toker, A.; **Khailaie, S.**; Huehn, J.; (2015) Foxp3^{+} regulatory T cell homeostasis quantitatively differs in murine peripheral lymph nodes and spleen. Eur. J. Immunol. 45: 153-66.
- **Khailaie, S.**; Robert, P.A.; Toker, A.; Huehn, J.; Meyer-Hermann, M.; (2014) A signal integration model of thymic selection and regulatory T cell commitment. J. Immunol. 193: 5983-96.
- **Khailaie, S.**; Bahrami, F.; Janahmadi, M.; Milanez-Almeida, P.; Huehn, J.; Meyer-Hermann, M.; (2013) A mathematical model of immune activation with a unified self-nonself concept. Front. Immunol. 4: 474.

Tagungsbeiträge

- **Khailaie, S.**; Robert, P.A.; Walker, L.S.K.; Sansom, D.M.; Meyer-Hermann, M.; (2014) CTLA4 trafficking model. (Poster) Quantitative Immunology, Les Houches, France.
- **Khailaie, S.**; Bahrami, F.; Janahmadi, M.; Milanez-Almeida, P.; Huehn, J.; Meyer-Hermann, M.; (2014) A mathematical model of immune activation with a unified self-nonself concept. (Poster) Systems Biology for Infection Research and Biotechnology, BRICS forum, Braunschweig, Germany.
- **Khailaie, S.**; Bahrami, F.; Janahmadi, M.; Milanez-Almeida, P.; Huehn, J.; Meyer-Hermann, M.; (2013) Theoretical analysis of peripheral immune tolerance. (Poster) 6th International PhD Symposium of the Helmholtz Graduate School for Infection Research, Braunschweig, Germany.
- **Khailaie, S.**; Toker, A; Huehn, J.; Meyer-Hermann, M.; (2013) Signal integration in thymocytes is crucial for thymic selection. Front. Immunol. Conference abstract: 15th International Congress of Immunology (ICI), Milan, Italy.
- **Khailaie, S.**; Meyer-Hermann, M.; (2012) TCR signaling dynamics in thymic selection. (Poster) 3rd Annual Retreat of the Helmholtz Graduate School for Infection Research, Bad Bevensen, Germany.
- **Khailaie, S.**; Meyer-Hermann, M.; (2011) Mathematical modeling and simulation of thymic selection. (Poster) 5th International PhD Symposium of the Helmholtz Graduate School for Infection Research, Braunschweig, Germany.

Auszüge dieser Arbeit wurden im Rahmen der oben genannten Vorveröffentlichungen in Fachzeitschriften veröffentlicht. Der Abdruck erfolgt mit freundlicher Genehmigung dieser Zeitschriften. Weiterhin wird darauf hingewiesen, dass Abschnitte, Resultate und Abbildungen dieser Dissertation zum Teil oder vollständig in zukünftigen Veröffentlichungen des Autors verwendet werden.

Abstract

A beneficial immune response must hold a balance between activation against internal/external disturbances and suppression to avoid damage to healthy tissues. Deviation from this balance results in autoimmunity/graft rejection at one side or cancer/chronic infection at the other side. Among numerous factors that control the immune balance, conventional T cells (Tconv), natural regulatory T cells (nTreg) and their interplay are the key factors. Tconvs and nTregs are selected from precursor cells which express randomly generated T cell receptors (TCR). Upon activation by antigen presenting cells (APC), Tconvs boost the immune response via the production of pro-inflammatory signals (cytokines), while nTregs suppress Tconvs in a cell-contact or cytokine-dependent manner. A defective selection of nTregs and Tconvs in thymus, in terms of cell numbers and quality, or disturbed interplay between these cells in periphery could result in unbalanced immune responses. In this study, induction and maintenance of the immune balance in different stages are analyzed by mathematical models.

An agent-based modeling approach, which is suitable to consider heterogeneity among cells, is employed to identify the critical factors that affect the outcome of thymic selection. A novel signal integration model of thymic selection is proposed and used to study TCR properties of cells that are selected as nTreg and Tconvs. This model takes into account the history of TCR stimulations perceived by precursor cells during their interactions with APCs. The model is advantageous in predicting how the balance between selected repertoires are changed by manipulations in thymic environment. This would help in a better understanding of unwanted tolerance induction and autoimmunity in peripheral T cell repertoires, and may suggest strategies for inducing or breaking immune tolerance for therapeutic purposes.

After thymic selection, quality and interplay of selected nTregs and Tconvs determines whether a major immune response can be initiated in periphery. A major proliferation of Tconvs, which is down-regulated by nTregs, is required for antigen clearance. Proliferation of T cells in addition to suppression of Tconvs by nTregs result in a nonlinear interplay between these two repertoires that demands a mathematical analysis. By constructing a set of hierarchical models based on ordinary differential equations (ODE), interplay of activated Tconvs and nTregs is studied. By using parametric stability and bifurcation analysis of proposed models, it is shown that the relative number of nTregs and Tconvs and their absolute numbers are the major determinants for an immune activation against an antigen. The model helps in understanding the nonlinear dynamics of the immune response and the emergence of chronic infections and inflammageing.

In addition to a direct pathway, nTregs indirectly suppress Tconvs via down-regulation of stimulatory capacity of APCs. By using a series of ODE-based mathematical models that represent the experimental protocols, Treg-associated regulation of immune stimulation is quantified.

By targeting different interdependent immunological stages, this theoretical study presents a multi-stage view on the induction and maintenance of immune balance, which cannot be gained solely by experimental studies.

Zusammenfassung

Eine erfolgreiche Immunantwort muss die Balance zwischen Abwehr interner und externer Beedrohungen und ihrer Unterdrückung zur Vermeidung von Schäden an gesundem Gewebe halten. Eine Abweichung von dieser Balance führt einerseits zu Autoimmunreaktionen und TransplantatabstoÃ§ung oder andererseits zu Krebs und chronischen Infektionen. Unter den zahlreichen Faktoren, welche die Balance des Immunsystems kontrollieren, nehmen konventionelle T-Zellen (Tconv), natürliche regulatorische T-Zellen (nTreg) und deren Wechselwirkungen eine Schlüsselposition ein. Tconvs und nTregs werden aus Vorläuferzellen selektiert, die zufällig generierte T-Zell Rezeptoren (TCR) exprimieren. Bei Aktivierung durch antigenpräsentierende Zellen (APC) verstärken Tconvs die Immunreaktion durch die Produktion proinflammatorischer Signale (Zytokine), während Tconvs von nTregs mittels Zellkontakt oder Zytokinen gehemmt werde. Eine fehlerhafte Selektion von nTregs und Tconvs im Thymus in Bezug auf die jeweilige Anzahl und Qualität oder ein gestörtes Zusammenspiel dieser Zellen können zu unausgeglichenen Immunreaktionen führen. In dieser Studie werden Herstellung des Immungleichgewichts und dessen Aufrechterhaltung in unterschiedlichen Stadien durch mathematische Modelle untersucht.

Es wird ein agentbasierter Modellierungsansatz verwendet, der eine Berücksichtigung der Heterogenität der Zellen ermöglicht, um Faktoren zu identifizieren, die kritisch für das Ergebnis der Selektion im Thymus sind. Ferner wird ein neuartiges Modell der Signalintegration bei der Selektion im Thymus eingeführt und die Eigenschaften des TCR von Zellen, die als nTreg oder Tconv selektiert werden, werden anhand dieses Modells untersucht. Dieses Modell beruht auf den TCR Stimulationen, welche die Vorläuferzellen während ihrer Interaktionen mit APCs in der Vergangenheit erfahren haben. Das Verfahren hat den Vorteil, Vorhersagen über den Einfluss von Manipulationen im Umfeld des Thymus auf das Gleichgewicht zwischen den selektierten Zellrepertoires zu ermöglichen. Es kann zu einem besseren Verständnis von unerwünschter Toleranz und Autoimmunität in peripheren T-Zellen beitragen und eine Empfehlung von Strategien zur Induktion oder Vermeidung von Immuntoleranz zu therapeutischen Zwecken ermöglichen.

Nach der Selektion im Thymus entscheiden Qualität und Zusammenspiel der selektierten nTregs und Tconvs darüber, ob eine Immunantwort in der Peripherie ausgelöst wird. Für die Beseitigung von Antigen ist eine massive Proliferation von Tconvs nötig, welche von nTregs heruntergeregelt werden. Proliferation von T-Zellen in Verbindung mit der Unterdrückung von Tconvs durch nTregs führt zu nichtlinearen Wechselwirkungen zwischen den beiden Repertoires, die eine mathematische Analyse nötig machen. Dieses Wechselspiel zwischen Tconvs und nTregs wird anhand eines Satzes hierarchischer Modelle auf der Basis von gewöhnlichen Differentialgleichungen (ODE) untersucht. Durch die Ausnutzung parametrischer Stabilitäts- und Bifurkationsanalyse der hier eingeführten Modelle kann gezeigt werden, dass die relative Anzahl von nTregs und Tconvs sowie ihre absolute Zahl die entscheidenden Faktoren für eine Immunreaktion gegen ein Antigen sind. Das Modell hilft bei dem Verständnis der nichtlinearen Dynamik der Immunantwort und des Entstehens chronischer Infektionen und Inflammageing.

Neben dem direkten Weg unterdrücken nTregs Tconvs durch das Herunterregulieren der stimulatorischen Kapazität von APCs. Mit Hilfe einer Reihe von ODE basierten mathematischen Modellen, welche die jeweiligen experimentellen Verfahren repräsentieren, wird die durch Tregs vermittelte Regulation von Immunstimuli quantifiziert.

Diese Studie ermöglicht durch die Untersuchung verschiedener voneinander abhängiger immunologischer Stadien einen Blick auf verschiedene Stadien der Herstellung und Aufrechterhaltung der Balance des Immunsystems, der nicht allein durch experimentelle Studien möglich ist.

To love of my life, Parvin.

Acknowledgements

First and foremost, I would like to express my deepest gratitude to Prof. Dr. Michael Meyer-Hermann, who have provided generous support and encouragement for my research. I would like to thank him for helping me in these initial steps in science. His excellent supervision, patience, caring, and specially giving the freedom to work was crucial for my work. I could not wish for a better or friendlier supervisor.

I would like to thank Prof. Dr. Dirk Langemann, for his contributions of time for revising the mathematical context of my thesis. I am thankful to Prof. Dr. Stefan Dübel who kindly accepted to review and evaluate my thesis, and to Prof. Dr. Martin Korte for kindly accepting to take part to the oral examination.

A special thanks to my colleague and friend, Philippe A. Robert, for his continuous support. My progress in the thymic selection project owes to his great contribution. He provided me worthwhile discussions and interesting arguments, not only about science.

I wish to thank Sebastian C. Binder for his help in writing my thesis and his technical supports. I also want to thank my dear friends Ghazal, Nima and Neda for their kind help and encouragements during the time of preparing my thesis. I am also thankful to my colleagues in department of systems immunology, who provided me with new ideas and helpful discussions, especially during the weekly seminars. I acknowledge my gratitude to my thesis committee members, Prof. Dr. Michael Meyer-Hermann, Prof. Dr. Jochen Huehn and Prof. Dr. Martin Korte for fruitful discussions. My very sincere thanks to my collaborators, Prof. Lucy S. K. Walker and Prof. David M. Sansom for their fruitful discussions. I acknowledge the Helmholtz International Graduate School for Infection Research, for their financial support during my PhD research.

At the end, I take this opportunity to deeply thank my family for their love, care, encouragement and endless support. I cannot express with words, how much thankful I am to my parents who raised me with love and prayed for me throughout every moment of my life. I deeply thank my loving, patient wife, Parvin, who is always supporting me with her kindness. Her smile always bring peace to my difficult moments.

Contents

List of Figures

List of Tables

Chapter 1

Introduction

Our immune system normally fights against a wide spectrum of pathogens reliably, thanks to a complex collaboration between diverse immune cells and proteins. The immune system usually initiates responses against external intruders (referred to as nonself or foreign) in a tightly regulated way to avoid any harm to self-tissues. However, diseases may arise when the pathogens find a way to deceive the immune system, or the immune system is not shaped or working properly. Understanding how the immune system works is essential for designing therapies to reduce debilitating effects that diseases bring.

Our understanding of the immune system has progressed significantly over recent decades. Several infectious diseases such as measles, tuberculosis and diphtheria are no longer uncontrolled threads to our community. However, still fundamental questions are remained to be answered. For example, a major challenge in immunology is to explain how self and nonself are discriminated by the immune system.

Among diverse immune cells, helper T cells has a critical role in coordinating the immune response. These cells belong to a branch of the immune system known as adaptive immune system, and can promote or suppress immune responses. Helper T cells release chemical messages, called cytokines, that are used to regulate immune responses. It is not irrelevant to call helper T cells as the "generals" of the immune system since they can order troops of other cells, such as B cells and cytotoxic T cells, to when and how tolerate or fight against an antigen (defined here as any protein that potentially could stimulate immune system).

Immune tolerance is the state of unresponsiveness of the adaptive immune system to antigens. Clearly, the immune system should tolerate self-antigens derived from healthy tissues, or harmless foreign-antigens such as those derived from food. In contrast, the immune system should lunch effective immune responses against foreign-antigens derived from pathogens, or self-antigens derived from altered-self tissues such as tumors. Excessive or misguided reactions that would harm the host should be avoided. For example, aberrant activation of self-reactive immune cells may harm self-tissues in autoimmune diseases. An excessive immune response against harmless foreign agents may damage healthy tissues like in allergy. Autoimmune diseases may also arise if stimulation of immune cells is indefinite and is not terminated properly. Therefore, immune response should have a suppressor arm to maintain homeostasis of the individual. However, a strong suppressor arm may induce immune tolerance to foreign or altered self antigens (such as tumor), or may result in an ineffective immune response that fails to clear an antigen. Hence, a balance between effector and suppressor mechanisms in the immune system is critical.

Conventional T cells (Tconv) and natural regulatory T cells (nTreg) are two types of helper T cells with opposing functions. Upon activation by antigen presenting cells (APC), Tconvs boost the immune response via the production of pro-inflammatory cytokines and other effector functions that lead to antigen clearance. In contrast, nTregs suppress Tconvs in a cell-contact or cytokine-dependent manner to down-regulate the immune response. These two different cell types are the key players in maintaining the homeostasis of the

individual, by balancing immune activation and suppression.

Immune tolerance is induced and maintained in multiple stages, with respect to time and place. At the construction phase in thymus, where helper T cells are generated, T precursor cells (known as thymocytes) with randomly generated antigen recognition receptors (T cell receptor or TCR) undergo a series of selections. During negative selection, those thymocytes that recognize self-antigens in thymus are eliminated. Self-tolerance induced by negative selection in thymus is called *central tolerance*. Negative selection is an error prone process, and some self-reactive thymocytes can escape thymus and enter periphery as autoreactive Tconv. A part of detected self-reactive thymocytes are differentiated into nTregs instead of being eliminated. nTregs are key players of inducing *peripheral tolerance*, by avoiding unwanted self-reaction or by regulating the magnitude of the immune response to foreign-antigens. nTregs tightly regulate effector functions of Tconvs, and the stimulatory capacity of APCs. Therefore, selection of nTregs and Tconvs in thymus and their interplay in periphery, as well as regulation of peripheral immune stimulation by nTregs are the critical stages where the balance between immune activation and suppression is affected.

In this thesis, induction and maintenance of the immune balance is studied by a series of mathematical models and computer simulations. A very simplistic view of the immune system is taken to construct a series of quantitative and qualitative models. At the stage of thymic selection, where adaptive immune system is shaped by selection of nTregs and Tconvs, an agent-based modeling approach is taken to study the properties of TCRs in nTregs and Tconvs. Biological evidences suggest that nTregs are self-reactive; however, little is known about their TCR specificities. Despite being self-reactive, nTregs react to foreign antigens, which seems contradictory to autoreactivity of nTregs. Agent-based modeling approach allows us to consider heterogeneity in TCR specificity of cells, to track their interactions with thymic environment, and to study differences between selected nTregs and Tconvs. The results of the thymic selection model are given in chapter 4, which are based on the published article [1].

After thymic selection, interplay of selected nTregs and Tconvs are studied qualitatively by a series of hierarchical models for immune activation. Basic components of the adaptive immune system is considered, and additional complexities are incrementally added to a degree that the balance between immune activation and suppression can be studied. Nonlinear dynamics emerging from immune stimulation, cell proliferation and immune suppression is characterized without relying on quantitative experimental data. These are mainly done by parametric linear stability and bifurcation analysis. The analysis of proposed immune activation models are given in chapter 5, which are based on the published article [2].

Immune response in periphery starts with stimulation of T cells by APCs. APCs express antigens and co-stimulatory molecules on their plasma membrane to stimulate interacting nTregs and Tconvs. In addition to Tconvs, APCs are tightly regulate by nTregs. By physically removing co-stimulatory molecules expressed by APCs, nTregs are able to control the level of immune stimulation and by that, indirectly regulate activation of Tconvs. This critical role of nTregs possibly determines the initiation, magnitude and termination of immune responses. In order to quantify this antigen-nonspecific pathway of immune regulation, a series of ODE-based mathematical models are constructed based on experimental protocols. By employing parameter estimation procedures, the sub-processes involved in nTreg-associated removal process of co-stimulatory molecules are quantified. The results are given in chapter 6.

This thesis is structured in the following chapters. Basic components of the immune system are introduced in chapter 2. But detailed knowledge and questions of interest in each part of the study are given separately in each chapter. In chapter 3, modeling strategies and mathematical methods that are used in this study are introduced. A review of previous theoretical attempts of studying the immune system is given in the same chapter. Chapter 4 is devoted to the analysis of thymic selection. Chapter 5 contains the analysis of interplay between nTregs and Tconvs during an immune response. In chapter 6, the regulation of immune stimulation by nTregs is studied. Finally, a summary, conclusion and outlook for the presented study are given in chapter 7.

Chapter 2

Biological background

The main goal of this thesis is to dissect how the immune system is shaped and designed to fight pathogens without being harmful to healthy tissues. Before entering in the depths of this thesis, some background knowledge on the immune system is given in this chapter, specially regarding the repertoire of one of the most important cellular components in the immune system, T cells.

2.1 Immune system

The immune system is a complex biological system comprises of collaborative components, interactions and processes within an organism with the aim of protection against internal or external disturbances. The immune system is divided in two main branches, the *innate* immune system and the *adaptive* immune system, which communicate with each other via different molecules and cellular components.

2.1.1 Innate immune system

The innate immune system is the first line of defense against invading pathogens in vertebrates, invertebrates and plants. It exhibits a great variety of humoral and cellular components that act upon antigens in a generic and non-specific manner. The innate immune system comprises different cell types, such as macrophages, neutrophils, natural killers etc., which express germline encoded *pattern recognition receptors* (PRRs). These receptors are only able to recognize features that are conserved among pathogens, known as *pathogen associated molecular patterns* (PAMPs), such as lipopolysaccharides and peptideoglycans that are commonly expressed in bacteria.

Recognition of conserved features among pathogens is not sufficient to face all different kinds of disturbances that might occur throughout lifetime of an individual, by considering the case where slow evolving vertebrates are exposed to a fast changing pathogens. For example, some pathogens might take advantage of a high mutation rate to change drastically their phenotype, and escape the detection by innate immune receptors. Therefore, despite providing immediate defense against pathogens, the innate immune system cannot provide long-lasting immunity to the host. However, the innate immune response has a crucial contribution to the activation of adaptive immune system which is aimed to provide a comprehensive and antigen-specific protection. Namely, innate cells such as dendritic cells, macrophages and natural killer cells link the innate and adaptive immune responses by activating lymphocytes.

2.1.2 Adaptive immune system

Unlike innate immune system which contains receptors that are encoded in the germline, the adaptive immune system is made of receptors that are acquired throughout the life. Acquisition of new receptors allows the adaptive immune system to prepare for future and unknown challenges. The adaptive immune system comprises of two class of lymphocytes, namely B and T cells, which carry out the antibody or cell-mediated immune responses, respectively. B and T cells exhibit their pathogen-specific receptor (called B cell receptor or BCR, and T cell receptor or TCR, respectively) on the cell membrane. These receptors are generated during B- and T-cell ontogeny by *somatic recombination*, the so-called V(D)J recombination process. This process allows a limited number of genes to generate a repertoire of antigen receptors with enormous diversity which could potentially recognize all pathogens present in nature.

Each antigen recognition receptor is expressed on each individual lymphocyte (with tens to hundreds of thousands copies). T and B lymphocytes can become activated when the innate immune cells, namely antigen-presenting cells (APCs) - such as dendritic cells (DCs), macrophages, or even B cells - present pathogen-derived antigens complexed with a carrier molecule like class I or class II major histocompatibility complex (MHC) molecules. Antigen-specific lymphocytes then recognize the presented antigen and initiate a very specific immune response.

This thesis focuses on T cell repertoire and, thus, more emphasis will be given to T cells in this general introduction.

2.2 T cell repertoire

2.2.1 $CD4^+$ and $CD8^+$ T cells

A majority ($\approx 95\%$) of the T cell pool is $\alpha\beta$ T cell repertoire that will be the focus of the thesis. These T cells are divided into two lineages: $CD4^+$ and $CD8^+$ T cells. These lineages express exclusively CD4 and CD8 molecules on the cell surface, respectively. These two molecules serve as co-receptors in the interaction of TCR with peptide-MHC complexes. The co-receptors are essential for efficient signal transduction, which ultimately lead to T-cell activation.

$CD4^+$ T cells (also known as helper T cells), have a central role in the immune system. They regulate innate immune cells, B cells and their $CD8^+$ counterparts to either mount or suppress major immune responses against self or foreign antigens. $CD4^+$ T cells recognize antigen-derived peptides complexed with MHC class II molecules on the surface of APCs. The importance of $CD4^+$ T cells is more evident in individuals infected with human immunodeficiency virus (HIV), where these cells are the target of HIV. When the number of $CD4^+$ T cells drops below a certain limit, the individual is not longer immune against other opportunistic infections that ultimately lead to death of the individual [3, 4].

$CD8^+$ T cells (also known as cytotoxic T cells) are capable of fighting against a wide range of infectious agents, such as, viruses, bacteria, or eliminating cancer or damaged cells. Unlike $CD4^+$ T cells, TCRs of $CD8^+$ T cells recognize antigens presented by class I MHC molecules on the surface of infected cells. $CD8^+$ T cells directly engage and eliminate target cells via release of several toxic molecules, such as perforin that lead to cytolysis and cell death.

2.2.2 Regulatory T cells

$CD4^+$ T cells are divided into two distinct lineages: regulatory T cells (Tregs) and conventional helper T cells (Tconvs). Unlike Tconvs that activate other immune cells such as $CD8^+$ cytotoxic T cells, B cells and macrophages, Tregs suppress potentially deleterious activities of Tconvs. Tregs are essential maintaining immune tolerance to healthy self-tissues, suppressing immune responses after elimination of pathogens, and limiting chronic inflammations. However, they are involved in limiting anti-tumor immunity. Considering

the positive and negative effects of Tregs, there is considerable interest in the generation and action of these cells.

Upon antigen-specific activation, Tregs suppress immune response in various ways. Tregs secrete cytokines like IL-10, IL-35 and transforming growth factor-β (TGFβ) that inhibits effector Tconvs. Human and mouse Tregs express granzyme A and B, respectively, that lead to the cytolysis (cell death) of activated Tconvs. Similar to Tconvs, Tregs consume IL-2 as a growth factor. Tregs highly express IL-2 receptor (indicating high IL-2 consumption) while they are unable to secrete IL-2. This suggests that Tregs may disrupt metabolic activity of proliferating effector T cells by depleting the IL-2. The direct suppression effect of Tregs on Tconvs is discussed in Chapter 5. However, Tregs may directly suppress APCs. Direct interactions between Tregs and APCs have been observed *in vivo*. These interactions were proposed to function in attenuating T cell stimulation capacity of APCs in a process that involves cytotoxic T-lymphocyte antigen-4 (CTLA4), which is an inhibitory molecule constitutively expressed by Tregs. CTLA4-based regulation is further discussed in Chapter 6.

Two types of Tregs are existing in peripheral lymph nodes, Tregs that are selected by thymus (called as natural regulatory T cells or nTregs), and Tregs that are differentiated from Tconvs (referred as induced Tregs or iTregs) in peripheral lymphoid organs. Molecular markers are essential tools for defining and for analyzing a sub-population of immune cells. Unfortunately, a Treg-specific molecular marker is not available [5]. CD25, CTLA4 and Foxp3 are the markers that widely used for identifying regulatory T cells, although these cannot exclusively discriminate Tconvs and Tregs, or nTregs and iTregs. This thesis investigate nTreg selection and functions. Our work regarding iTreg generation is given elsewhere [6]. Similar to other T cells, nTregs are selected in the thymus from progenitor cells during a selection process known as thymic selection. Like other T cells, Tregs bear TCRs generated by V(D)J recombination process, which can recognize specific antigens via interacting with cognate ligands (ligands that activate mature T cells).

2.3 Thymic selection

T cell antigen recognition is achieved via TCR. When the adaptive immune system is under construction, there is not any information about pathogens that the individual will encounter through life. Therefore, an enormous diversity of TCRs in immune system seems required for recognition of the entire antigenic universe. Indeed, this diversity is generated early in life in an specialized organ called thymus. V(D)J recombination is a unique process of genetic recombination that randomly rearrange variable (V), joining (J) and diversity (D) gene segments and therefore, generates novel TCRs. The TCR repertoire resulted from random rearrangement process are able to react to any antigen, including self-antigens. Therefore, the repertoire has to be shaped to efficiently react to harmful pathogens (bacteria, viruses, parasites, worms and altered-self such as cancer cells) and at the same time, tolerate healthy tissues. Thymus is active during the first two decades of life and maintains the diversity of T cell repertoire. Afterwards, the thymically generated diversity is partially maintained through life via homeostatic proliferation of T cells.

Shaping of randomly generated (pre-selection) TCRs is occurred via a series of distinct selection steps. These steps that are defined by the expression of co-receptors are the double-negative (DN) stage, in which T precursors (thymocytes) do not express any co-receptor, followed by the double-positive (DP) stage when thymocytes express both co-receptors in addition to $\alpha\beta$ TCR, ending up in the single-positive (SP) stage when thymocytes uniquely express one type of co-receptor molecules (CD4 or CD8).

$\alpha\beta$ TCRs are expressed in double-positive stage. After expression of TCRs, thymocytes sequentially encounter various APCs (mainly thymic epithelial cells) each expressing diverse self-peptides on the cell surface. On each APC, self-peptides are presented by individual's MHC molecules and are corresponding to proteins that build individual's healthy tissues. It is believed that thymocyte-APC encounters and the quality of self-antigen recognition is the primary determinant of cell fates, namely cell maturation and differentiation, or cell death. Thymocytes that complete the maturation steps leave the thymus as $CD8^+$ Tconvs, or $CD4^+$ Tconvs or $CD4^+CD25^+Foxp3^+$ Tregs (or nTregs).

2.3.1 Affinity model of thymic selection

The strength of the binding between two interacting proteins is called affinity. The affinity is commonly represented by a dissociation constant (K_{d}), which indicates how easy it is to separate protein complex into its constituents. A smaller K_{d} indicates a stronger or higher affinity interaction. In the context of protein interactions bound to interacting cells, avidity indicates the combined strength of interacting proteins. Abundance of a peptide indicates to the fraction of APCs that express the peptide (**Figure 2.1**). If a peptide is highly abundant, thymocytes interact with the peptide with high frequency.

The classical affinity/avidity model of thymocyte selection relies on the affinity/avidity between TCR and self-peptide-MHC complex (spMHC) as determinant of cell fate (**Figure 2.2**). According to this model, during positive selection, weak affinity/avidity interactions are required for maturation of double-positive thymocytes to single positive thymocytes and to protect them from cell death by neglect. In contrast, during negative selection (also known as clonal deletion), double-positive or single-positive thymocytes that encounter high affinity/avidity interactions undergo apoptosis (cell death) [7]. This model does not state how nTregs are selected.

2.3.2 Selection of regulatory T cells

TCR-transgenic mice models were extensively used for studying thymic selection. In these genetically engineered models, all thymocytes express identical $\alpha\beta$ TCR with known specificity. By manipulating the antigen presentation in thymus and expression of a ligand with known TCR affinity via a second transgene, the role of affinity/avidity in thymic selection can be investigated.

According to TCR-transgenic studies, high-affinity interactions were shown to deviate clonal deletion to nTreg differentiation. This suggests that nTregs may be selected from thymocytes with autoreactive (self-reactive) TCRs. A modified version of the affinity model is currently favored in which nTreg selection occurs within an affinity-window between positive selection and negative selection (**Figure 2.3**).

However, the alternative models exist in which nTreg differentiation are, at least partially, independent of TCR specificity to self-antigens. These models are summarized in **Figure 2.4**. In this thesis, we propose a signal integration model of thymic selection in which thymocyte fate determination relies on the

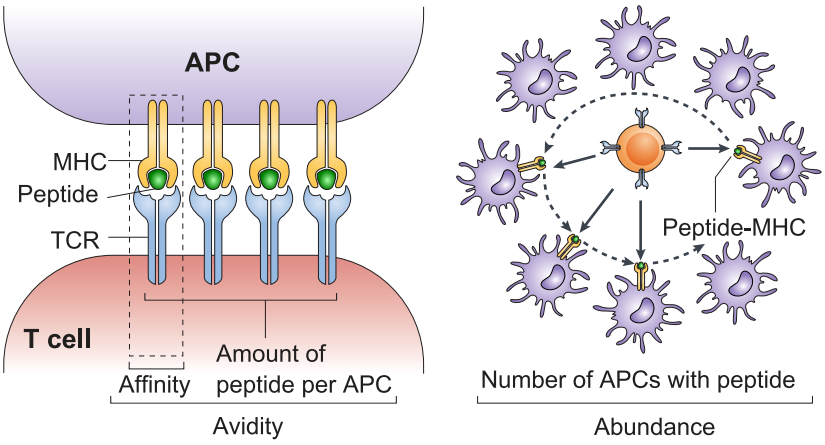

Figure 2.1: Affinity, avidity and abundance of ligands. Affinity is the strength of interaction between TCR and a single peptide-MHC complex. Avidity is the combined strength of interaction between TCRs on a single T cell and multiple peptide-MHC complex on the APC. Abundance of a ligand indicates the fraction of thymic APCs that express the ligand.

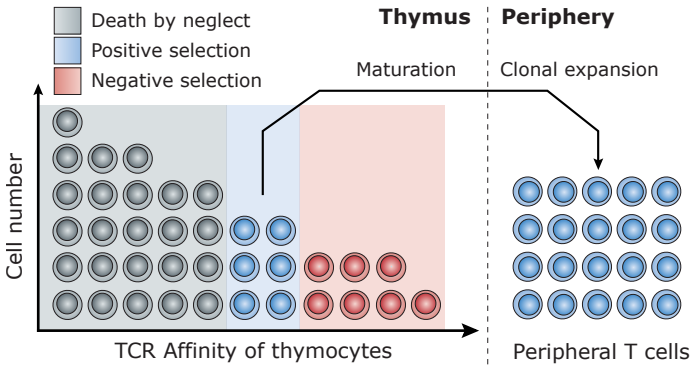

Figure 2.2: Affinity/avidity model of thymic selection. Most thymocytes (≈90% of pre-selection cells) express TCRs that do not bind spMHCs, do not receive a survival signal and die by neglect (grey cells). Low affinity interactions of TCRs with spMHCs rescue cells from death (blue cells), whereas high-affinity interactions induces cell death (red cells). Positively selected thymocytes undergo cell maturation and migrate out of the thymus and enter the peripheral T cell pool.

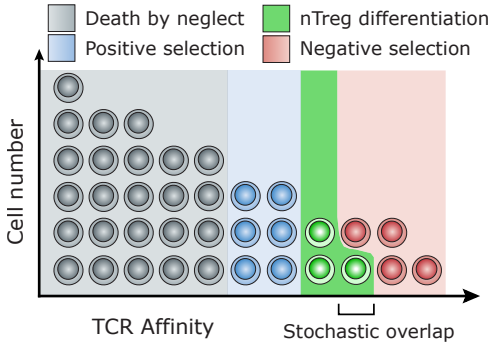

Figure 2.3: Modified affinity model of thymic selection. nTreg selection occurs within an affinity-window between positive selection and negative selection. This window is subjected to some stochastic influences. For example, in TCR-transgenic systems, expression of a high affinity ligand may induce either nTreg or Tconv selection, or nTreg selection and clonal deletion. A broad range of affinities seems to be permissive for nTreg differentiation.

integrated TCR signal over a sequence of thymocyte-APC interactions. In the proposed model, not only affinity/avidity contributes to the fate decision, but abundance of presented self-peptides play a major role (peptide abundance is defined in **Figure 2.1**). Signal integration model is presented in chapter 4.

2.4 Immune activation and response

After maturation in thymus, T cells migrate to peripheral lymphoid organs and continuously scan the environmental antigen presentation. T cells cannot recognize "free" antigens, but only when they are processed by other cells (like APCs) and presented via carrier molecules such as MHC molecules. $CD8^+$ T cells respond to their specific antigens when presented by MHC I molecules. MHC I molecules are expressed by most cells in the body. $CD4^+$ cells recognize their specific antigens that are carried by MHC II molecules. MHC II molecules are only expressed by professional APCs such as macrophages and dendritic

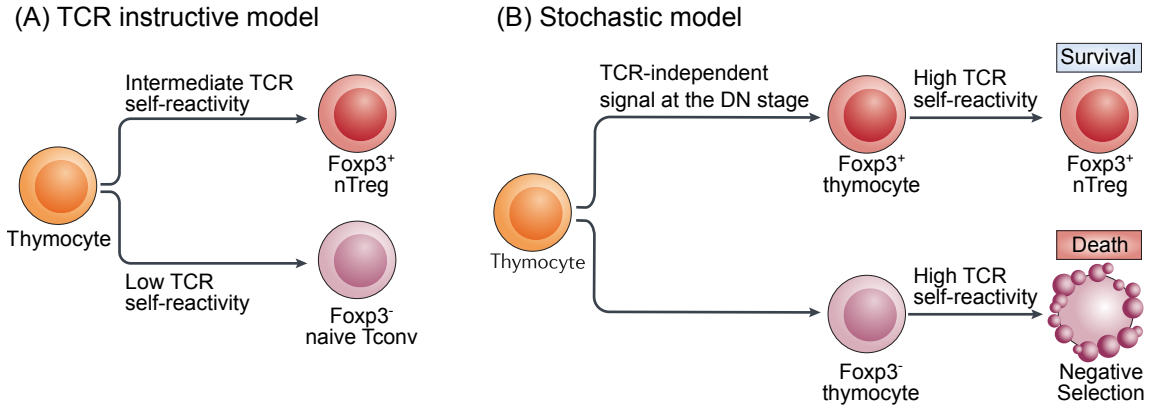

Figure 2.4: Models of nTreg selection. The current models are divided into (A) TCR instructive and (B) stochastic. According to TCR instructive (affinity) model, intermediate levels of TCR stimulation Foxp3 expression, whereas higher levels and lower levels induce clonal deletion and Tconv selection respectively. In stochastic model, the Foxp3 expression is induced in some thymocytes by an early TCR-independent signal during double-negative stage (before expression of TCR). As the result, these cells become more resistant to clonal deletion than Foxp3^{-} thymocytes whenever interact with their specific spMHCs. Therefore, these autoreactive TCRs can survive and build nTreg repertoire. Figure is modified from [8].

cells.

The activation of immune response starts with phagocytosis of invaded pathogen by APCs. The engulfed material are digested and presented on the cell surface in the form of antigen fragments (peptides) complexed to MHC molecules. Among all the antigen fragments, only a few may stably bind MHC molecules (see **Figure 2.5**). If APCs encounter a dangerous pathogen, they express costimulatory ligands CD80 and CD86, on their plasma membrane (cell surface). CD80 expression is poor on professional APCs, but increases several days after interaction with T cells. In contrast, CD86 is constitutively expressed on professional APCs, which increases rapidly after antigen presentation to T cells [9]. The expression of costimulatory ligands on APCs is critical for T cell activation. Ligation of TCR with cognate pMHC can leads to T cell activation, proliferation and differentiation into effector cells only when costimulatory receptors on T cells, called CD28, is sufficiently ligated with costimulatory ligands [10, 11]. If the costimulation is not provided to T cells within hours of TCR engagement, they convert to an unresponsive state known as anergy, or undergo apoptosis.

Another receptor of T cells that bind to costimulatory ligands, is CTLA4. Unlike CD28 that is expressed by nearly all T cells in steady state and during infection, CTLA4 is maximally expressed by Tconvs 1-2 days after T cell activation [12]. In steady state, CTLA4 expression is confined to Tregs. CTLA4 and CD28 differs in their binding affinity to co-stimulatory ligands. CTLA4 binds to both costimulatory ligands with higher affinity and avidity than does CD28 (**Figure 2.6**). Therefore, it is believed that CTLA4 can act as an antagonist of CD28-ligand interactions, meaning that by winning the competition, CTLA4 interferes the induction of costimulation. In CTLA4-deficient mice (mice that are unable to express CTLA4), conventional T cells undergo unregulated proliferation in lymph nodes which results in death in 3-4 weeks after birth. Further, blocking CTLA4 receptor in mice models resulted in amplification of T cell response. These experimental evidences clearly indicate to inhibitory function of CTLA4. However, how CTLA4 works is widely debated. Namely, it is not clear that CTLA4 inhibition is cell-intrinsic, or rather CTLA4 acts on other cells via cell-extrinsic mechanisms. Chapter 6 is devoted to the study of unusual cellular trafficking of CTLA4 molecules and its possible role on cell-extrinsic inhibition of immune activation.

Once activated, CD4^{+} T cells orchestrate different phases of adaptive immune response (**Figure 2.7**).

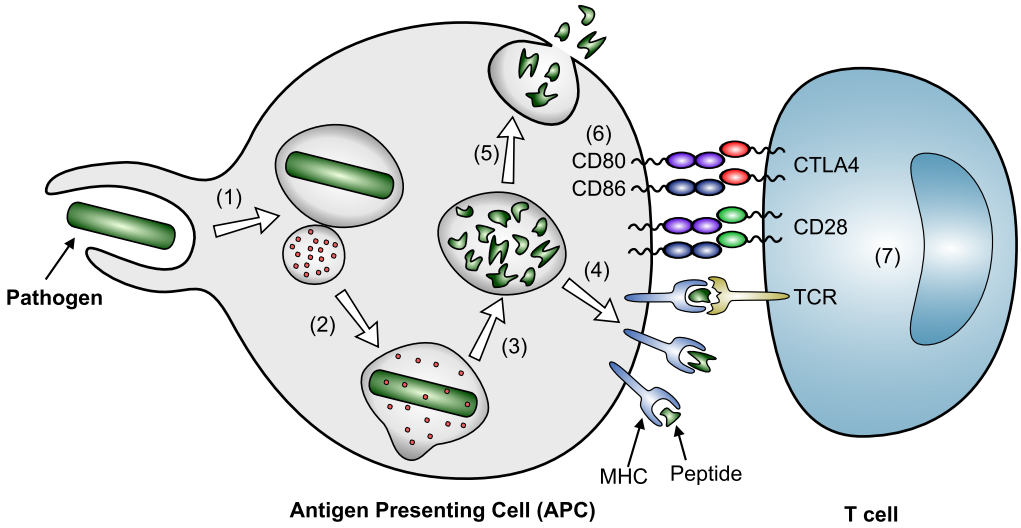

Figure 2.5: Antigen presentation. (1) APCs continuously scan their local environments and engulf dead cells, invaded substances, microbes and cancer cells. (2) In cytoplasm (inside the cell), the phagosomes that carry the engulfed material are fused with lysosomes. (3) Then, the engulfed material are digested by special enzymes and broken into small fragments (peptides). (4) Those fragments that successfully bind to MHC molecules are then expressed to the cell surface. (5) Left over fragments are either released by exocytosis or assimilate. (6) If APCs encounter a dangerous pathogen, in addition to the expression of peptide-MHC complex, they express CD80 and CD86 molecules which are known as co-stimulatory ligands. CD28 and CTLA4 are the receptors on T cells that can bind co-stimulatory ligands. (7) Upon ligation of specific TCRs with pMHC molecules and CD28 with CD80/CD86 ligands, T cells can be activated. Otherwise, activation does not occur.

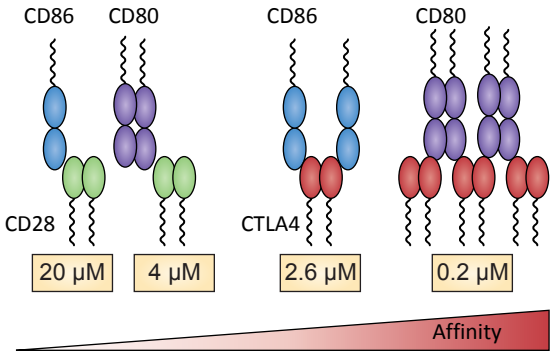

Figure 2.6: Costimulatory receptor-ligand interactions [13]. The numbers shown represent the values of the monovalent solution dissociation constant (K_d), measured in [14]. This figure is taken from [13].

$CD4^+$ helper T cells proliferate and differentiate into effector cells by acquiring effector functions such as cytokine secretion. For example, effector Tconvs secrete the cytokine interleukin-2 (IL-2), which is a growth factor that stimulates clonal expansion (proliferation) of the antigen-specific T cells. Some Tconvs secrete cytokines that stimulate leukocyte recruitment and production of microbicidal substances in phagocytes (like macrophages). Other $CD4^+$ helper Tconvs secrete cytokines that help B cells produce antibodies which are substances that identify and neutralize invaders such as bacteria and viruses.

When $CD4^+$ T cells orchestrate an effective immune response that successfully eliminates the threat, a contraction phase occur druing which effector T cells are reduced and homeostasis is restored. However, long-lived memory cells will remain for years after the infection to re-initiate another effective immune response upon re-stimulation by the same pathogen. In each phase of immune response, Tregs function as regulators. Before T cell activation, Tregs control the homeostatic proliferation of Tconvs that may limit their clonal size (thymocytes with identical TCR make a clone). Further, they continuously interact with APCs and control the expression of costimulatory ligands. Once activated, Tregs undergo cell proliferation and expand their clonal size. By acquiring cytokine-driven or cell-contact dependent inhibitory functions, Tregs regulate the population size of activated Tconvs and stimulatory capacity of APCs.

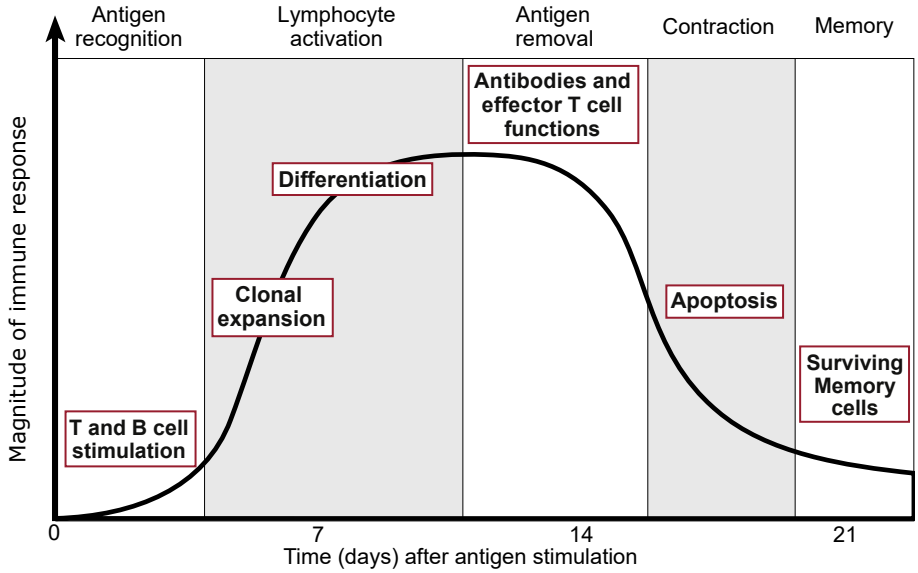

Figure 2.7: Time-course of T cell response. T cell response consist of distinct phases. Interaction with activated APCs lead to recognition of antigen by specific T cells. Upon activation T cells expand their clonal size and effector response until the antigen is eliminated (the effector phase). The response declines by apoptosis of effector cells and Treg-associated suppression. This restores T cell homeostasis. Some antigen-specific T cells remain as memory T cells for immunity against later invasion of pathogen. The duration of each phase may vary depending on pathogen and associated immune responses.

2.5 Scope of the study

A state in which the immune system does not elicit a response to an antigen or a set of antigens is called immune tolerance. This does not imply that TCRs recognizing the tolerated antigen do not exist in the repertoire, rather the overall status of immune system (such as antigen density, number of antigen specific Tconvs versus Tregs etc.) for the antigen does not allow an antigen-specific immune response. In other words, immune tolerance is not inability to recognize an specific antigen, but it is an antigen-specific suppressive response. Immune tolerance can be also achieved under conditions that effector immune response is suppressed after initiation. Immune tolerance is clearly required for proteins that build healthy tissues, and should be broken for foreign-antigens and altered self-antigens. How immune tolerance is induced, is kept and is broken in the immune system is the driving force behind this study. In this thesis, tolerance induction in helper T cells is studied in different stages, namely T cell selection, T cell activation

and response. We start with thymic selection during which central tolerance (the result of negative selection or clonal deletion) is induced in T cells repertoire by eliminating thymocytes with self-reactive TCRs. Although negative selection eliminates a vast majority of self-reactive TCRs, this process still leaking some autoreactive TCRs. Therefore, generation of nTregs that keeps immune tolerance in periphery (called peripheral tolerance or dominant tolerance) is critical. It is important to know which TCRs are deviated to nTreg differentiation instead of clonal deletion. Next, nTregs and Tconvs are considered after thymic selection when they migrate to peripheral lymphoid organs. Interplay between nTregs and Tconvs after they are stimulated by antigen (both self and nonself) is studied by a series of simple mathematical models. It is shown how different functions and properties of nTreg and Tconvs lead to emergence of antigen-specific immune response and tolerance. In addition to antigen-specific immune tolerance, immune system benefits from antigen-nonspecific mechanisms to keep the tolerance. A major antigen-nonspecific suppression mechanism which is imposed by T cells-associated inhibitory receptor CTLA4 is studied.

Chapter 3

Mathematical background

Mathematical models can quantitatively describe, in a systematic and dynamic way, immunological processes which contain complex networks with nonlinear interactions. These models help in interpretation of experimental data, extraction of information from a large amount of complex data, behavioral prediction of the immune system in different scenarios, and finding new drug or vaccine target. Two major theoretical approaches have been utilized to study the immune system: unbiased data-driven modeling approach that aims to identify, from massive amounts of quantitative data, cellular and molecular components of the immune system and their possible interactions; and hypothesis-based modeling approach aiming to understand the functioning principles of the immune system by extracting a minimal and fundamental set of variables and their underlying rules [15]. This thesis takes hypothesis-based modeling approach and, therefore, different strategies and methods that have been used in this modeling approach to study the immune system is briefly reviewed.

3.1 Hypothesis-based modeling approach

In hypothesis-based modeling approach, one asks a question based on a specific hypothesis, and then by employing models tries to answer the question of interest. These models are simplified version of immune mechanisms, and are developed by translating presumed knowledge about the system of interest into mathematical formulations. Different hypothesis require different equations that lead to different predictions, which can then be compared to experimental data. Comparison between model predictions and validating experimental data reveals the most relevant hypothesis that best matches the observations. Depending on complexity, quantity and quality of experimental data, different strategies may be taken to study the immune system.

3.1.1 Conceptual modeling

In theory, it is possible to develop mathematical models of immunological networks, and study them by means of classical analysis and simulation tools. But, this is not easy to achieve in practice, as experimental data with sufficient quantity and quality are usually not available for kinetic parameters of most immunological systems. Moreover, complex models with many variables are highly nonlinear and consist of different time-scales, making the model analysis difficult to handle with analytic and computational approaches. To cope with system complexity and lack of sufficient experimental data, one can take conceptual modeling approach in which the immunological system is translated into the mathematical formulation just in an abstract and mechanistic way. The biological details of components and their interactions are usually

neglected. Although this approach may not provide accurate quantitative conclusions about the system of interest, it may provide qualitative insights about the regime in which the system is functioning.

A typical example of such modeling strategy, is modeling of the interaction between antigens and antibodies. Perelson and Oster [16] developed a simple model to estimate the probability that an antigen can be recognized by, at least, an antibody (or antigen receptor) from a set of distinct and randomly generated antibodies. A "shape space" concept to represent the binding of antigen and antibody was introduced. In shape space, each point corresponds to an antigen or antibody. When two points representing an antigen and antibody are located in sufficiently close proximity, there exists a probability of antigen-antibody binding (**Figure 3.1**). This does not imply an actual proximity in physical space. By using their simplifying assumptions, authors approximated the size of an immune repertoire that would be required in order to provide immunity against an infinite number of antigenic variants. Note that in the model, it is assumed that the antibodies in the repertoire are randomly distributed in shape space. This assumption is certainly not strictly satisfied. Antibodies are not made by a fully random process, but generated from random rearrangement of a finite set of genes. Further, the model cannot map the shape space to physical space and make statements in the protein level.

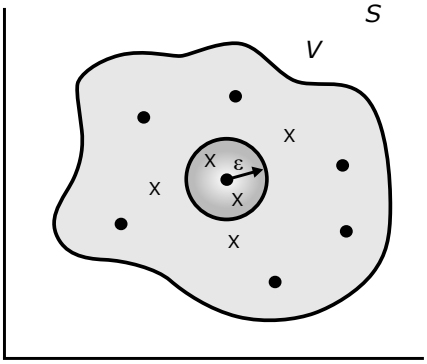

Figure 3.1: Shape space for antigen-antibody binding [16]. Within shape space S there is a volume V in which the shapes of antibody combining site (•) and antigenic determinant (X) are located. All the antigens that are within a distance ϵ of an antibody are assumed to be recognized by the antibody.

3.1.2 Data-driven mechanistic modeling

Once appropriate biological data is available, one can analyze biological theories by data-driven modeling approach. This approach starts with developing models based on underlying immunological mechanisms and theories. For building models, one should carefully understand experimental protocols, observations and possible interpretations regarding the immunological process. In general, models are constructed by parameters of interest with unknown biologically relevant value; by using experimental measurements the biological value of parameters may be estimated. In case that measurements are not enough for estimation of all parameters, new experiments can be designed to specifically estimate parameters that were not identified. Models should be validated by comparing mathematical and experimental results which were not used in the parameter estimation step. The model has to be modified until such a validation achieved. Then, the established model can be used to predict system behavior in new scenarios and suggest new hypothesis and experiments to test the predictions. An example of steps that is followed in data-driven modeling approach is shown in **Figure 3.2**.

We took this modeling strategy to study homeostasis of regulatory T cells [6]. The aim of our study was to quantify the contribution of different mechanisms that sustain the homeostatic cell number of

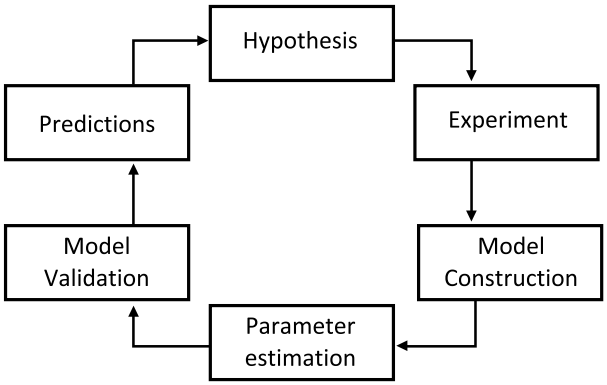

Figure 3.2: Data-driven mechanistic modeling approach. This figure shows an example of a workflow that is followed in data-driven modeling approach. Not all the steps in this workflow can be done in every case; for example, model validation and verification of predictions in some cases might not be feasible due to limitations in technology.

regulatory T cells, an important phenotype of T cells that is critical for self-tolerance. These mechanisms are thymic output, migration of cells between different lymphoid organs, cell proliferation/death, and in particular, induction of regulatory T cells from conventional naïve T cells (conversion mechanism) (**Figure 3.3**). Although the Tconv-Treg conversion is a well documented mechanism [17], its contribution to the homeistatic number of Tregs is not experimentally quantified, mainly due to paucity of unique markers to distinguish thymically-selected (natural) and Tregs [18]. By using a combined *in vivo* and *in silico* approach, the first estimation of the peripheral regulatory T cell conversion rate is provided, which cannot be verified experimentally for the moment. This is an exciting example of employing hypothesis-based modeling strategy in estimation of a critical biological parameter which cannot be quantified experimentally with the current technology.

3.1.3 Hierarchical modeling

Clearly, simple (minimal) models cannot fully describe details of a complex system. Using highly simplistic models is often necessary due to practical limitation and uncertainties. Despite their limitations, simple models can give valuable insights about the system and drive predictions that raise motivation for further investigations. Despite being simplistic, simple models are attractive as they can be treated with variety of analytic tools and, thereby, provide a better understanding. The importance of using minimal models is represented by some quotes. According to principle of parsimony (also known as Ockham's razor), among competing hypotheses that has similar prediction quality, the one with the fewest assumptions should be chosen. Using simplest model is also demanded by Albert Einstein, "Make everything as simple as possible, but not simpler".

It is not always easy to find the minimal model that can sufficiently describe the functioning principles of the system. Further, minimal model may not be unique, and multiple minimal models may equally able to describe the system under study. Essentially, as George Box said, all models are wrong, but some are useful [19]. For finding a useful model, the degree of model complexity and details has to be chosen, which depends on the purpose of the model. One way to construct a model with minimal but necessary degree of complexity, is to start with very basic model, and then by adding complexity in a hierarchical manner, obtain the simplest model that could match to the experimental findings. Along with the procedure, useful information can be gained about the deficits of simpler models and the contribution of each additional complexity.

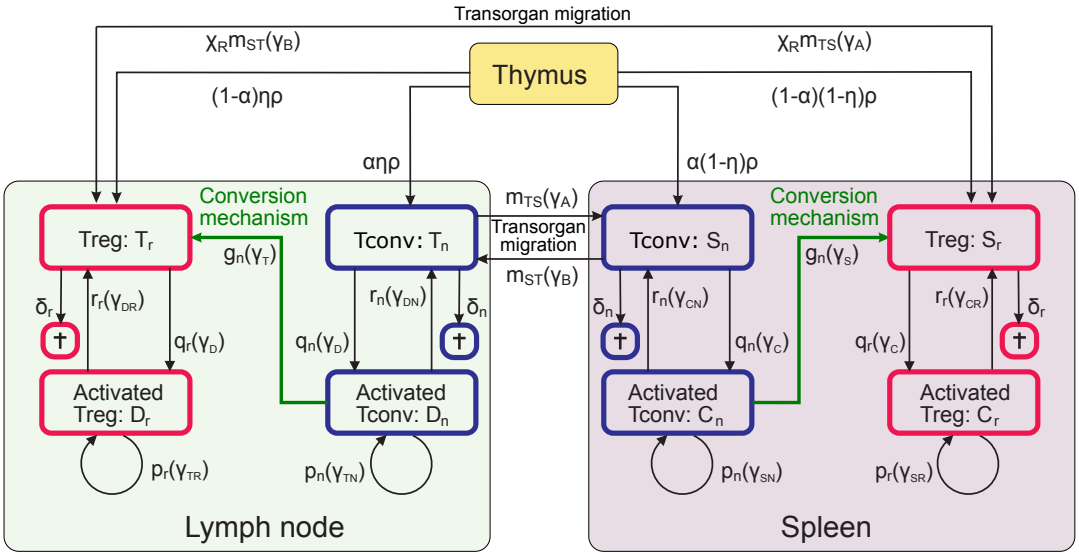

Figure 3.3: A multiorgan mathematical model of T cell homeostasis including LNs and spleen [6]. The thymus generates naïve T cells (fraction α) and Treg cells (fraction $1-\alpha$) at rate ρ; both fractions distribute to LNs (fraction η, left) and spleen (fraction $1-\eta$, right). Naïve T cells and Treg cells die with rate δ_{n} and δ_{r}, are activated to homeostatic division with rate $\mathrm{q_n}$ and $\mathrm{q_r}$, divide with rate $\mathrm{p_n}$ and $\mathrm{p_r}$, and return to the resting state with rate $\mathrm{r_n}$ and $\mathrm{r_r}$ in both organs, respectively. Activated Treg cells modulate naïve T cell activation, while activated naïve T cells modulate Treg cell activation. Activated naïve T cells convert into Treg cells with rate $\mathrm{g_n}$. Resting T cells migrate between both organs with rate $\mathrm{m_{ST}}$ from spleen to LNs and back with rate $\mathrm{m_{TS}}$. Treg-cell transorgan migration is reduced by the factor $0 \leq \chi_{\mathrm{R}} \leq 1$. A mice strain was used to transiently eliminate Tregs and observe their rebound. The best parameter set was obtained to fit rebound kinetics. Experimentally, it is not possible to quantify Tconv-Treg conversion. This model was used to estimate the conversion rate.

A classical example of such modeling strategy is the study of de Boer and Hogeweg [20], where the authors studied emergence of self/nonself discrimination by cytotoxic and helper T cells with incorporating varying degree of immunological complexity. Self/nonself discrimination emerged in their models from nonlinearities that were assumed in the T cell activation and proliferation processes. In their simplest model (**Figure 3.4**), helper and cytotoxic T cells are not discriminated. The authors assumed that memory cells accumulate when the antigen stimulation is low. Such conditions occur when the antigen density or the affinity between TCR and antigen is low. According to this critical assumption, the authors suggested that the continuous self stimulation in immune system does not allow memory accumulation for self-reactive T cell clones that have high affinity to self. Therefore, self-tolerance can emerge. In contrast, T cells with low self-reactivity are accumulated as memory T cells, which upon high affinity foreign-antigen stimulation are converted to effector T cells and, therefore, immunity arises.

In the next model, helper and cytotoxic T cells were treated as separate populations: cytotoxic T cells eliminate the antigen, and helper T cells produce IL-2. Both populations use IL-2 for proliferation. Later, the difference of antigen recognition by helper versus cytotoxic T cells was included. Finally, the expression of IL-2 receptors on cytotoxic T cells was assumed to be regulated by a factor derived from helper T cells. By comparing the hierarchical models, authors concluded that only the most complex and the simplest models can represent self-nonself discrimination sufficiently well which is resulted from memory cells accumulation with low self-affinity.

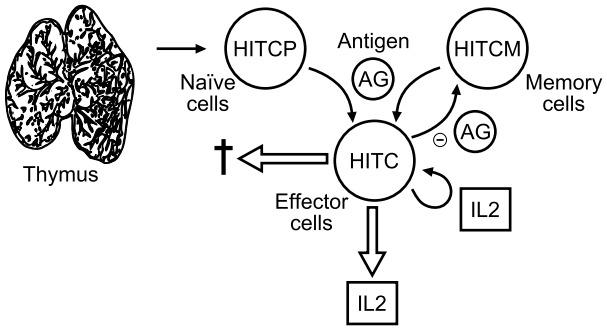

Figure 3.4: Helper independent cytotoxic T cell model. Naïve cell (Tconv) population is maintained by thymic export at a constant rate; these cells can be activated by antigen-stimulation, or they undergo cell death. Activated cells acquire effector functions in the presence of antigenic stimulation, which are IL-2 secretion (a growth factor) and IL-2-dependent proliferation, convert to memory cells in the absence of antigenic stimulation, undergo cell death, and can eliminate antigen. Memory cells are generated from effector cells; By re-stimulation they convert into effector cells, or they undergo cell death. Effector cells, which needs continuous antigen stimulation, compete with other sub-populations to occupy antigenic petides.

3.1.4 Model selection

Often, there is a set of competing hypotheses for explaining a set of observations. These different hypotheses have different mathematical representation among which the best model can be selected. The "best" model has controversial meanings. Although the models with more complexity may fit better to the observations, the additional complexities may not represent useful information/mechanism. Therefore, the best model should balance the goodness of fit and simplicity. When more than one model have similar quality of fitness and degree of complexity, one has to rely on the differences in model predictions. Due to differences in governing rules of models, one can find a (simple) scenario in which the predictions of competing models diverge. It is challenging to find the simple scenario which can be tested by current technologies. Then, the best model can be chosen by validation of simple prediction. Curve fitting problems, where a curve that best fits to data points given by a function, is a standard example of model selection.

3.2 Methods

3.2.1 Ordinary differential equations-based model

Models based on ordinary differential equations (ODEs) are the most popular models in studying the immune system. They have been extensively employed in cancer immunology [21, 22], T cell responses [23, 24], regulatory T cell dynamics [6, 25–27] and B cell responses [28, 29] to name a few example. Most of this popularity owes to the mature theories that exist for analysis of these models and huge informative literature of their applications in population dynamics, reaction kinetics and other physical systems. Additionally, analysis of these systems is simpler than other modeling approaches due to high efficiency of numerical methods for solving these models. The literature about the methods for ODE-based dynamical system modeling and analysis is enormous. In the following, a brief introduction is given solely for the methods that have been employed in this thesis.

Trajectories that follow evolution rules as functions of *time* on a set of *states* (phase space) are called *dynamical systems*. The behavior of dynamical systems can be analyzed according to the properties of their phase space (denoted by M). In this thesis, we consider systems of order n with continuous phase

space that is $\mathbb{R}^n$ with a continuous time variable, $t \in \mathbb{R}$. Relation between a function and its derivatives is a *differential equation*. A differential equation is called *ordinary* if the function depends only on a single variable; otherwise, it is called *partial*. The general system of first order ODEs can be written in the form of

$$\dot{x} = f(t, x), \quad x = x(t) \in M \subseteq \mathbb{R}^n \tag{3.1}$$

where x represents the states of the system. $f(t, x)$ determines the velocity at point x and at time t; consequently, $f : \mathbb{R} \times M \to \mathbb{R}^n$. A dynamical system is called *autonomous* when it does not depend explicitly on time, which can be written in the form of

$$\dot{x} = f(x), \quad x = x(t) \in M \subseteq \mathbb{R}^n. \tag{3.2}$$

In (3.2), the function $f : M \to \mathbb{R}^n$ which assigns a velocity (the direction and speed of motion in a point) at each point in the phase space M is called *vector field*. The problem of finding a solution $x(t)$ of a physical system represented in the form of (3.2) that satisfies initial value $x(t_0) = x_0$ at a given time t_0 is called the *initial value problem*.

In this thesis, we are dealing with obtaining analytic and numerical solutions of initial value problems, bifurcation analysis and parameter estimation in autonomous systems. Therefore, methods that have been used in this study are briefly introduced.

3.2.1.1 Analytic solutions

Consider initial value problem for a system of the form (3.2). A solution $x(t; c)$ that depends on a set of parameters c called the *general solution* of the system if for any initial value x_0, there exists a choice of c such that $x(t_0; c) = x_0$.

The goal in theory of ODEs is to find the general solution of ODE systems in a closed form. However, usually this goal cannot be achieved since the solutions can become highly complex. The only case where always the general solution can be found is autonomous linear ODE systems. In chapter 6, we are dealing with models described by linear ODEs, which are solved analytically. Next, we briefly introduce the methods used in this study to obtain the analytic solutions.

3.2.1.1.1 Homogeneous linear ODEs

Linear differential equations describe systems in which the response is proportional to the input. Such linear systems are described by

$$\frac{dx}{dt} = Ax, \quad x \in \mathbb{R}^n \tag{3.3}$$

where A is an $n \times n$ matrix. For solving this linear system, we can use the *eigenvalues* and *eigenvectors* of the matrix A. An eigenvector v is a nonzero solution to the equation $Av = \lambda v$ for an eigenvalue λ. For this equation, a solution exists only when the characteristic polynomial $Q(\lambda) = \det(\lambda I_n - A)$ is equal to zero; I_n is the identity (unit) matrix of size n. If n linearly independent eigenvector can be found, then a general solution to equation (3.3) exists which is of the form

$$x(t) = \Phi(t)c = \sum_{j=1}^{n} c_j e^{\lambda_j t} v_j \tag{3.4}$$

for any values of the constants c_j. The non-singular matrix-valued function $\Phi(t)$ is called *fundamental matrix*.

3.2.1.1.2 Nonhomogenous linear ODEs

An autonomous linear system that is exposed by an external force can be represented by the following set of ODEs

$$\dot{x} = Ax + g(t), \quad x(t_0) = x_0. \tag{3.5}$$

where $g(t)$ is a continuous vector-valued function, and A is an $n \times n$ matrix. The solution of the system is of the form

$$x(t) = x_c(t) + x_p(t) \tag{3.6}$$

where $x_c(t)$ is the solution of the homogeneous equation and has the form (3.4), and $x_p(t)$ is called a particular solution of the nonhomogeneous equation. Let $\Phi(t)$ be the fundamental matrix for the homogeneous version of the system. Let's replace c in the general solution of homogeneous system given in (3.4) with variable vector-function $u(t)$. Additionally, let's assume that the particular solution of the system has the following form

$$x_p(t) = \Phi(t)u(t). \tag{3.7}$$

Then, by taking a time derivative, we have

$$\dot{x}_p(t) = \dot{\Phi}(t)u(t) + \Phi(t)\dot{u}(t). \tag{3.8}$$

Next, by substituting this into differential equation (3.5), we obtain

$$\dot{\Phi}(t)u(t) + \Phi(t)\dot{u}(t) = A(t)\Phi(t)u(t) + g(t). \tag{3.9}$$

By knowing that equation (3.4) is the solution of the homogeneous system, or equivalently $\dot{\Phi}(t) = A\Phi(t)$, then, $\dot{\Phi}(t)u(t) = A\Phi(t)u(t)$. Therefore, equation (3.9) can be simplified to

$$\Phi(t)\dot{u}(t) = g(t) \Rightarrow u(t) = \int \Phi^{-1}(t)g(t)dt. \tag{3.10}$$

Since $\Phi(t)$ is reversible, $u(t)$ can be obtained. Therefore, the analytic solution of the nonhomogeneous system (3.5) is

$$x(t) = \Phi(t)c + \Phi(t) \int \Phi^{-1}(t)g(t)dt. \tag{3.11}$$

The method presented here is variation of parameters, which is used in chapter 6. An alternative to this method is the method of undetermined coefficients. In contrast to the method of variation of parameters, which works for any form of functions $g(t)$ in (3.5), the method of undetermined coefficients can only be applied to a restricted class of functions $g(t)$.

3.2.1.2 Numerical solutions

Most ODE models cannot be solved analytically. However, an approximate solution can be obtained by numerical methods. Among diverse methods, we explain in the followings two methods used in this thesis for obtaining numerical approximation of initial value problem, which is of the form

$$\dot{x} = f\left(t, x\right), \quad x(t_0) = x_0 \tag{3.12}$$

where f is a function that maps $[t_0, \infty) \times \mathbb{R}^n \to \mathbb{R}^n$, and the initial condition $x_0 \in \mathbb{R}^n$ is a given vector.

Theorem 3.1 *Consider the initial value problem of the form (3.12). If $f\left(t, x(t)\right)$ and $\frac{\partial f}{\partial x}$ are continuous functions in $\alpha < t < \beta$ and $\gamma < x(t) < \delta$ containing the point (t_0, x_0), then a unique solution to the initial value problem exists in an interval $t_0 - h < t < t_0 + h$ that is contained in $\alpha < t < \beta$.*

3.2.1.2.1 Euler method

The most basic explicit method for numerical integration of ODEs is the (forward) Euler method. Consider an initial value problem of the form (3.12), which satisfies the conditions of theorem 3.1 in an interval that contains $t = t_0$. From the problem itself, we know the derivative at $t = t_0$

$$\dot{x}(t_0) = f\left(t_0, x(t_0)\right). \tag{3.13}$$

The tangent line to the solution at $t = t_0$ is

$$\widehat{x}(t) = x(t_0) + f\left(t_0, x(t_0)\right)(t - t_0). \tag{3.14}$$

By choosing a $t = t_1$ sufficiently close to t_0, the corresponding point on the tangent line

$$x_1 = \widehat{x}(t_1) = x(t_0) + f(t_0, x(t_0))(t_1 - t_0) \tag{3.15}$$

should be close to $x(t_1)$, the actual value of the solution at $t = t_1$. By using the approximated value x_1 instead of the exact solution $x(t_1)$, the approximate solution x_2 in the next time point $t = t_2$ that is sufficiently close to t_1 can be obtained. In the same fashion, approximate solution in next time steps (t_{n+1}) can be obtained from previous ones (t_n)

$$x_{n+1} = x_n + f(t_n, x_n)h \tag{3.16}$$

where $h = t_{n+1} - t_n$ for every n is called step-size.

The Euler method is a first-order method, i.e. local error (error per step) is proportional to the square of the step-size, and the global error (error at a given time) is proportional to the step size. The explicit Euler method is equivalent to the first-order explicit *Runge-Kutta* method.

3.2.1.2.2 Classical Runge-Kutta method

Explicit Euler method is not very accurate and suffers from instabilities when the ODE is highly nonlinear. Explicit Runge-Kutta methods are alternative methods which are based on making multiple Euler steps. In the following, we present a motivation for the formulation of explicit 4^{th} order Runge-Kutta method.

Consider that $x(t)$ is the solution to initial value problem. A typical solution curve is shown in **Figure 3.5A** in the first time interval $[t_0, t_1]$ with step-size $h = t_1 - t_0$. The value f_1 is the slope of the solution curve at time t_0, f_2 and f_3 are two different estimates in the middle of time interval, and f_4 is the estimate at the end of time interval. These slopes are

$$\begin{aligned} f_1 &= f\left(t_0, x(t_0)\right), \quad f_2 = f\left(t_0 + \frac{h}{2}, x(t_0) + \frac{h}{2} f_1\right), \\ f_3 &= f\left(t_0 + \frac{h}{2}, x(t_0) + \frac{h}{2} f_2\right), \quad f_4 = f\left(t_0 + h, x(t_0) + h f_3\right). \end{aligned} \tag{3.17}$$

The actual next point $(t_1, x(t_1))$ can be obtained by integrating the slope function (**Figure 3.5B**)

$$x(t_1) - x(t_0) = \int_{t_0}^{t_1} f\left(t, x\left(t\right)\right) dt. \tag{3.18}$$

By applying Simpson's rule step-size $h/2$, the integral in (3.18) can be approximated to

$$\int_{t_0}^{t_1} f\left(t, x\left(t\right)\right) dt \approx \frac{h}{6}\left[f\left(t_0, x(t_0)\right) + 4f\left(t_{1/2}, x(t_{1/2})\right) + f\left(t_1, x(t_1)\right)\right]. \tag{3.19}$$

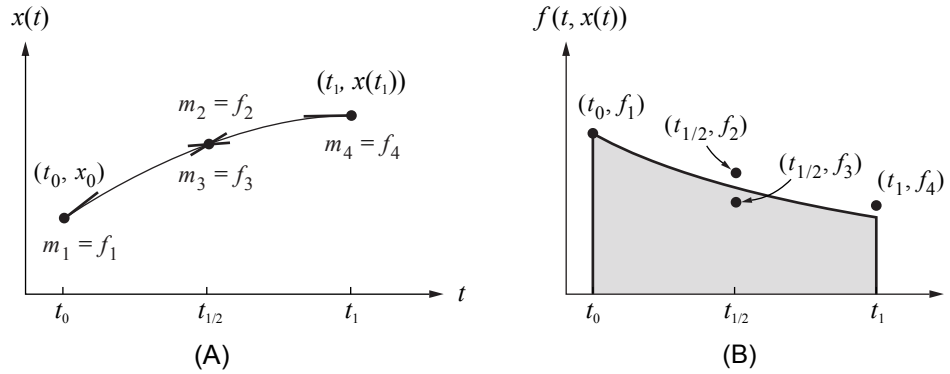

Figure 3.5: 4^{th} order Runge-Kutta. (A) Estimated slopes m_j of the solution curve $x(t)$. (B) Integral approximation $x(t_1) - x(t_0) \approx \frac{h}{6}(f_1 + 2f_2 + 2f_3 + f_4)$.

where $t_{1/2}$ is the middle time point of the interval. We use the following approximations for the values of function $f(t, x(t))$ in the time interval:

$$\begin{aligned} &f(t_0, x(t_0)) = f_1, \\ &f\left(t_{1/2}, x(t_{1/2})\right) \approx \frac{f_2 + f_3}{2}, \\ &f(t_1, x(t_1)) \approx f_4. \end{aligned} \tag{3.20}$$

These values are substitute into (3.19), which is used in equation (3.18) to get an approximate to $x(t_1)$, which is x_1

$$x(t_1) \approx x_1 = x_0 + \frac{h}{6}(f_1 + 2f_2 + 2f_3 + f_4). \tag{3.21}$$

In the same fashion, the approximate solution of $x(t_1)$ will be used to approximate next data point. The Runge-Kutta method presented here (4^{th} order) has a local error (error per step) proportional to h^5, and the global error (error at a given time) proportional to h^4.

In addition to the explicit methods presented here and other explicit methods exist in the literature, one can choose implicit methods, such as implicit Euler or Runge-Kutta methods, especially when the ODE is stiff, i.e. exact solution of ODE $x(t)$ contains a term that decays exponentially to zero as t increases, but whose derivatives are much greater in magnitude than the term itself. For example, consider the initial value problem $\dot{x}(t) = -100x(t)$ with $x(0) = 1$. The exact solution of this ODE is $x(t) = e^{-100t}$, which rapidly decays to zero as t increases. If we employ Euler method with step size $h = 0.1$, we have $x_{n+1} = x_n - 100hx_n = -9x_n$ which yields to a exponentially growing approximate solution $x_n = (-9)^n$. If we choose $h = 10^{-3}$, we obtain approximate solution $x_n = (0.9)^n$, which correctly capture the qualitative behavior of the exact solution. Explicit methods need to take small step size to accurately estimate the solution, which increases the computational cost. Implicit methods allow for a more reasonable step size for stiff ODEs. In this thesis, we are not dealing with stiff ODEs, and the rate of changes in the immunological processes that we study is smooth. Therefore, Euler and Runge-Kutta methods are sufficient to obtain numerical solutions of our proposed models.

3.2.1.3 Steady state and linear stability analysis

A constant solution $x(t) \equiv x^*$ is called a steady state (equilibrium, critical or fixed point) for a differential equation. It is a solution where the value of $x(t)$ does not change over time. In other words, the steady state values (x^*) are the solutions which satisfy $\dot{x} = f(x) = 0$.

A steady state x^* in $\mathbb{R}^n$ is called *stable* if for every neighborhood $\mathcal{O}$ of x^*, a neighborhood $\mathcal{O}_1$ exists such that every solution with initial condition $x(0) = x_0$ inside $\mathcal{O}_1$ is defined and stays in $\mathcal{O}$ for all $t > 0$. Additionally, if $\mathcal{O}_1$ exists such that x^* is stable and $\lim_{t\to\infty} x(t) = x^*$, then x^* is *asymptotically stable*. The equilibrium x^* is called *unstable* if there exists a neighborhood $\mathcal{O}$ of x^* such that for *every* neighborhood $\mathcal{O}_1$ of x^* in $\mathcal{O}$, at least one solution $x(t)$ starting at $x(0) \in \mathcal{O}$ can be found which does not entirely remain in $\mathcal{O}$ for all $t > 0$. In simpler words, steady state x^* that is not stable, is unstable.

To see how we can check the asymptotic stability of an autonomous system of the form (3.2), let's take multivariate Taylor expansion of the right-hand side of equation (3.2)

$$\dot{x} = f(x) = f(x^*) + (x - x^*) \left.\frac{\partial f}{\partial x}\right|_{x=x^*} + \text{higher order terms.} \tag{3.22}$$

Since x^* is the equilibrium point, $f(x^*) = 0$ in (3.22). For function $f(x)$, the partial derivative at point x is defined as the Jacobian matrix

$$J(x) = \frac{\partial f}{\partial x} = \begin{pmatrix} \frac{\partial f_1}{\partial x_1} & \frac{\partial f_1}{\partial x_2} & \cdots & \frac{\partial f_1}{\partial x_n} \\ \frac{\partial f_2}{\partial x_1} & \frac{\partial f_2}{\partial x_2} & \cdots & \frac{\partial f_2}{\partial x_n} \\ \vdots & \vdots & \vdots & \vdots \\ \frac{\partial f_n}{\partial x_1} & \frac{\partial f_n}{\partial x_2} & \cdots & \frac{\partial f_n}{\partial x_n} \end{pmatrix} \tag{3.23}$$

For x sufficiently close to x^*, the higher order terms in (3.22) will be close to zero when function $f(x)$ is sufficiently smooth, and therefore, we can drop them to obtain the following approximation

$$\dot{x} = f(x) \approx J(x^*)(x - x^*) \tag{3.24}$$

Let's define the *perturbation state* as $\delta x = x - x^*$. By taking time derivative, we have $\dot{\delta x} = \dot{x}$. Therefore, by using the approximation in (3.24), we have the following linear system

$$\dot{\delta x} = J(x^*)\delta x. \tag{3.25}$$

The matrix $J(x^*)$ is a constant, and hence, equation (3.25) is a linear differential equation. Therefore, we know that the solution of (3.25) is of the form (3.4), where λ_j is the set of eigenvalues of the Jacobian matrix at $x = x^*$. Let $\lambda_j = \mu_j + iv_j$, where μ_j and v_j are the real and imaginary parts of the eigenvalue respectively. Then, each of the exponential terms in the expansion (3.4) can be written as

$$e^{\lambda_j t} = e^{\mu_j t}\left(\cos(v_j t) + i\sin(v_j t)\right) \tag{3.26}$$

Therefore, the contribution of imaginary part of the eigenvalue is limited to the oscillatory component of the solution. If real part of eigenvalue (μ_j) is positive for any j, there exists an exponential component of the solution which grows with time and hence, equilibrium point x^* is unstable.

Theorem 3.2 *Let $f : M \to \mathbb{R}^n$ be C^1 and have an equilibrium point x^* such that all the eigenvalues of $J(x^*)$ have negative real parts. Then x^* is asymptotically stable. If among the eigenvalues, at least one has a positive real part, the equilibrium point is unstable.*

Note that we made a local linear approximation of the vector field in (3.22); thus, an analysis based on this theorem is a *linear stability analysis*. Theorem 3.2 is silent about the stability of the system, when there exists eigenvalue with zero real parts; the higher order terms that we neglected in (3.22) determine the stability in this case. In theory, a system might have eigenvalues with repeated real parts; in this case, the

stability of the equilibrium points depends on linearly independence or orthogonality of eigenvectors that are associated with repeated eigenvalues, and determination stability in equilibrium points requires further analysis. In practice, however, identical eigenvalues for real life systems are rare, and one can assume that eigenvalues are different and very close but not identical, and employ theorem 3.2.

The *HartmanâĂŞGrobman* theorem gives insight about how the solution of linearized system and full system are related. This theorem states that the nonlinear system has the same qualitative structure as the linear system in the neighborhood of a *hyperbolic* equilibrium point, which is a point where all the eigenvalues of the Jacobian matrix have nonzero real part.

Theorem 3.3 (Hartman-Grobman). *Let $x^{â}ĹŮ$ be a hyperbolic equilibrium point of a C^1 vector field $f(x)$ with flow $\phi_t(x)$. Then, there is a neighborhood N of $x^{â}ĹŮ$ such that ϕ is topologically conjugate to its linearization on N.*

Note that the *flow* $\phi_t(\bullet)$ is defined such that $\phi_t(x(0)) = x(t)$ according to $\dot{x} = f(x)$. Also, a function is $C^1(M)$ - i.e. continuously differentiable - if the elements of Jacobian matrix $J(x)$ are continuous on the open set M.

3.2.1.4 Bifurcation analysis

A bifurcation is a drastic qualitative change in trajectories in the phase space, or equivalently, in the structure of solutions of a dynamical system upon a small change in a parameter. Let's consider a family of continuous-time systems depending on a parameter,

$$\dot{x} = f(x, \alpha), \quad x \in \mathbb{R}^n, \quad \alpha \in \mathbb{R}^1 \tag{3.27}$$

where α is the parameter of interest and f_α is differentiable for all degrees (C^∞) with respect to α. The simplest types of bifurcations occur when the number and stability of equilibrium solutions changes as α varies. Saddle-node (fold) and Hopf bifurcations are common examples of such simple bifurcations. In the following, fold and Hopf bifurcations are introduced.

Consider one-dimensional dynamical system below

$$\dot{x} = \alpha + x^2. \tag{3.28}$$

At $\alpha = 0$, the system above has a nonhyperbolic equilibrium point $x_0 = 0$, with eigenvalue $\lambda = 0$. For $\alpha < 0$, two equilibrium points $x_{1,2}(\alpha) = \sqrt{\alpha}$ exists, with positive equilibrium point x_1 being unstable, and negative equilibrium point x_2 being stable node. For $\alpha > 0$, no real equilibrium point exists. By increasing the value of α from negative to positive, two equilibrium points x_1 and x_2 (unstable and stable, respectively) collide at $\alpha = 0$, and disappear (see **Figure 3.6**).

The equation $f(x, \alpha) = 0$ is shown in **Figure 3.7** in (x, α)-plane, which is called a bifurcation diagram which shows at the same time equilibrium manifold and the stability of equilibrium points.

Theorem 3.4 (Saddle-Node bifurcation). *Consider first order differential equation (3.27) for which $f_{\alpha_0}(x_0) = 0, \dot{f}_{\alpha_0}(x_0) = 0, \ddot{f}_{\alpha_0}(x_0) \neq 0, \frac{\partial f_{\alpha_0}}{\partial \alpha} \neq 0$. Then, a saddle-node bifurcation occurs at $\alpha = \alpha_0$.*

Consider the following two-dimensional dynamical system that depends on parameter α

$$\begin{aligned} \dot{x}_1 &= \alpha x_1 - x_2 - x_1(x_1^2 + x_2^2) \\ \dot{x}_2 &= \alpha x_1 + \alpha x_2 - x_2(x_1^2 + x_2^2) \end{aligned} \tag{3.29}$$

This system has the equilibrium point $(x_1, x_2) = (0, 0)$ irrespective of the value α. The Jacobian matrix of system (3.29)

$$\mathsf{J} = \begin{pmatrix} \alpha & -1 \\ 1 & \alpha \end{pmatrix}. \tag{3.30}$$

has eigenvalues $\lambda_{1,2} = \alpha \pm i$. Let's define complex variable $z = x_1 + ix_2$ with the following properties

$$\bar{z} = x_1 - ix_2, \quad |z|^2 = z\bar{z} = x_1^2 + x_2^2. \tag{3.31}$$

By taking time derivative of variable z, we have the following differential equation

$$\dot{z} = \dot{x}_1 + i\dot{x}_2 = \alpha(x_1 + ix_2) + i(x_1 + ix_2) - (x_1 + ix_2)(x_1^2 + x_2^2), \tag{3.32}$$

By using equation (3.32), we can rewrite system (3.29) in the following complex form

$$\dot{z} = (\alpha + i)z - z\,|z|^2\,. \tag{3.33}$$

By replacing representation $z = \rho e^{i\phi}$ in equation (3.33), we obtain

$$\dot{z} = \dot{\rho}e^{i\phi} + \rho i\dot{\phi}e^{i\phi}, \tag{3.34}$$

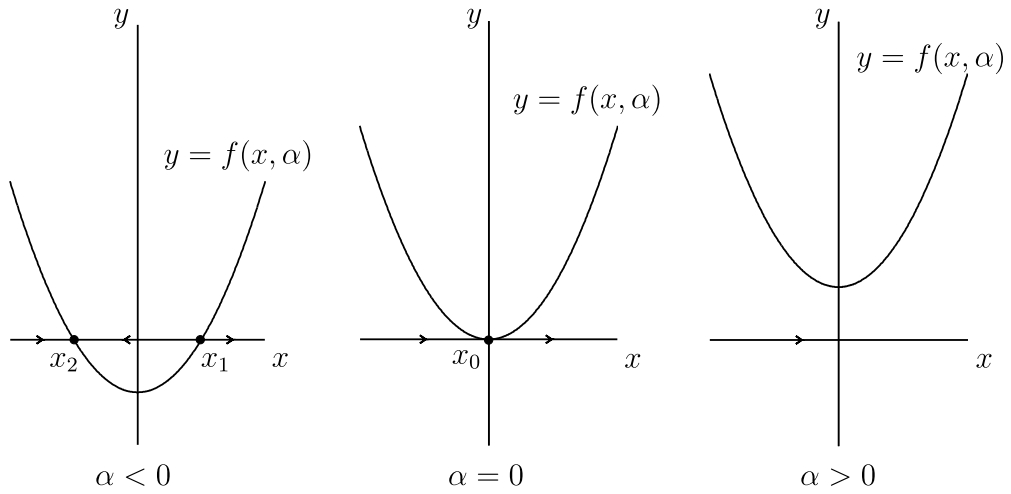

Figure 3.6: Fold bifurcation. Fixing some α, the number of equilibrium points in the system (3.28) can be easily determined. At $(x, \alpha) = (0, 0)$, a fold bifurcation occurs in which unstable and stable equilibrium points collide.

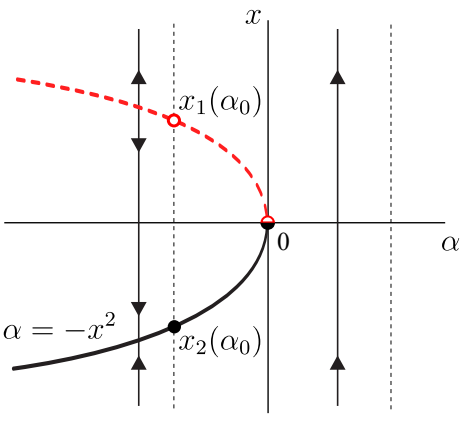

Figure 3.7: Fold bifurcation in the phase-parameter space. Black solid line shows the stable equilibrium points and red dashed line shows unstable equilibrium points. The equilibrium points in a particular case $\alpha = \alpha_0$ is shown by circles.

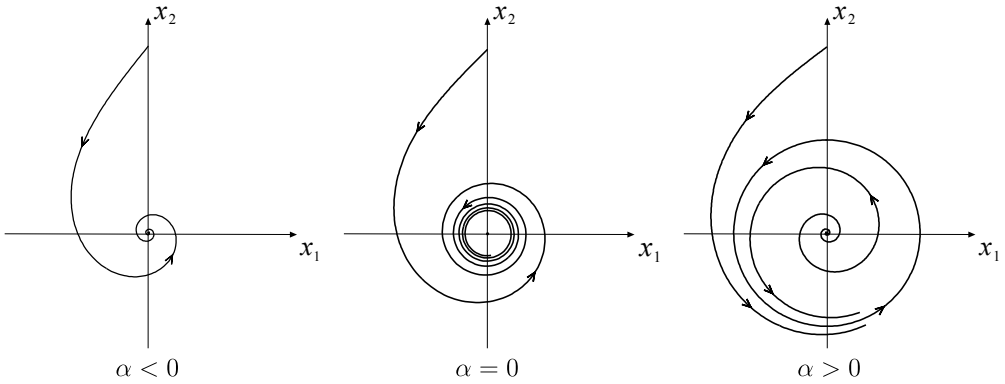

Figure 3.8: Supercritical Hopf bifurcation. System (3.36) has an equilibrium point at the origin which is a stable focus for $\alpha < 0$ and an unstable focus for $\alpha > 0$. At $\alpha = 0$, the equilibrium point is a weakly attracting focus, which is nonlinearly stable and topologically equivalent to the focus. For $\alpha > 0$, this equilibrium point is surrounded by an isolated closed orbit (so-called *limit cycle*) that is unique and stable. The stable cycle is a circle with radius $\rho_0(\alpha) = \sqrt{\alpha}$. Every Orbit that starts from a non-zero initial point inside or outside of the cycle approaches to the cycle as $t \to \infty$. This bifurcation is also called Andronov-Hopf bifurcation.

or equivalently,

$$\dot{\rho}e^{i\phi} + i\rho\dot{p}hie^{i\phi} = \rho e^{i\phi}(\alpha + i - \rho^2), \tag{3.35}$$

which gives the polar form of system (3.29)

$$\begin{aligned} \dot{\rho} &= \rho(\alpha - \rho^2) \\ \dot{\phi} &= 1. \end{aligned} \tag{3.36}$$

System (3.36) consists of uncoupled equations for ρ and ϕ, and therefore, suitable for analyzing bifurcations of phase portrait when α passes through zero. The first equation of system (3.36) has equilibrium point $\rho = 0$ for all values of α. This equilibrium point is linearly stable if $\alpha < 0$, remains stable at $\alpha = 0$ nonlinearly (i.e. rate of convergence of the solution to zero is not exponential), and become unstable when $\alpha > 0$. Another equilibrium point of first equation is $\rho = \alpha$ for $\alpha > 0$ which is linearly stable. The second equation of system (3.36) describes a rotation with constant speed. Therefore, two dimensional system (3.36) has a bifurcation diagram shown in **Figure 3.8**. This bifurcation can also be presented in (x_1, x_2, α)-space (**Figure 3.9**).

3.2.1.5 Parameter estimation

Consider a system represented by the following ODEs

$$\begin{aligned} \dot{x}(t) &= f\left(x(t), u(t), p\right) \\ y(t) &= g\left(x(t), s\right) + \epsilon \end{aligned} \tag{3.37}$$

where $u(t)$ is an external force, p is the parameter set of the system, g is an m-dimensional mapping of the system states to observations $y(t)$ which involves scaling and offset parameters s, and $\epsilon(t)$ is noise in observations.Typically, complex systems are partially observed, which is equivalent with dimension m of

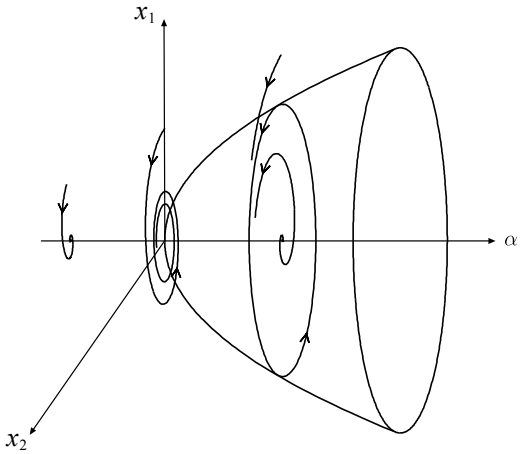

Figure 3.9: Supercritical Hopf bifurcation in the phase-parameter space of system (3.29).

observations being smaller than the dimensions n of system states. Together with the initial value of states $x(0)$ for system (3.37) we define

$$\theta = \{p, x(0), s\}\,. \tag{3.38}$$

as set of parameters necessary to fully specify the system. The quality of fitting of the model prediction to the experimental measurements is typically measured by an objective function, such as

$$\chi^2(\theta) = \frac{1}{\sum_{k=1}^{m} d_k} \sum_{k=1}^{m} \sum_{l=1}^{d_k} \left(\frac{\widehat{y}_{kl} - y_k(\theta, t_l)}{\max\left(\{\widehat{y}_{kl}\}_{l=1}^{d_k}\right)} \right)^2 \tag{3.39}$$

where $\widehat{y}_{kl}$ denotes d_k data-points for observable k, measured at time-points t_l and $y_k(\theta, t_l)$ denotes the k-th observable as predicted by parameters θ for time-point t_l. The best parameters set can be estimated numerically by minimizing the objective function

$$\widehat{\theta} = argmin\left[\chi^2(\theta)\right]. \tag{3.40}$$

We use differential evolution algorithm for finding the parameter set that minimizes this objective function.

3.2.1.6 Differential evolution

Differential evolution (DE) is an evolutionary computation method suitable for real-valued problems. DE tries to optimize an objective function by improving a population of candidate solutions in a stochastic manner. The core idea behind this method is to use differences between candidate solutions for perturbing the population. This method starts with a random generation of a solution set according to user-defined ranges for parameter set. These solutions are modified to moved around in the search parameter space and improve the value of objective function, until a satisfactory criterion is met.

In **pseudo-code 1**, description of DE algorithm we use in this thesis is given. In this pseudo-code, each generation consists of N_p candidate solutions each with n parameters. Trial solutions are created by mutation and crossover. If the trial solutions yield better value for objective function, they replace the old solutions; otherwise, the old solution remains for next generation. Once a termination criterion is satisfied or the maximal number of generations is reached, the algorithm terminates.

Generate N_p initial solutions ($G_0 = \{x_1, x_2, \ldots, x_{N_p}\}$) each with n parameters randomly distributed in appropriate intervals;
for $k \leftarrow 0$ **to** $G_{\max}$ **do**
  check the best candidate solution;
  if *termination criterion* **then**
    break;
  end
  for $i \leftarrow 1$ **to** N_p **do**
    select different parent solutions p_1, p_2, p_3 from G_k excluding x_i;
    generate mutated solution: $v_i = p_1 + F.(p_2 - p_3)$;
    pick random integer $r \in [1, n]$;
    for $j \leftarrow 1$ **to** n **do**
      generate a random number s;
      if $j = r$ *or* $s < CR$ **then**
        take parameter from mutated solution: $u_j = v_{ij}$;
      else
        take parameter from old solution: $u_j = x_{ij}$;
      end
    end
    evaluate objective function for new solutions;
    if $\chi^2(u_j) < \chi^2(x_j)$ **then**
      replace x_i by u_i for next generation G_{k+1};
    else
      retain x_i for next generation G_{k+1};
    end
  end
end
return best candidate;

Pseudo-code 1: Differential evolution algorithm.

3.2.2 Agent-based model

In contrast to PDE models which are dealing with collective populations, agent-based models (ABM) relies on the concept of discrete and distinguishable agents, such as individual cells or isolated molecules. It is easier to study probabilistic uncertainty or stochasticity in biological interactions by ABMs. For example, an individual agent may changes its state or location at a certain probability but not by a deterministic process.

Partial differential equations are widely used for studying dynamics of biological systems. However, the usage of PDEs are restricted to applications where the system of interest has a large density of interacting components, the local fluctuations are smoothed by high diffusion rates, and no delay is existing between cause and effect [30]. These conditions are not fully satisfied in most cellular systems. Further, biological systems are composed of discrete entities that make microscopic inhomogeneity in the system. Neglecting such inhomogeneity by PDE models sometimes lead to false interpretation. For example, Shnerb et al. [31] presented diverging outcomes from an agent-based and a PDE-based representation of a simple system.

In this system, the interaction of two agents, immortal A and mortal B, is considered. It is assumed that A is uniformly distributed on an area with density n_A and move with diffusion coefficient D_A. Agents B spread in the area with initial uniform distribution $n_B(0)$ and move with diffusion coefficient D_B. Further it is assumed that agents B die with a constant rate (μ) and proliferate in the presence of agents A (with rate λ). The dynamic of B population is as follows

$$\frac{\partial n_B}{\partial t} = D_B \nabla^2 n_B + (\lambda n_A - \mu) n_B. \tag{3.41}$$

When the proliferation rate is lower than the death rate, the PDE-based model predicts an extinction for B, and uniformization for A. In contrast, an agent-based implementation of the same system shows that agents B are resilient and trace agents A as they randomly walks, allowing agents B to place their center of mass in A's location and grow (see **Figure 3.10**). The authors concluded that inhomogeneity and fluctuations among interacting populations are the nature of the discrete structure of such systems that cannot be represented by PDE models or their stochastic version [30].

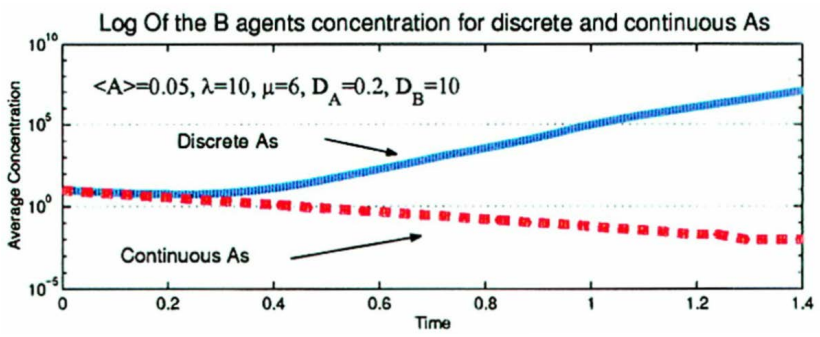

Figure 3.10: Discrete versus continuous model [31]. This figure shows different predictions of PDE-based and agent-based representation of a system with two interacting populations, A and B. See equation (3.41) for the PDE-based model.

ABMs are attractive tools for immunological application and their usage is growing. To name a few examples, Catron et al. [32] employed a complex model for interaction between T cells and dendritic cells to extract the frequency of interactions and duration of T cell stimulation required for activation from imaging data. In [33], authors developed a simulation model to study T cell competition for specific and nonspecific stimuli presented by APCs. For a scenario with low antigen expression by APCs, the antigen-driven competition between T cells is evident which results in coexistence of different T cell clones specific for different target antigens. However, this competition vanishes when the antigen expression is high, which allow the highly reactive T cell clones to exclude other T cell population.

The main advantage of ABMs that is used in this thesis is the ability to account for probabilistic uncertainty and individual diversity within a large population. This advantage make agent-based modeling approach suitable for studying thymic selection where diverse premature T cells interact with a finite number of APCs for fate determination. However, assuming such individual diversity in ABMs has the cost of huge computational complexity that accompanies such sophisticated models.

Chapter 4

A signal integration model of thymic selection

The sections of this chapter are partially reprinted from published article [1], which can be accessed by the link: `http://www.jimmunol.org/content/193/12/5983.full`.

4.1 Background

A functional and self-tolerant T cell repertoire is required for a robust immune defense. Functionality of a T cell repertoire refers to the ability to effectively recognize foreign pathogen, and self-tolerance refers to avoiding destruction of healthy self-tissues. Initially produced with rearranged surface T cell receptors (TCRs) that could theoretically bind any antigen fragments, T cells complete their development in the thymus through multiple processes of selection, necessary to restrict a randomly generated (pre-selection) TCR pool to a functional and self-tolerant repertoire. In thymus, $CD4^+$ $CD8^+$ thymocytes (T progenitor cells) migrate through a directive path from thymic cortex to thymic medulla. During this migration, thymocytes repeatedly interact with their environmental cells. The thymic environmental cells are cortical (cTEC) and medullary (mTEC) thymic epithelial cells, thymic resident dendritic cells and those migrated from peripheral lymphoid organs. These environmental cells express a collection of self-peptides by MHC I and MHC II molecules, and therefore, they are acting as antigen presenting cells (APCs). During migration in thymus, thymocytes perceive the self-reactivity level of their TCR - i.e. the ability to bind to self-peptides MHC complexes (spMHC) - by sequentially interacting with APCs and scanning diverse self-peptides [34]. It is believed that the decision of thymocytes to exit the thymus as mature T cells or not is made by these thymocyte-APC interactions.

The classical theory of thymic selection (affinity/avidity model) is based on the premise that thymocytes with no self-reactivity die by neglect, with weak self-reactivity are positively selected, and highly self-reactive cells are clonally deleted by negative selection [35]. In **Figure 2.2**, a graphical presentation of affinity/avidity model of thymic selection is given.

It is believed that thymocytes with inability to bind to MHC molecules would not be rescued by positive selection process, and thymocytes that are specific for self-peptides would be clonally deleted by negative selection process; this would ensure that potentially dangerous self-peptide specific T cells are absent in the peripheral lymphoid organs [36]. However, in an interaction of TCR with self-peptide-MHC complex, both self-peptide and MHC molecules contribute to the affinity of interaction as a single complex, but not as separate molecules (**Figure 4.1**). Therefore, the level of (self-) reactivity for a TCR is resulted from both, the loaded peptide and the MHC affinities. The relative importance of these two components,

MHC and self-peptide, in thymic selection processes is not yet known. A T cell repertoire recognizes foreign-peptides when presented by self-MHC molecules [37–39]. Intuitively, for increasing the chance of recognizing foreign-peptides, T cells should at least be able to bind presenting MHC molecules.

According to early experimental evidences, the specificity of T cell-mediated immune responses is biased towards antigens presented by MHC molecules by which T cells were selected in the thymus (referred to as self- or selecting-MHC); However, the immune response is not fully restricted to selecting-MHC molecules [40–44]. The notion of MHC-restriction in T cell responses which indicates to the restriction of T cell recognition of antigens presented by one MHC but not other MHCs, was discovered from chimeric experiments (described in **Figure 4.2**) [40, 41, 45]. These experiments indicates the major contribution of thymus in MHC-restriction. However, there is no clear mechanistic explanation of how and to what degree such a self-MHC specificity might be imposed on the T cell repertoire during thymic selection.

In addition to MHC molecules, the set of MHC-bound self-peptides influences the T cell selection. In mice models, by reducing the diversity of thymically expressed self-peptides, the thymic output reduces [46–48]. This suggests that some TCRs are specific for the thymically-expressed self-peptides, and only can be selected in their presence. Another possibility would be that selection of some TCRs may not solely depend on a particular self-peptide, but rather depends on a "gemisch" (a mixture) of self-peptides [49,50]. Theoretically, a thymocyte with low self-MHC affinity can be selected by a self-peptide when it provides sufficient signal for positive selection. Also, a TCR that is highly specific for a self-peptide might be able to escape negative selection by having a low MHC specificity.

While self-peptide specific T cells are observed in the periphery even in healthy individuals [51], their activation is regulated by natural Tregs (nTregs), a subpopulation of T cells arising from the thymus [52]. nTregs are characterized by CD4, Foxp3 and high CD25 expressions. In thymus, nTreg precursor cells display high levels of TCR signaling [53], but the mechanisms underlying the fate diversion (nTreg differentiation versus clonal deletion) are not fully understood.

For explaining the overall observations in nTreg generation studies, a few general models have been proposed (reviewed in [8]): a TCR instructive model, where selection of nTregs depends exclusively on higher level of TCR self-reactivity, which is at or near the negative selection threshold; a two-step model where TCR instruction facilitates IL-2 dependent expression of Foxp3; a stochastic model according to which the fate of nTreg differentiation is decided randomly earlier than negative selection phase, which makes nTregs resistant to clonal deletion (see **Figure 2.4**).

TCR transgenic mice models are the models that generate thymocytes with a identical and known TCR sequence. In TCR transgenic mice that express high affinity peptides for a particular TCR in the thymus, nTregs were observed [54–56]. These observations suggest that TCRs which shows higher reactivity

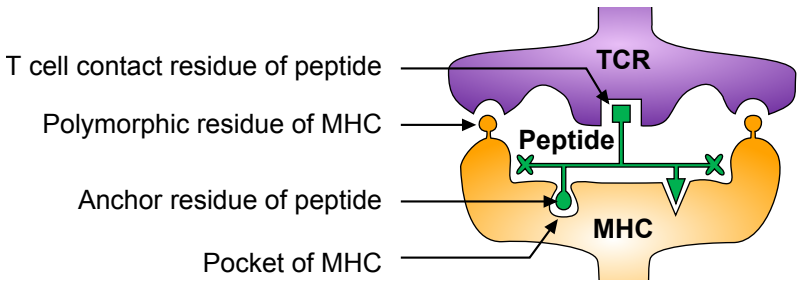

Figure 4.1: Interaction surface of T cell receptor and peptide-MHC complex. Peptides bind to MHC molecules via a non-covalent interaction mediated by residues in the clefts of the MHC molecules (pocket) and in the peptides (anchor residue). The amino acid side chains of peptides that is accessible from the open top of the cleft of the MHC molecule by a specific TCR. At the same time, TCR bind to polymorphic residues of the α helices of the MHC molecule.

(affinity/avidity) to thymically expressed self-peptides than conventional T cells (Tconv), would appear in the peripheral nTreg TCR repertoire. This idea would predict that nTreg and Tconv repertoires carry T cells with distinct TCR specificities, with nTreg TCRs being more specific to self-peptides. The different requirements of self-reactivity level for selection of nTreg versus Tconv repertoires have been validated by using TCR signaling reporter mouse model [53] (see **Figure 4.3**).

If one assumes an extreme case of affinity-based nTreg selection hypothesis, i.e. each self-peptide selects a specific TCR as nTregs, then the resulting diversity of TCR specificities in nTreg repertoire would be equal and limited to the diversity of self-peptide pool. In the context of experimental observations, however, overlap between the specificities of nTregs and Tconvs has been observed [58–62]. Further, there is evidence that nTregs are diverse [58, 61, 63–67] and are activated by foreign antigens in the periphery [68–71]. It is not know how diverse TCR specificities in nTreg repertoire could be resulted from a selection with high self-reactivity criterion, and how this repertoire contains TCRs that can recognize foreign antigens. By additionally considering that nTregs represent only 5% to 10% of the overall $CD4^+$ T cell pool in mice and human [67], how can such a small fraction can cover antigenic space, i.e. both foreign- and self-peptide pool?

A single TCR-spMHC interaction cannot determine the fate of a cell, but interacting with many spMHCs repeatedly is required for completing the selection [72, 73]. Blocking thymocyte-APC interactions or TCR signaling at different selection stages prevents successful positive selection[72–74]; this implies to the requirement of sustained TCR signals for a successful positive selection. In contrast to positive selection, negative selection which requires strong TCR signaling event is a fast process [75]. It was shown that negative selection was preceded by a strong and transient increase in the level of TCR-mediated signals

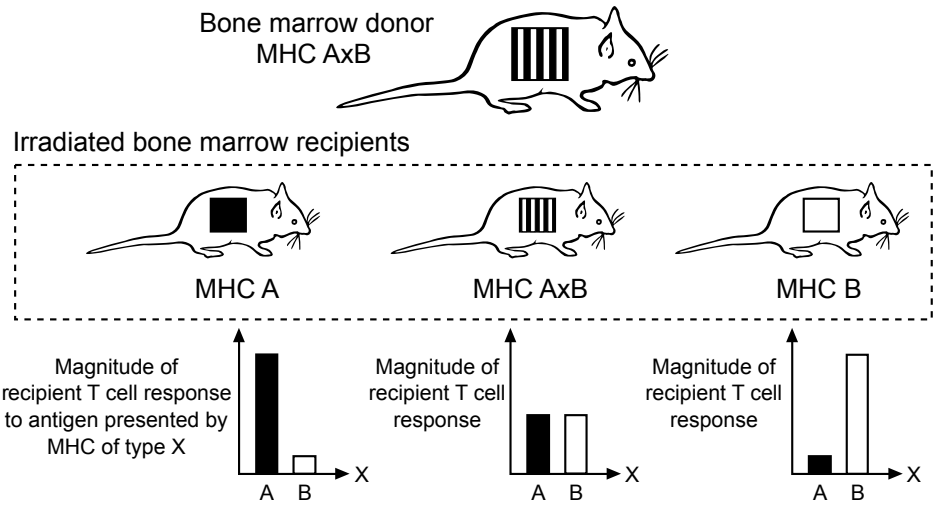

Figure 4.2: MHC-restriction. MHC-restriction indicates to the restricted ability of T cells to recognize antigens presented by MHC molecules that were available in thymus, but not by other MHC molecules. Bone marrow chimeras were used to show the MHC-restriction concept. In these experiments, bone marrow from a AxB donor is transplanted in recipient individuals expressing MHC A, B or both in their thymuses. The thymocytes derived from AxB donor can express TCRs that can potentially be selected by MHC A and MHC B. The recipient mice are irradiated so that the they cannot produce thymocytes from their own bone marrow, but the epithelial cells and APCs are not affected and they present antigens in the context of their own MHC. The resulted T cell repertoire is then stimulated by antigens presented by MHC A or B. The magnitude of T cell responses shows that MHC-restriction, although is not complete, is imposed by MHC molecules which drive the thymic selection.

[76]. Additionally, by using reporter mouse model in which GFP levels were correlated with TCR signal strength [53], it was observed that nTreg precursor cells perceive higher levels of sustained TCR signaling than Tconv precursor cells during thymic selection (see **Figure 4.3**).

An experimental paper [75] was published when our manuscript [1] was under revision, which nicely showed different TCR signaling requirements for positive and negative selection of $CD8^+$ T cells. A mouse model was engineered in which TCR signaling can be inhibited in a ZAP70-dependent manner by special inhibitors. By using inhibitors in various regimes, it was shown that even a small duration of TCR signaling inhibition can disrupt positive selection significantly. In contrast, a transient TCR signaling is sufficient for efficient negative selection (see **Figure 4.4**).

Different temporal TCR signaling patterns (sustained and transient signals) that are shown to be associated thymocyte fate decisions (positive and negative selections) [74–81], indicate to the relevance of the TCR signaling dynamics for fate decisions. Hence, for a model of thymic selection, the history of TCR signaling has to be taken into account. Furthermore, the TCR signaling strength perceived by cells at any given time might depend on previous interactions (in a short time-window) in addition to the current thymocyte-APC integration. Due to the limitations of experimental methods, mathematical modeling would be a well-suited tool to investigate the information that might be encoded in the dynamics of TCR signaling.

Numerous theoretical models were employed to study thymic selection and its impact on the TCR specificity and cross-reactivity of the T cell repertoire [82–86]. In [83], an affinity based model was investigated by using random numeric sequences as a representation for TCR and spMHC sequences. By checking for all possible interactions between TCR and spMHCs, the maximum affinity was was translated to cell removal only if it is insufficient (positive selection) or excessive (negative selection). By using the model, it was predicted that negative selection would remove TCRs with high cross-reactivity from the repertoire. In [84], a thymic selection model was proposed in which the activation threshold of cells was adaptable. According to this model, by assuming that TCR stimulations can decrease signaling sensitivity for the next interactions, it was shown that different levels of T cell cross-reactivity could be resulted. In the aforementioned theoretical studies, the stochastic nature of interactions, the abundance of spMHCs and different dynamical criteria in TCR signaling for positive versus negative selections were not considered. Further, nTreg differentiation as additional outcome of thymic selection was not considered. Recently, a theoretical study investigated thymic selection by incorporating nTreg differentiation [87]. It was assumed

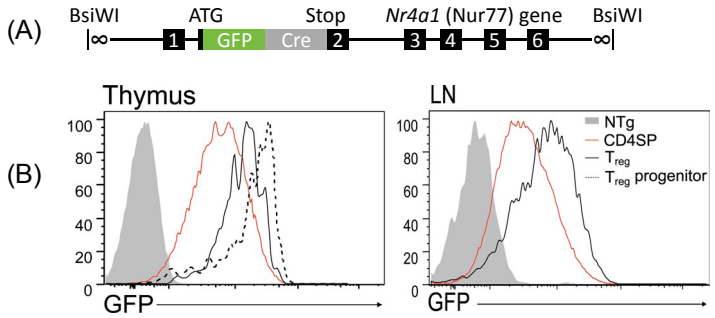

Figure 4.3: TCR signal strength in nTreg versus Tconv [53]. A reporter mouse is developed in which the level of a fluorescent protein reflects the strength of antigen receptor signal. In this transgenic mouse model, GFP is inserted into the Nr4a1 (Nur77) locus of a bacterial artificial chromosome (BAC). Nur77 is an immediate early gene, which is a gene that can be transiently and rapidly activated by TCR stimulation in thymocytes and T cells [57]. (B) According to reporter mouse model, nTregs express higher GFP levels compared with Tconvs, both in thymus and lymph nodes (LN). nTreg progenitors were defined as CD4SP $CD25^+CD122^{hi}Foxp3^+$. NTg: nontransgenic.

that binding strengths for the TCR-spMHC interactions have a log-normal distribution; by underlying to this distribution, variations in TCR sensitivity and the numbers of simultaneous TCR-spMHC interaction per APC were studied. This model recapitulated experimental observations where the numbers of Tconv and nTregs were affected by changing the amount of thymically expressed self-peptides [88]. In all these theoretical studies, maximum encountered TCR-spMHC affinities were the only determinant of cell fates, and except [87], nTreg differentiation was not incorporated in the proposed models.

In this chapter, we investigate a signal integration model for thymic selection by considering a random polyclonal (multiple clones of TCRs) repertoire of thymocytes. In particular, we consider the contribution of the two binding regions of the TCR (MHC and self-peptide) in the interaction affinity. By employing an agent-based simulation, we consider sequential interactions of thymocytes with diverse spMHCs during which affinity-dependent TCR ligation signals are integrated. The characteristics of the integrated signal, namely sustained and transient signaling levels (SSL and TSL, respectively), are of the focus in this model. These signaling components are quantified for each thymocyte during thymic selection. We assume a SSL threshold for positive selection after which 10% of the total thymocyte pre-selection pool are kept. For negative selection, we assume a TSL-based negative selection threshold after which 50% of the positively selected cells are eliminated. Further, 5% of the remaining cells with highest SSL are considered to be selected as nTregs. By using the proposed model, we show that the strength and dynamics of the integrated

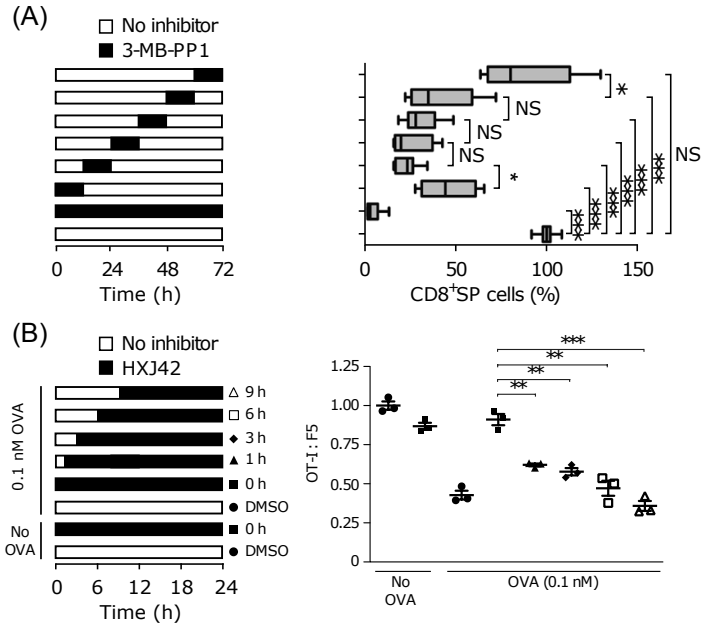

Figure 4.4: TCR signaling requirements for positive and negative selection [75]. (A) Thymocytes expressing the OT-I TCR transgene (a TCR that is specific for ovalbumin-OVA peptide) are added to thymic tissue slices containing positive selecting ligands. TCR signaling inhibitor is added for 12 hours after different TCR signaling duration. These inhibitions, especially between 12 h and 48 h, all resulted in markedly impaired positive selection. (B) For identifying the TCR signaling requirement for negative selection, high affinity ligands (OVA peptide) is added to thymic slices containing thymocytes with OT-I TCR. Additionally, to quantify negative selection, thymocytes expressing F5 TCR transgene (specific for influenza nucleoprotein peptide) that can be positively selected in this system were also used. In the presence of high affinity ligands, negative selection is significant. Negative selection is significantly impaired only when TCR signaling is fully inhibited.

signal would be a successful basis for extracting specificity/affinity of thymocytes to MHC and detecting the existence of cognate spMHC in the presentation pool. These information would be essential for selecting a self-MHC-biased self-tolerant T cell repertoire. A nTregs selection based on the high SSL results in an nTreg repertoire that contains TCRs with higher affinity to MHC than in Tconv repertoire. Such nTreg repertoire is more ready for activation than Tconvs due to higher signaling status, and consequently, nTreg repertoire is more cross-reactive with the ability to recognize both self- and foreign-peptides. According to the signal integration model, for selecting a self-MHC-biased T cell repertoire, thymically expressed self-peptide pool has to be diverse and low-abundant.

4.2 Model

In order to be able to study the thymic selection, the model should be able to represent diversity in TCR sequences. Further, biologically relevant assumptions for TCR-pMHC interactions and their properties has to be made. Next, in the cellular level the interaction of thymocytes and APCs in thymus has to be represented. In this section, we try to make biologically relevant assumptions to investigate the thymic selection *in silico*.

4.2.1 Representation of proteins and their binding affinity

In order to make a sufficient diversity in TCR sequences, we use take binary sequences as a simplified structural representations of proteins. This simplification has been used in several studies [83–86]. This allows us to create a large set of TCRs and peptides and to generate different possible affinities of binding interaction. We use the following approach to calculate the affinity of a TCR-pMHC interaction:

Assume that X and Y are binary sequences with length l, which represent the "facing" binding regions of two proteins

$$X = \{x_i\}_{i=1}^{L} \quad , Y = \{y_i\}_{i=1}^{L} \text{ with } \; x_i, y_i \in \{0, 1\}. \tag{4.1}$$

We consider that a site in the sequence X is "matching" (contributing to the interaction) if the respective site in the other sequence Y is complementary (opposite value). We call a binary sequence of matching sites as "Complementarity sequence" C, defined as

$$C(X, Y) = X \oplus Y = \{c_i\}_{i=1}^{L} \text{ with } \; c_i = \begin{cases} 1 & x_i \neq y_i \\ 0 & x_i = y_i \end{cases}. \tag{4.2}$$

Since adjacent matching sites (AMS) may contribute more to the global affinity than other sparse single matching sites, AMS sizes are listed in the "Adjacency Match" M in the following way:

$$\begin{aligned} &M(C) = m_j \;\text{ with }\; m_j = p_j - q_j + 1 \\ &s.t.\ \{p_j, q_j \in [1, L] \mid (\forall i \in [p_j, q_j] : c_i = 1) \wedge (c_{p_j - 1} \subseteq 0) \wedge (c_{q_j + 1} \subseteq 0)\}, \end{aligned} \tag{4.3}$$

Therefore, adjacency match M is the list of lengths of consecutive 1s that exist in the complementarity sequence C. Here, p_j and q_j are the locations of the first and last 1s in j-th AMS. Next, we define global affinity (A) of the interaction as the sum of the sizes of the AMS raised to power r, called specificity parameter, normalized to the maximum possible value.

$$A(X, Y) = \frac{\sum_j (m_j)^r}{L^r}, \tag{4.4}$$

With the specificity parameter (r), we can tune the relative contribution of the largest AMS in the global affinity; this dependency is illustrated in **Figure 4.5**. By increasing the value of r, the dependency of the affinity to the largest AMS increases, which results in a high sensitivity of affinity to a single bit alteration in this region and dramatic decrease in the interaction affinity. Such a dependency to single point mutations has been observed experimentally [89].

Through the TCR complementarity regions (CDR1/2/3), a T cell can interact with a peptide when it is loaded on a MHC. CDR3 is positioned at the center of the binding interface which can establish contact with both, the peptide and the MHC; CDR1/2 loops are mostly in contact with the top of MHC helices and surround the central CDR3-peptide region [90–92]. While CDR1 and CDR2 are mostly conserved, CDR3 loop is a hypervariable element of the TCR which is mediates a major part of the interaction between MHC and TCR. Due to hypervariability of CDR3, various affinities to MHC would be resulted from randomly generated TCRs. In the model, we assume that the variable part of TCR binds to both the peptide and the borders of MHC surrounding the peptide. Since the conserved part of TCR interacting with MHC would contribute equally to each TCR-pMHC interaction, it is not considered in the model. It is assumed that binary sequences of TCR and pMHC proteins are aligned in such a way that the middle part of the TCR sequence with length L_p contacts the peptide sequence, whereas the sides of the TCR sequence, each with length $L_{\mathrm{MHC}}/2$, contact the MHC sequence; this is illustrated in **Figure 4.5**. The affinity of TCR-pMHC interaction is computed using equation (4.4)

$$A_{\mathrm{pMHC}} = A(\mathrm{TCR}, \mathrm{pMHC}). \tag{4.5}$$

In order to distinguish between the specificity of a TCR to a MHC and a peptide, we calculate TCR affinity to MHC by just considering the MHC binary sequence without peptide and the corresponding part of the TCR binary sequence

$$A_{\mathrm{MHC}} = A(\mathrm{TCR}, \mathrm{MHC}). \tag{4.6}$$

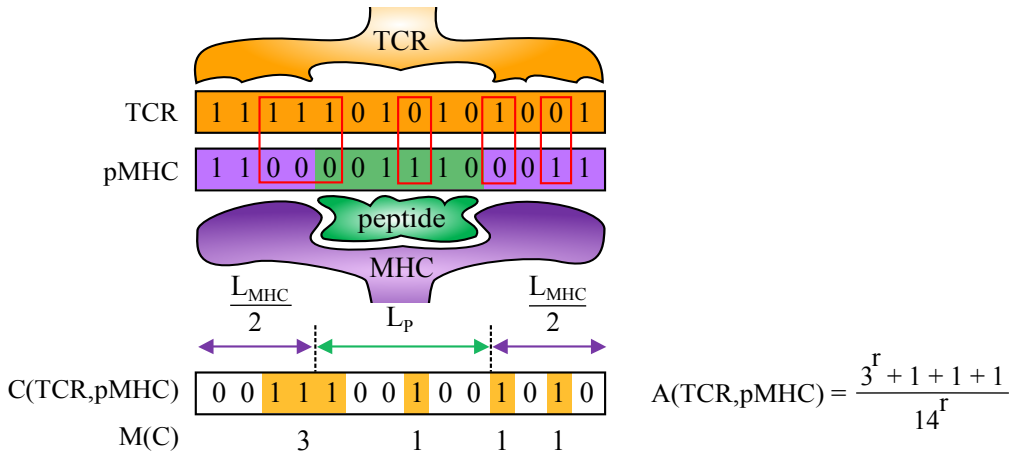

Figure 4.5: A binary representation of the TCR-pMHC binding interface. In this particular example, with $r = 1$ in equation (4.4), the contribution of the largest adjacency match to the affinity is 50%, whereas this contribution increases to 75% with $r = 2$. A single bit mutation in TCR or pMHC in the center of the largest adjacency match region decreases the affinity approximately by 17% and 58% with $r = 1$ and $r = 2$, respectively. See Table 4.1 for the simulation values.

In a similar fashin, the affinity of TCR to a single self-peptide (sp) is computed by using the binary sequence of the self-peptide and the corresponding part of the TCR sequence

$$A_{\mathrm{sp}} = A(\mathrm{TCR}, \mathrm{sp}). \tag{4.7}$$

The separation of TCR-pMHC interaction affinity to MHC and peptide affinities is artificial and not biologically relevant; it only provides us with an index to characterize TCRs according to their specificities to a particular MHC and peptide (higher affinities indicate to higher specificities). We further define the average self-peptide affinity of a TCR to all N_{sp} self-peptides as

$$\bar{A}_{\mathsf{sp}} = \frac{\sum_{i=1}^{N_{\mathsf{sp}}} A_{\mathsf{sp},i}}{N_{\mathsf{sp}}} \tag{4.8}$$

where i enumerates the self-peptides and $A_{\mathrm{sp},i}$ is calculated with equation (4.7). Note that we consider only a small subset of all possible peptide-MHCs (pMHCs) as thymically expressed ligands. In general, since TCRs are specific only to a few pMHCs, $\bar{A}_{\mathsf{sp}}$ is low for a sufficiently large subset of possible pMHCs; however, by considering a small subset of high-affinity pMHCs, this value increases.

4.2.2 Signal integration

4.2.2.1 Importance of time in TCR signaling

Each T cell express unique TCR with thousands of copies [93]. Upon cell movement, T cells continuously sample their environment. In a the course of few hours, T cells interact with a considerable number of APCs [94]. In the context of a single TCR-pMHC interaction, the affinity is low and the resulting intracellular signals, such as ERK or calcium flux [95], are transient, short-lived and insufficient for activating T cell. In order to overcome an activation threshold, signaling events have to be prolonged for several hours and maintain translocation of transcription factors to the nucleus [96]. Frequent TCR-spMHC interactions, even though not activating the T cell [97–99], are required for maintaining the TCR-mediated intracellular signals at a level sufficient for cell survival, homeostasis [100–102] and responsiveness to foreign pMHCs [103,104]. In order to represent the aforementioned time-dependent properties of signaling, we assume that thymocytes (or T cells in periphery) collect TCR signals and quantify them by activation and accumulation of downstream intracellular signals. This assumption is irrespective of the nature of presented antigen (self and foreign pMHCs).

4.2.2.2 Integrated TCR signal

In our simulation, each cell from the pool of thymocytes interaction with a series of APCs. During this *in silico* APC scanning, an APC is assigned to a thymocyte at each time point or, when there exists a low number of APCs, a thymocyte may stay without interaction until the next time point. For each thymocyte, we simulate a TCR signaling level. This allows us to describe, for each thymocyte, the characteristics of TCR signaling resulting from scanning different peptides over time. At any time point, the signaling level can increases as a function of the affinity of all simultaneous TCR-pMHC interactions. This signaling level also decays with a constant rate. Each thymocyte expresses n_{TCR} identical TCRs. We assume that an affinity-dependent TCR ligation signal $p_i(t)$ is induced via ligation of its i-th TCR (TCR_i) with a pMHC molecule:

$$p_i(t) = \begin{cases} A_i & \text{during thymocyte-APC interaction} \\ 0 & \text{no thymocyte-APC interaction} \end{cases} \tag{4.9}$$

where A_i is the TCR$_i$-pMHC interaction affinity computed by equation (4.4). Each of the TCR ligation events give rise to TCR-mediated intracellular signals $S(t)$

$$\frac{\mathrm{d}S(t)}{\mathrm{d}\,t} = \alpha \sum_{i=1}^{n_{\mathrm{TCR}}} p_i(t) - \delta S(t) \tag{4.10}$$

where n_{TCR} is the number of expressed TCRs by thymocyte/T cell, α is the accumulation rate and δ is the degradation rate of TCR-mediated intracellular signals. In the rest of this manuscript, we call $S(t)$ as integrated TCR signal (ITS). Since foreign peptides are not normally presented by thymic resident APCs, ITS of thymocytes encodes the level of TCR self-reactivity.

4.2.3 Simulation settings: thymocyte-APC interactions and signal integration

4.2.3.1 Settings of cells and peptides

We consider a set of N_{sp} random sequences (non-identical) as self-peptide pool, which is only a subset of all possible presentable peptides (binary sequences with length L_p); the remaining ones are considered as foreign-peptides. We assume only a single type MHC in the thymus (the selecting-MHC) which is presented by all APCs. Peptide sequences are combined with MHC sequences in similar way shown in **Figure 4.5**.

Let's assume a thymic selection with n_{APC} number of APCs which express n_{spMHC} spMHCs randomly from the pool of spMHCs. If the size of the self-peptide pool is greater than the number of spMHCs expressed by each APC ($N_{\mathrm{sp}} > n_{\mathrm{spMHC}}$), we make sure that a self-peptide is presented by an APC with only a single copy. In this way, presented spMHCs have identical density among all APCs. Then, each self-peptide is presented, on average, by a fraction of APCs equal to

$$F = \frac{n_{\mathrm{spMHC}}}{N_{\mathrm{sp}}} \tag{4.11}$$

When we decrease the diversity of self-peptides and keep the total number of ligands (spMHCs) presented in the thymus (n_{APC} and n_{spMHC} and consequently $n_{\mathrm{APC}} \times n_{\mathrm{spMHC}}$), the abundance of self-peptides increases (see **Figure 2.1** for definition of abundance of a ligand). By decreasing the abundance of a particular self-peptide, the probability of finding it in subsequent APC interactions increases. To represent the experimental observation that self-peptides in thymic cortical region are diverse and low-abundant [105,106], F in equation (4.11) is assumed sufficiently small, i.e. self-peptide diversity is sufficiently larger than the carrying capacity of an APC. In biological context, an APC expresses approximately 10^5 molecules for MHC I and MHC II, and presents approximately 10^4 different bound peptides, each with 1 to 10^3 copies per APC [107]. It has been estimated that thr total possible self-peptide with presentable length (8 to 10 amino acids) in the mouse proteome is around 3×10^7 [108], and a typical MHC may present 3% of all possible nonameric peptides [109], yielding to $0.03 \times 3 \times 10^7 = 9 \times 10^5$ self-peptides presentable by each MHC. Thus, each APC may present $10^4/(9 \times 10^5)$ ≈1% of all self-peptides. Since our model is a simplified and reduced form of the reality, we keep a close value of peptide abundance (F =2%) instead of generating a high dimensional model.

4.2.3.2 T cells and *in silico* scanning of APCs

A subset of total possible (distinct) TCR binary sequences (2^L) are assigned to thymocytes with population size n_T. At any given time-point, we assign a random interaction event between thymocytes and APCs. Then, for each thymocyte, we calculate the affinity of TCRs to the presented spMHCs and we update the integrated signal $S(t)$. We assume that the duration of thymocyte-APC interaction Δt is identical for all cell interactions. For having a uniformly distributed self-peptides, we have to assume a sufficiently

large number of APCs ($n_{\mathrm{APC}} \gg n_{\mathrm{spMHC}}$). After a critical value, more larger numbers of APCs does not affect the results of the simulation. When the number of thymocytes is equal to or smaller than the number of APCs ($n_T \leq n_{\mathrm{APC}}$), no competition for APCs exists in the simulation and therefore, tymocytes have independent fates. In this case, the number of thymocytes (n_T) does not represent any physiological number and only has statistical significance. In contrast, when the number of APCs is smaller than the number of thymocytes ($n_T > n_{\mathrm{APC}}$), thymocytes compete for interacting with APCs at any given time and with a uniform probability. As the result, at any time step, a subset of thymocytes remain without interaction. The parameters used in the presented results are given in **Table 4.1**.

4.2.4 Dynamics of integrated TCR signal and fate determination

Herein, after a simulation with parameter values given in **Table 4.1**, we checked the temporal properties of TCR signaling in the scale of single cell. In **Figure 4.6**, some typical ITS curves are shown. As it can be seen in this figure, ITS generally shows fluctuations; however, due to repeated interactions with APCs and affinity contribution from the MHC which presents a mixture of self-peptides, the signal never goes to zero.

In addition to steady fluctuations, some strong signaling peaks in ITS can be observed (**Figure 4.6**). By recalling the fact that all the APCs in the simulation carry identical MHCs, one possible reason for strong peaks could be encountering of cell to high affinity peptide; another possibility would be encountering of cell to multiple peptides with moderate affinities presented by one APC, which creates a high avidity thymocyte-APC interaction; or, consecutive moderate affinity interactions with APCs could lead to an increase of the TCR signaling.

In order to investigate the information lies within ITS dynamics, we decompose the signal of each cell into two distinct components: the basal value of ITS after a stabilization time-window, called "Sustained Signaling Level" (SSL) which is determined by the minimum value of the ITS (**Figure 4.6**); the peak value, hereby called "Transient Signaling Level" (TSL), obtained as the maximum value of the ITS during the APC scanning period. These signaling components obtained for each thymocyte during simulation, will be used for thymocyte fate determination.

Table 4.1: Thymic selection model: parameter descriptions and values

Parameter	Value	Description
N_{sp}	500	Diversity of self-peptides
n_{T}	10^6	Number of different thymocytes/TCR sequences
n_{APC}	10^6	Number of APCs
α	1	Activation/accumulation rate of TCR signaling
δ	0.1	Degradation rate of TCR signaling
r	7	Specificity parameter
L	24	Sequence length of TCR and self/foreign-peptide-MHC
L_{MHC}	8	Sequence length of MHC
L_{p}	16	Sequence length of self/foreign-peptides
n_{spMHC}	10	Number of distinct spMHCs presented by each APC
n_{TCR}	10	Number of TCRs on surface of each thymocyte/T cell
$S(0)$	0	Initial condition of integrated TCR signals
Δt	0.5 hours	Thymocyte-APC interaction duration
T_{s}	$500\Delta t$	Thymic selection time-window

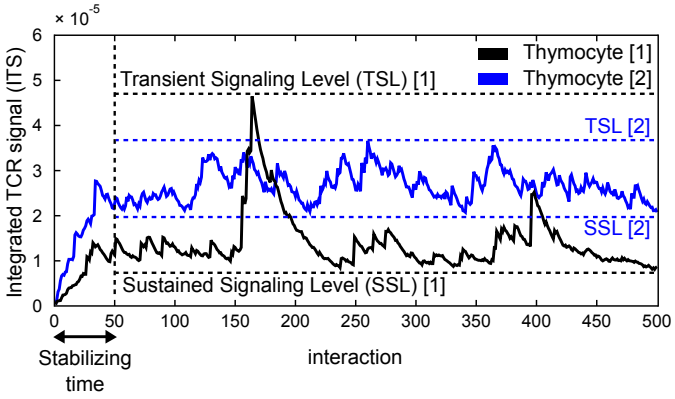

Figure 4.6: Integrated TCR signal (ITS). Dynamic changes of integrated TCR signal (ITS) of two different thymocytes are shown. The fluctuations are resulted from sequential interactions with APCs which are presenting diverse spMHCs. The sustained signaling level (SSL) is defined as the minimum value of the ITS in a window of sequential interactions. The transient signaling level (TSL) is determined by the maximum ITS value in the same window of interactions. Note that SSL and TSL are individual properties of thymocytes, which depends on the specificity of TCR to encountered spMHCs. In the shown example, thymocyte 1 (black curve) has a low SSL and a high TSL, whereas thymocyte 2 (blue curve) displays a higher SSL and a lower TSL than thymocyte 1.

4.2.4.1 SSL-based positive selection

It is geneally believed that thymocytes with TCRs unable to recognize any of encountered spMHCs in thymic cortex cannot receive a TCR-mediated survival signal and therefore, die by programmed-cell death, a process known as death by neglect [110]. Further, thymocytes have short life-spans and a few engagements with spMHCs are not sufficient for their survival and maturation. Hence, repeated engagements of TCRs with spMHCs are require in order to sustain TCR-mediated signaling in a sufficient level to prevent cell death [72]. Evidences showing that sustained levels of TCR-mediated signals, such as ERK or calcium flux, are associated with positive selection [74, 76–81] further supports the idea that positive selection relies on sustained TCR-mediated signals in the thymic selection process.

In the context of our model, we incorporate this notion of positive selection as the elimination of thymocytes that have low SSL. We remove thymocytes that are unable to sustain their ITS at a higher level than positive selection SSL threshold (**Figure 4.7**).

Out of all pre-selection thymocytes, approximately 5% are able to mature and enter the periphery [111]. By relying on the estimation that 50% of positively selected thymocytes are clonally deleted by negative selection [112], we can assume that 90% of the cells die by neglect during positive selection.

4.2.4.2 TSL-based negative selection

In contrast to positive selection, it has been shown that negative selection is associated with a strong transient increase in TCR-mediated signals [74, 76, 77, 81], and therefore, negetive selection relies on a transient event. In the context of our model, we assume that all cells with a TSL above a threshold are negatively selected (**Figure 4.7**), and therefore, clonally deleted. We estimate this TSL threshold in such a way that it eliminates 50% of the positively selected cells.

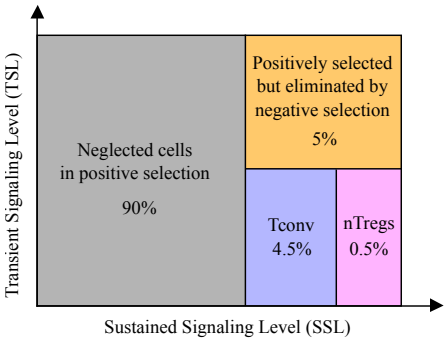

Figure 4.7: Signal integration model of thymic selection. SSL- and TSL-based rules for thymic selections and nTreg commitment.

4.2.4.3 SSL-based nTreg selection

In the presented study, we focus on the selection of $CD4^+$, and out aim is to incorporate a signal-based nTreg fate commitment; however, the previous definitions apply for both contexts of $CD4^+$ and $CD8^+$ T cell development. Various experimental evidences have shown that selection of nTregs in the thymus depends on interactions of MHC class II-restricted TCRs with high affinity/avidity ligands [54,55,113–115]; therefore, the dominant hypothesis for nTreg selection is that these cells express self-reactive TCRs [116] and they perceive stronger TCR signals than their Tconv progenitor counterpart [53]. Further, it has been suggested that nTregs originate from thymocytes expressing TCRs with affinities/avidities to self-peptides that lie between the affinities/avidities that drive positive and negative selection [8, 117, 118].

The ability of nTregs to sustain high strength TCR signals is not only required for nTreg differentiation, but also for their homeostasis and functionality in the periphery [119]. In the context of out model, we assume that the selection of nTregs requires a sufficiently high SSL. We consider an SSL-threshold for nTreg selection after which only 5% of the selected repertoire can be selected as nTreg phenotype (physiological value: 5%-10% of total peripheral $CD4^+$ T cells [67] or 4%-6% of total $CD4^+$ thymocytes in mice [63]) (**Figure 4.7**).

A typical simulation of thymic selection follows the flow chart in **Figure 4.8**. According to different experiments, different modifications are made to the configurations of antigen presentation.

4.3 Results

4.3.1 Sustained and transient components of integrated TCR signal (ITS): MHC and cognate peptide affinities are segregated by the sustained and transient components of ITS

It has been suggested that specificity of T cell responses is biased toward foreign-antigens presented by the MHC molecules that they have been selected on (referred to as selecting- or self-MHC) [40–43] (see **Figure 4.2** for MHC-restriction concept). Yet, T cells are tolerant to self-antigens presented by the same MHC in the periphery. Therefore, thymocytes should be sensitive to MHC affinity and be able to detect cognate self-peptide during the selection process. Here, we checked how signal integration would allow thymocytes to interpret the TCR signals they perceived by APC scanning in a way that allows distinction of MHC and peptide affinities.

A repertoire of thymocytes with random TCR sequences was generated and allowed to sequentially interact with APCs (described in **section 4.2**). Thereafter, the components of the TCR signaling history

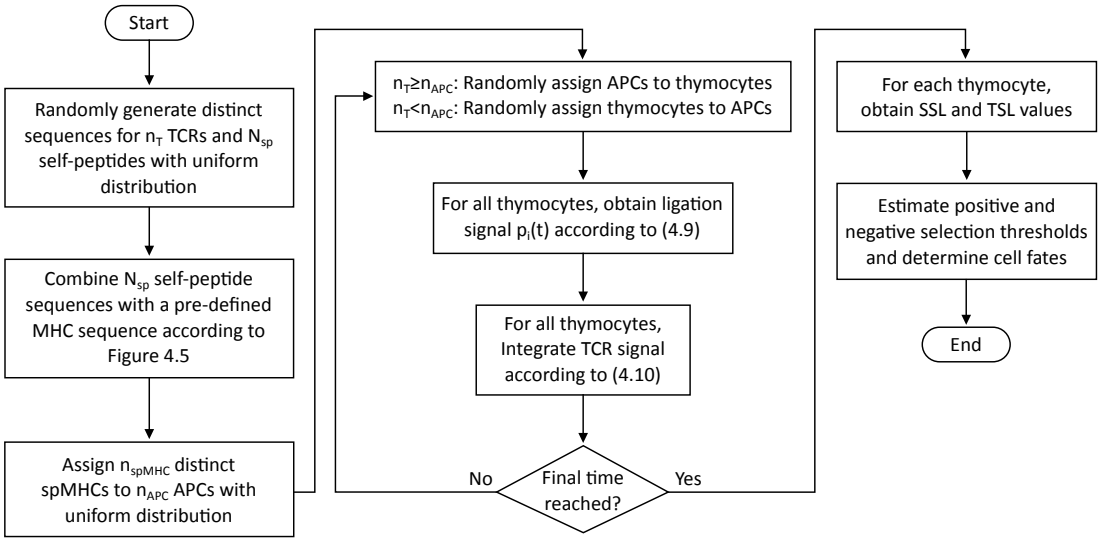

Figure 4.8: Simulation flow chart.

for each thymocyte (SSL and TSL, defined in **Figure 4.6**) were obtained and the potential relation between the signaling components and affinity of cells to MHC as well as spMHCs was investigated on the population level. A correlation analysis showed that MHC affinity of thymocytes correlated with their SSL (**Figure 4.9A**). No significant correlation between MHC affinity and TSL was observed (data not shown). Instead, TSL correlated with the affinity of the best spMHC existing in the thymus (**Figure 4.9B**). No significant correlation could be observed between maximum spMHC affinity and SSL (data not shown), showing that MHC affinity and maximum spMHC affinity are encoded by two independent components of ITS, namely SSL and TSL, respectively. This offers a biological mechanism of how cells could discriminate between their affinity to MHC and cognate self-peptide by relying on the temporal properties of their signaling.

4.3.2 Positive selection based on SSL: positive selection ensures a high MHC affinity of thymocytes

As positive selection requires sustained TCR signaling [74–81], we asked how the MHC specificities would be shaped if the TCR repertoire is selected based on SSL. For this, the average MHC affinity of the positively selected population was calculated. Note that we do not aim to give absolute affinity values since TCRs are represented by a simplified and artificial binary space. Therefore, no realistic affinity values can be extracted, but rather a distribution of possible affinities. Selection of 10% of the cells (**Figure 4.10**) caused an 8-fold increase in the average MHC affinity (from ≈ 0.013 to ≈ 0.1, see **Figure 4.11**). Despite neglecting the majority of thymocytes, the resulting average MHC affinity was still low in comparison to the higher average of MHC affinity that could be acquired with a more stringent positive selection, i.e. higher positive selection threshold (**Figure 4.11**). This suggests a trade-off between selecting the cells with higher MHC affinity and selecting a large number of cells. The TSL-distribution of the repertoires of the different fates (**Figure 4.12**) showed that positively selected cells displayed higher TSL levels. However, having a high TSL did not guarantee positive selection for a substantial number of cells (cells in dotted area of **Figure 4.12**).

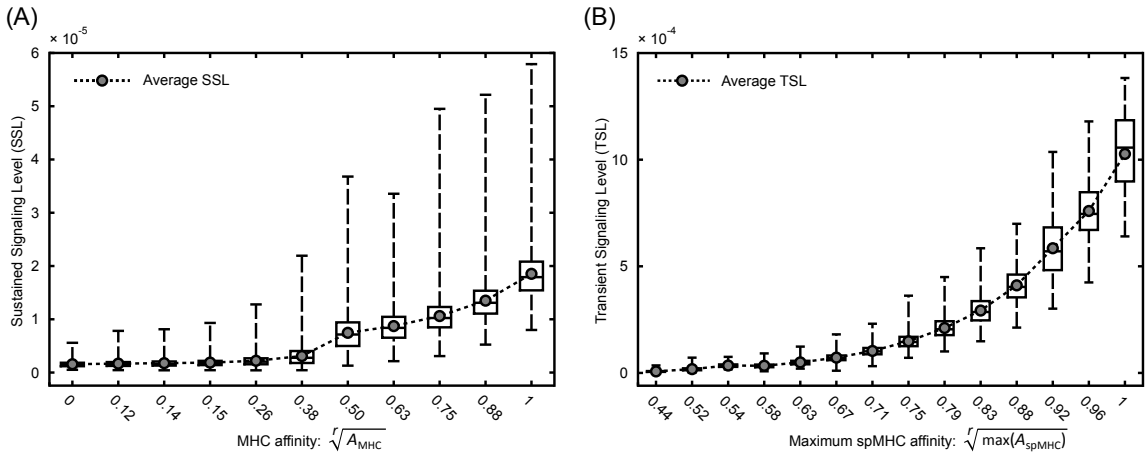

Figure 4.9: SSL and TSL versus TCR-MHC affinity. (A) Boxplot of SSL distribution (showing the maximum, minimum, median and quartiles of SSL) of thymocytes with respect to their MHC affinity. A positive correlation between MHC affinity and SSL is found. (B) Boxplot of TSL distribution of thymocytes with respect to their maximum spMHC affinity among the total pool of self-peptides. A positive correlation between TSL and the maximum existing spMHC affinity is found. Note that because of the binary representation of proteins, only finite sets of MHC and spMHC affinities are possible. For the sake of clear presentation, the thymocytes with close proximity of affinity values are grouped. This applies to all subsequent figures.

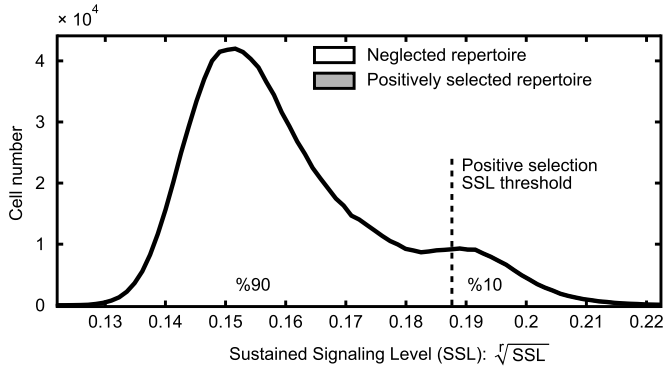

Figure 4.10: Distribution of thymocyte SSLs. The positive selection SSL threshold is determined by selecting the 10% thymocytes with highest SSL. The different peaks of the SSL-distribution are reflecting discrete possible values of MHC affinities (and consequently, SSL values) and the decreasing number of cells with higher MHC affinity.

4.3.3 Negative selection based on TSL: negative selection limits the number of MHC-specific thymocytes

We asked whether the MHC affinity of the repertoire is only controlled by positive selection, or whether negative selection also plays a role. Negative selection was based on the TSL. 50% of the positively selected cells with highest TSL were deleted. The distribution of thymocytes was investigated with respect to their MHC affinity for the whole population (pre-selection repertoire), positively selected and selected (after

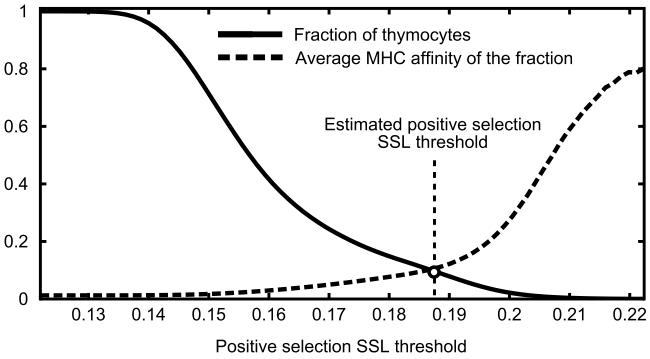

Figure 4.11: Positive selection threshold versus MHC affinity of repertoire. Fraction of thymocytes that are selected by different positive selection SSL thresholds (solid line), and the corresponding average MHC affinity of the selected fraction (dashed line) are shown. A higher positive selection SSL threshold results in a stronger MHC-bias (MHC-affinity or MHC-specificity) and strong reduction of surviving cell numbers. A healthy immune system requires a sufficient daily production of T cells by thymus. Therefore, SSL threshold for positive selection cannot be extremely high. Consequently, positive selection can only impose a maximum MHC-bias in the repertoire (here represented by average MHC-affinity of cell population) that is lower than theoretically possible value.

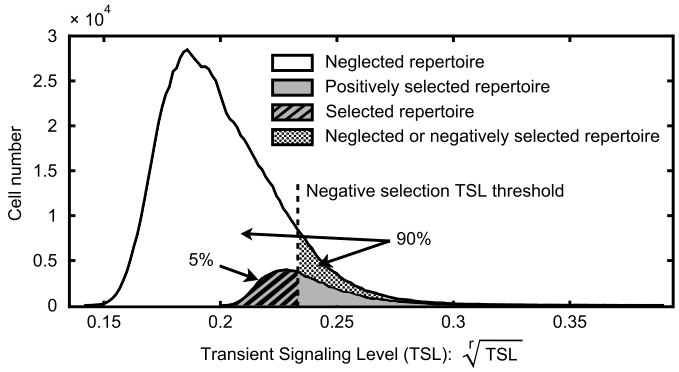

Figure 4.12: Distribution of repertoires with respect to TSL. The graph distinguishes thymocytes that were not positively selected (white area), positively selected cells (gray area), cells which were not positively selected but would have been removed by negative selection anyway (dotted area) as well as the final selected repertoire (hatched area).

both selections) repertoires (**Figure 4.13A**). Additionally, these distributions are shown as the fraction of the total population (**Figure 4.13B**). First, while positive selection imposed a lower bound on the MHC affinity of the selected repertoire (**Figure 4.13A-B**), which is consistent with an increased MHC affinity after positive selection (**Figure 4.11**), a wide range of MHC affinities survived positive selection. Note that all the MHC-specific cells (MHC Affinity $= 1$) were kept by positive selection (**Figure 4.13B**, solid line). Secondly, looking at the fraction of the selected repertoire distinguished by MHC affinities (**Figure 4.13B**, dash-dotted line), the whole spectrum of MHC affinities was affected by negative selection. In particular, a higher fraction of MHC-specific thymocytes was deleted (average MHC affinity of positively selected repertoire ≈ 0.1 and selected repertoire ≈ 0.08). Therefore, negative selection based on TSL

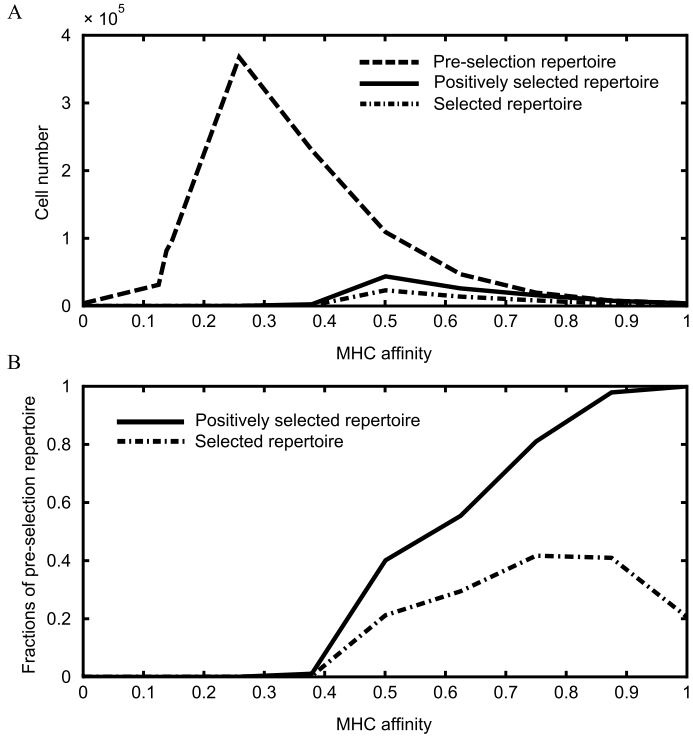

Figure 4.13: Distributions of MHC affinity in different repertoires. (A) Distribution of cell numbers and (B) fraction of all cells that are positively selected (solid line) and selected (dash-dotted line) with respect to their MHC affinities. Positive selection imposed a minimum MHC affinity on the repertoire and highly impacted the lower-end of MHC affinity spectrum, whereas negative selection impacted the whole spectrum with a higher impact on higher-end spectrum.

limited the MHC affinity of the repertoire by preventing MHC-specific cells to survive.

4.3.4 Shaping self-peptide and MHC specificity in thymus: selected thymocytes are either affine to MHC or to self-peptide but not both

As shown before, positive selection increased the affinity for MHC on a population level. However, cells with an above threshold MHC affinity (**Figure 4.13B**, solid and dash-dotted lines) might be able to complete positive selection by having proper self-peptide affinity. For this reason, we monitored the average self-peptide affinity of thymocytes according to equation (4.8), including the whole pool of self-peptides. This quantity was calculated for groups of thymocytes with similar MHC affinity (**Figure 4.14**). The self-peptide affinity displayed a large spectrum of possible values (not shown), as expected from uniform random TCR generation. Therefore, the average self-peptide affinity of the whole population before any selection was independent of MHC affinity by construction (**Figure 4.14**, see dashed line).

After positive selection, the cells with lower MHC affinity exhibited higher self-peptide affinity and this tendency was conserved after negative selection. Therefore, low MHC affinity thymocytes required a stronger specificity for self-peptides to survive positive selection. In contrast, the cells with higher MHC affinity were not influenced by positive selection in terms of self-peptide affinity. Negative selection constrained the self-peptide affinity on the whole spectrum of MHC affinities, with a higher impact on

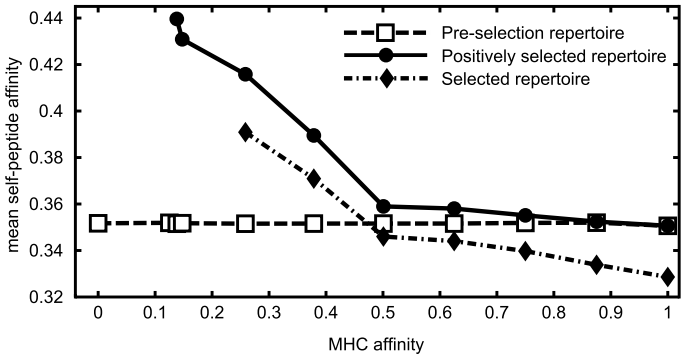

Figure 4.14: Average self-peptide affinity of the thymocyte repertoires at different stages of thymic selection. Equation (4.8) is calculated for groups of thymocytes with defined MHC affinity. Positive selection affects the lower-end spectrum of MHC affinity, whereas negative selection affects the whole spectrum.

thymocytes with strong affinity for MHC (**Figure 4.14**, compare solid and dash-dotted lines). The combination of positive and negative selection imposed constraints on both MHC and self-peptide affinity and consequently, the selected repertoire showed a compromise between these two constraints.

4.3.5 MHC-specificity of nTreg repertoire: nTreg repertoire is enriched with MHC-specific TCRs

Negative selection is not perfect and autoreactive T cells may escape it [51]. This also happens in the model because of its stochastic nature and the probabilistic scan of APCs in a limited time frame. Selection of nTregs, which respond to the autoreactive stimuli together with Tconvs, would limit autoreactive responses in the periphery mediated by these accidental self-reactive T cells. nTregs were shown to have a higher sustained TCR signal than Tconvs in thymus and periphery [53] (see **Figure 4.3**). This property motivated the definition of nTregs in the model (see **Model** section 4.2). The 5% of selected thymocytes with highest SSL were committed to the nTreg phenotype while all others acquired the Tconv phenotype.

To investigate the TCR characteristics of nTregs versus Tconvs, their respective distributions were monitored in dependence on their MHC affinity (**Figure 4.15A-B**). As expected from the definition of the nTreg commitment, nTregs were biased towards higher MHC affinity whereas Tconvs are composed of cells with lower MHC affinity. However, the overlap of both subsets in terms of MHC affinities was large (**Figure 4.15A-B**).

The compromise between MHC affinity and average self-peptide affinity that was observed in the selected repertoire (**Figure 4.14**), was also conserved in nTreg and Tconv repertoires (**Figure 4.16**).

4.3.6 Autoreactivity of pre- and post-selection repertoires

Starting from an initial random sequence of thymocyte-APC interactions, we checked how many cells from the pre-selection repertoire would be autoreactive. The cells which crossed their signaling level over negative selection TSL-threshold being defined as autoreactive cells. Next, the fate of these particular autoreactive cells was examined with a different random sequence of thymocyte-APC interactions. Out of 10% of the pre-selection thymocytes that showed autoreactivity in the initial random sequence of thymocyte-APC interactions, nearly 50% failed to pass positive selection in the second random sequence of thymoycte-APC interactions due to low MHC affinity (average MHC affinity ≈ 0.006). Note that in contrast to the whole

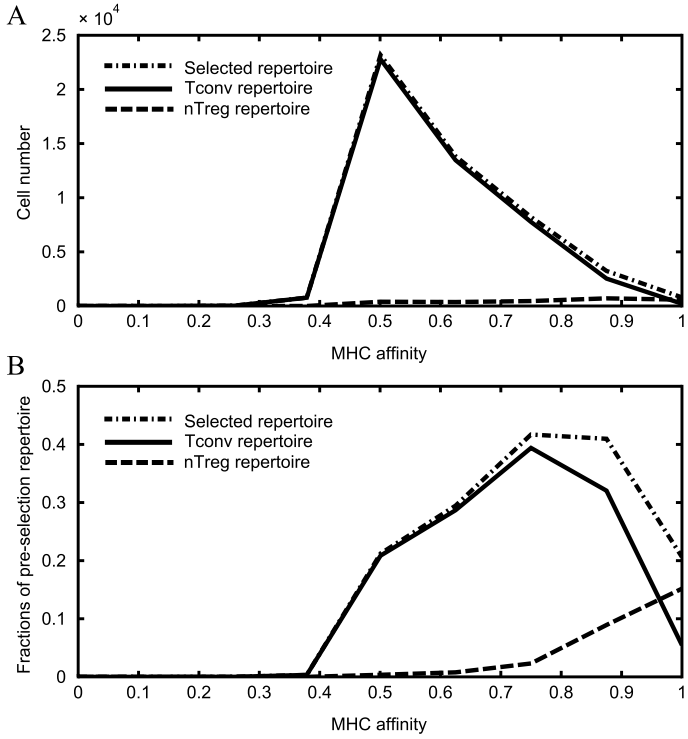

Figure 4.15: Distributions of MHC affinity of nTreg versus Tconv repertoires. (A) Distribution of cell numbers and (B) fraction of all cells that are selected (dash-dotted line), selected as Tconvs (solid line) and selected as nTregs (dashed line) with respect to their MHC affinity. Tconvs and nTregs have a large overlap in their MHC affinity spectrum. nTreg repertoire is more enriched in MHC-specific TCRs than Tconv repertoire.

population where only 10% survived positive selection, autoreactive thymocytes reached 50% of survival due to high MHC affinity (with average MHC affinity ≈ 0.13).

From the positively selected autoreactive thymocytes, approximately 88% were negatively selected by the second random sequence of thymoycte-APC interactions. Therefore, autoreactive TCRs were more targeted by negative selection. From the escaped autoreactive cells, a high number (89%) matured as Tconv. Note that the escaped autoreactive Tconvs had a lower MHC affinity (in average ≈ 0.06) than negatively selected autoreactive thymocytes (average ≈ 0.13) or autoreactive cells that selected as nTregs (average ≈ 0.33). We also observed that the fraction of autoreactive TCRs in nTreg repertoire was approximately 2.5-fold higher than autoreactive TCRs in Tconv repertoire, proving higher autoreactivity of nTreg than Tconv repertoire in our model.

These results show that some autoreactive TCRs ended up in the Tconv repertoire due to stochastic variations of thymocyte interactions with APCs within a limited time-frame. Negative selection was more efficient than nTreg differentiation in restricting the autoreactive TCRs in the Tconv repertoire. But the nTreg repertoire was more enriched with autoreactive TCRs (and with higher affinity for MHC) than the Tconv repertoire.

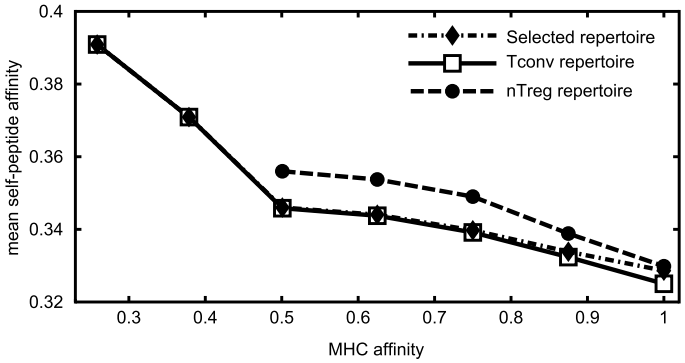

Figure 4.16: Average self-peptide affinity of the nTreg and Tconv repertoires. Equation (4.8) is calculated for groups of thymocytes with defined MHC affinity. In contrast to nTreg repertoire, Tconv repertoire contains low MHC affinity TCRs which are skewed to recognize self-peptides in an average fashion. In overlapping spectrum of MHC affinity, nTreg repertoire has TCRs with higher self-peptide affinities than Tconv repertoire, which is consistent with nTregs being more self-reactive than Tconvs.

4.3.7 Cross-reactivity and degeneracy of thymic and peripheral repertoires: nTregs are more cross-reactive than Tconvs

Recognition and activation of individual T cell is not limited to a unique specific peptide sequence, but multiple peptide sequences with sufficient specificity can be recognized by an individual T cell [120]. This allows the immune system to provide a comprehensive immunity against the antigen universe and cope with antigenic variations during infection [121]. This feature can be observed in two different forms: an individual T cell is able to recognize multiple non-homologous peptides, defined as cross-reactivity here, or T cells are able to respond to variants of their agonist antigen (i.e. point-mutations in amino acid sequences), defined as degeneracy here.

In order to assess the degree of cross-reactivity in the selected T cell repertoire and the impact of positive and negative selection on shaping cross-reactivity, the ability of cells to recognize multiple foreign-peptides was examined. First, a set of non-identical and random foreign-peptide sequences was generated and combined with the self-MHC sequence (as shown in **Figure 4.5**) to set up a pool of 100 distinct foreign-peptide-self-MHC (fpMHC) sequences. Then, all the cells were stimulated for 2 days by APCs each carrying extra fpMHC. The pool of APCs was configured with the same settings as for thymic selection, and the negative selection TSL-threshold was considered as activation threshold. The autoreactive cells that responded to the APCs without loading any foreign-peptide were excluded from the analysis.

We observed that while most cells from the pre-selection repertoire were not activated, a high percentage of positively selected or selected cells got activated (not shown). This is due to the fact that in our system, which is a reduced-scale of the physiological system, the number of foreign-peptides tested (100 distinct foreign-peptides) is large (20% of the pool of self-peptides). However, this is required to allow for a statistical analysis of responsiveness to foreign-peptides. Activated thymocytes from the pre-selection repertoire were separated in groups depending on how many of the foreign peptides they could recognize. For each group, the percentage of pre-selection cells remaining after positive and negative selections were obtained (**Figure 4.17**). The results showed that positive selection avoided the selection of cells with low cross-reactivity. In contrast, negative selection mainly affected the cells with higher cross-reactivity.

The cross-reactivity was examined for Tconv and nTregs. We observed that foreign peptides led to the activation of both nTregs and Tconvs (4.8$\pm$1.6% of nTregs and 2.3$\pm$0.4% of Tconvs responded to each of the foreign peptides; not shown). Additionally, the distribution of the number of foreign-peptides

recognized by the same cells (**Figure 4.18**) showed that more nTregs than Tconvs were able to recognize multiple foreign peptides. This shows that the *in silico* nTreg repertoire exhibits higher cross-reactivity than Tconvs.

The degree of degenerate recognition in cells was assessed by measuring the ability of cells to recognize variations in their cognate foreign-peptide. First, all the cells were stimulated by one foreign peptide. Then, the reactive cells were stimulated by altered foreign-peptides generated by single-bit mutations in the binary sequence of initially considered foreign-peptide.

We observed that positive selection allowed the selection of cells that were more degenerate in recognizing altered cognate peptides. In contrast, negative selection largely restricted the cells with high degeneracy (**Figure 4.19**). The same analysis on nTreg and Tconv repertoires showed that as compared to Tconvs, the distribution of nTregs was shifted towards a more degenerate recognition of altered peptides

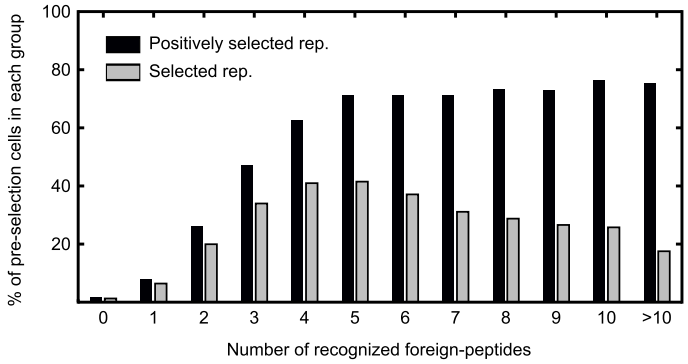

Figure 4.17: Cross-reactivity assay: A set of 100 randomly generated foreign-peptides was presented by all the APCs by adding one MHC loaded with a single type of foreign-peptide on each APC. The stimulation was done by two days of APC scanning and the TSL-based activation threshold is assumed to be equal to the negative selection threshold. The cells in the pre-selection repertoire were grouped according to the number of peptides that could activate them. For each group, the percentage of cells that remain after positive selection (black bars) and subsequently, after negative selection (gray bars) are given. For instance, among the cells activated by 5 of the foreign peptides, nearly 70% were kept by positive selection while only 40% completed thymic selection.

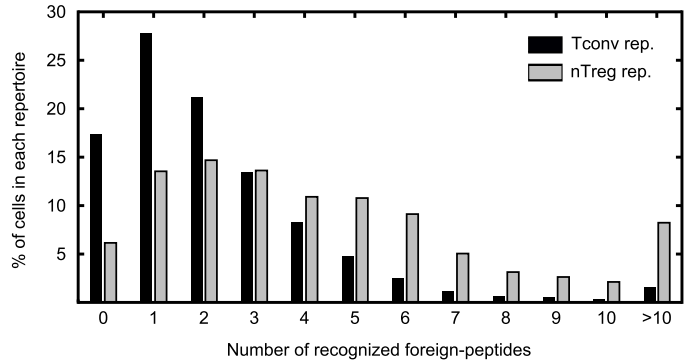

Figure 4.18: Distribution of the number of foreign-peptides recognized by Tconvs and nTregs in cross-reactivity assay.

(**Figure 4.20**).

4.3.8 Role of self-peptide diversity: diversity of self-peptides in the thymus is required for selection of a self-MHC-biased repertoire

Next, the role of self-peptide diversity in the selection of self-MHC-biased repertoire was analyzed. As shown in **Figure 4.9A**, in a thymus with diverse low-abundant self-peptides the SSL of thymocytes was correlated with their MHC affinity. We calculated the correlation coefficient between the SSL of thymocytes and their MHC affinity for different diversities of self-peptides (**Figure 4.21**). The positive correlation between SSL and MHC affinity increases and saturates with higher diversity of self-peptides presented in the thymus. This implies that SSL-based positive selection requires a large self-peptide diversity to select a self-MHC-biased T cell repertoire.

To examine the impact of restricting APC availability onto the MHC-specificity of the repertoire, the correlation coefficients between SSL and MHC affinities were obtained for various APC numbers. As

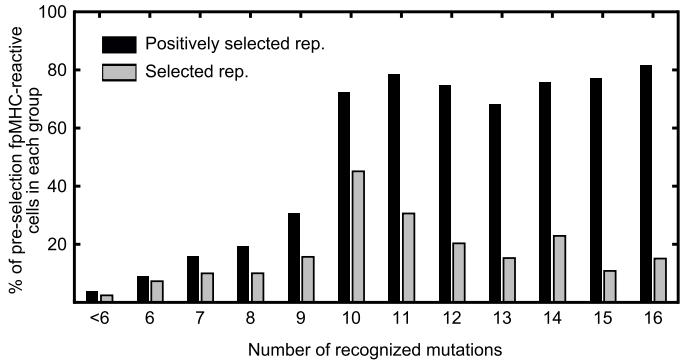

Figure 4.19: Degeneracy assay: starting from a random foreign peptide, all reactive cells were considered. These were stimulated by every possible single-point mutations of the initial foreign peptide. The stimulation was done for 2 days by APCs fully expressing the same mutated peptide. The cells in the pre-selection repertoire were grouped according to the number of single-point mutated peptides that could activate them. For each group, the percentage of cells that remain after positive selection (black bars) and subsequently, after negative selection (gray bars) are given.

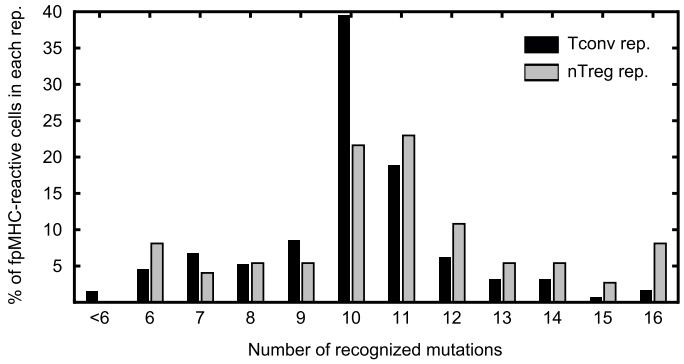

Figure 4.20: Distribution of the number of single-point mutated peptides recognized by Tconvs and nTregs.

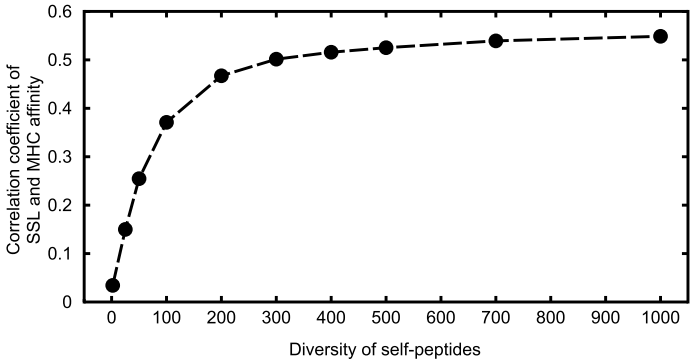

Figure 4.21: Impact of self-peptide diversity on self-MHC-bias. The correlation coefficient between SSL of thymocytes and their MHC affinity in thymuses with varying self-peptide diversity.

depicted in the **Figure 4.22**, the SSL-MHC affinity correlation was lost when the number of APCs was critically low. Therefore, the number of APCs could be a limiting factor in the thymus for selecting a MHC-biased T cell repertoire.

4.3.9 Thymic selection with single peptide: single spMHC selects a repertoire with wider range of MHC affinity

Although a diverse set of self-peptides is essential for selection of diverse TCR specificities, expression of a single self-peptide-MHC molecule was shown to allow for the selection of a large number of T cells [48, 49, 122] and that these cross-react with allogeneic MHC [48]. Here, an MHC that is not expressed in the thymus is called allogeneic MHC or allo-MHC. In order to analyze the extent of self-MHC-bias of the repertoire selected by single spMHC presented in the thymus, the diversity of self-peptides in the model was decreased to a single spMHC but with the same density of total peptide presentation as in the diverse system.

Despite the abundant expression of a single peptide, it was possible to positively select 7.5% (compare to 10% in the model based on diverse spMHCs), and to select 4% (compare to 5% in the model based on diverse spMHCs) of the pre-selection repertoire, showing a decreased yet considerable amount of selected thymocytes. In experimental systems expressing a single spMHC, about 20%-50% of the normal number of T cells are selected (*in silico*, this corresponds to 80% of the normal T cell number) [49]. Presentation of the single spMHC in these experimental systems is not efficient and constitutes approximately one-tenth of the wild type antigen presentation level, and the expression level of spMHCs is shown to be important for the outcome of the thymic selection [49]. Therefore, the absolute number of thymic output in our model with abundant presentation of a single spMHC was an upper limit; by decreasing the density of the single spMHC per APC, the number of selected cells decreased further (not shown).

As shown in **Figure 4.23A-B**, a single spMHC selected a repertoire with a wider range of MHC affinity in comparison to the repertoire selected by diverse spMHCs, indicating that the thymic output by a single spMHC was less self-MHC-biased. Therefore, the fact that T cells specific to different allogeneic MHCs exist in the single spMHC-based model is a natural result in the framework of the presented model of thymic selection. Nearly 20% of the cells positively selected in the model based on diverse spMHCs were also positively selected in the model based on single spMHC. This overlap was decreased to 10% by negative selection, which shows that the thymic outcome is different in both models. This is consistent with the observations that TCRs with known specificities were not selected by single spMHC, despite being selected in normal mice which express diverse spMHCs [122–124].

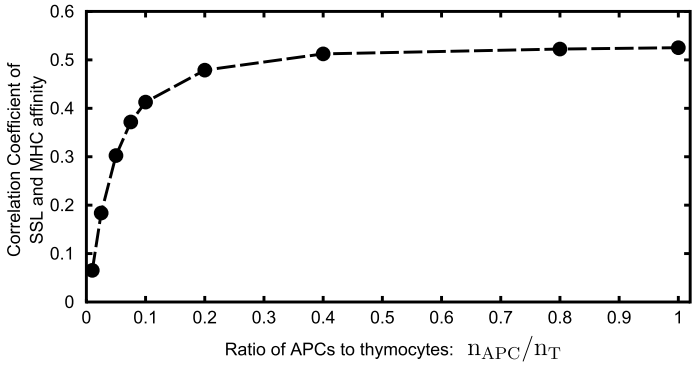

Figure 4.22: Impact of APC availability on self-MHC-bias. The correlation coefficient between SSL of thymocytes and their MHC affinity in thymuses with varying cell number ratio of APCs to thymocytes.

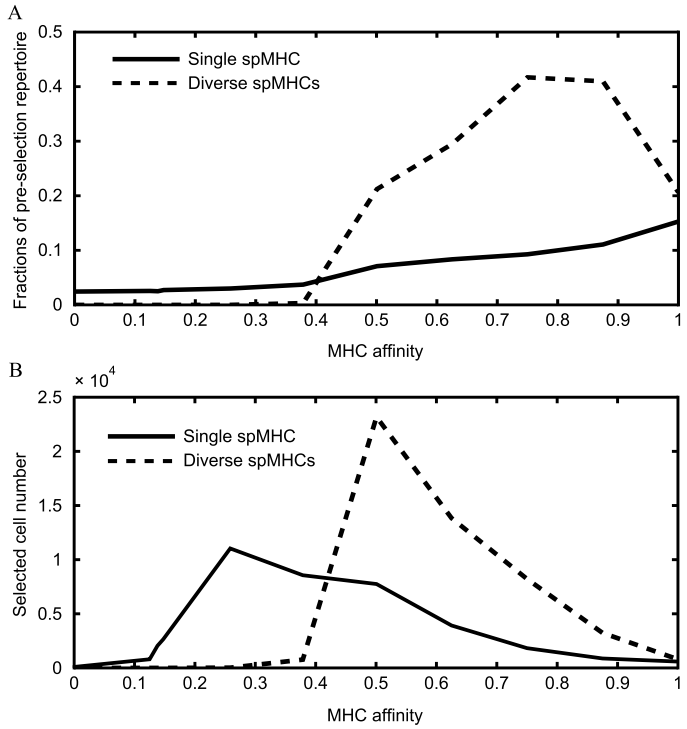

Figure 4.23: Thymic selection with single peptide. (A) Fraction and of pre-selection thymocytes and (B) number of thymocytes that are selected by single spMHC (solid line) versus diverse spMHCs (dashed line) in dependence on their MHC affinity. Compared to a selection based on diverse spMHC presentation, a restriction of APC presentation to a single spMHC leads to selection of thymocytes with a wider range of MHC affinities.

The relative number of selected cells in both models was dependent on the specificity parameter r that controls the relevance of specific adjacency matching sites (see **Model** section 4.2). By considering low values of r, and keeping the same SSL- and TSL-selection thresholds, the number of positively selected

cells in the single spMHC-based model was higher than in the diverse spMHCs model (not shown) which is not consistent with experimental observation. Consistency between model and experiment was found with $r \geq 7$, which emphasizes the relevance of specific adjacency matching sites [see equation (4.4)]. The biological implication of requiring such a large specificity parameter (r) is that for a signal-integration-based positive selection, a group rather than sparse complementing features between binary sequences is required in TCR-spMHC interactions during thymic selection; otherwise, positive selection would become highly and unrealistically peptide-promiscuous (peptide-independent).

4.3.10 MHC-restriction versus MHC-bias: after thymic selection, T cell recognition is self-MHC-biased but not self-MHC-restricted

It has been suggested that thymic selection biases the T cell repertoire towards recognizing foreign peptides in the context of the selecting-MHCs, referred here as self-MHC-bias (see [125] for a review and **Figure 4.2** for the concept of MHC-restriction). However, T cell responses are not self-MHC-restricted as T cells selected with one MHC may respond to other (allogeneic) MHCs as well [126, 127]. Here, we assessed the degree of MHC-bias and MHC-restriction in our model by an *in silico* alloreactivity experiment. First, 33 distinct MHCs with different levels of similarity to self-MHC were taken as allo-MHCs. Among the foreign-peptide sequences, 100 sequences were combined with these allo-MHC sequences. Then, all the pre-selection cells were stimulated with APCs fully loaded with one of these combinations and categorized based on the fates they would have during thymic selection. The negative selection TSL-threshold was used as activation threshold. The level of alloreactivity to each allo-MHC was measured by examining the extent of T cell cross-reactivity to allo-MHCs, i.e. the number of foreign-peptides (presented by alloMHC) recognized by each T cell. The distributions of T cell cross-reactivity to each allo-MHC were compared with respect to the degree of similarity between allo- and self-MHCs (**Figure 4.24**).

The T cell repertoire selected with diverse spMHCs was more reactive to the self-MHC than to allo-MHCs. Further, the level of alloreactivity depended on how similar the examined allo-MHCs were to the self-MHC. This result shows that thymic selection does not guarantee self-MHC-restriction, despite imposing self-MHC-bias for recognition of foreign peptides. The cells selected with diverse spMHCs were more biased to the self-MHC than the cells selected by single spMHC (**Figure 4.24A**, compare gray and black boxplots). This is an additional support for the result given in **Figure 4.21**, showing that diversity of self-peptides was required for self-MHC-biased T cell recognition.

Next, the contribution of positive and negative selection in MHC-restriction was assessed by performing the same analysis on the cells that were either not positively selected or eliminated by negative selection (in a thymus with diverse spMHCs). In that way, the cells that were both neglected and negatively selected (the cells existing in dotted area of **Figure 4.12**) were included in both pools, making sure that the impact of positive and negative selection were examined independently.

The distributions of cell cross-reactivity to each allo-MHC were compared with respect to the degree of similarity between allo- and self-MHCs (shown in **Figure 4.24B**). The result shows that positive selection was more efficient than negative selection in avoiding the cells recognizing allo-MHCs that were not similar to self-MHCs. However, with increasing the similarity to self-MHC negative selection became more efficient and the efficiency of positive selection decreased.

Another way to quantify the efficiency of positive and negative selection in restricting alloreactivity is to look at the number of cells that can be activated by each foreign-peptide presented by an allo-MHC. This number was averaged over 100 foreign-peptides per allo-MHC. The average was then normalized to the population size of each repertoire (**Figure 4.24C**). The same trend of efficiencies as **Figure 4.24B** was found.

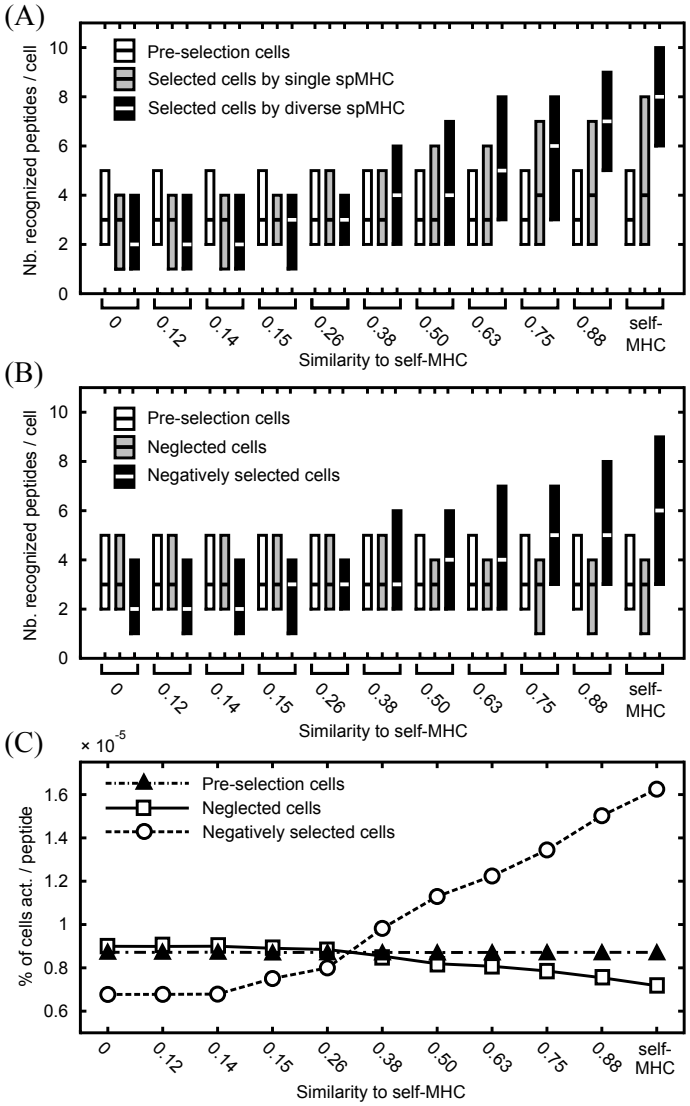

Figure 4.24: Self-MHC-bias versus self-MHC-restriction of T cell repertoire. (A) A set of 100 foreign-peptide sequences were combined with a set of allo-MHC sequences. For each of allo-MHCs, all the cells were stimulated for 2 days by allogeneic APCs fully loaded with a single-type foreign-peptide-allo-MHC. (A,B) The cross-reactivity to each stimulating-MHC, i.e. number of foreign-peptides recognized by each cell, was obtained. These distributions were compared for all allo-MHCs with respect to the degree of similarity between allo- and self-MHC. Similarity is measured by equation (4.4) using the sequence of one MHC and the complementary sequence of another MHC. The analysis was done for (A) cells selected by single or diverse spMHCs, and (B) for cells removed from the repertoire in different stages of selection with diverse spMHCs. Box-plots show median and quartiles. (C) Reactivity to foreign peptide, i.e. the average number of cells activated by one foreign peptide was obtained for the repertoire of cells neglected by positive selection or eliminated by negative selection. The plot represents the percentage of cells among their corresponding repertoire.

4.4 Discussion

4.4.1 Selection of a self-MHC-biased T cell repertoire

Affinity of a TCR-peptide-MHC interaction is resulting from the combination of a peptide and a MHC molecule rather than a peptide alone (see **Figure 4.1**). The signaling strength of a single TCR-peptide-MHC interaction is not enough for a thymocyte to discriminate between the contribution of peptide and MHC molecules. The requirement that T cells should recognize foreign peptides in the context of their own individual MHC molecules for a proper immune response, implies that thymic selection should impose a bias towards recognition of self-MHC in a pre-selection repertoire that potentially bears TCRs with different MHC specificities. In this paper, we studied a potential mechanism allowing thymocytes to extract information regarding their MHC- and self-peptide-specificities in the course of the selection process.

We proposed a TCR signal integration model capturing the requirement of repeated interactions for successful T cell selection/activation. From the TCR stimulation history generated by sequential interactions with different spMHCs, two distinct components emerged, namely sustained and transient signaling levels (SSL and TSL). The model showed that SSL is correlated with the TCR affinity to MHC, which can serve as an indirect measure of MHC affinity to the cell. Indeed, we illustrated that a SSL-based positive selection imposes a lower limit on the MHC affinity range of the repertoire, which gives a signal-based explanation for the selection of a self-MHC-biased T cell repertoire (see **Figure 4.13**).

According to the model, the SSL relies on the frequency of successful (signal providing) interactions during APCs scanning. To provide a positively selecting stimulus from the peptide component, positively selecting self-peptides would have to be highly abundant in order to provide sustained signaling above the SSL-threshold of positive selection. The observation that self-peptides are diverse and rare in the thymic cortical region [105, 106] implies that finding enough positively selecting self-peptides for multiple subsequent interactions is unlikely. Since the common component in low-abundant spMHCs during sequential interactions is the MHC sequence, the SSL largely correlates with the MHC affinity and less with the affinity to self-peptides. Consequently, an increased abundance of self-peptides would result in an increased likelihood of finding repeated and identical signal-providing sequences (for some TCRs) that may even exceed the likelihood of finding signal-providing sequences in the MHC (if $L_{\mathrm{p}} > L_{\mathrm{MHC}}$). Indeed, we showed that a repertoire selected with an adundant single-type spMHC is less self-MHC-biased. This is further supported by the observations that the repertoire selected with a single (and abundant) ligand is cross-reacting with allogeneic APCs [48]. Therefore, presentation of diverse and low-abundant self-peptides by MHC molecules is required in the thymus for efficient quantification of self-MHC affinity and selection of a MHC-biased T cell repertoire.

According to Gemisch model, postulated by Bevan [50], a TCR could be positively selected by multiple peptides with sufficient aggregate contribution, but with low affinity for each. This can naturally occur in the signal integration model in two ways: multiple low affinity peptides can raise the avidity of one thymocyte-APC interaction, but also different peptides in consecutive APCs can sustain an integrated TCR signal sufficient for positive selection. According to our model, selection with a single spMHC could not select cells that were selected based on diverse spMHCs, implying that *in silico* positive selection of these cells depended on one or multiple other self-peptides. This prediction of the signal integration model is in agreement with the gemisch selection model.

4.4.2 Negative selection and peptide specificity

In contrast to the sustained component of the TCR signaling, the strong transient increase (TSL) is a property that occurs at specific interactions and harbors a more stochastic nature than the sustained component (**Figure 4.6**). The emergence of a strong TSL could result from the ligation of TCRs with cognate spMHCs, suggesting TSL as an indicator of self-peptide reactivity. Indeed, we showed that the

TSL is correlated with the affinity of TCRs to the most specific spMHC in the ligand repertoire (**Figure 4.9B**). It can be concluded that the discrimination between sustained and transient components in TCR signaling offers a mechanism for separate detection of self-MHC and cognate self-peptide.

We observed that a TSL-based negative selection reduced the self-reactive TCR repertoire. Negative selection targeted TCRs with a wide-spectrum of MHC affinities with a dominant effect on the higher end (**Figure 4.13A-B**). However, due to the stochastic nature of finding cognate spMHC in a limited number of interactions, a TSL-based negative selection was prone to error, as experimentally detected [51]. Consistently, the model predicts that self-peptide reactive T cells exist in both nTreg and Tconv repertoires which would cross the negative selection TSL threshold if a sufficient number of cell interactions were allowed. *In silico*, increasing the frequency of interactions in thymus decreased the number of escaped self-reactive cells.

4.4.3 Impact of selections on the cross-reactivity of repertoires

As extensively discussed by Mason [128], TCR cross-reactivity enables recognition of a larger spectrum of peptides without requiring an enormous number of T cells that respond specifically to single foreign-peptides. In our model, this cross-reactivity was already present in pre-selection repertoire and was pronounced by positive selection during which cross-reactive cells were enriched (**Figure 4.17**). This guarantees a comprehensive peptide coverage by the positively selected repertoire. However, a repertoire with cells cross-reacting with self-peptides bears the potential of autoimmunity. Negative selection has to cope with cells reacting with different affinities for a large range of peptides, and a 100% efficient negative selection would delete all T cells because of cross-reactivity. Therefore, there is a tradeoff between self-tolerance and cross-reactivity of the selected repertoire [128, 129].

4.4.4 The efficiency of positive and negative selection for MHC-restriction depends on the extent of similarity between allo- and self-MHCs

It has been suggested that all MHC proteins in the genome of one species might share some features and that germline-encoded TCR variable elements might have an inherent predisposition to react with these shared features in all MHCs [127,130]. Although we did not assume any bias in random generation of TCR sequences, we showed that in the case of existing similarities between selecting- and allo-MHCs, negative selection is more efficient in MHC-restriction than positive selection. This *in silico* result is consistent with the work of Huseby et al. [126,127] using single-point amino-acid mutations of the selecting-MHC to assess alloreactivity in vitro. However, our model predicts the opposite trend in the case of dissimilar MHCs, meaning that negative selection is not efficient to restrict alloreactive T cells. A noteworthy point is that the conclusion drawn by Huseby et al. [126,127] that negative selection is responsible for MHC-restriction relied on the assumption that a thymus with single-peptide presentation disrupts negative selection but not positive selection. According to our model, cells that were not normally selected by diverse self-peptides were selected based on single-peptide. Moreover, these cells were less self-MHC-biased. Therefore, the results in [126,127] might be influenced by the cells that were not normally selected in a wild-type model. Our result regarding the importance of negative selection in controlling the specificity of T cells to foreign peptides by removing cross-reactive T cells is also in agreement with the work of Huseby et al. [126,127].

4.4.5 Selection of regulatory T cells

It is believed that the activation of escaped autoreactive T cells is suppressed by regulatory T cells in the periphery [131]. nTregs can be derived from antigens over-expressed in the thymus of TCR transgenic mice, and the selected nTregs exhibit a high affinity to these antigens [54]. This suggests a self-peptide specific repertoire of nTregs and led to the TCR instructive model. According to this view, self-specific

TCRs generate nTregs whereas less self-specific TCRs (but more foreign specific) generate Tconvs (see **Figure 2.4A**).

The TCR-instructive model predicts that the respective specificities of the Tconv and nTreg repertoires are distinct and that the diversity of nTregs is limited by the diversity of selecting ligands in the thymus. While several studies argued for distinct repertoires of Tconvs and nTregs [132, 133], there is also evidence for an overlap between them and for similar diversity [58–62]. Although the nTreg repertoire is a minority of the whole $CD4^+$ T cell population, nTregs can recognize both self- and foreign-peptides. One possible explanation would be that nTreg activation is non-specific. There is evidence that the suppressive activity of Tregs is triggered in an antigen-specific manner and relies on recognition of cognate antigen [55,67,134,135]. However, once Tregs are activated, they can suppress Tconvs with different antigen specificities *in vitro* [67, 134] and *in vivo* [136–138], implying that they may suppress in a non-specific manner [139]. Another possible explanation would be that the nTreg repertoire consists of cross-reactive TCRs. Cross-reactivity was indeed observed in TCRs [120, 121], but the extent of cross-reactivity in nTregs versus Tconvs has not been experimentally evaluated. Here, we defined the nTreg population based on the observation that nTregs show higher sustained signaling [53], and we managed to reproduce the aforementioned observations. We found that, under the hypothesis of higher SSL, nTregs show higher MHC specificity (linked to sustained signaling) as well as higher cross-reactivity (lower peptide sensitivity) compared to Tconvs.

In the model, cross-reactivity emerged from two different mechanisms. First, nTregs could recognize foreign peptides since their higher MHC affinity removed strong bias toward self-peptides. Second, having higher MHC affinity resulted in a higher level of signaling close to the level required for their activation. Hence, they required less peptide affinity contribution for activation. This resulted in the recognition of a wider range of activating ligands and represented a signal-based cross-reactivity (not affinity-based). This nTreg cross-reactivity would be a way to allow 5% of the $CD4^+$ population to recognize a broad spectrum of possible peptides and be the safekeeper of immune activation, while Tconv are designed to be more peptide-specific. In the model, we observed that peptides could activate both nTreg and Tconvs suggesting that an immune reaction for these peptides would activate simultaneously a pro-inflammatory response and a suppressive response. It would be of interest to know the amount of peptides recognized only by Tconv as they could be more pathogenic, or the relative populations of nTregs versus Tconvs recognizing the same antigen depending on its similarity to self-peptides. In the next chapter, I show that the ratio of antigen-specific Tregs to Tconvs and their absolute numbers are the major determinants for the onset of an immune response against the antigen [2].

Given an abundant source of signaling, any cell can become an nTreg according to the SSL-based selection model. If diverse and low-abundant self-peptides are presented, the MHC affinity is the major determinant of SSL. However, under the condition of high abundance of selecting self-peptides, our integration model would predict that self-peptide specific cells (existing in pre-selection repertoire due to random TCR rearrangement) would be selected as nTregs. In the case of transgenic TCRs, an additional requirement to become a nTreg would be to provide a peptide with sufficient affinity (in a level that does not exceed negative selection threshold). In agreement with this, thymocytes differentiate to nTregs in transgenic mouse models in which an additional selecting peptide is abundantly expressed [54]. *In silico*, no nTregs would be selected if the quality of the abundant peptide is not high enough for the transgenic TCR, consistently with experimental observations [54].

If the density of a particular self-peptide per APC was increased on a small fraction of APCs, it would not be sufficient to sustain the TCR signal for nTreg differentiation. However, this would affect the efficiency of negative selection. In a recent theoretical work by Bains et al. [87], the authors were able to recapitulate *in vivo* experiments where a controllable expression of one agonist-peptide in the thymus leads to selection of a varying number of nTregs and Tconvs from thymocytes with transgenic TCR [88]. Selection of T cells in the work of Bains et al. was assumed to rely on the maximum and minimum thymocyte-APC TCR signal strength. Tconv and nTreg repertoires were distinguished by an intermediate threshold between the positive and negative selection thresholds. The over-expressed peptide had an affinity to the TCR that

induce nTreg selection or deletion by negative selection. In an alternative scenario, the authors assumed that the sensitivity of the TCR increased step-wise such that the interaction with the over-expressed peptide led to different fates with time. This article gave insights on the impact of thymic selection manipulation *in vivo* by over-expression of an agonist peptide for a transgenic TCR, and provided a simple mechanistic explanation for the non-intuitive variation in the amounts of selected nTregs and Tconv. Note that cell fates in the model of Bains et al. are determined by single interactions and independent of TCR stimulation history, which is the focus in the present model.

4.4.6 Roles of TCRs on the borders of MHC-affinity spectrum

As shown, thymic selection imposes higher and lower limits on the MHC spectrum of the selected repertoire. The low end of the MHC affinity spectrum encompasses Tconvs with higher average affinity to self-peptides as a consequence of the pressure of positive selection. One could speculate that these cells would cause autoimmunity and be potentially pathogenic. However, this has to be mitigated by the following ideas. First, due to the low MHC affinity, they have the lowest SSL in the repertoire, which means that activation under homeostatic conditions is hard. Furthermore, self-peptides could only activate them under over-presentation condition by increasing the integrated signal level. This would not naturally happen unless self-peptide disturbances occurred as a result of non-homeostatic conditions such as cancerous cells or self-similar pathogens. Therefore, these cells would be good candidates to recognize such self-disturbances. I explain this idea in the next chapter [2]. Secondly, they are less self-MHC-biased. Hence, upon interacting with allogeneic APCs, they might recognize foreign MHCs. These are the cells that would reject grafts via recognizing foreign MHCs on the donor's APCs.

The high end of the MHC affinity spectrum contains Tconvs and nTregs with lower average affinity to self-peptides as a consequence of the pressure of negative selection. We showed that these cells are more cross-reactive for the peptides. However, they might be easily detected in the thymus due to their higher SSL. Efficient negative selection or differentiation of these cells to nTregs are two processes that minimize the risk of having a pathogenic autoreactive response.

According to the model, the borders of the MHC affinity spectrum change by variations in the diversity of self-peptides that bind to a MHC molecule. In the extreme case, we showed that a selection with single spMHC comprises cells with no MHC-bias.

4.4.7 Heterogeneity of antigen presentation in the thymus

Thymic APCs are heterogeneous in the type of self-peptides they present and in signaling resources they provide to thymocytes (particularly by differential co-stimulation levels). Thymic APCs can be categorized into cTEC and migratory DCs in the cortex and mTEC, migratory and resident DCs in the medulla. Some peptides, denoted as *private* self-peptides [7], may only be presented by cTECs but by no other thymic and peripheral APCs. Some other peptides are presented by all the cells, known as *ubiquitous* peptides. AIRE-dependent *Tissue-Restricted-Antigens* (TRA) are presented by mTECs allowing to mimic the peripheral self-peptides. Additionally, a spectrum of peripheral antigens is presented by migratory DCs. As potential extensions to the model, such heterogeneity could be translated by considering sets of peptides with different abundance [different values of F, see equation (4.11)] and density per APC: a set of self-peptides with low-abundance but higher density to represent TRAs, and a highly abundant set representing the ubiquitous peptides (presented by a higher fraction of APCs) [7].

Regarding the role of co-stimulation, as generally accepted in T cell activation, higher co-stimulation provides higher signaling strength and increases the sensitivity of T cells to antigen stimulation [140]. By assuming this property, the model can potentially be adapted in two ways by either associating different co-stimulation levels to particular peptides i.e. allowing muliple copies of particular self-peptides on APCs; or by associating co-stimulation to particular APCs i.e. provide a stronger TCR signal integration rate (higher

α, see **Table 4.1**). Incorporating heterogeneity of APCs and self-peptides in a realistic biological way would increase the number of unknown parameters (e.g. the number of APCs of each kind, the difference in peptide presentation capacity and co-stimulation expression heterogeneity, the degree of abundance of each different type of self-peptides) and would therefore reduce the predictive power of the model. Therefore, we restricted ourselves to simpler representations of APCs and reserve the distinction of different APC subsets to future work.

4.5 Summary

The extent of TCR self-reactivity is the basis for selection of a functional and self-tolerant T-cell repertoire, and is quantified by repeated engagement of TCRs with a diverse pool of self-peptides complexed with self-MHC molecules. The strength of a TCR signal depends on the binding properties of a TCR to the peptide and the MHC, but it is not clear how the specificity to both components drive fate decisions. In this chapter, we proposed a TCR signal-integration model of thymic selection that describes how thymocytes decide among distinct fates, not only based on a single TCR-ligand interaction, but taking into account the TCR stimulation history. These fates are separated based on sustained accumulated signals for positive selection and transient peak signals for negative selection. This spans up the cells into a 2-dimensional space where they are either neglected, positively selected, negatively selected, or selected as natural regulatory T cells (nTregs).

We showed that the dynamics of the integrated signal can serve as a successful basis for extracting specificity of thymocytes to MHC and detecting the existence of cognate self-peptide-MHC. It allows to select a self-MHC-biased and self-peptide-tolerant T cell repertoire. Further, nTregs in the model are enriched with MHC-specific TCRs. This allows nTregs to be more sensitive to activation and more cross-reactive than conventional T cells. The presented model provided a mechanistic model showing that the time integration of the TCR-mediated signals, as opposed to single-cell interaction events, is needed to gain a full view on the properties emerging from thymic selection. See **Figure 4.25** for a summary and highlights of signal integration model of thymic selection.

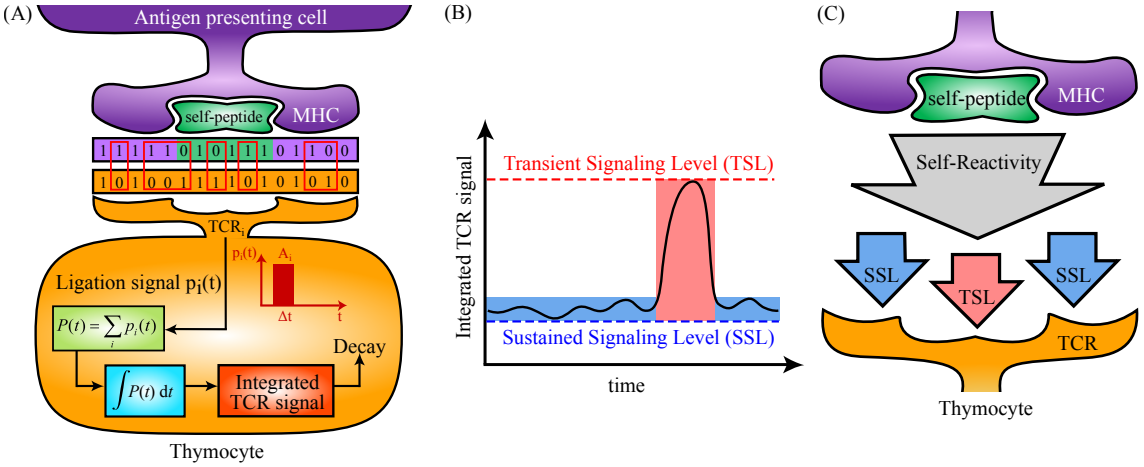

Figure 4.25: A summary for signal integration model. Thymocytes are generated, selected and mature in the thymus to create a diverse, functional and self-tolerant T cell repertoire. Self-reactivity of thymocytes is quantified by repeated engagement of their TCRs with a diverse repertoire of self-peptides complexed with self-MHC molecule (spMHC) and may originate from either part of the complex. The fact that the selected T cell repertoire is MHC-biased, requires a good mechanistic explanation of how thymocytes are able to quantify their affinity to MHC. In order to analyze how thymocytes quantify their self-reactivity, extract their MHC affinity, and how they use this information for cell fate determination, we developed a signal integration model for thymic selection, mimicking the requirement of repeated TCR signaling for successful selection and cell maturation. (A) A polyclonal repertoire of thymocytes sequentially interact with diverse spMHCs and integrate the affinity-dependent TCR ligation signals. Proteins are represented by binary sequences. Binding affinity between TCR and self-peptide-MHC (spMHC) depends on the complementarity of sequences. (B) Schematic for a dynamic change of integrated TCR signal (ITS) upon sequential interactions with APCs presenting diverse and low-abundant spMHCs is shown. The sustained signaling level (SSL) is determined by the minimum value of the ITS in a window of sequential interactions. The transient signaling level (TSL) is defined as the maximum ITS value in the same window of interactions. SSL and TSL are individual properties of thymocytes and correlate with MHC affinity and cognate spMHC affinity, respectively. In thymic selection model, both the strength and dynamics of the integrated signal is taken as a reference for cell fate determination. (C) MHC and cognate self-peptide affinities are segregated by the sustained and transient components of ITS. Therefore, quantification of the integrated signal and discrimination between its sustained and transient dynamics turns out as a successful basis for extracting affinity of thymocytes to MHC, detecting the existence of cognate self-peptide, and selecting a MHC-biased self-tolerant T cell repertoire. We provided a mechanistic model that questions the view that affinity to self-peptides is the major determinant of cell fates in thymic selection and highlights two central points instead: MHC specificity and peptide specificity are different properties of TCRs, and the time integration of the TCR-mediated signals during APCs scanning is necessary to gain a full view of the properties emerging from thymic selection.

Chapter 5

Immune activation model

The sections of this chapter are partially reprinted from published article [2], which can be accessed by the link: `http://journal.frontiersin.org/article/10.3389/fimmu.2013.00474/full`.

5.1 Background

The immune system is continuously exposed to a wide variety of disturbances. Such disturbances are recognized by T cells via antigen presentation. Antigen presentation is a process in which antigen presenting cells (APCs) capture the antigens, break them into small peptides, combine them with MHC molecules and present them on the cell surface, thus enabling their recognition by T cells [141–143]. Antigen presentation process is described in **Figure 2.5**). The majority of disturbances that the immune system encounters are pathogenic nonself (foreign). Since the APCs break down the nonself antigens into smaller peptides and present them on their surface, the presented peptide of nonself antigen might share some similarities with self peptides [144, 145]. In addition, rapidly evolving nonself pathogens, such as Hepatitis C virus, might acquire similarities to self antigens by high rate of mutation [146]. Apart from nonself, altered self such as cancer cell is also a disturbance that has to be recognized by the immune system. Therefore, an ideal immune system has to find a solution for dealing with nonself, self-similar nonself, and altered self disturbances (**Figure 5.1**).

As a general solution, the immune system generates T cell clones in thymus with random specificities that could potentially recognize any peptide, including self-peptides. The classical idea that the T cell repertoire has to be self-tolerant and T cells should not react to self-peptides, assumes that self-reactive T cells should be eliminated in the thymus. This assumption is partially true, as T cell clones which fully recognize self-peptides in the thymus undergo clonal deletion, in the so-called negative selection process [147, 148], which is studied in chapter 4.

The self-tolerance resulting from negative selection is called central tolerance. A stringent central tolerance induction and deletion of all autoreactive T cells is believed to create holes in the specificity space of the T cell repertoire [149, 150] by removing T cells that are able to initiate immune responses against self-similar nonself and altered self. Such holes may facilitate persistence and growth of cancer cells. Further, they allow highly mutating pathogens to acquire self-similar structures and take advantage of self-tolerance. Hence, a too stringent central tolerance does not seem beneficial. In line with this idea, there is evidence that negative selection only partially deletes autoreactive T cells mainly because availability of self-peptides required for negative selection in the thymus is limited. Additionally, T cells spend only a limited time in the thymus and may not interact with high-affinity self-peptides [151–153]. *In silico*, we also observed that some self-reactive thymocytes escape the negative selection chapter 4. Autoreactive T cells normally exist in healthy individuals and are quiescent in the presence of their cognate

self-antigen [154]. However, involvement of escaped autoreactive T cells in autoimmunity has been shown [155].

Escaped autoreactive T cells are under the control of peripheral tolerance mechanisms in healthy individuals. A prominent mechanism of peripheral tolerance among others (reviewed in [156]) is induced by $CD4^+$ $Foxp3^+$ regulatory T cells (Tregs) [8]. The majority of these cells, known as natural Tregs (nTreg), are hypothesized to be selected from self-reactive T cells in the thymus [54, 157] (see **Figure 2.4A** for TCR instructive model of nTreg selection). Tregs suppress effector functions of conventional T cells (Tconvs) and by that, regulate the immune response.

Despite the necessity of suppression by Tregs for avoiding autoimmunity [158, 159], production of a too large amount of Tregs by the thymus might prevent beneficial effector responses. Therefore, a too stringent induction of peripheral tolerance by selection of a large number of Tregs in the thymus does not seem favorable.

In the view of this background, how does the immune system balance the tolerance mechanisms in order to ensure immune responses to any type of disturbances including self-disturbances, yet being tolerant to self in a healthy homeostasis? Here, we address this question by using a mathematical model of immune activation that relies on identical components for self and nonself, i.e. using the same set of ordinary differential equations. The proposed model considers the thymic production of Tregs and Tconvs as well as the dynamic interplay between Tregs, Tconvs and IL-2 molecules in the presence of antigen(Ag)-stimulation in the periphery. The model is exploited to reveal the parametric regime of the immune system in which an immune response against self is restricted, but not impossible.

The interplay between Tregs and Tconvs during immune responses is a topic of extensive mathematical modeling [25–27, 160–163]. León and co-workers [160] proposed a series of models for studying immune tolerance by considering APCs, Tconvs and Tregs. Their models rely on the assumption that regulatory interaction between Tregs and Tconvs takes place only in simultaneous conjugation with an APC. As a result of this assumption, efficient suppression of Tconvs requires a minimum population of Tregs per APC [164]. As an extension, a crossregulation model is proposed by Carneiro and co-workers [26] in an attempt to incorporate Tregs in a coherent theory of the immune system. Their model shows a bistable behavior. Bistability is a property of dynamical systems with two stable steady states. In such systems, depending on the initial condition, the states of the system evolve towards one or the other steady state (see **Figure 5.2**). According to crossregulation model, immunity to a given Ag arises as competitive exclusion of Tregs by the expansion of Tconvs, and tolerance results from limited APC availability or above threshold Treg

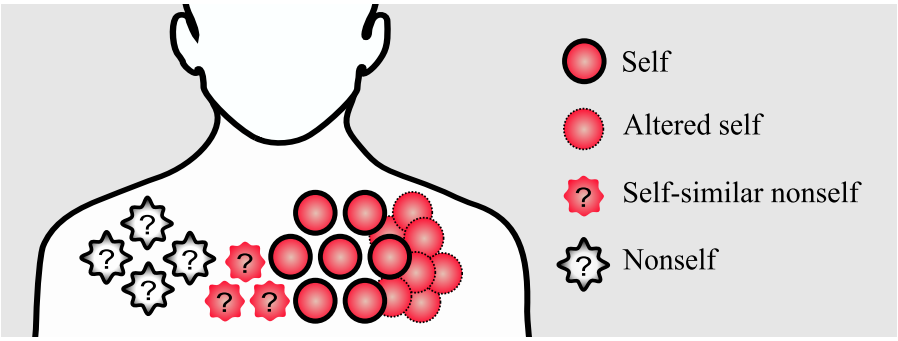

Figure 5.1: Conceptual figure of different disturbances in the immune system. Pathogenic nonself are recognized and attenuated by nonself-specific T cells. However, recognition and attenuation of altered self and self-similar nonself disturbances are challenging for the immune system due to the existence of self-tolerance mechanisms; without self-specific immune cells, the immune system is not able to initiate an immune response against these disturbances.

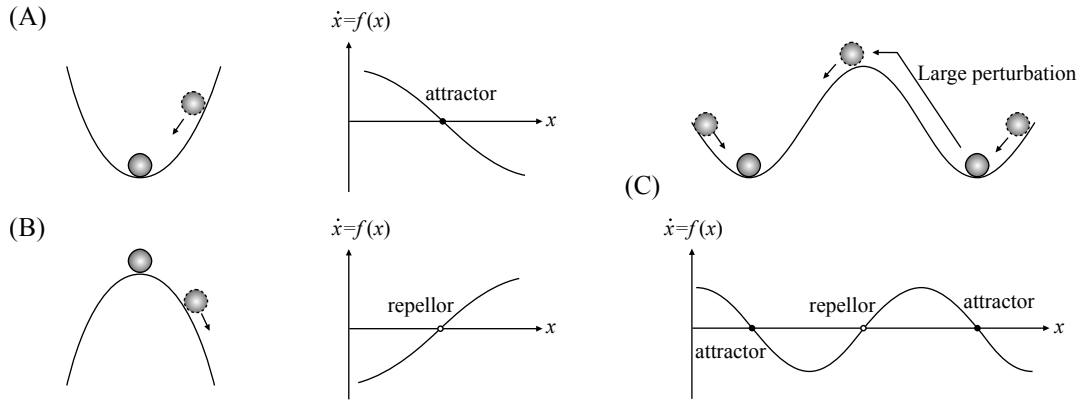

Figure 5.2: Stable, unstable and bistable dynamical systems. In a 1-dimensional dynamical system $\dot{x} = f(x)$, equilibrium points can be determined by the slope in intersections of dynamic function $f(x)$ with the x-axis. (A) Equilibrium point is attractor when the slope of the dynamical function is negative and corresponds to a stable state for perturbations. (B) Equilibrium point is repellor when the slope of the dynamical function is positive and corresponds to an unstable state for perturbations. (C) A bistable dynamical system has two attractors, separated by an repellor. Unlike systems with only one attractor, a bistable dynamical system exhibit a threshold associated with the presence of repellor between two attractors. While each attractor corresponds to a stable state for small perturbations, when the magnitude of the perturbation exceeds a critical threshold, the system can cross the potential barrier imposed by the repellor, and move from one attractor to the other.

numbers. Since the interactions between Tregs and Tconvs is assumed to depend on the density of the APCs, increasing the APC availability decreases the simultaneous conjugate formation of Tregs and Tconvs with the same APCs and hence, it is sufficient to break the immune tolerance.

An alternative concept was brought forward in a model proposed by Carneiro and co-workers [161] that assumes APC-independent interactions between Tconvs and Tregs for immune suppression which will be also used in our model. A direct suppressive interactions of Tconvs and Tregs was identified by experiments [139]. The authors concluded that efficient immune suppression still requires a minimum population of Tregs regardless of the number of APCs.

In contrast to the aforementioned studies, we do not consider the conjugate formation of Tregs and Tconvs with APCs and therefore, there is not a competition between these cells for Ag presented by APCs. Instead, the role of APCs is indirectly captured by an Ag-stimulation factor which is the activation rate of naïve T cells and resting Tregs with identical Ag-specificity by APCs that present cognate Ag. In addition, we explicitly consider the dependency of Tregs on Tconvs through the growth factor IL-2.

Burroughs and co-workers [25] investigated Treg-induced inhibition of cytokine secretion by effector T cells. By assuming that Tregs are activated by self Ag and locally maintained by nonlinear competition for tissue-derived cytokines that are solely utilized by Tregs, the authors analyzed the role of local active Treg population size in the balance between suppressor and effector responses. Stimulation of Tregs and Tconvs is described by independent parameters. In contrast to their model, thymic output maintains the homeostatic population of Tregs in our model. Another essential difference is that Ag-stimulation of Tregs and Tconvs is described with a unified self-nonself concept and Tregs are assumed to also respond to nonself Ag-stimulation, which has been shown experimentally [69].

Parametric steady state and stability analysis of the model provides insights about the physiological range of model parameters, and determines the overall conditions under which immune responses against self are possible. Furthermore, the impact of model parameters on the requirements for the initiation of

immune reactions against self is analyzed. The model proposes that disturbed homeostatic balance between autoreactive T cells and Tregs increases the susceptibility to autoimmunity or cancer.

5.2 Model

For constructing a simple immune activation model, the conceptual and hierarchical modeling approaches are taken (described in 3.1.1 and 3.1.3 respectively). In the conceptual modeling approach, it is aimed to model the qualitative behavior of the immune response. However, a data-driven modeling approach can be taken once the experimental data exist. As the simplest model, only essential components of an effector immune response is considered. These components include the dynamics of Tconv activation, Tconv proliferation and secretion of growth factor IL-2. Then, the compatibility of the model to the immune system is discussed. If the model cannot be validated in a qualitative fashion, by taking the hierarchical modeling approach, additional complexities are incrementally added to the model to a degree allowing for validation and analysis of tolerance versus immunity. This approach allows us to investigate the contribution of added complexities and biologically relevant range of their associated parameters. The scheme of the most complex model in this study is depicted in **Figure 5.3**, which is constructed and analyzed in sequential steps. Note that the model is conceptually independent of the self/nonself nature of the immune response. Instead, differences in the immune responses against self versus nonself are derived from different parameter values of the same model.

5.2.1 Conventional T cell response: an immune response requires sufficient division and IL-2 secretion of activated T cells

In peripheral lymphoid organs, only a few T cell clones in the naïve Tconv pool are able to recognize an antigen. Effector functions of a few activated Tconv are not sufficient to effectively remove a pathogen, especially pathogens with high growth rate. Therefore, a growth mechanism in activated T cell population would allow the expansion of a few initially activated T cells. This growth mechanism is mainly via growth factor IL-2 which is secreted by activated Tconvs. IL-2 secretion and consumption by activated T cells lead to T cell division and production of daughter cells. This processes is called cell proliferation. An effective immune response arises from massive proliferation of activated T cells and their subsequent effector functions. Our simplest model attempts to capture the dynamic characteristics of such expansion in T cells population (represented by T) by secretion and consumption of IL-2 molecules (represented by I)

$$\begin{aligned} \dot{T}(t) &= aI(t)T(t) - bT(t), \\ \dot{I}(t) &= dT(t) - eI(t)T(t) - fI(t). \end{aligned} \tag{5.1}$$

In model (5.1), activated T cells have a mean lifespan $1/b$, and secrete IL-2 (I) with rate d. Available IL-2 decays with rate f and is consumed by activated T cells with rate e. Activated T cells are able to proliferate in the presence of IL-2. This IL-2 dependent proliferation rate is a linear function of IL-2, in the form of $aI(t)$. The impact of considering a nonlinear proliferation rate (a Hill-function of IL-2) instead of the linear term $aI(t)$ will be given in section (5.2.5).

Remark: Model (5.1) with $d = 0$ and $f < 0$ is in the form of classical predator (Tconv) - prey (IL-2) model. But this particular case of parameter range does not represent the regime of IL-2 dependent Tconv proliferation. In contrast to predator-pray model, the production of IL-2 in model (5.1) depends on the consumers of IL-2 when $d \neq 0$. Further, IL-2 molecules cannot reproduce themselves, meaning that $f > 0$.

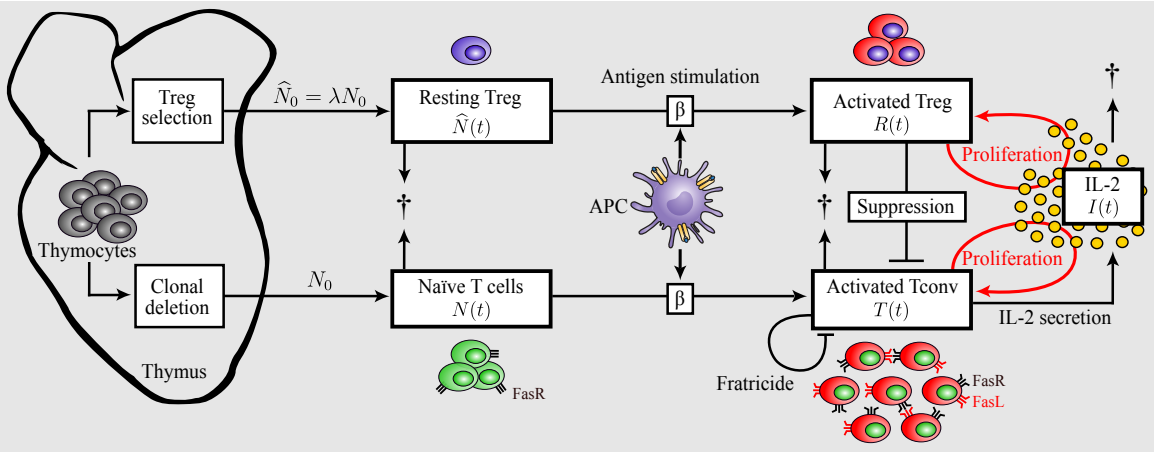

Figure 5.3: Model of dynamic interplay between conventional T cells and regulatory T cells: Nonself-specific as well as some self-specific thymocytes that escaped negative selection in thymus and were not selected as Tregs enter the periphery as naïve T cells. A part of detected autoreactive thymocytes differentiate into Tregs in the thymus and reside in the periphery in resting state. Upon Ag-stimulation by APCs, naïve T cells and resting Tregs become activated. In contrast to activated T cells, activated Tregs do not secrete IL-2, but both activated populations proliferate in dependence on IL-2 [165]. Activated Tregs suppress activated T cells in a cell-contact dependent and cytokine-driven manner. Activated T cells undergo Fas-induced apoptosis by interacting with each other (fratricide). In contrast, Tregs are resistant to Fas-induced apoptosis [166].

Proposition 5.1 *Assume that all parameters are positive and* $ad - be > 0$ *in model (5.1), then there exists a super-threshold for initial conditions that allow for unlimited proliferation of activated Tconvs, or equivalently,* $\lim_{t\to\infty} T(t) = \infty$.

Proof. In order to show the existence of such super-threshold, we characterize the dynamical behavior of the model (5.1) in its phase space. This model has two equilibrium points

$$(I_1, T_1) = (0, 0), \quad (I_2, T_2) = \left(\frac{b}{a}, \frac{bf}{ad - be}\right). \tag{5.2}$$

The parameters of the model are representing biological processes and therefore, they are assumed to be positive. According to (5.2), the nontrivial equilibrium point (T_2, I_2) is positive if and only if

$$ad - be > 0. \tag{5.3}$$

The linear stability of equilibrium points can be determined from the sign of the real part of the eigenvalues of linearized model in equilibrium points. An equilibrium point is asymptotically stable if all eigenvalues of the Jacobian matrix J evaluated at the equilibrium point have negative real parts, and it is unstable if at least one of the eigenvalues has a positive real part.

General notation: Time-variant states of the model are indicated explicitly with time argument (such as $T(t)$ and $I(t)$); states without time argument (such as T and I) indicates to steady state values.

The Jacobian matrix of model (5.1) is

$$\mathrm{J} = \begin{pmatrix} aI - b & aT \\ d - eI & -eT - f \end{pmatrix}. \tag{5.4}$$

From Jacobian matrix, the following characteristic polynomial can be obtained

$$Q(\lambda) = \det(\lambda I_n - J) = \begin{vmatrix} \lambda - aI + b & -aT \\ -d + eI & \lambda + eT + f \end{vmatrix}$$
$$= \lambda^2 + (eT + f + b - aI)\lambda + (-afI + beT + bf - adT). \tag{5.5}$$

where I_n is the identity (unit) matrix of size n, and n is the number of states in the model. The eigenvalues $\lambda_{1,2}$ in trivial equilibrium point (I_1, T_1) are obtained by solving the following characteristic equation, which is derived by evaluating characteristic polynomial (5.5) in (I_1, T_1)

$$Q(\lambda, I_1, T_1) = \lambda^2 + (f + b)\lambda + bf = 0. \tag{5.6}$$

From quadratic equation above, $\lambda_1\lambda_2 = bf$ is positive and $\lambda_1 + \lambda_2 = -(f + b)$ is negative. Therefore, eigenvalues $\lambda_{1,2}$ are negative and the trivial equilibrium point (I_1, T_1) is asymptotically stable.

For checking the stability of nontrivial equilibrium point (I_2, T_2), the characteristic equation (5.6) is obtained by evaluation of polynomial (5.5) in (I_2, T_2)

$$Q(\lambda, I_2, T_2) = \lambda^2 + \left(\frac{afd}{ad - be}\right)\lambda - bf = 0. \tag{5.7}$$

If we assume that condition (5.3) is satisfied, the coefficient of λ in (5.7) is positive. The sign of coefficients in quadratic equation $Q(\lambda, I_2, T_2)$ changes only once. According to Routh-Hurwitz stability Criterion (RHC), only one eigenvalue in (I_2, T_2) has a positive real part. Therefore, the nontrivial equilibrium point (I_2, T_2) is a saddle point and unstable.

Remark: Equilibrium point x_0 of saddle type in a system of differential equations $\dot{x} = f(x)$, with $x \in \mathbb{R}^n$ and the map $f : \mathbb{R}^n \to \mathbb{R}^n$, has stable and unstable manifolds, denoted by $W^s(x_0)$ and $W^u(x_0)$, respectively. These manifold are defined as

$$W^s(x_0) := \{x \in \mathbb{R}^n | \lim_{t\to\infty} \phi^t(x) = x_0\}, \tag{5.8}$$
$$W^u(x_0) := \{x \in \mathbb{R}^n | \lim_{t\to\infty} \phi^{-t}(x) = x_0\}, \tag{5.9}$$

where ϕ^t is the flow of the system. Trajectories on the stable (unstable) manifold converge to equilibrium point x_0 forward (backward) in time. Manifolds organize the dynamics on the phase space. For example, stable manifolds may form boundaries of basins of attraction.

The stable manifold of saddle equilibrium point (I_2, T_2) imposes a threshold for initial conditions of the model in which the activated Tconvs proliferate unlimitedly, i.e. $\lim_{t\to\infty} T(t) = \infty$, which in this model, corresponds to a major immune response. This can be visualized by the phase portrait of the model as shown in **Figure 5.4**. ■

In the biological context, condition (5.3) imposes a quality constraint on activated T cell clones which can enter a highly proliferative state. The condition implies that among T cell clones that are in the activated state, only T cell clones with a sufficiently high proliferation rate (a) or IL-2 secretion rate (d) are able to significantly contribute to the major immune response against Ag. Since both, the proliferation and IL-2 secretion rate of activated T cells depend on the affinity/avidity of their TCR to the presented Ag [168–170], condition (5.3) implies that the existence of T cell clones with sufficiently high specificity (high affinity) for the presented Ag is required for induction of a major immune response. Similar implications can be derived from a model that considers a nonlinear IL-2 dependent proliferation rate of activated T cells (Model will be given in section 5.2.5).

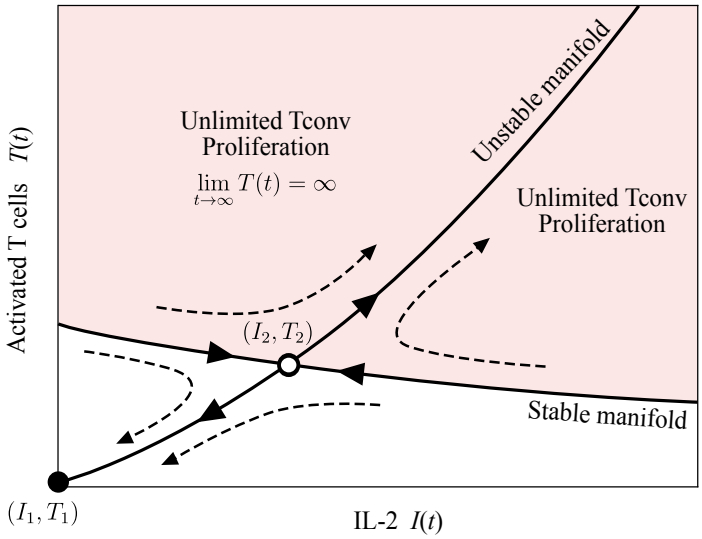

Figure 5.4: Qualitative phase portrait of Tconv response model (5.1). Stable equilibrium point (I_1, T_1) is shown with black circle, and saddle equilibrium point (I_2, T_2) is shown in black circle. Arrows with dashed line show trajectories of the model. In the phase plane, the stable manifold of saddle point (shown with arrows with solid line) defines a separatrix curve in the phase plane that sharply distinguishes the sub-threshold initial conditions, i.e. initial conditions that tends to stable equilibrium point as $t \to \infty$, from super-threshold initial conditions that allow for unlimited proliferation of activated Tconvs, i.e. $\lim_{t\to\infty} T(t) = \infty$ and $\lim_{t\to\infty} I(t) = \infty$. To compute stable manifold numerically, two initial conditions can be considered that are slightly displaced from two different sides of saddle point along the direction of the eigenvector with negative eigenvalue; an integration backward in time is an approximation to stable manifold. For obtaining unstable manifold, two trajectories has to be computed by integration forward in time. These trajectories start from initial conditions slightly displaced from two different sides of saddle point along the direction of eigenvector with positive eigenvalue [167].

The major focus of central tolerance in thymus is to eliminate T cells with self-specific TCRs. Therefore, it is unlikely that highly self-specific T cells escape from central tolerance, as they are more effectively detected and eliminated in the thymus upon interactions with cognate self-peptides [152, 170]. It is thus expected that autoreactive T cells in the periphery are less aggressive than the ones that undergo clonal deletion in the thymus, and may not fulfill condition (5.3).

Remark: model (5.1) can be simplified to a dimensionless system by scaling variables in the following way

$$\tau = \theta_t t, \qquad \widehat{T}(\tau) = \theta_T T(t), \qquad \widehat{I}(\tau) = \theta_I I(t). \tag{5.10}$$

By assuming the following parametric values for scaling factors

$$\theta_t = b, \qquad \theta_T = \frac{b}{e}, \qquad \theta_I = \frac{b}{a}, \tag{5.11}$$

model (5.1) is converted to the following simple form

$$\begin{aligned} \dot{\widehat{T}}(\tau) &= \widehat{I}(\tau)\widehat{T}(\tau) - \widehat{T}(\tau) \\ \dot{\widehat{I}}(\tau) &= p_1\widehat{T}(\tau) - \widehat{I}(\tau)\widehat{T}(\tau) - p_2 I(\tau) \end{aligned} \tag{5.12}$$

where

$$p_1 = \frac{ad}{be}, \qquad p_2 = \frac{f}{b} \tag{5.13}$$

are dimensionless parameters. The simplified model has less number of parameters and therefore, makes the analysis easier. However, since we add additional mechanisms to model (5.1), the number of parameters increases unless a new set of scaling factors is determined. Hence, we keep the model of Tconv response in its initial form given in (5.1).

5.2.2 Homeostatic population and antigen stimulation: initiation of an immune response requires a minimum homeostatic population of naïve T cells and antigen stimulation

Continuous thymic production of naïve T cells maintains the peripheral number and diversity of mature naïve T cells [171], although involvement of other mechanisms such as homeostatic proliferation resulted from stimulation of T cells with low-affinity self-antigens and IL-7 has been shown [172]. Upon Ag-stimulation by activated APCs, which express both antigen and costimulation, naïve T cells with high affinity/avidity to the presented Ag become activated. Here, dynamics of the naïve T cell population (denoted by $N(t)$) and T cell activation by Ag-stimulation (with rate β) are taken into account. It is assume that naïve T cells with identical Ag-specificity (one T cell clone) have a homeostatic population in the periphery that is established by naïve T cell renewal (with rate N_0) and natural cell death (with rate g)

$$\begin{aligned}
\dot{N}(t) &= f(N) = N_0 - gN(t) - \beta N(t),\\
\dot{T}(t) &= aI(t)T(t) - bT(t) + \beta N(t),\\
\dot{I}(t) &= dT(t) - eI(t)T(t) - fI(t).
\end{aligned} \tag{5.14}$$

Note that coupling between added variable $N(t)$ to model (5.1) is via the rate that naïve conventional T cells are stimulated ($\beta N(t)$) and enter to the activated state. In the case of $\beta = 0$, no coupling exists between $N(t)$ and other variables. T cell activation $k(t)$ is defined as

$$k(t) = \beta N(t), \tag{5.15}$$

which indicates to the number of naïve T cells activated by Ag-stimulation (β) per unit of time.

Proposition 5.2 *Assume that condition (5.3) is satisfied for model (5.14), and N_0 is larger than a critical T cell activation k_-,*

$$N_0 > k_-, \tag{5.16}$$

with the following value for k_-

$$k_- = \frac{adf}{e^2}\left(1 - \sqrt{1 - \frac{be}{ad}}\right)^2. \tag{5.17}$$

By increasing Ag-stimulation β from $\beta = 0$, a critical point β_- exists with the following value

$$\beta_- = \frac{gk_-}{N_0 - k_-}, \tag{5.18}$$

after which activated Tconvs proliferate unlimitedly, or equivalently, $\lim_{t\to\infty} T(t) = \infty$.

Proof. According to (5.18), a biologically meaningful (positive) value for β_- that corresponds to k_- exists when $N_0 > k_-$. In the case of $N_0 < k_-$, no positive β_- can be found. Next, we study the steady state and linear stability of model (5.14) with respect to T cell activation (k), to prove that for k larger than k_- given in (5.17), we have $\lim_{t\to\infty} T(t) = \infty$.

In the followings, we show that model (5.14) has either 2 or no equilibrium points depending on the steady state value of T cell activation (k), and k_- given in (5.17) is the critical point where the number of equilibrium points in the model changes, such that for $k > k_-$ or equivalently, for $\beta > \beta_-$, model (5.14) does not have any positive equilibrium point and therefore, $\lim_{t\to\infty} T(t) = \infty$.

The equilibrium points of model (5.14) with the definition of T cell activation $k(t)$ given in (5.15) can be obtained from the followings

$$N = \frac{k}{\beta} = \frac{N_0}{g+\beta}, \tag{5.19}$$

$$I = \frac{dT}{eT+f} = \frac{bT-k}{aT}, \tag{5.20}$$

$$(ad-be)T^2 + (ek-bf)T + fk = 0. \tag{5.21}$$

According to (5.21), by keeping the assumption (5.3), the equilibrium points ($T_{1,2}$), if exist, are positive ($T_{1,2} > 0$) if the coefficient of T in (5.21) is negative

$$ek - bf < 0 \quad \rightarrow \quad k < \frac{bf}{e}. \tag{5.22}$$

Otherwise, the equilibrium points $T_{1,2}$ are negative ($T_{1,2} < 0$). According to (5.20), if $T \geqslant 0$, then $I \geqslant 0$. The equilibrium values for $T_{1,2}$ can be obtained from equation (5.21)

$$T_{1,2} = \frac{-(ek-bf) \pm \sqrt{(ek-bf)^2 - 4(ad-be)fk}}{2(ad-be)}. \tag{5.23}$$

where $(ad-be) > 0$, according to assumption (5.3). Real equilibrium points $T_{1,2}$ exists if

$$\Delta = (ek-bf)^2 - 4(ad-be)fk = (ek+bf)^2 - 4adfk \geq 0. \tag{5.24}$$

Our aim is to obtain a range for T cell activation (k), in which real equilibrium points $T_{1,2}$ exists. Therefore, we have to obtain k_+ and k_- in which Δ in (5.24) is zero. We can rewrite Δ in (5.24) as $\Delta = \Delta_1\Delta_2$, where

$$\Delta_1 = \left(ek + bf + 2\sqrt{afdk}\right), \qquad \Delta_2 = \left(ek + bf - 2\sqrt{afdk}\right). \tag{5.25}$$

Since all the parameters are positive, $\Delta_1 > 0$. Hence, $\Delta = 0$ can only be resulted from equation $\Delta_2 = 0$, which has the following roots

$$k_+ = \frac{adf}{e^2}\left(1 + \sqrt{1 - \frac{be}{ad}}\right)^2, \qquad k_- = \frac{adf}{e^2}\left(1 - \sqrt{1 - \frac{be}{ad}}\right)^2. \tag{5.26}$$

Model (5.14) does not have any equilibrium points for $k_- < k < k_+$, and two equilibrium points otherwise. The number of equilibrium points differs between two sides of critical points k_+ and k_-, where the bifurcation in the model occurs. It can be verified that by keeping assumption (5.3), we have

$$0 < k_- < \frac{bf}{e} < k_+. \tag{5.27}$$

Therefore, the existence criterion of equilibrium points ($k < k_-$ or $k > k_+$) and the criterion for having positive equilibrium points, given in (5.22), are combined to the following criterion

$$0 < k < k_- \tag{5.28}$$

In other words, for $0 < k < k_-$, condition (5.22) is satisfied and the model has two positive equilibrium points. Further, for $k > k_+$, condition (5.22) is not satisfied and model has two negative equilibrium points. As shown, for $k > k_-$, model (5.14) does not have any stable positive equilibrium point and therefore in this caes, $\lim_{t\to\infty} T(t) = \infty$. ■

Next, as we learned that bifurcation occurs in k_- and k_+, we check the type of bifurcation by evaluating the linear stability of model in equilibrium points. In the first case, consider that model (5.14) has two different positive equilibrium points ($0 < k < k_-$).

Lemma 5.3 *Model (5.14) for $0 < k < k_-$ has two equilibrium points of type stable node and saddle.*
Proof. We evaluate the linear stability of the model in equilibrium points. The Jacobian matrix of the model is

$$\mathsf{J} = \begin{pmatrix} -g-\beta & 0 & 0 \\ \beta & aI-b & aT \\ 0 & d-eI & -eT-f \end{pmatrix} \tag{5.29}$$

from which, the following characteristic equation can be obtained

$$Q(\lambda) = \det \begin{pmatrix} \lambda+g+\beta & 0 & 0 \\ -\beta & \lambda-aI+b & -aT \\ 0 & -d+eI & \lambda+eT+f \end{pmatrix} = Q_1(\lambda)Q_2(\lambda) = 0 \tag{5.30}$$

where

$$Q_1(\lambda) = \lambda + (g+\beta), \qquad Q_2(\lambda) = (\lambda - aI + b)(\lambda + eT + f) + aT(eI - d). \tag{5.31}$$

From $Q_1(\lambda) = 0$, the model has a negative eigenvalue $\lambda = -(g+\beta)$ for all equilibrium points. For the other two remaining eigenvalues, equation $Q_2(\lambda) = 0$ has to be checked for existence of positive roots. We rewrite $Q_2(\lambda)$ in the form of $Q_2(\lambda) = \lambda^2 + U\lambda + V$, where the coefficients U and V are

$$U = eT + f + b - aI, \qquad V = -afI + beT + bf - adT. \tag{5.32}$$

From (5.20) it can be easily verified that $b - aI > 0$ and hence, coefficient U is positive. Therefore, the linear stability depends on the sign of coefficient V. We substitute $I = dT/(eT+f)$, given in (5.20), in coefficient V

$$V = -\frac{afd}{eT+f}T - (ad - be)T + bf. \tag{5.33}$$

In order to determine the sign of V in equilibrium points, we simplify polynomial V by obtaining new expressions with identical sign and from multiplication of V with positive expressions.

$$V_1 = TV = -\frac{afd}{eT+f}T^2 - [(ad-be)T^2 + (ek - bf)T + fk] + k(eT+f). \tag{5.34}$$

According to (5.21), the expression in the brackets of equation above is equal to zero. Then, V_1 is simplified to

$$V_1 = -\frac{afd}{eT+f}T^2 + k(eT+f). \tag{5.35}$$

Next, we further simplify V_1 like below

$$V_2 = \frac{1}{k(eT+f)} V_1 = -\frac{af}{kd}\left(\frac{dT}{eT+f}\right)^2 + 1. \tag{5.36}$$

From (5.20), we use $I = dT/(eT+f)$ in V_2 to obtain a I-dependent expression

$$V_2 = -\frac{af}{kd} I^2 + 1. \tag{5.37}$$

According to (5.20) and (5.21), values of equilibrium points $I_{1,2}$ are:

$$I_1 = \frac{1}{2}\left(\frac{(ek+bf) - \sqrt{\Delta}}{af}\right), \qquad I_2 = \frac{1}{2}\left(\frac{(ek+bf) + \sqrt{\Delta}}{af}\right) \tag{5.38}$$

where $I_2 > I_1$ and Δ is given in (5.24). Next, the sign of V_2, which is similar to V_1 and V, has to be checked in the equilibrium points. By substituting the value of I_2, given in (5.38), in V_2, we have

$$V_2(I_2) = -\frac{1}{2fkad}\left[\Delta + (ek+bf)\sqrt{\Delta}\right] \tag{5.39}$$

From the existence criterion of equilibrium points, we know that $\Delta > 0$, and parameters are positive. Therefore, the expression inside bracket of equation above is positive and V_2, V_1 and V are negative for I_2. By reminding that coefficient U is positive, this equilibrium point has one positive eigenvalue and hence, is saddle and unstable. With substituting I_1 in V_2 and using (5.24), we have

$$V_2(I_1) = -\frac{\sqrt{\Delta}}{2fkad}\left[\sqrt{(ek+bf)^2 - 4fkad} - (ek+bf)\right]. \tag{5.40}$$

It can be easily verified that expression inside brackets of equation above is negative, and therefore, V_2, V_1 and V are positive for I_1. Thus, all the eigenvalues in (I_1, T_1) are negative and hence, it is asymptotically stable.

From the linear stability analysis presented above, it is shown that by increasing k from $k < k_-$, a bifurcation occurs at $k = k_-$ which results from coalescence of saddle point (I_2, T_2) and stable node (I_1, T_1). This is called a fold or saddle-node bifurcation (described in section 3.2.1.4). ■

Lemma 5.4 *Model (5.14) for $k > k_+$ has two equilibrium points of type unstable node and saddle.*
Proof. We evaluate linear stability of the model in equilibrium points. For this, it is sufficient to obtain the sign of coefficients U and V in (5.32). Remind that for $k > k_+$, two real equilibrium points exist and the steady state values of $T_{1,2}$ are negative. From (5.20), the equilibrium values of $I_{1,2}$ are positive when $T_{1,2} < 0$. From (5.20), and the fact that $T < 0$, we have

$$T = \frac{k}{b - aI} < 0 \rightarrow b - aI < 0. \tag{5.41}$$

From (5.20), and the fact that $I > 0$ and $T < 0$, we have

$$I = \frac{dT}{eT+f} > 0 \rightarrow eT + f < 0. \tag{5.42}$$

Therefore, coefficient U in (5.32) is negative, and at least one positive eigenvalue exists in both equilibrium points. Next, we check the sign of coefficient V in equilibrium points. From (5.20), we use $T = k/(aI-b)$ in V to obtain I-dependent expression below

$$V = -f(aI-b) + (ad-be)\frac{k}{aI-b}. \tag{5.43}$$

We simplify polynomial V by multiplication with positive expressions. From (5.20), we use $aI-b=-k/T$, which is a positive expression since $T<0$

$$V_2=(aI-b)V=-f(aI-b)^2+(ad-be)\,k=-f\frac{k^2}{T^2}+(ad-be)\,k. \tag{5.44}$$

$$V_3=\frac{T^2}{fk^2}V_2=-1+\left(\frac{ad-be}{fk}\right)T^2. \tag{5.45}$$

The sign of V_3 in (5.45), which is the same as the sign of V in (5.32), is determined by substituting $T_{1,2}$ with their equilibrium values given in (5.23)

$$V_3(T_2)=\frac{1}{4(ad-be)fk}[2\Delta-2\sqrt{\Delta}(ek-bf)] \tag{5.46}$$

By referring to our assumption in (5.3), the sign of V_3 in (5.46) only depends on the sign of the expression inside the brackets. Further, we have considered the case $k>k_+$ in **Lemma 5.4**; therefore, according to (5.27), $(ek-bf)>0$. The fact that we are studying real equilibrium points implies that Δ given in (5.24) is positive. By substituting Δ from (5.24) in (5.46), it is easily verified that V_3, or equivalently, V is positive in (I_2,T_2). By reminding that the coefficient U in (5.32) is also negative for (I_2,T_2), this equilibrium point has only one positive eigenvalue. Hence, (I_2,T_2) is a saddle and unstable equilibrium point.

For (T_1,I_1), we have

$$V_3(T_1)=\frac{1}{4(ad-be)fk}[2\Delta+2\sqrt{\Delta}(ek-bf)] \tag{5.47}$$

By referring to our assumptions in (5.3), and knowing from $k>k_+$ and (5.27) that $(ek-bf)>0$, and the fact that we have real equilibrium points ($\Delta>0$), it is easily verified that V_3 in (5.47), or equivalently, V is positive for (I_1,T_1). By reminding that the coefficient U in (5.32) is negative for (I_1,T_1), therefore, the equilibrium point (T_1,I_1) has two positive eigenvalues and hence, it is unstable node. Note that by decreasing k from $k>k_+$, a bifurcation occurs at $k=k_+$ which is resulted from the coalescence of a saddle and an unstable node. ■

In summary, model (5.14) has either 2 or no equilibrium points dependent on the steady state value of T cell activation (k). According to the bifurcation diagram of the model depicted in **Figure 5.5**, which is obtained by treating k as bifurcation parameter, model (5.14) has no biologically meaningful (positive) equilibrium points for $k>k_-$, with k_- given in (5.17), which corresponds to the unlimited proliferation state of activated T cells. Therefore, condition $k>k_-$ has to be satisfied for initiation of an immune response. However, according to (5.19), the steady state value of T cell activation (k) is

$$k=\frac{\beta N_0}{g+\beta} \tag{5.48}$$

which is limited by rates of naïve T cell renewal (N_0) and Ag-stimulation (β). Therefore, according to (5.48) and the requirement of $k>k_-$ for initiation of a major immune response, there exists an Ag-stimulation range $\beta>\beta_-$, with β_- given in (5.18), in which an immune response is initiated if condition (5.16) is satisfied. Condition (5.16) implies that the renewal rate of naïve T cells plays a critical role for the initiation of immune responses. Without a sufficient renewal rate of naïve T cells, the immune response cannot be initiated by any Ag-stimulation. Instead, Ag-stimulation results in a subcritical immune response which is interpreted as insufficient for pathogen clearance. By increasing the proliferation rate or IL-2 secretion of activated T cells or the renewal rate of naïve T cells, the threshold of Ag-stimulation required for initiation of an immune response is decreased (see equations (5.17) and (5.18)). Therefore,

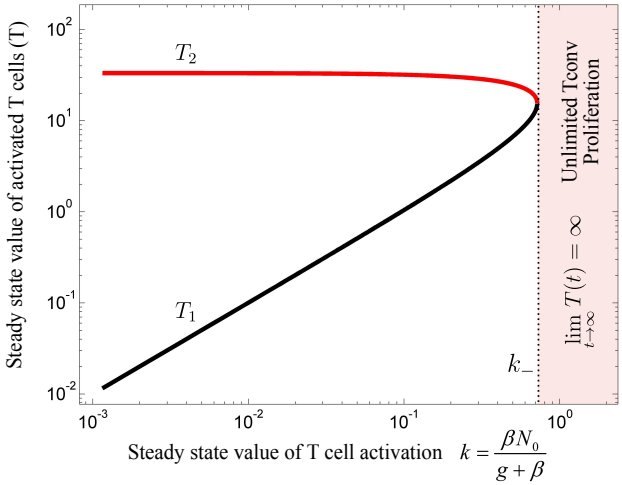

Figure 5.5: Bifurcation diagram of T cell activation model (5.14) by treating k as bifurcation parameter. Stable (node) and unstable (saddle) equilibrium points are shown by black and red lines, respectively. A fold bifurcation at $k = k_-$ occurs which is resulted from coalesce of saddle and stable node. For $k > k_-$, no stable equilibrium point exists and the immune response enters the regime of unlimited T cell proliferation, i.e. $\lim_{t\to\infty} T(t) = \infty$. In the immune system, despite massive T cell proliferation, T cell population is limited to a high cell number. Such saturation cannot be represented by model (5.14). Numerical result is obtained with parameters given in table 5.1.

central tolerance in thymus is able to tune the initiation criterion of self reaction not only by limiting the quality of autoreactive T cells, but additionally by restricting the renewal rate of autoreactive T cells. As central tolerance does not limit nonself-specific T cells, according to the model, these cells exhibit a lower threshold of activation by nonself Ag-stimulation.

5.2.3 T cell fratricide: a mechanism to limit but not to suppress immune responses

The immune response in model (5.14) is characterized by unlimited proliferation of activated T cells which is physiologically unrealistic. The linear death term that represents natural death of activated T cells in model (5.14) is not sufficient to limit cell proliferation. Any other linear death term, such as $\widehat{b}T(t)$, is incorporated to natural cell death rate (b)

$$\dot{T}(t) = aI(t)T(t) - bT(t) - \widehat{b}T(t) + \beta N(t) = aI(t)T(t) - (b+\widehat{b})T(t) + \beta N(t) \tag{5.49}$$

By defining $\bar{b} = b + \widehat{b}$, modified model keeps the structure as is in (5.14). By replacing b with $\bar{b}$ in the analysis given for model (5.14), it is verified that still a saturated T cell level cannot be achieved. Therefore, such saturation requires a nonlinear limiting factor.

A potential mechanism of limiting the immune response is activation-induced cell death (AICD) in activated T cells, known as fratricide [173]. Upon T cell activation, death ligand (FasL) and receptor (Fas) proteins are expressed on the surface of T cells. Followed by expression of these proteins, T cells eliminate themselves in a cell contact-dependent manner. A death mechanism based on cell contacts requires a cell density-dependent death term. If it is assumed that cells are well-mixed in the space and meet randomly, the rate of cell contacts and consequently, fratricide death rate increases if the number (or density) of cells

increases. If the number of cells are doubled, the potential encounter for each cell is doubled. Additionally, the number of cells that can make cell contacts is also doubled. Therefore, the total number of encounters in the system is quadruples. In general, encounter rate of cells is proportional to $T^2(t)$; assuming a constant rate (c) of Fas-mediated fratricide for each cell encounter, the overall rate of cell death is represented by a nonlinear death term $cT^2(t)$ [173]:

$$\begin{aligned}
&\dot{N}(t) = f(N) = N_0 - gN(t) - \beta N(t),\\
&\dot{T}(t) = aI(t)T(t) - bT(t) - cT^2(t) + \beta N(t),\\
&\dot{I}(t) = dT(t) - eI(t)T(t) - fI(t).
\end{aligned} \tag{5.50}$$

In the following, we obtain a proper range for fratricide-associated death rate c, in which a saturated level for the population of activated Tconv is obtained.

Proposition 5.5 *In model (5.50), assume that condition (5.3) is satisfied and $\beta = 0$. There exists a critical value c_- for fratricide-associated death rate, with the following value*

$$c_- = f^{-1}(\sqrt{ad} - \sqrt{be})^2, \tag{5.51}$$

such that for

$$0 < c < c_- \tag{5.52}$$

model (5.50) is bistable with two stable nodes. The larger stable node corresponds to a saturated level for the population of activated Tconv.

Proof. First, we analyze the number and linear stability of equilibrium points of model (5.50) in the case of $\beta = 0$, i.e. no coupling exists between $N(t)$ and the other two variables $T(t)$ and $I(t)$ in (5.50). These equilibrium points are

$$I_1 = 0, T_1 = 0, N_1 = \frac{N_0}{g}, \tag{5.53}$$

$$N_{2,3} = \frac{N_0}{g}, \tag{5.54}$$

$$ceT^2 + (cf + be - ad)T + bf = 0, \begin{cases} T_2 = -\frac{1}{2ce}(-(cf + be - ad) - \sqrt{\Delta}) \\ T_3 = -\frac{1}{2ce}(-(cf + be - ad) + \sqrt{\Delta}) \\ \Delta = (cf + be - ad)^2 - 4cfbe \end{cases} \tag{5.55}$$

$$I_{2,3} = \frac{cT_{2,3} + b}{a}. \tag{5.56}$$

According to (5.55), equilibrium points $T_{2,3}$, if exist, are positive only if

$$cf + be - ad < 0 \rightarrow c < f^{-1}(ad - be) \tag{5.57}$$

Model (5.50) has two different real equilibrium points $T_{2,3}$ when

$$\Delta = (cf + be - ad)^2 - 4cebf = f^2c^2 - 2f(ad + be)c + (ad - be)^2 > 0. \tag{5.58}$$

The above condition is equivalent to the following condition

$$\{c < c_-\} \cup \{c > c_+\} \tag{5.59}$$

where

$$\left[c_- = f^{-1}\left(\sqrt{ad} - \sqrt{be}\right)^2\right] < f^{-1}(ad - be) < \left[c_+ = f^{-1}\left(\sqrt{ad} + \sqrt{be}\right)^2\right] \tag{5.60}$$

Therefore, according to (5.57), (5.59) and (5.60), two positive equilibrium points exist only if

$$0 < c < c_-. \tag{5.61}$$

Next, we assume that the condition (5.61) is satisfied, and we analyze the stability of the equilibrium points. The Jacobian matrix is

$$\mathsf{J} = \begin{pmatrix} -g-\beta & 0 & 0 \\ \beta & aI - b - 2cT & aT \\ 0 & d - eI & -eT - f \end{pmatrix} \tag{5.62}$$

from which the following characteristic equation is obtained

$$\begin{aligned} Q(\lambda) &= \det \begin{pmatrix} \lambda + g + \beta & 0 & 0 \\ -\beta & \lambda - aI + b + 2cT & -aT \\ 0 & -d + eI & \lambda + eT + f \end{pmatrix} \\ &= (\lambda + g + \beta)(\lambda^2 + U\lambda + V) \end{aligned} \tag{5.63}$$

where

$$U = eT + f + b - aI + 2cT, \quad V = -afI + 2ceT^2 + beT + bf + 2cfT - adT. \tag{5.64}$$

All the equilibrium points have a negative real eigenvalue $\lambda = -g - \beta$. For determining the type of other eigenvalues, the sign of coefficients U and V in (5.64) has to be checked in equilibrium points. These coefficients are positive for (N_1, T_1, I_1) and therefore, all eigenvalues have negative real values. Hence, (N_1, T_1, I_1) is asymptotically stable. For stability analysis of other equilibrium points, the sign of U and V in (5.64) has to be analyzed. We use $b - aI = -cT$ from (5.56) in U

$$U = eT + f + cT. \tag{5.65}$$

According to (5.65), coefficient U is positive for positive equilibrium points ($T_{2,3} > 0$). Therefore, the stability depends on the sign of V in (5.64). We use $b - aI = -cT$ from (5.56) in V

$$V = ceT^2 + \left[ceT^2 + (cf + be - ad)\,T + bf\right] - bf = ceT^2 - bf. \tag{5.66}$$

According to (5.55), the expression inside the brackets of equation above is zero. Then, V is simplified to

$$V = ceT^2 - bf. \tag{5.67}$$

We evaluate coefficient V at equilibrium point T_3 given in (5.55)

$$V(T_3) = \frac{\sqrt{\Delta}}{2ce}\left(\sqrt{\Delta} - (cf + be - ad)\right), \tag{5.68}$$

where Δ, given in (5.57), is positive since we are considering the case that real equilibrium points exist by assuming (5.61). According to (5.57), it is verified that V in (5.68) is positive and hence, equilibrium point (N_3, T_3, I_3) is a stable node. Next, we evaluate the sign of coefficient V for T_2

$$V(T_2) = \frac{\sqrt{\Delta}}{2ce}\left(\sqrt{\Delta} + (cf + be - ad)\right) \tag{5.69}$$

According to (5.57), and by replacing Δ from (5.55), it is verified that the sign of V for T_2 is negative. By reminding that the sign of coefficient U in (5.63) for (N_2, T_2, I_2) is positive, this equilibrium point has one eigenvalue with positive real part, and therefore, it is a saddle point and unstable. Note that the value of stable node T_3 is larger that saddle T_2. Now that the stability of equilibrium points is revealed, the bifurcation that occurs at c_- by increasing the fratricide death rate c from $c < c_-$, is of type fold which is resulted from the coalescence of a saddle (T_2) and an stable node (T_3). Note that since the aim of introducing fratricide death mechanism is to have a saturated population for activated Tconvs, we have to assume a fratricide death rate in the range given in (5.52), where the model (5.50) is bistable. ■

The equilibrium points of the model with $\beta > 0$ and by considering $\beta N(t) = k(t)$ are obtained by solving:

$$-ceT^3 - (cf + be - ad)\,T^2 + (ek - bf)\,T + kf = 0, \tag{5.70a}$$

$$I = \frac{dT}{eT + f}. \tag{5.70b}$$

By keeping our assumptions (5.3) and (5.61), the equation (5.70a) has either one positive real equilibrium point or three positive real equilibrium points depending on the value of k. The stability of equilibrium points that are obtained from (5.70a) and (5.70b) by varying the value of k is hard to be checked analytically; instead, it is analyzed numerically by obtaining eigenvalues from characteristic equation (5.63) for equilibrium points.

In summary, model (5.50) for $\beta = 0$ has either 3 or 1 equilibrium points, depending on the value of fratricide death rate c. The bifurcation diagram of the model (5.50) with respect to c is depicted in **Figure 5.6A** for $\beta = 0$. When c satisfies (5.52), the stable node (T_3) exists that corresponds to a saturated population of activated Tconv. When the conditions (5.3) and (5.52) are fulfilled, the model (5.50) exhibits the bifurcation diagram plotted in **Figure 5.6B** with respect to the steady state value of T cell activation k. The fratricide mechanism added a large stable node (T_3) to the model which imposes a saturation level to the activated T cell population. The larger the c, the smaller the saturated population of activated T cells is. Similar to model (5.14), model (5.50) shows an initiation threshold of the immune response ($k > k_i$). Despite solving the issue of unlimited proliferation of activated T cells by the fratricide mechanism, model (5.50) bears a hysteresis characteristic so that the immune response cannot be suppressed when Ag-stimulation (β) is removed.

5.2.4 Dynamic interplay of activated conventional and regulatory T cells

Tregs are essential in maintaining self-tolerance and immune homeostasis by preventing autoimmunity and limiting chronic inflammation in the periphery. However, they might also limit beneficial responses by inducing tolerance to pathogens [174, 175] or limiting anti-tumor immunity [176, 177]. One functional role of Tregs is to shut down the cell-mediated immune response via cell contact-dependent and inhibitory cytokine-driven suppression of activated T cells [178]. As an extension for model (5.50) in which immune response is not suppressed after resolving Ag-stimulation, we add Treg population for immune suppression. Two different subsets of Tregs were identified. Natural Tregs are the dominant subset of peripheral Tregs [179] and are selected in the thymus. In our model, we consider only natural Tregs and neglect the induced Treg subset that differentiates from naïve T cells. Like for naïve T cells, the thymus contributes to the renewal of resting Treg pool ($\widehat{N}$) by continuously selecting them from self-reactive thymocytes. The renewal of resting Tregs is assumed to occur with rate $\widehat{N}_0$. Our aim is to obtain the size of Treg population (Treg selection or renewal rate) such that immune activation to foreign and self antigens are allowed, but is tightly restricted for self antigens. We choose the relative renewal of resting Tregs and naïve T cells as the parameter of interest. We assume that

$$\widehat{N}_0 = \lambda N_0. \tag{5.71}$$

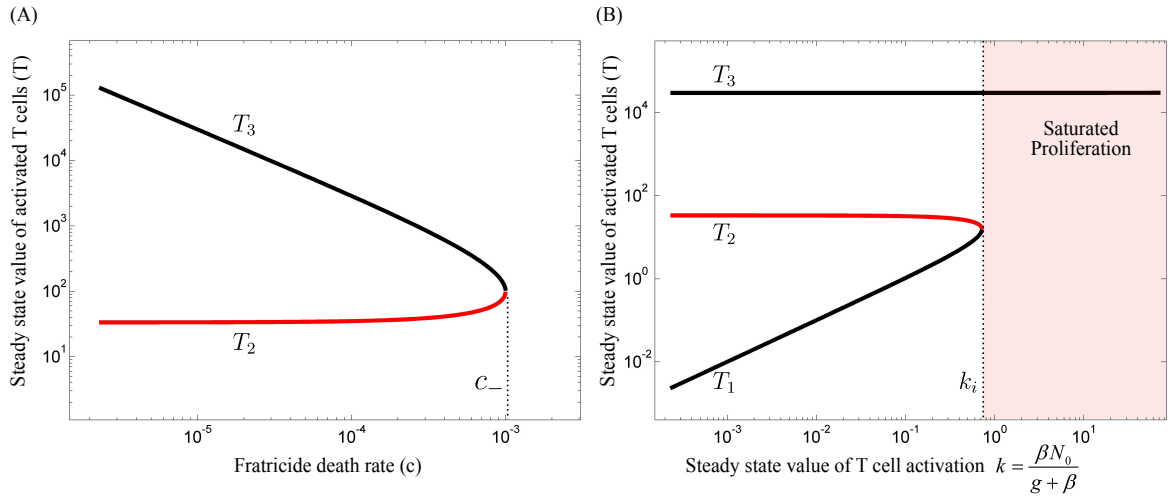

Figure 5.6: Fratricide mechanism. (A) Bifurcation diagram of model (5.50) with $\beta = 0$ using the fratricide death rate c as bifurcation parameter. A fold bifurcation occurs at $c = c_-$. No immune response exists for fratricide death rates larger than c_- due to extensive activation-induced cell death. The trivial equilibrium point ($T_1 = 0$) of type stable node is omitted in this figure. (B) Bifurcation diagram of model (5.50) using k as bifurcation parameter. A fold bifurcation occurs at $k = k_i$. An immune response can be initiated for large values of k ($k > k_i$). However, due to hysteresis characteristic in this model, the immune response is not suppressed after decreasing T cell activation (k). Stable and unstable equilibrium points are shown by black and red lines, respectively. Numerical results are obtained with parameters given in table 5.1.

Tregs remain in the resting state until they are stimulated by Ag (β) and become activated in a TCR-dependent manner. The dynamic population of the resting Treg compartment is assumed to be the same as the naïve T cell compartment in (5.14) and (5.50) ($\mathrm{d}\widehat{N}/\mathrm{d}t = f(\widehat{N})$). Activated Tregs ($R$) are assumed to suppress activated T cells (by rate γ). Survival and proliferation of activated Tregs depends strictly on IL-2, produced by activated non-Tregs [165, 180, 181]. The IL-2 dependent proliferation rate of Tregs is considered as a linear function of IL-2 (a nonlinear case will be given in section 5.2.5). In contrast to activated T cells, activated Tregs lack the ability to secrete IL-2 [182]. The relative proliferation rate of activated Tregs and activated T cells is controlled by the parameter ϵ:

$$\begin{aligned}
\dot{N}(t) &= \lambda N_0 - gN(t) - \beta N(t),\\
\dot{\widehat{N}}(t) &= \lambda N_0 - g\widehat{N}(t) - \beta\widehat{N}(t),\\
\dot{T}(t) &= aI(t)T(t) - bT(t) - cT(t)^2 - \gamma R(t)T(t) + \beta N(t),\\
\dot{R}(t) &= \epsilon aI(t)R(t) - bR(t) + \beta\widehat{N}(t),\\
\dot{I}(t) &= dT(t) - eI(t)\left(T(t) + R(t)\right) - fI(t).
\end{aligned} \tag{5.72}$$

The description and values of model parameters are given in **Table 5.1** and the model components are illustrated in **Figure 5.3**. We define Treg activation $\widehat{k}(t)$ as

$$\widehat{k}(t) = \beta\widehat{N}(t) \tag{5.73}$$

and indicates to the rate of resting Treg activation by Ag-stimulation (β) per unit of time. According to (5.48) and (5.71), the steady state value of Treg activation ($\widehat{k}$) is given by

$$\widehat{k} = \lambda \frac{\beta N_0}{g+\beta} = \lambda k. \tag{5.74}$$

Model (5.72) for $\beta N(t) = k(t) = 0$ has five equilibrium points with following values:

$$(T_1, I_1, R_1, N_1) = \left(0, 0, 0, \frac{N_0}{g}\right) \tag{5.75}$$

$$T_{2,3} : ceT_{2,3}^2 + (cf - ad + be)T_{2,3} + bf = 0, I_{2,3} = \frac{dT_{2,3}}{eT_{2,3}+f}, R_{2,3} = 0, N_{2,3} = \frac{N_0}{g} \tag{5.76}$$

$$T_4 = \frac{b(eR_5+f)}{\epsilon ad - be}, I_4 = \frac{b}{\epsilon a},$$
$$R_4 = \left(\frac{b}{\epsilon}\right)\left(\frac{-\epsilon(cf+be-ad)+be(\epsilon-1)-\epsilon(\epsilon ad-be)}{cbe+\gamma(\epsilon ad-be)}\right), N_4 = \frac{N_0}{g} \tag{5.77}$$

$$T_5 = 0, I_5 = \frac{b}{\epsilon a}, R_5 = \frac{-f}{e}, N_5 = \frac{N_0}{g} \tag{5.78}$$

For resting Treg population, steady state values are $\widehat{N}_i = \lambda N_i$ for $i \in \{1, \cdots, 5\}$. The sign of the equilibrium point T_4 changes by changing the Treg-associated parameters (ϵ,γ). T_4 is positive if

$$\epsilon ad - be > 0, R > -\frac{f}{e} \tag{5.79}$$

or

$$\epsilon ad - be < 0, R < -\frac{f}{e} \tag{5.80}$$

The physiologically relevant regime of the model occurs by satisfying condition (5.79) which means positive R_4 is allowed.
The equilibrium points of model (5.72) for $\beta N(t) = k(t) \neq 0$ can be obtained from the following

$$N = \frac{\beta N_0}{g+\beta} \tag{5.81}$$

$$R = \frac{-\lambda k}{\epsilon aI - b} \tag{5.82}$$

$$T = \frac{-I(-e\lambda k + f\epsilon aI - bf)}{(\epsilon aI - b)(-d+eI)} \tag{5.83}$$

$$P_5 I^5 + P_4 I^4 + P_3 I^3 + P_2 I^2 + P_1 I + P_0 = 0 \tag{5.84}$$

where

$$P_5 = a^3 f \epsilon^2 e \tag{5.85}$$

$$P_4 = -bf\epsilon^2 a^2 e + cf^2\epsilon^2 a^2 - k\epsilon^2 a^2 e^2 - a^3 f\epsilon^2 d - 2\,a^2 f\epsilon\, be - a^2 e^2 \lambda\, k\epsilon \tag{5.86}$$

$$P_3 = be^2\lambda\, k\epsilon\, a - 2\,cf^2\epsilon\, ab + ae^2\lambda\, kb + 2\,a^2 f\epsilon\, bd + \gamma\,\lambda\, kf\epsilon\, ae + ab^2 fe + bf\epsilon^2 a^2 d$$
$$+ 2\,k\epsilon^2 a^2 de - 2\,ce\lambda\, kf\epsilon\, a + 2\,b^2 f\epsilon\, ae + a^2 e\lambda\, k\epsilon\, d + 2\,k\epsilon\, abe^2 \tag{5.87}$$

$$P_2 = 2\,ce\lambda\, kbf - 4\,k\epsilon\, abde - \gamma\,\lambda\, kbfe - b^2 e^2\lambda\, k - kb^2 e^2 - be\lambda\, k\epsilon\, ad - b^3 fe - ae\lambda\, kbd + cb^2 f^2$$
$$+ ce^2\lambda^2 k^2 - ab^2 fd - k\epsilon^2 a^2 d^2 - \gamma\,\lambda^2 k^2 e^2 - 2\,b^2 f\epsilon\, ad - \gamma\,\lambda\, kf\epsilon\, ad \tag{5.88}$$

$$P_1 = \gamma\,\lambda^2 k^2 ed + b^2 e\lambda\, kd + 2\,kb^2 de + 2\,k\epsilon\, abd^2 + b^3 fd + \gamma\,\lambda\, kbfd \tag{5.89}$$

$$P_0 = -kb^2 d^2 \tag{5.90}$$

Table 5.1: Parameters of immune activation model.

Parameter	Value	Description	Dimension
a	0.4	Proliferation rate of activated T cells	molecule^{-1}time^{-1}
b	0.1	Natural death rate of activated T cells and Tregs	time^{-1}
c	10^{-5}	Fratricide death rate of activated T cells	cell^{-1}time^{-1}
d	0.01	IL-2 secretion rate by activated T cells	molecule cell^{-1}time^{-1}
e	0.01	IL-2 consumption rate by activated T cells and Tregs	cell^{-1}time^{-1}
f	1	IL-2 decay rate	time^{-1}
g	b	Natural death rate of naïve T cells and resting Tregs	time^{-1}
β	$[0, \infty)$	Ag-stimulation of naïve T cells and resting Tregs	time^{-1}
γ	0.1	Treg-mediated suppression rate	cell^{-1}time^{-1}
ϵ	0.6	Proliferation rate ratio Treg / Tconv	-
N_0	4	Renewal rate of naïve T cells	cell time^{-1}
λ	0.006 0.02	ratio of renewal rate of resting Tregs to naïve T cells $\widehat{N}_0/N_0$	-
$\widehat{N}_0$	λN_0	Renewal rate of resting Tregs	cell time^{-1}

Parameters are chosen arbitrarily according to conditions given in (5.3), (5.52) and (5.79). Any other parameters choice that satisfies these conditions results in similar qualitative behaviors shown for the proposed models.

By incorporating the Treg compartment to model (5.50), two additional equilibrium points (T_4 and T_5) emerged for $\beta = 0$. The equilibrium point of interest (T_4), which depends on the Treg-associated parameters (ϵ,γ), has an impact on the topology of the phase portrait under variations of bifurcation parameter k. The value of ϵ and γ are assumed to be in a range where the model does not inherit the hysteresis characteristics of immune responses from model (5.50) in which the immune response is not suppressed after resolving Ag-stimulation (β). Then, the bifurcation diagrams of model (5.72) for two different values of λ are obtained by treating k as the bifurcation parameter (**Figure 5.7**). Depending on the value of k, the model has either 5 or 3 equilibrium points (positive and negative).

By varying the relative renewal rates of resting Tregs and naïve T cells (λ in (5.71)) a λ_{th} can be found, such that for $\lambda > \lambda_{\text{th}}$, no immune response can be initiated for any value of k (**Figure 5.7A**). For $\lambda < \lambda_{\text{th}}$ (**Figure 5.7B**), there exists a T cell activation threshold (k_i) such that for $k > k_i$ the major immune response can be initiated. However, in contrast to model (5.50), the immune response is completely suppressed by activated Tregs if k decreases to a lower value than k_i (grey region in **Figure 5.7B**). For persistent Ag-stimulation with $k > k_i$, two scenarios are possible. An oscillating immune response is induced when k remains in the range of $k_i < k < k_s$ (red region in **Figure 5.7B**). For $k > k_s$ the immune response is suppressed after its initiation to a minor immune response, with an activated T cell population T_4, due to over-suppression of activated T cells by over-activation of Tregs (magenta region in **Figure 5.7B**). In the latter case ($k > k_s$), despite proper T cell stimulation, only a minor immune response is induced (and antigen is not cleared). Instead a chronic co-existence of antigen and inefficient immune activity is established. Therefore, according to the model, a range of T cell and Treg activation ($k_i < k < k_s$) exists in which an efficient immune response is induced. Outside of this range, the antigen persists because of under-stimulation of naïve T cells, or over-stimulation of Tregs. According to (5.48), the

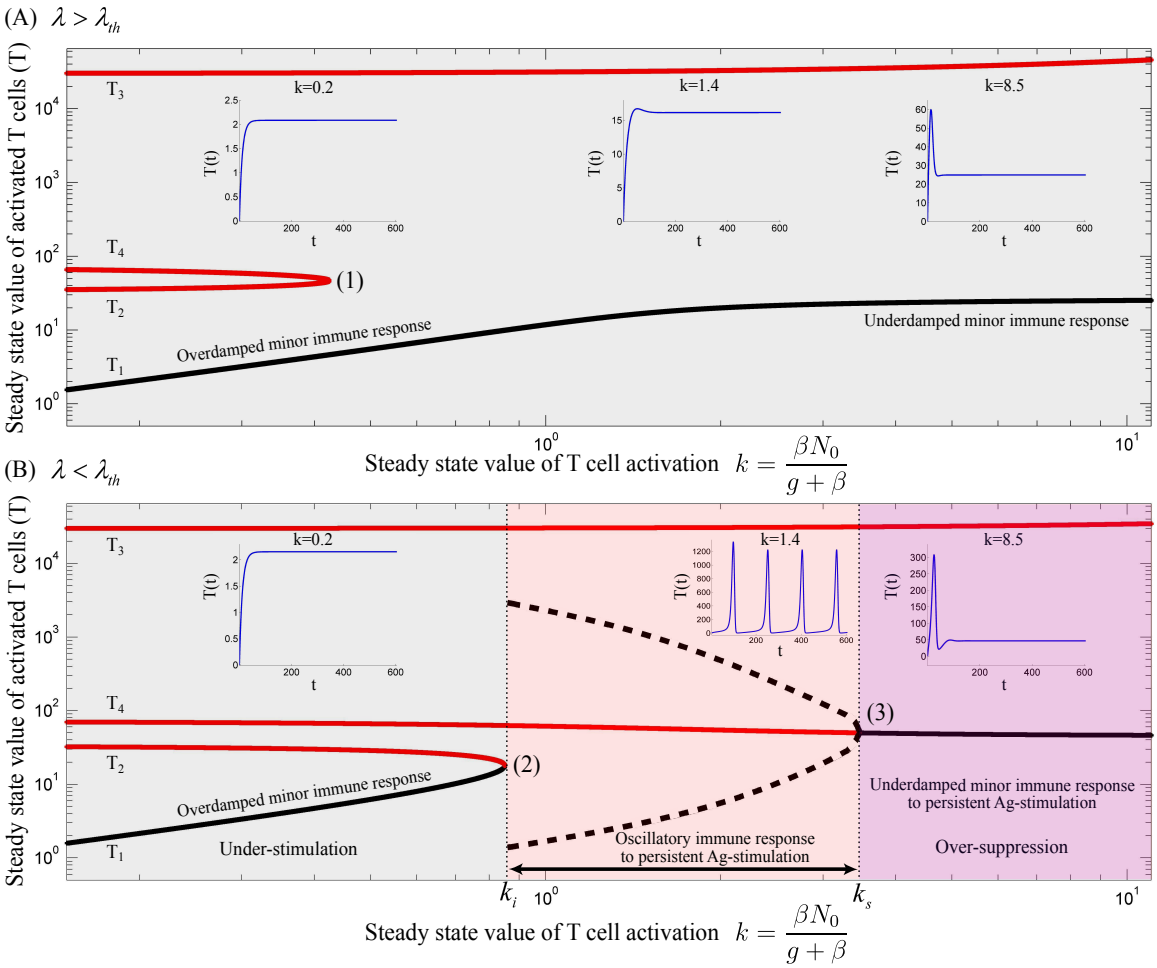

Figure 5.7: Bifurcation diagram of Treg-Tconv model (5.72) using k and λ as the bifurcation parameter with (A) $\lambda = 0.02$ and (B) $\lambda = 0.006$. Stable and unstable equilibrium points are drawn by black and red solid lines, respectively. Dashed black lines represent the stable limit cycles by showing the maximum and minimum populations of oscillating activated T cells for persistent k. Depending on the values of λ and k, an immune response is not initiated (grey), is initiated (red) or over-suppressed (magenta). With parameter values given in Table 5.1, $\lambda_{\rm th} = 0.01183$. The time-courses of the activated T cell population $T(t)$ were deduced from a numerical solution (using $4^{\rm th}$ order explicit Runge-Kutta method) of model (5.72) with zero initial conditions and persistent β. The unstable negative equilibrium point (T_5) is not shown in the plots. In critical point (1), a bifurcation occurs by coalescence of two saddle points. In point (2), a fold bifurcation occurs resulting from coalescence of the saddle and stable node. In point (3), an Andranov-Hopf (subcritical Hopf) bifurcation occurs by which the stable limit cycle disappear by increasing k. Only in case of $\lambda < \lambda_{\rm th}$, a major immune response can potentially arises (k_i exists); however, the actual initiation of major immune response depends on N_0, or equivalently, the homeostatic population of naïve T cells. By choosing different values of N_0 for self versus nonself, the Ag-stimulation (β) requires for starting immune response against self versus nonself can be tuned.

existence of Ag-stimulation thresholds β_i and β_s which correspond to the values of k_i and k_s, respectively, depends on the renewal rate of naïve T cells (N_0); β_i exists if $N_0 > k_i$ and β_s exists if $N_0 > k_s$. Increasing the renewal rate of naïve T cells reduces the Ag-stimulation required for initiation(β_i)/over-suppression(β_s) of the immune response.

The peak immune response depends on the value of the Treg-associated equilibrium point (T_4) which in turn depends on Treg-associated parameters. However, the fratricide-associated equilibrium point (T_3) is a limiting factor for the maximum population of activated T cells if the fratricide death rate (c) is sufficiently high.

According to our model, sufficient activated Tregs are required to suppress the proliferative response of activated T cells. These are supplied by two processes: Treg activation ($\widehat{k}$) which depends on Ag-stimulation (β), and Treg proliferation which depends on the IL-2 secretion by activated T cells. With a low Ag-stimulation and insufficient Treg activation ($\widehat{k} = \beta\widehat{N}$), Treg proliferation has to account for immune suppression. Since Treg proliferation is dependent on the availability of IL-2, sufficient activated T cells are required to secrete IL-2 and induce immune suppression. Therefore, activated T cells undergo the proliferation up to a level that sufficient IL-2 is available for Treg proliferation and subsequent immune suppression. In contrast, by facilitated Treg activation ($\widehat{k}$), less Treg proliferation is required for suppressing activated T cells which means that the dependency of immune suppression on proliferation of activated T cells decreases. Consequently, by increasing Ag-stimulation (β) in the range of $\beta_i < \beta < \beta_s$ (red region in **Figure 5.7B**), Treg activation ($\widehat{k}$) increases as well which results in a reduced maximum population of activated T cells (**Figure 5.7B**, dashed black line) and an increased frequency of oscillations. By further increasing Ag-stimulation to $\beta > \beta_s$ (magenta region in **Figure 5.7B**), Treg activation ($\widehat{k}$) completely prevent oscillating immune response.

In the same way, by increasing the relative homeostatic population of resting Tregs and naïve T cells ($\lambda > \lambda_{\text{th}}$), Treg activation increases up to a level that Treg suppression does not depend on the proliferative response of activated T cells. Thus, activated T cells are not able to enter the massive proliferation for any Ag-stimulation level, as shown in **Figure 5.7A**. Similar results can be derived from a model that considers a nonlinear IL-2 dependent proliferation rate of activated T cells and Tregs, which is presented in the next section.

5.2.5 Nonlinear proliferation rate of conventional and regulatory T cells

In the models (5.1), (5.14), (5.50), and (5.72) it is assumed that proliferation rate of Tconvs and Tregs is a linear function of IL-2. In the biological context, IL-2-dependent proliferation of Tconvs and Tregs may not be linear, and may require a critical IL-2 level for effective proliferation. In previous models, a linear IL-2-dependent proliferation is assumed in order to allow parametric stability analysis of the model in a closed form and to find explicitly the dependency between parametric variations and topological changes of the model. Here, we show that our simplifying assumption does not affect the three regimes of qualitative immune responses that could be derived from the model. Therefore, the linear IL-2-dependent proliferation rate is replaced with a nonlinear function of IL-2, named $\Phi(I)$ in models (5.1), (5.14) and (5.72)

$$\begin{aligned} \dot{T}(t) &= \Phi\left(I(t)\right) T(t) - bT(t) + k(t), \\ \dot{I}(t) &= dT(t) - eI(t)T(t) - fI(t) \end{aligned} \tag{5.91}$$

where $\Phi\left(I(t)\right)$ is considered as a Hill function of IL-2

$$\Phi\left(I(t)\right) = a\frac{I^n(t)}{h^n + I^n(t)}. \tag{5.92}$$

With choosing proper parameters n and h in (5.92), requiring a critical level of IL-2 for effective proliferation can be imposed to the model. The models (5.1) and (5.91) are compared by steady state analysis. The

equilibrium points of the modified model (5.91) (with $k = \frac{\beta N_0}{g+\beta} = 0$) are

$$(I_1, T_1) = (0, 0), \tag{5.93}$$

$$(I_2, T_2) = \left(h \left(\frac{b}{a-b} \right)^{\frac{1}{n}}, \frac{fI_2}{d - eI_2} \right). \tag{5.94}$$

The nontrivial equilibrium point (I_2, T_2) is positive and biologically meaningful only if

$$(a-b)d^n - be^n h^n > 0. \tag{5.95}$$

The local stability of the equilibrium points can be determined by obtaining the eigenvalues from the characteristic equation

$$Q(\lambda) = \det \begin{pmatrix} \lambda - a\frac{I^n}{h^n+I^n} + b & -aT\frac{nh^n I^{n-1}}{(h^n+I^n)^2} \\ -d + eI & \lambda + eT + f \end{pmatrix} = \lambda^2 + \left[eT + f - a\frac{I^n}{h^n + I^n} + b \right] \lambda$$
$$+ \left[\left(-a\frac{I^n}{h^n + I^n} + b \right) (eT + f) + aT\frac{nh^n I^{n-1}}{(h^n + I^n)^2} (-d + eI) \right] = 0 \tag{5.96}$$

By checking Routh-Hurwitz stability criterion, it can be easily confirmed that the eigenvalues have negative real parts for trivial equilibrium point since all the coefficients of polynomial $Q(\lambda)$ are positive, and hence, the trivial equilibrium point (I_1, T_1) is asymptotically stable. For checking the stability of the non-trivial equilibrium point, the characteristic equation (5.96) is evaluated in (I_2, T_2)

$$Q(\lambda, I_2, T_2) = \lambda^2 + U\lambda + V = 0 \tag{5.97}$$

where

$$U = eT_2 + f, \quad V = -\frac{nbh^n T_2}{I_2(h^n + {I_2}^n)}(d - eI_2). \tag{5.98}$$

By assuming that condition (5.95) is satisfied, the coefficients U and V in (5.97) are positive and negative respectively. Therefore, there exists an eigenvalue with positive real part, and consequently, nontrivial equilibrium point (I_2, T_2) is a saddle point and unstable.

Similar to the model (5.1), the stable manifold of saddle point in the model (5.91) defines a threshold for initial conditions that allow for unlimited proliferation of activated T cells. By comparing the conditions (5.95) and (5.3), the dependencies of these conditions to the model parameters, specifically the proliferation rate (a) and IL-2 secretion rate (d), are positively correlated. In other words, in both models, only T cell clones with sufficiently high proliferation rate (a) and/or high IL-2 secretion rate (d) are able to undergo major T cell proliferation.

For $k \neq 0$, the equilibrium points of the model (5.91) are obtained from the following equations

$$T = \frac{fI}{d - eI}, \tag{5.99}$$

$$[(a-b)f - ke]\, I^{n+1} + [kd]\, I^n - [h^n(bf + ke)]\, I + kdh^n = 0. \tag{5.100}$$

The stability of equilibrium points is analyzed by evaluating the characteristic equation and is shown in **Figure 5.8** for parameter values given in **Table 5.1** and Hill-function parameters $n = 2$ and $h = 0.5$. By comparing the bifurcation diagram in **Figure 5.8** and **Figure 5.5**, the qualitative similarity between model (5.14) and (5.91) is evident. This qualitative similarity also holds true between model (5.72) and the following model

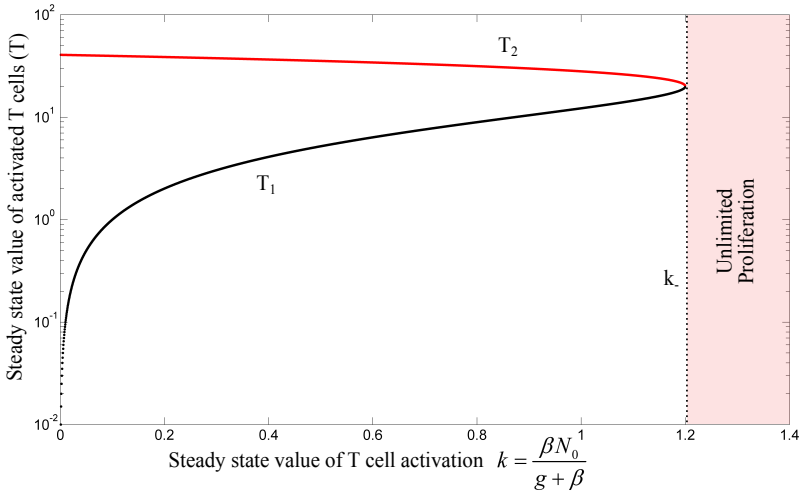

Figure 5.8: Bifurcation diagram of T cell activation model (5.91) with nonlinear proliferation rate. Hill-function parameters are $n = 2$ and $h = 0.5$. k is treated as bifurcation parameter. Stable and unstable equilibrium points are shown by black and red lines, respectively. For $k > k_{-}$, the immune response enters the regime of unlimited proliferation. The unstable negative equilibrium point is omitted in this figure.

$$\begin{aligned}
\dot{T}(t) &= \Phi\left(I(t)\right) T(t) - bT(t) - cT^2(t) - \gamma R(t)T(t) + k(t),\\
\dot{R}(t) &= \epsilon\Phi\left(I(t)\right) R(t) - bR(t) + \widehat{k}(t),\\
\dot{I}(t) &= dT(t) - eI(t)\left(T(t) + R(t)\right) - fI(t)
\end{aligned} \tag{5.101}$$

where $\Phi\left(I(t)\right)$ is identical to (5.92).

The equilibrium points of model (5.101) are calculated and their stability is analyzed by deriving the characteristic equation of the model and obtaining the eigenvalues. By keeping assumption (5.71), the bifurcation diagrams of model (5.101) for two different values of λ are obtained by treating $k = \frac{\beta N_0}{g+\beta} > 0$ as the bifurcation parameter (depicted in **Figure 5.9**). Depending on the value of k, the model has either 8 or 6 equilibrium points (4 or 2 equilibrium points with $T > 0$, identical to model (5.72)) with parameter values given in **Table 5.1** and Hill-function parameters $n = 4$ and $h = 1$. The additional equilibrium points resulted from considering the Hill-function nonlinearity are all in the negative space of the model variables. As it can be seen from **Figure 5.9**, similar to the model (5.72), the three qualitatively different responses still could be derived from the modified model. It is clear that the value of k_i, k_s and λ_{th} are different from their corresponding values in the model (5.72).

In summary, imposing the nonlinear IL-2 dependent proliferation rate of cells results in a more restricted condition for initiation of an immune response in comparison to the linear IL-2 dependent proliferation rate, namely the requirement of higher T cell avidity (higher a and d), higher Ag-stimulation (increased β_i) and lower Treg/Tconv ratio (lower λ_{th}); but three qualitatively different immune reactions depending on the critical levels of Ag-stimulation could still be derived, very similar to model (5.72).

5.3 Discussion

In this study, a model of the dynamic interplay between effector and regulatory immune responses was examined to investigate the requirements for the initiation of an immune response by Ag-stimulation. The

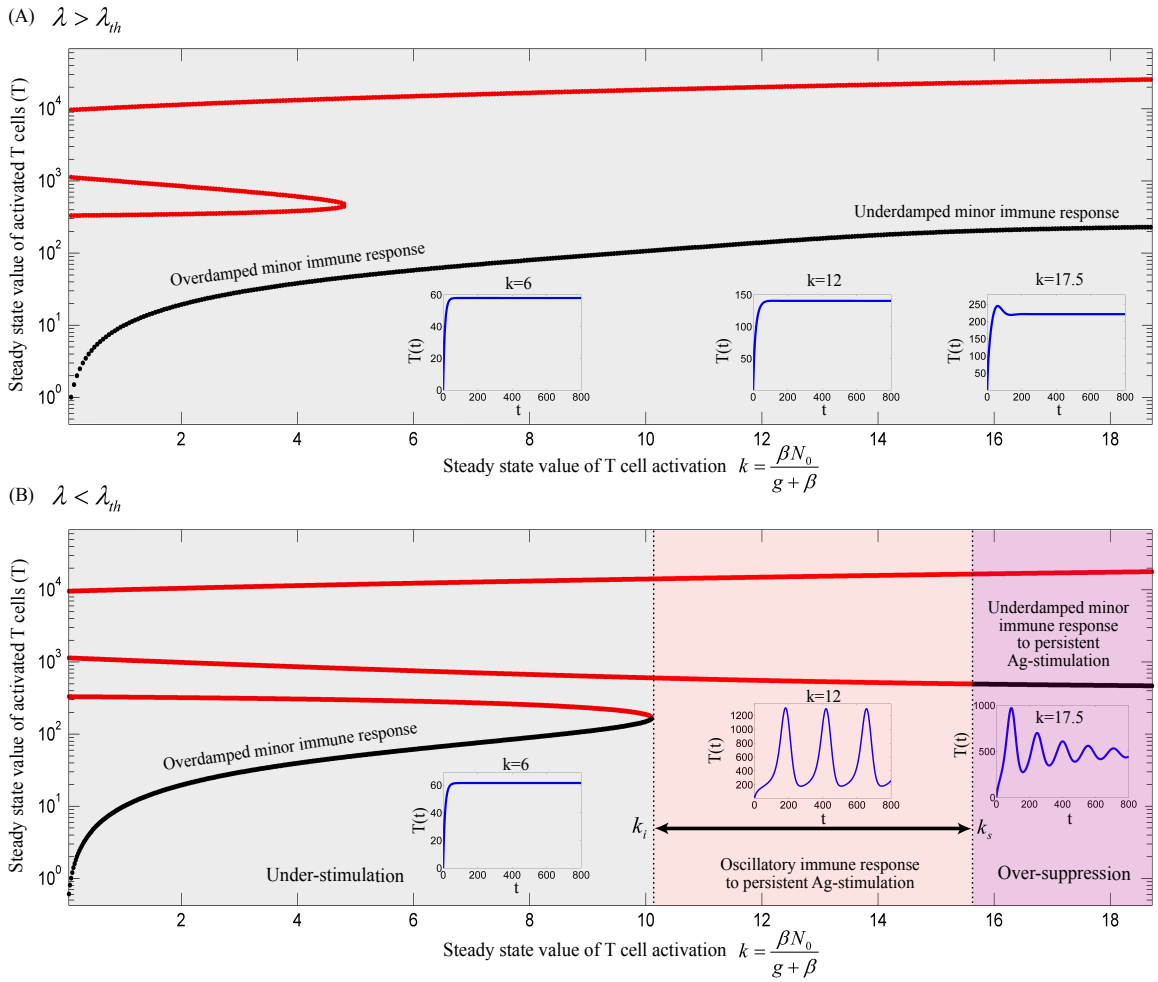

Figure 5.9: Bifurcation diagram of Treg-Tconv model (5.101) with with nonlinear proliferation rate. Hill-function parameters are $n = 4$ and $h = 1$. k and λ are treated as bifurcation parameters with (A) $\lambda = 0.0016$ and (B) $\lambda = 0.0008$. Stable and unstable equilibrium points are drawn by black and red solid lines, respectively. The stable limit cycles are not shown for all value of $k_i < k < k_s$ except for $k = 12$. Depending on the values of λ and k, an immune response is not initiated (grey), is initiated (red) or over-suppressed (magenta). With parameter values given in Table 5.1 and Hill-function parameters $n = 4$ and $h = 1$, the threshold becomes $\lambda_{\rm th} = 0.00111$. The time-courses of the activated T cell population $T(t)$ were deduced from a numerical solution of model (5.101), by using $4^{\rm th}$ order explicit Runge-Kutta method, with zero initial conditions and persistent β. The negative equilibrium points which are all unstable are not shown in the plots.

model unifies several components developed in previous studies, such as IL-2 dependent proliferation of T cells [20], fratricide-induce programmed cell death [173], IL-2 competition between activated T cell and activated Tregs [25], and Treg-mediated immune suppression [25, 27, 161]. Homeostatic division of T cell compartments was not considered in the present study, such that the main renewal source of T cells in the absence of Ag-stimulation is the thymus. While the presented model is still simplifying the real situation in many aspects, the stability analysis revealed a number of reasonable results matching many experimental findings and allowing for an analysis of reasons for immune failure and autoimmunity.

The model predicts three qualitatively different immune responses depending on the level of antigenic stimulation. At first, a threshold stimulation β_i is required in order to get an immune response at all. Secondly, in a limited range of Ag-stimulation $\beta \in (\beta_i, \beta_s)$ an efficient immune response is induced. Tregs limit the duration of the immune response. If the antigen was cleared by the first immune response, further immune activity would be suppressed by Tregs. However, if the first peak of the immune response fails to clear the antigen, but keeps the antigen in the stimulation range $\beta_i < \beta < \beta_s$, the immune system attempts to clear the antigen with subsequent immune responses, which corresponds to the oscillatory solution depicted in **Figure 5.7B**. If the immune response failed to control the antigen spread, antigenic stimulation would be further increased to $\beta > \beta_s$, leading to the third class of immune responses. Tregs are over-stimulated and suppress immune activity. In this situation, a chronic persistence of the antigen would develop. Treg-mediated over-suppression of immune responses in chronic infections is well-established (reviewed in [183]). According to our model, depletion of resting Tregs restores the immune response by transiently decreasing λ and by this increasing β_s. This notion is consistent with the experimental model of chronic infections according to which depletion of Tregs results in the restoration of effector immune response and restriction of antigen spread [184, 185]. A key feature of our model is that the immune response does not rely on a stable equilibrium point with a dominant population of activated T cells which is typically derived from existing bistable models. It rather relies on a transient response (or stable limit cycles in the case of persistent Ag-stimulation) which originates from T-cell-mediated suppression and IL-2 consumption by Tregs. Moreover, the role of Tregs in the chronic state of the immune response is not represented by available models.

According to our model, the qualitatively different immune responses and their requirements are dependent on the quality and quantity of Tconv and Treg clones responding to the Ag-stimulation. The proliferation rate of activated T cells, which depends on their avidity to the stimulating antigen determines the existence of an Ag-stimulation threshold (β_i) which is required for the initiation of an immune response. The absolute renewal rate of naïve T cells (N_0) adjusts the Ag-stimulation threshold β_i, which exists when the renewal rate of resting Tregs remains below a threshold value ($\lambda < \lambda_{\mathrm{th}}$). Further Treg-associated parameters, namely the proliferation rate of Tregs (ϵ) and the Treg-mediated suppression rate (γ), also affect the existence and the level of the Ag-stimulation required for initiation (β_i) and over-suppression (β_s) of immune responses. By increasing the proliferative (ϵ) and suppressive (γ) activity of Tregs, β_i increases, whereas β_s decreases up to a level where the initiation of an immune response is completely impossible for any Ag-stimulation. Interestingly, when proliferation rate of activated Tregs exceeds the one for activated T cells ($\epsilon > 1$) a massive proliferation of activated T cells is still required for subsequent immune suppression by Tregs. Thus, IL-2 secretion by sufficiently large numbers of activated T cells is a strict requirement for immune suppression. Note also that without Tregs, a return to the homeostatic state is not possible, even when the antigen was cleared.

Considering all aforementioned parameters controlling the initiation of an immune response, is it beneficial for the immune system to completely avoid self reaction, or is there a benefit in allowing self reaction? Clearly, autoreactive T cells exist in the periphery of healthy individuals as a normal component of the T cell repertoire [152, 155, 186, 187]. These cells respond to self-tissue destruction even in the presence of Tregs and without genetic predisposition to autoimmunity [154]. Although the activation of autoreactive T cells has been shown to be involved in autoimmunity [152], several lines of evidences indicate that these cells are required for limiting self-destruction by supporting self-regenerative processes [188–190]. In addition, the

anti-tumor immune responses evoked by autoreactive T cells are beneficial [170, 191]. Therefore, it seems unlikely that autoreactive T cells escaping from the thymus are simply a result of thymic selection error that can disturb self-tolerance under certain physiological conditions. Instead, these evidences imply that beneficial self reaction is allowed in the immune system. According to the mathematical model, immune reactions against self are only possible with a critical homeostatic population of autoreactive T cells (or sufficient renewal rate N_0) which is balanced by a proper number of Tregs ($\lambda < \lambda_{\rm th}$) which corresponds to region (C) in **Figure 5.10**. Since the T cell repertoire is normally stimulated with an endogenous level of self antigens in the periphery which does not evoke any self reaction, the Ag-stimulation threshold for initiating an immune response (β_i) should be sufficiently high in comparison to a typical nonself Ag-stimulation. According to our model, this is achieved by ensuring a low renewal rate (N_0) of low-avidity autoreactive T cells and a high, but balanced renewal rate of Tregs (high λ but lower than $\lambda_{\rm th}$). In other words, according to **Figure 5.10**, by choosing N_0 close to k_i and higher value of k_i which is obtained by higher λ, a large Ag-stimulation threshold (β_i) for the initiation of immunity against self can be achieved.

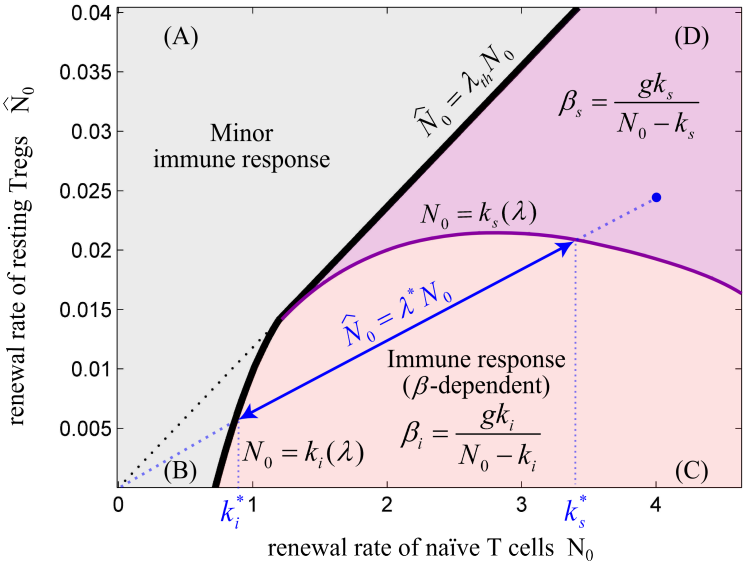

Figure 5.10: The balance between renewal rate of naïve T cells and resting Tregs. The relative renewal rate of naïve T cells and resting Tregs ($\lambda = \hat{N}_0/N$) determines the existence of an immune response. The initiation of an immune response requires a sufficient renewal rate of naïve T cells (N_0). (A) For $\lambda > \lambda_{\rm th}$, the immune response does not exist for any value of N_0 and Ag-stimulation (β). (B) For $N_0 < k_i$, no immune response can be initiated for any value of β. (C) For $N_0 > k_i$, immune response can be initiated for $\beta > \beta_i$. In this regime, the Ag-stimulation that results in over-suppression of immune response (β_s) does not exist. (D) In this regime, immune response is initiated for $\beta > \beta_i$, and is over-suppressed for $\beta > \beta_s$. Note that k_i and k_s are dependent on the value of λ. For any point in the plane (e.g. blue point), the values of k_s^* and k_i^* are obtained by projecting the intersections of the line created by connecting the point to the origin (slope=λ^*) with the nonlinear curves $N_0 = k_i(\lambda)$ and $N_0 = k_s(\lambda)$ onto the N_0-axis. By decreasing λ^*, the effective range of T cell activation ($k_s^* - k_i^*$) or equivalently, the effective range of Ag-stimulation ($\beta_s^* - \beta_i^*$) which evoke immune response without over-suppression increases. We hypothesize that a healthy individual bears the potential to evoke self reaction and therefore its immune system is located in parametric regime (C); however, higher self Ag-stimulation compared to nonself Ag-stimulation is required for initiating immune response due to low renewal rate of autoreactive T cells (N_0).

Aging of the immune system, the so-called immunosenescence, is characterized by involution of thymus, decreased number of thymic output, contraction in T cell diversity and disturbed T cell homeostasis which all result in attenuated immune function and susceptibility to infectious diseases and cancer in the elderly [192,193]. By decreasing thymic output, the homeostatic population of some T cell clones diminishes which leads to the creation of holes in the T cell repertoire [194]. According to our model, a decreased renewal rate of a naïve T cell clone (N_0) per se could prevent an immune response or increase the Ag-stimulation level required for initiation of an immune response. In addition, as shown in many studies, the frequency of Tregs increases with age [195,196] which results in a disturbed balance between the population of naïve T cells and resting Tregs (increased λ). In line with these results, in the mathematical model an increased λ prevents the initiation of an immune response corresponding to the age-related immune hyporesponsiveness in infection and cancer.

Based on the reasonable and physiologically realistic results that we could derive from the model, we dare to speculate about the self versus nonself concept emerging from the model. As mentioned before, the naïve T cells and resting Tregs are two major components of the immune reaction. The model does not distinguish self and nonself, but rather derives different responses to self and nonself from quantitative differences in the nature of Ag-stimulation. According to the model, by adjusting different parameters, different requirements in terms of Ag-stimulation level are found for the initiation of immune responses to self versus nonself. If the immune system responds according to a universal set of Ag-stimulation thresholds, regardless of whether the stimulus arises from self or nonself antigens, a change of systemic parameters can lead to immune failure or autoimmunity. Self is no more considered as self if it exceeds an Ag-stimulation threshold determined by the stringency of central and peripheral tolerances. Similarly, nonself is considered as self if it does not properly stimulate the T cell repertoire. Autoimmunity might occur due to either a failure in tuning the Ag-stimulation threshold by the thymus that leads to unwanted self reaction in the periphery, or a chronic self Ag-stimulation in the periphery that leads to an oscillating self reaction and tissue destruction like in type 1 diabetes [197] and multiple sclerosis [198]. Cancer or chronic infection would arise as the result of an imbalance in central and peripheral tolerances such as insufficient release of autoreactive T cells as well as high production or induction of Tregs that results in over-suppression of immune responses.

An early elegant mathematical modeling study analyzed a series of models to investigate self/nonself discrimination by T cells without explicitly considering suppressive Tregs [20]. As a result of their critical assumption that memory cells accumulate in poor stimulatory conditions, the authors suggested that due to high stimulation by self antigen the lack of memory accumulation for T cell clones with high affinity to self accounts for self tolerance. Also in our model, a high self Ag-stimulation ($\beta > \beta_s$ in **Figure 5.7B**) results in over-activation of Tregs and by this in over-suppression of self reaction. In both models an increased stimulation by self antigen would not lead to autoimmunity. The fact that autoreactive T cells do respond in the presence of Tregs when their stimulatory requirements are provided [154] makes it unlikely that this is the mechanism of self-tolerance induction. In the framework of our model, the view is supported that immune tolerance is induced by an increased stimulation threshold for self antigen and keeping self Ag-stimulation in a subcritical regime ($\beta < \beta_i$).

Undoubtedly, other mechanisms besides clonal deletion and Treg selection in the thymus also contribute to the fine tuning of the Ag-stimulation threshold required for initiation of immune reactions to self and nonself, such as anergy in the periphery [199] or activation threshold tuning in the thymus [84, 200]. However, our simple model emphasizes the subtle balance between the generation of Tregs and autoreactive T cells which are both needed for beneficial autoimmunity. The model supports the view according to which self and nonself do not differ on a qualitative level. It is rather quantitative differences of the immune status and Ag-stimulation level that determine which molecule is treated as self or nonself.

5.4 Summary

The adaptive immune system reacts against pathogenic nonself, whereas it normally remains tolerant to self. The initiation of an immune response requires a critical antigen(Ag)-stimulation and a critical number of Ag-specific T cells. Autoreactive T cells are not completely deleted by thymic selection and partially present in the periphery of healthy individuals that respond in certain physiological conditions. A number of experimental and theoretical models are based on the concept that structural differences discriminate self from nonself.

In this chapter, we presented a series of mathematical models for immune activation in which self and nonself are not distinguished. The most complete model considers the dynamic interplay of conventional T cells, regulatory T cells (Tregs) and IL-2 molecules and shows that the renewal rate ratio of resting Tregs to naïve T cells as well as the proliferation rate of activated T cells determine the probability of immune stimulation. The actual initiation of an immune response, however, relies on the absolute renewal rate of naïve T cells. This result suggests that thymic selection reduces the probability of autoimmunity by increasing the Ag-stimulation threshold of self reaction which is established by selection of a low number of low-avidity autoreactive T cells balanced with a proper number of Tregs.

The stability analysis of the ordinary differential equation model reveals three different possible immune reactions depending on critical levels of Ag-stimulation: A subcritical stimulation, a threshold stimulation inducing a proper immune response, and an overcritical stimulation leading to chronic co-existence of Ag and immune activity. The model exhibits oscillatory solutions in the case of persistent but moderate Ag-stimulation, while the system returns to the homeostatic state upon Ag clearance. In this unifying concept, self and nonself appear as a result of shifted Ag-stimulation thresholds which delineate these three regimes of immune activation.

Chapter 6

Regulation of immune stimulation

In Chapters 4 and 5, induction of central tolerance by removing self-antigen specific cells and peripheral tolerance by antigen-specific activation and regulatory function of regulatory T cells (Treg) were discussed. However, antigen-nonspecific mechanisms for maintaining immune tolerance exist in the immune system. One mechanism by which the immune system is able to maintain a balance between immune activation and inhibition is to use different antigen-nonspecific receptors for different cellular outcomes. In this chapter, one of the most important inhibitory receptors of the immune system, Cytotoxic T lymphocyte antigen 4 (CTLA4), is discussed.

6.1 Background

Activation of T cells requires close contacts with antigen presenting cells (APCs). This cell-cell contact forms immunological synapses that allow membrane receptors of one cell to effectively interact with their ligands on the surface of opposing cell [201, 202]. "Two-signal" activation model of T cells is the widely accepted model of how T cells become activated. This model states that optimal T-cell activation requires two signals: antigen-specific and antigen non-specific signals. First signal is induced by interaction of TCRs expressed by T cells with major histocompatibility complex (MHC)-bound peptides presented by APCs. Second signal is induced by interaction of CD28 receptors expressed by T cells with costimulatory molecules (CD80 and CD86 molecules) expressed by APCs [203, 204] (see **Figure 2.5**). It is generally believed that costimulatory molecules increase the sensitivity of T cells to antigen-specific signals, and allowing them to become activated by few high-affinity antigens presented by APCs.

Providing abundant costimulation to T cells may lead to uncontrolled T cell activation and clonal expansion which may damage healthy tissues. Especially, abundant costimulation may lead to T cell activation against self-peptides that is normally expressed by APCs. CTLA4 is an inhibitory receptor expressed by T cells that controls the outcome of costimulatory signals. CTLA4 binds to the same ligands for CD28, which are CD80 and CD86. CD28 molecules are expressed on the surface of resting and activated conventional T cells. In contrast, CTLA4 is only expressed approximately 2 days after activation of conventional T cells in mice [205] and humans [206]. CTLA4 is expressed by both $CD4^+$ and $CD8^+$ T cells, but the its expression on $CD4^+$ may be more important, since the unbalance immune regulation can be avoided in CTLA4-deficient animals by eliminating $CD4^+$ T cells [207]. Unlike conventional T cells, CTLA4 is expressed by Tregs in resting state [208–210]. This expression is upregulated after Treg activation [211].

CTLA4 is a receptor that binds to its specific ligands on the cell surface (it is a transmembrane protein). However, the cellular distribution of CTLA4 molecules contrasts with its function; CTLA4 is mostly located inside the cell (in cytoplasm). This unusual distribution for a transmembrane protein raises questions about

the functionality of CTLA4. For example, it is not clear whether a small amount of CTLA4 on the plasma membrane (cell surface) under steady-state condition (without inflammation) is sufficient for the inhibitory effects of CTLA4. A possible answer for this question would be that higher affinity interactions of CTLA4 with CD80/CD86 molecules should be limited in order to allow stimulation of lower affinity interactions of CD28 with the same costimulatory molecules. Another question is whether the distribution of CTLA4 molecules corresponds to a static behavior of CTLA4 molecules, or rather it is resulted from a dynamic trafficking process. In each case, there should be an explanations about what the immune system gains if CTLA4 is located stably, or highly traffics between plasma membrane and cytoplasm.

It is generally believed that CTLA4 molecules impact on the cell that express them. This is generally referred as cell-intrinsic pathway of immune inhibition. Such a cell-intrinsic mechanism would predict that if CTLA4 is removed from the immune system (in a CTLA4-deficient mouse model), T cells undergo uncontrolled activation from which autoimmunity arises. Indeed, this prediction is validated by experimental observations. However, cell-intrinsic inhibition idea would predict that if a mixture of CTLA4-deficient and CTLA4-sufficient T cells exists in an individual (a chimeric experiment), CTLA4-deficient T cells become activated. In contrast to this prediction, it has been shown (in chimeric experiment) that all T cells remain in their quiescent state. Recently, a new function of CTLA4 has been discovered which is compatible with observations in chimeric experiments. It has been shown that CTLA4 molecules on T cells are able to detach and internalize costimulatory molecules from the surface of APCs, a process known as trans-endocytosis (**Figure 6.1**). Trans-endocytosis is an unusual mechanism for regulating molecule expression in the immune system. Trans-endocytosis allows CTLA4-expressing T cells to regulate the expression of CD80/CD86 molecules by APCs, and by that, regulate the activation of other interacting T cells. In such a cell-extrinsic inhibitory mechanism, the dynamics of CTLA4 trafficking is critical. In contrast to a fast trafficking CTLA4 machinery, static model of CTLA4 expression would not allow an efficient removal of costimulatory molecules. In this chapter, a series of experiments and their corresponding mathematical models are employed to quantify sub-processes involved in CTLA4 trafficking. Once the trafficking rates are obtained, they can be used to predict the contribution of trans-endocytosis mechanism in immune regulation.

6.2 Modeling

Cells express a variety of proteins in cytoplasm (CP) and on plasma membrane (PM). These proteins are usually maintained in homeostatic numbers by multiple trafficking sub-processes. These sub-processes are regulated depending on different environmental stimuli which leads to the changes of protein distributions. Typical trafficking sub-processes are protein synthesis, secretion of proteins to PM (exocytosis), internal-

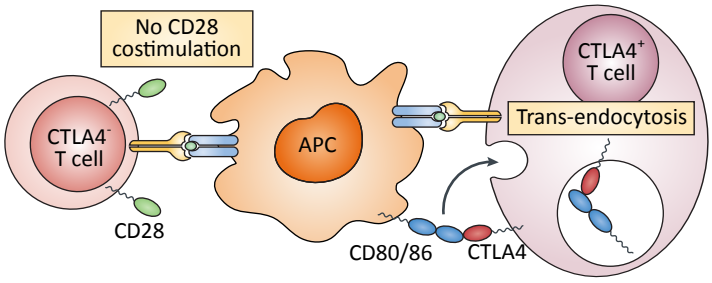

Figure 6.1: Trans-endocytosis, a T cell extrinsic function of CTLA4 [13]. CTLA4-expressing cell removes costimulatory molecules (CD80/86) from surface of antigen presenting cell (APC). This removal mechanism deprive other interacting T cells from costimulatory signals from APC.

ization of proteins from PM to CP (endocytosis), protein degradation and protein diffusion on plasma membrane which is the process of protein movements from one location to another. The rates of trafficking sub-processes differ among different proteins. For example, CD28 molecules are stably present on the plasma membrane, which resulted from low endocytosis and exocytosis rates. In order to identify the trafficking rates for CTLA4 molecules without any priori knowledge, the model has to be constructed by all the aforementioned sub-processes and associated rates. Then, by using experimental measurements, the contribution of each process can be quantified.

Experimental data obtained from CTLA4-labeling experiments given in [212] and [213] are used. In these experiments, CTLA4 molecules were expressed in Chinese Hamster Ovary (CHO) cells. These cell are widely used for production of various proteins. The modeling starts with a general model for CTLA4 trafficking. Since various experimental protocols have been used to observe CTLA4 molecules, such as using labeling antibodies, the general model is modified to often more complex models to represent these experimental protocols.

6.2.1 Model 1: ligand-independent trafficking model of CTLA4 receptors

First, we consider CTLA4 molecules without cell interactions. General model is constructed by considering fundamental processes in protein trafficking, namely protein synthesis, recycling, internalization and degradation (**Figure 6.2**). General model relies on the following assumptions:

- CTLA4 molecules are synthesized at a constant rate σ_i with dimension of molecule number ($\#$) per minute. Protein synthesis results in the maintenance of homeostatic number of CTLA4 molecules in the plasma membrane (R_{ip} with dimension $\#$) and subsequently in the cytoplasm (R_{ic} with dimension $\#$) after internalization. This assumes that newly synthesized CTLA4 molecules are not directly undergo the degradation pathway that exists in the cytoplasm, but only after exocytosis to plasma membrane and subsequent internalization to cytoplasm. The subscript i is taken from *inhibition* as an indication to inhibitory role of CTLA4 molecules. Letter R is taken from *Receptor* and will be used for number of CTLA4 molecule. L (taken from *Ligand*) will be used for co-stimulatory (CD80/CD86) or labeling molecules. The subscripts c and p indicate to the location of molecules (taken from Cytoplasm and Plasma membrane, respectively).
- The cytoplasmic CTLA4 molecules are degraded in a lysosomal-dependent manner with a constant rate δ_{il} (with dimension of min^{-1}). To quantify the degradation of CTLA4 in non-lysosomal-dependent manner, we assume that CTLA4 molecules also degrade with a constant rate δ_{in} (with dimension of min^{-1}). Total cytoplasmic degradation rate is $\delta_{ic} = \delta_{il} + \delta_{in}$.
- The intracellular CTLA4 molecules (R_{ic}) are exocytosed (recycled) to the plasma membrane by a constant rate k_{ir} (with dimension of min^{-1}).
- The surface CTLA4 molecules (R_{ip}) are internalized with a constant rate k_{ii} (with dimension of min^{-1}) and are added to the cytoplasmic CTLA4 molecules (R_{ic}).

The general model, depicted in **Figure 6.2**, can be written as the following nonhomogeneous linear system of ordinary differential equations (ODE):

$$\begin{pmatrix} \dot{R}_{ic}(t) \\ \dot{R}_{ip}(t) \end{pmatrix} = \begin{pmatrix} -(k_{ir} + \delta_{ic}) & k_{ii} \\ k_{ir} & -k_{ii} \end{pmatrix} \begin{pmatrix} R_{ic}(t) \\ R_{ip}(t) \end{pmatrix} + \begin{pmatrix} 0 \\ \sigma_i \end{pmatrix} \tag{6.1}$$

where $\delta_{ic} = \delta_{il} + \delta_{in}$. Steady state values of model (6.1) are the followings:

$$\begin{aligned} R_{ic} &= \frac{\sigma_i}{\delta_{ic}}, \\ R_{ip} &= \frac{k_{ir} + \delta_{ic}}{k_{ii}} R_{ic} = \frac{\sigma_i (k_{ir} + \delta_{ic})}{k_{ii} \delta_{ic}}. \end{aligned} \tag{6.2}$$

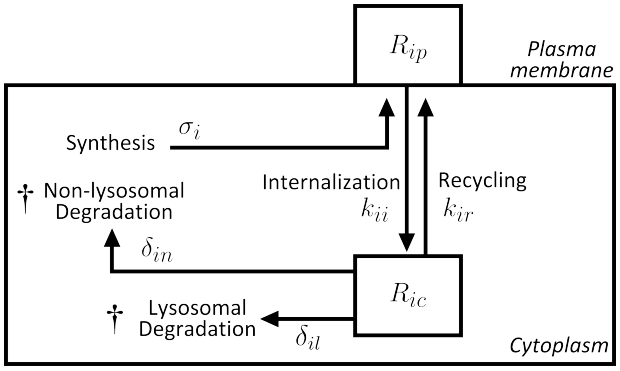

Figure 6.2: General model: Ligand-independent model of CTLA4 trafficking.

Before starting each experiment, the number of CTLA4 moleculse are assumed to be at their steady state values given in (6.2).

6.2.2 Model 2: ratio of plasma membrane to internalized receptors

In the first ligand-independent experiments, CTLA4-expressing CHO cells are pulsed at $37\,^{\circ}\mathrm{C}$ for 30 minutes with an unlabeled anti-CTLA4. Unlabeled anti-CTLA4 is a primary antibody without any color and binds to CTLA4 molecules. This primary antibody can also bind to secondary antibodies with different colors, once they are provided in the medium. In $37\,^{\circ}\mathrm{C}$, CTLA4 molecules undergo a natural trafficking. Therefore, once CTLA4 molecules appear on the plasma membrane (newly synthesized or recycled molecules), they can bind to unlabeled anti-CTLA4 molecules. We refer to this compound as marked CTLA4. After being marked, CTLA4 molecules can be subsequently internalized or recycled again.

Next, by putting cells on ice, the CTLA4 trafficking was blocked. Then, by using a fluorescently labeled secondary antibody (red), marked CTLA4 molecules (without color) on the plasma membrane were labeled by red color. Subsequently, the cells were permeabilized and stained with an alternate secondary antibody (green). Note that with permeabilization, secondary antibodies can diffuse to cytoplasm and bind to intracellular marked CTLA4 molecules. Since the CTLA4 molecules were labeled with the red labels, they cannot be labeled with green antibody. Finally, CHO cells were analyzed by confocal microscopy and the ratio of red mean fluorescent intensity (MFI) to green MFI was obtained (see **Figure 6.3**). Confocal microscope is capable of showing a plane of focus from within a sample and eliminating out of focus objects.

Model of this experiment, depicted in **Figure 6.4A** schematically, is representing the labeling process during the natural trafficking of CTLA4 molecules. It is assumed that free CTLA4 molecules on the plasma membrane $R_{ip}(t)$ can bind to primary labeling molecules (unlabeled anti-CTLA4 molecules L_p), which has no color in this particular experiment, and make marked CTLA4 compounds $R^*_{ip}(t)$ on the plasma membrane in CTLA4+$\mathrm{L_p} \rightleftarrows$ CTLA4* reaction. This reaction has a constant binding rate k_L and unbinding rate $\widehat{k}_L$. Free CTLA4 molecules and marked CTLA4 compounds on the cell surface ($R_{ip}(t)$ and $R^*_{ip}(t)$, respectively) are internalized with a constant rates k_{ii} and k^*_{ii}, respectively. Once the marked CTLA4 molecules are in cytoplasm ($R^*_{ic}(t)$), free primary labeling molecules $L_c(t)$ appear in cytoplasm due to the unbinding of the marked CTLA4 to its reactants (CTLA4$^* \rightleftarrows$ CTLA4 + $\mathrm{L_c}$), which further can bind to free cytoplasmic CTLA4 molecules $R_{ic}(t)$. Note that internalization is the only pathway that primary labeling molecules can enter cytoplasm from extracellular environment. With these aforementioned

assumptions, model of labeling experiment is the following

$$\dot{R}_{ic}(t) = -\left(\delta_{ic} + k_{ir} + k_L L_c(t)\right) R_{ic}(t) + k_{ii} R_{ip}(t) + \widehat{k}_L R^*_{ic}(t) \tag{6.3}$$

$$\dot{R}_{ip}(t) = k_{ir} R_{ic}(t) - \left(k_L L_p + k_{ii}\right) R_{ip}(t) + \widehat{k}_L R^*_{ip}(t) + \sigma_i \tag{6.4}$$

$$\dot{R}^*_{ip}(t) = k_L L_p R_{ip}(t) - \left(\widehat{k}_L + k^*_{ii}\right) R^*_{ip}(t) + k^*_{ir} R^*_{ic}(t) \tag{6.5}$$

$$\dot{R}^*_{ic}(t) = k_L L_c(t) R_{ic}(t) + k^*_{ii} R^*_{ip}(t) - \left(\widehat{k}_L + k^*_{ir} + \delta^*_{ic}\right) R^*_{ic}(t) \tag{6.6}$$

$$\dot{L}_c(t) = -k_L L_c(t) R_{ic}(t) + \widehat{k}_L R^*_{ic}(t) - \delta_L L_c(t) \tag{6.7}$$

where $R^*_{ip}(t)$ and $R^*_{ic}(t)$ are the number of CTLA4 molecules on plasma membrane and in cytoplasm, respectively, which are marked with binding to the unlabeled anti-CTLA4 (no color). L_p and $L_c(t)$ are the number of unlabeled anti-CTLA4 molecules in the medium and cytoplasm, respectively. The nonlinearity of this model arises from forward reaction of CTLA4 labeling (CTLA4 + L $\rightarrow$ CTLA4*). In a typical labeling experiment, the following assumptions are taken in order to interpret the data:

(A) L_p is constant and sufficiently large

(B) k_L is sufficiently large in comparison to other reaction rates.

(C) $\widehat{k}_L$ is smaller than other rates and is approximated to zero.

(D) $\delta^*_{ic} = \delta_{ic}$, $k^*_{ir} = k_{ir}$ and $k^*_{ii} = k_{ii}$.

Assumption (A) indicates to the experimental procedure, where sufficient anti-CTLA4 molecules are provided into the medium, and labeling molecules are not a limiting factor for CTLA4 observation. Assumption (B) and (C) imply that labeling molecules bind to CTLA4 with a very high rate and remain bound during the time of sample observation. This represents the experimental definition of a labeling molecule. Assumption (D) represents the approximation that trafficking rates of labeled CTLA4 molecules is similar to free CTLA4 molecules. We apply these assumptions to model equations.

According to the assumptions (A) and (B), we can assume that marking CTLA4 molecules on the plasma membrane R_{ip} with unconjugated unlabeled anti-CTLA4 is at quasi steady state. By setting

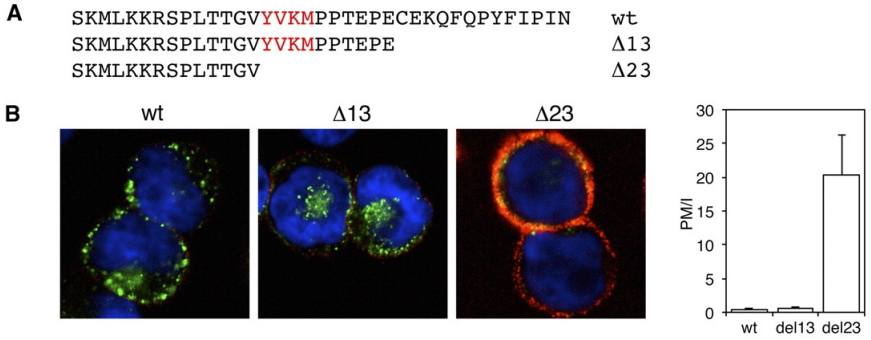

Figure 6.3: Ratio of plasma membrane (PM) to internalized (I) CTLA4 [212]. CHO cells expressing either wild type (wt), $\Delta 13$, or $\Delta 23$ CTLA4 were incubated with unlabeled anti-CTLA4 at $37\,^{\circ}\mathrm{C}$ for 30 minutes. $\Delta 13$ and $\Delta 23$ are mutants of CTLA4 molecules, and $\Delta 23$ turned out to be a non-endocytic mutant. After labeling, cells were then cooled to $4\,^{\circ}\mathrm{C}$, and CTLA4 that remained on the cell surface were stained with a fluorescently labeled secondary antibody (red). Cells were then fixed, permeabilized, and stained with a different secondary antibody (green) and imaged by confocal microscopy. The ratio of plasma membrane to internalized CTLA4 fluorescence (PM/I) was calculated and is shown in the right panel.

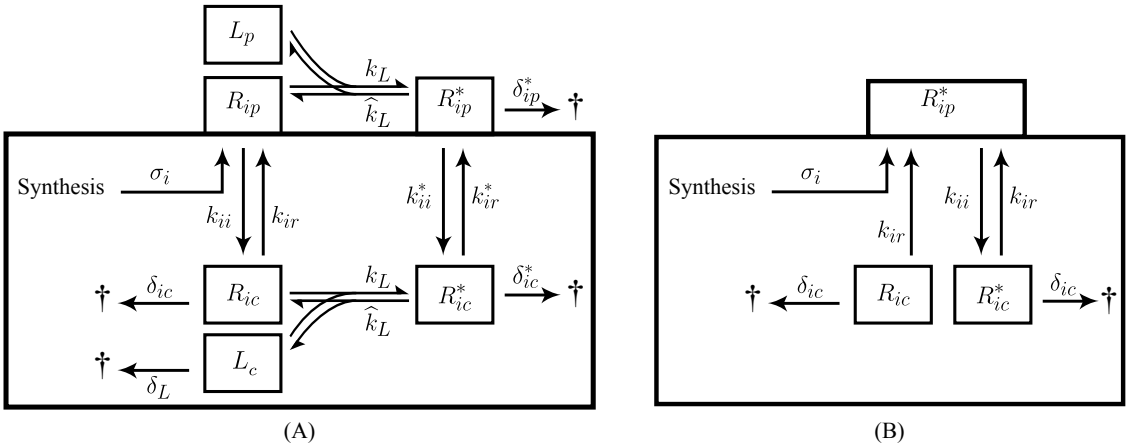

Figure 6.4: Model of CTLA4 labeling process. (A) Complete model of PM/I experiment and (B) the simplified version.

$\dot{R}_{ip}(t) = 0$ in (6.4), we have

$$\dot{R}_{ip}(t) = 0 \rightarrow R_{ip} = \frac{k_{ir}R_{ic}(t) + \widehat{k}_L R^*_{ip}(t) + \sigma_i}{k_L L_p + k_{ii}} \tag{6.8}$$

Since the cytoplasmic unconjugated unlabeled anti-CTLA4 $L_c(t)$ appears during the unbinding process of internalized marked CTLA4 compound (R^*_{ic}), its initial value ($L_{c,0}$) at starting time of the labeling process is zero. By employing assumption (C), we evaluate (6.7) by $\widehat{k}_L = 0$,

$$\dot{L}_c(t) = -(k_L R_{ic}(t) + \delta_L)L_c(t), \tag{6.9}$$

with initial condition $L_{c,0} = L_c(0) = 0$. Since $(k_L R_{ic}(t) + \delta_L)$ in (6.9) is positive for every t, then

$$L_c(t) = 0. \tag{6.10}$$

Next, we employ (6.8) and (6.10) in (6.3),

$$\dot{R}_{ic}(t) = -(\delta_{ic} + k_{ir})R_{ic}(t) + \frac{k_{ii}k_{ir}}{k_L L_p + k_{ii}}R_{ic}(t) + \frac{k_{ii}\widehat{k}_L}{k_L L_p + k_{ii}}R^*_{ip}(t) + \frac{\sigma_i k_{ii}}{k_L L_p + k_{ii}}. \tag{6.11}$$

According to assumptions (A) and (B), we extract $k_L L_p \gg k_{ii}k_{ir}$, $k_L L_p \gg k_{ii}\widehat{k}_L$ and $k_L L_p \gg \sigma_i k_{ii}$. Therefore, ratios in (6.11) are approximated to zero and the equation is simplified to

$$\dot{R}_{ic}(t) = -(\delta_{ic} + k_{ir})R_{ic}(t). \tag{6.12}$$

Next, we evaluate (6.5) according to (6.8), (6.10) and assumptions (C) and (D).

$$\dot{R}^*_{ip}(t) = \frac{k_L L_p}{k_L L_p + k_{ii}}(k_{ir}R_{ic}(t) + \sigma_i) - k_{ii}R^*_{ip}(t) + k_{ir}R^*_{ic}(t) \tag{6.13}$$

From assumptions (A) and (B), we extract $k_L L_p \gg k_{ii}$. Therefore, $k_L L_p/(k_L L_p + k_{ii}) \approx 1$, and above equation is simplified to

$$\dot{R}^*_{ip}(t) = k_{ir}R_{ic}(t) + \sigma_i - k_{ii}R^*_{ip}(t) + k_{ir}R^*_{ic}(t). \tag{6.14}$$

Finally, we evaluate (6.6) according to (6.8), (6.10) and assumptions (C) and (D).

$$\dot{R}^*_{ic}(t) = k_{ii}R^*_{ip}(t) - (k_{ir} + \delta_{ic})R^*_{ic}(t). \tag{6.15}$$

As the result of biologically relevant assumptions, the nonlinear model of labeling process is simplified to the following nonhomogeneous linear ODE model

$$\begin{pmatrix} \dot{R}_{ic}(t) \\ \dot{R}^*_{ip}(t) \\ \dot{R}^*_{ic}(t) \end{pmatrix} = \begin{pmatrix} -(k_{ir} + \delta_{ic}) & 0 & 0 \\ k_{ir} & -k_{ii} & k_{ir} \\ 0 & k_{ii} & -(k_{ir} + \delta_{ic}) \end{pmatrix} \begin{pmatrix} R_{ic}(t) \\ R^*_{ip}(t) \\ R^*_{ic}(t) \end{pmatrix} + \begin{pmatrix} 0 \\ \sigma_i \\ 0 \end{pmatrix}. \tag{6.16}$$

Model (6.16) is equivalent to the labeling process schematically depicted in **Figure 6.4B**. According to the simplified model, all free CTLA4 molecules ($R_{ip}(t)$) on the plasma membrane are labeled at the moment of adding labeling molecules into the medium. Hence, the initial value of marked CTLA4 molecules $R^*_{ip,0}$ is equal to the steady state number of free CTLA4 molecules on the plasma membrane in general model (6.1) given in (6.2). Initial number of free cytoplasmic CTLA4 molecules ($R_{ic,0}$) can be taken from its steady state value given in (6.2). No marked CTLA4 molecule exists at starting time of the experiment. In summary, model (6.16) has the following initial condition

$$R_{ic,0} = \frac{\sigma_i}{\delta_{ic}}, \quad R^*_{ip,0} = \frac{\sigma_i(k_{ir} + \delta_{ic})}{k_{ii}\delta_{ic}}, \quad R^*_{ic,0} = 0. \tag{6.17}$$

Initial conditions are used to obtain the time-varying solution of model (6.16). In **Appendix B.1**, steps to obtain the following solutions are given.

$$R_{ic}(t) = \frac{\sigma_i}{\delta_{ic}} e^{-(k_{ir}+\delta_{ic})t}, \tag{6.18}$$

$$R^*_{ip}(t) = R^*_{ip,0} = \frac{\sigma_i(k_{ir} + \delta_{ic})}{k_{ii}\delta_{ic}}, \tag{6.19}$$

$$R^*_{ic}(t) = \frac{\sigma_i}{\delta_{ic}} \left(1 - e^{-(k_{ir}+\delta_{ic})t}\right). \tag{6.20}$$

In (6.19), a constant value for marked CTLA4 molecules on plasma membrane is obtained, which is identical to its initial value. This is the result of uninterrupted CTLA4 synthesis during the labeling process and subsequent binding to labeling molecules which is a very fast process. According to (6.18), free CTLA4 molecules in cytoplasm disappear as $t \to \infty$. This is resulted from the assumption that all newly synthesized molecules are directly go to the plasma membrane, and all molecules on the plasma membrane are marked with labeling molecules. Consequently, no free CTLA4 molecule exists on the plasma membrane to be subsequently internalized and to sustain the pool of free CTLA4 molecules in the cytoplasm.

We are interested in the ratio of marked CTLA4 molecules on the plasma membrane (PM) to marked CTLA4 molecules in the cytoplasm (I) which are resulted from internalization process. This ratio (PM/I) can be obtained by using (6.19) and (6.20),

$$\frac{R^*_{ip}(t)}{R^*_{ic}(t)} = \frac{k_{ir} + \delta_{ic}}{k_{ii}} \frac{1}{1 - e^{-(k_{ir}+\delta_{ic})t}} \tag{6.21}$$

As $t \to \infty$, the fraction (6.21) converges to steady state ratio of free CTLA4 molecules on plasma membrane to free cytoplasmic CTLA4 molecules in the general model (6.1), given in (6.2). Since the labeling process was only done for 30 minutes, a larger ratio than steady state ratio was obtained.

Note that in confocal microscopy, only a focus plane is visible, meaning that a fraction of total CTLA4 on plasma membrane and in cytoplasm were quantified with confocal microscopy. Therefore, this fraction

has to be considered in the theoretical value of PM/I ratio. By considering a visible area A_{vis} and a visible volume V_{vis} of a spherical cell in confocal microscopy, observed number of molecules are

$$R^*_{ip,\mathrm{vis}}(t) = \frac{A_{\mathrm{vis}}}{A} R^*_{ip}(t), \tag{6.22}$$

$$R^*_{ic,\mathrm{vis}}(t) = \frac{V_{\mathrm{vis}}}{V} R^*_{ic}(t) \tag{6.23}$$

where A and V are the area of plasma membrane and volume of cytoplasm of a spherical CHO cell. The total and visible area and volume of the cell can be obtained from the followings

$$\begin{aligned} A_{\mathrm{vis}} &= 2\pi R z_s, \\ A &= 4\pi R^2, \\ V_{\mathrm{vis}} &= \frac{\pi z_s}{6}\left(6R_s^2 + z_s^2\right), \\ V &= \frac{4}{3}\pi R^3, \end{aligned} \tag{6.24}$$

where R is the radius of spherical cell, R_s is the radius of top focal plane, z_s is the thickness of cell slice that is visible in confocal microscopy (see **Figure 6.5**). Therefore, the experimentally quantified fraction of (6.21) is

$$Y_{\mathrm{PM/I}}(t) = \frac{R^*_{ip}(t)}{R^*_{ic}(t)} = \frac{k_{ir} + \delta_{ic}}{k_{ii}} \frac{1}{1 - e^{-(k_{ir}+\delta_{ic})t}} \frac{A_{\mathrm{vis}}}{A} \frac{V}{V_{\mathrm{vis}}}. \tag{6.25}$$

Note that CTLA4 molecules on plasma membrane and in cytoplasm are visualized by two different labeling antibodies, and hence, might show different fluorescent intensities with identical stimulation. This difference which is directly affecting the quantified PM/I ratio was not quantified in [212]. From observer (6.25), the rate of CTLA4 synthesis (σ_i) cannot be observed. By measuring the reaction kinetics of labeling process CTLA4+L$\rightleftarrows$CTLA4*, and obtaining the number of labeling molecules available in the vicinity of each CHO cell (L_p), an error that may arise from modeling assumptions (A), (B) and (C) can be extracted.

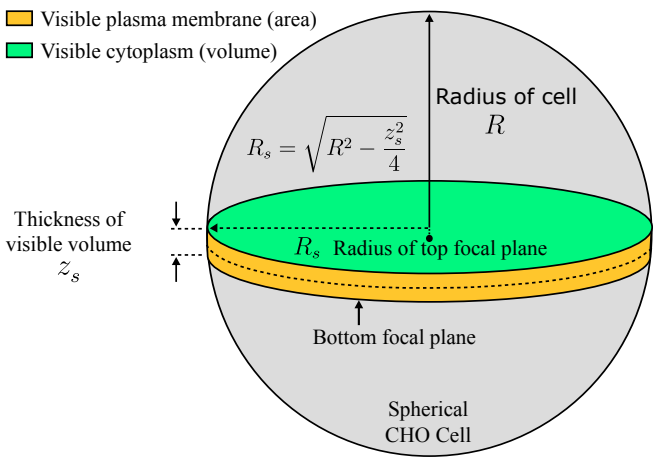

Figure 6.5: Visible area and volume of a spherical cell in confocal microscopy

6.2.3 Model 3: receptor internalization

To determine the rate of internalization, CTLA4-expressing CHO cells were labeled at $4\,^{\circ}\mathrm{C}$ with a primary fluorescently conjugated anti-CTLA4 (primary antibody with a predetermined color). Since in $4\,^{\circ}\mathrm{C}$, natural trafficking is stopped, only CTLA4 molecules on the plasma membrane were labeled. Then, the cells were washed, so that no further labeling was allowed. Then, cells are warmed to $37\,^{\circ}\mathrm{C}$ for various durations. Next, the cells were put on ice ($4\,^{\circ}\mathrm{C}$) to stop CTLA4 trafficking. Finally, those initially labeled CTLA4 molecules that were still existing on the cell surface (remained on or recycled to plasma membrane) were detected via a fluorescently conjugated secondary antibody. Note that the secondary antibody could not bind to free CTLA4 molecules on the plasma membrane, but only to CTLA4 molecules that were initially labeled with primary antibody. The fraction of the initially labeled CTLA4 molecules that were detected on plasma membrane by confocal microscopy was obtained at different time points (**Figure 6.6A**).

In the presented internalization experiment, only the trafficking of an initially labeled CTLA4 molecules is observed. Therefore, the corresponding model is a simplified version of model (6.16) shown in , without CTLA4 synthesis and cytoplasmic pool of free (unlabeled) CTLA4 molecules (compare **Figure 6.4B** and **Figure 6.6B**). The model of this experiment can be written as the following homogeneous linear ODE model

$$\begin{pmatrix} \dot{R}^*_{ip}(t) \\ \dot{R}^*_{ic}(t) \end{pmatrix} = \begin{pmatrix} -k_{ii} & k_{ir} \\ k_{ii} & -(k_{ir}+\delta_{ic}) \end{pmatrix} \begin{pmatrix} R^*_{ip}(t) \\ R^*_{ic}(t) \end{pmatrix} \tag{6.26}$$

where $R^*_{ip}(t)$ is the subset of CTLA4 molecules which are initially labeled and can be detected on the plasma membrane, and $R^*_{ic}(t)$ is the cytoplasmic number of labeled CTLA4 molecules. Labeled CTLA4 molecules can only appear in the cytoplasm via internalization process, which is blocked by ice at starting time of the experiment; therefore, initial value of the cytoplasmic number of labeled CTLA4 molecules ($R^*_{ic,0}$) is zero. Note that since we track only a subset of CTLA4 molecules that were initially labeled on ice, and labeling molecules were no further available in the medium after washing, no newly synthesized CTLA4 molecules contribute to the pools we observe in later time points. The initial number of labeled

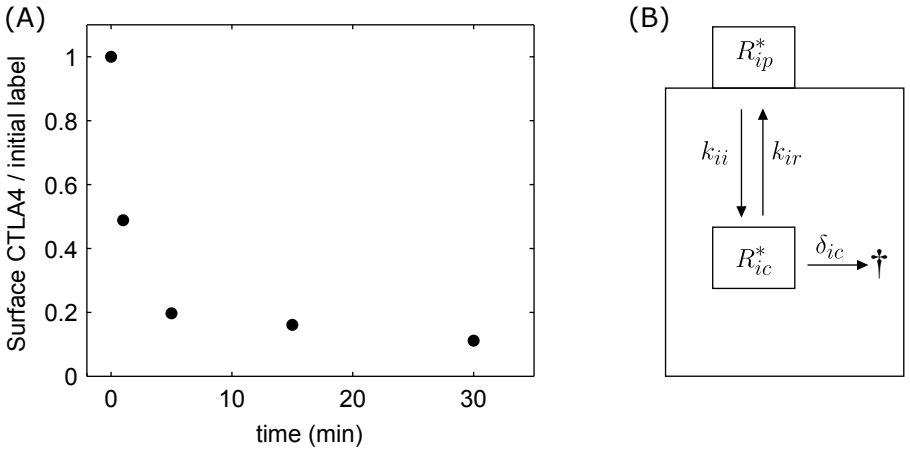

Figure 6.6: CTLA4 internalization. CTLA4-expressing CHO cells were labeled at $4\,^{\circ}\mathrm{C}$ with anti-CTLA4 PE to label surface CTLA4. Cells were then warmed to $37\,^{\circ}\mathrm{C}$ for the time indicated. Then CTLA4 remaining on the surface was detected on ice with a fluorescently conjugated anti-mouse secondary antibody. (A) The time course of surface labeling is plotted against initial labeling. Data points are normalized to the initial data points. The data are reported in [212]. (B) Schematic of the internalization model (6.26).

CTLA4 molecules on the plasma membrane ($R^*_{ip,0}$) is equal to the steady state number of free CTLA4 molecules on the plasma membrane obtained from general model (6.1) which is given in (6.2)

$$R^*_{ip,0} = \frac{\sigma_i(k_{ir} + \delta_{ic})}{k_{ii}\delta_{ic}}, \tag{6.27}$$

$$R^*_{ic,0} = 0. \tag{6.28}$$

The solution of the model with the above initial conditions are (see **Appendix B.2**):

$$R^*_{ip}(t) = -\frac{k_{ii} + \lambda_2}{\lambda_1 - \lambda_2} R^*_{ip,0} e^{\lambda_1 t} + \frac{k_{ii} + \lambda_1}{\lambda_1 - \lambda_2} R^*_{ip,0} e^{\lambda_2 t}, \tag{6.29}$$

$$R^*_{ic}(t) = \frac{k_{ii}}{\lambda_1 - \lambda_2} R^*_{ip,0} e^{\lambda_1 t} - \frac{k_{ii}}{\lambda_1 - \lambda_2} R^*_{ip,0} e^{\lambda_2 t}, \tag{6.30}$$

where λ_1 and λ_2 are the eigenvalues of the model:

$$\lambda_1 = \frac{1}{2}\left[-(k_{ii} + k_{ir} + \delta_{ic}) - \sqrt{(k_{ii} + k_{ir} + \delta_{ic})^2 - 4k_{ii}\delta_{ic}}\right], \tag{6.31}$$

$$\lambda_2 = \frac{1}{2}\left[-(k_{ii} + k_{ir} + \delta_{ic}) + \sqrt{(k_{ii} + k_{ir} + \delta_{ic})^2 - 4k_{ii}\delta_{ic}}\right]. \tag{6.32}$$

The quantified value in experiment is the fraction of initially labeled CTLA4 molecules that remained on the plasma membrane

$$\frac{R^*_{ip}(t)}{R^*_{ip,0}} = \frac{1}{\lambda_2 - \lambda_1}\left((k_{ii} + \lambda_2)e^{\lambda_1 t} - (k_{ii} + \lambda_1)e^{\lambda_2 t}\right). \tag{6.33}$$

Theoretically, the measured fraction in (6.33) at $t = 0$ is 1. Similarly, the experimental value for this fraction at $t = 0$ is 1, because all the data points are normalized to the initial data point at $t = 0$. By using normalized data and the fraction given in (6.33), we force a zero estimation error for initial data point. To avoid this, we introduce a scaling parameter S_{int} which allows the parameter estimation process to estimate the initial data point as well. Therefore, we use the following modified theoretical fraction for parameter estimation:

$$Y_{\text{int}}(t) = S_{\text{int}}\frac{R^*_{ip}(t)}{R^*_{ip,0}} = S_{\text{int}}\frac{1}{\lambda_2 - \lambda_1}\left((k_{ii} + \lambda_2)e^{\lambda_1 t} - (k_{ii} + \lambda_1)e^{\lambda_2 t}\right) \tag{6.34}$$

With this modified fraction, the estimated initial data point is $1/S_{\text{int}}$ fold of the measured value. Note that different antibodies were used to label CTLA4 molecules on the plasma membrane at starting time of the experiment (at $t = 0$) and remaining initially labeled CTLA4 molecules on the plasma membrane. In the theoretical value given in (6.34), it is assumed that antibodies are equally sensitive to visualization. However, difference in fluorescent intensities resulted from equal stimulation can directly affect the fraction given in (6.33) and (6.34). From observer (6.34), the rate of protein synthesis (σ_i) cannot be observed.

6.2.4 Model 4: blocking lysosomal degradation

To quantify the rate of CTLA degradation, two independent experiments were done. In the first experiment, CTLA4 molecules were labeled by 60 minutes pulse with a labeling antibody (anti-CTLA4 PE) at $37\,^{\circ}\text{C}$. Since the labeling was performed at $37\,^{\circ}\text{C}$, CTLA4 molecules undergo a normal trafficking. Consequently, labeled CTLA4 molecules appeared on the plasma membrane and in the cytoplasm. During 60 minutes of labeling process, only a fraction of total CTLA4 molecules could be labeled. After 60 minutes, cells were washed, such that no further labeling was allowed. This means that protein synthesis did not contribute

to the pool of labeled CTLA4 molecules after labeling process was ended. Next, two different samples with and without addition of Ammonium chloride (NH_4Cl) into the medium were prepared. NH_4Cl is known to block lysosomal-degradation pathway. In the presence and absence of NH_4Cl, degradation of labeled CTLA4 molecules were tracked for different time points by flow cytometry, which measures the fluorescent intensity arising from cellular labeled CTLA4 molecules (summation of CTLA4 molecules on plasma membrane and in cytoplasm) in a population of cells. Data of this experiment is shown in **Figure 6.7A**.

In order to construct the model of this experiment, in the first step, we assume that $R^*_{ip,0}$ and $R^*_{ic,0}$ number of CTLA4 molecules were labeled after 60 minutes on the plasma membrane and in the cytoplasm, respectively. Topology of the labeling model is similar to the model given in (6.16). By referring to equations (6.19) and (6.20), the number of labeled CTLA4 molecules are

$$\begin{aligned} R^*_{ip,0} &= \frac{\sigma_i(k_{ir}+\delta_{ic})}{k_{ii}\delta_{ic}}, \\ R^*_{ic,0} &= \frac{\sigma_i}{\delta_{ic}}\left(1-e^{-(k_{ir}+\delta_{ic})t_0}\right) \text{ at } t_0\text{=60 min}, \end{aligned} \tag{6.35}$$

where $\delta_{ic} = \delta_{il} + \delta_{in}$. In the second step, after 60 minutes of labeling, the cells were washed and the lysosomal degradation of CTLA4 was blocked by NH_4Cl, which is equivalent to $\delta_{il} = 0$. The second step of this experiment can be modeled by the following differential equation (depicted in **Figure 6.7B** schematically)

$$\begin{pmatrix} \dot{R}^*_{ip}(t) \\ \dot{R}^*_{ic}(t) \end{pmatrix} = \begin{pmatrix} -k_{ii} & k_{ir} \\ k_{ii} & -(k_{ir}+\delta_{in}) \end{pmatrix} \begin{pmatrix} R^*_{ip}(t) \\ R^*_{ic}(t) \end{pmatrix} \tag{6.36}$$

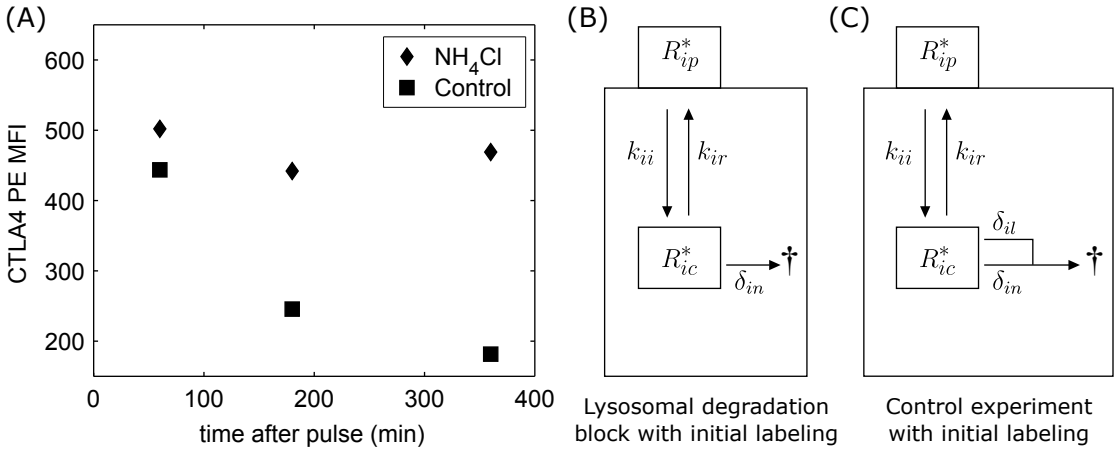

Figure 6.7: CTLA4 degradation block. (A) CTLA4-expressing CHO cells were labeled with a 1-hour pulse of anti-CTLA4 PE. Cells were then washed and incubated for various time-points in the presence or absence of NH_4Cl and analyzed for CTLA4 expression by flow cytometry. (B) Schematic of the model for NH_4Cl-dependent lysosomal degradation block with initial labeling, given in (6.36). (C) Schematic of the model for control experiment with initial labeling.

with initial conditions given in (6.35). The complete solution of this model is (see **Apendix B.3**):

$$R^*_{ip}(t) = C_1 e^{\lambda_1 t} + C_2 e^{\lambda_2 t}, \tag{6.37}$$

$$R^*_{ic}(t) = C_1 \frac{k_{ii} + \lambda_1}{k_{ir}} e^{\lambda_1 t} + C_2 \frac{k_{ii} + \lambda_2}{k_{ir}} e^{\lambda_2 t}, \tag{6.38}$$

where

$$\lambda_1 = \frac{1}{2}\left[-(k_{ii} + k_{ir} + \delta_{in}) - \sqrt{(k_{ii} + k_{ir} + \delta_{in})^2 - 4k_{ii}\delta_{in}}\right], \tag{6.39}$$

$$\lambda_2 = \frac{1}{2}\left[-(k_{ii} + k_{ir} + \delta_{in}) + \sqrt{(k_{ii} + k_{ir} + \delta_{in})^2 - 4k_{ii}\delta_{in}}\right] \tag{6.40}$$

are the eigenvalues of the model and

$$C_1 = -R^*_{ic,0} \frac{k_{ir}}{\lambda_2 - \lambda_1} + R^*_{ip,0} \frac{k_{ii} + \lambda_2}{\lambda_2 - \lambda_1}, \tag{6.41}$$

$$C_2 = R^*_{ic,0} \frac{k_{ir}}{\lambda_2 - \lambda_1} - R^*_{ip,0} \frac{k_{ii} + \lambda_1}{\lambda_2 - \lambda_1} \tag{6.42}$$

are the constant coefficients. The experimentally quantified value (observer) which is reported in **Figure 6.7A-NH_4Cl**, is equivalent to the following theoretical value

$$Y_{\mathrm{NH_4Cl},1}(t) = R^*_{ip}(t) + R^*_{ic}(t). \tag{6.43}$$

In the same experiment where NH_4Cl was missing in the medium, the similar model as (6.36) can be used by replacing δ_{in} with $\delta_{ic} = \delta_{il} + \delta_{in}$ (see **Figure 6.7C**). The theoretical value below is equivalent to experimentally quantified values shown in **Figure 6.7A-Control**

$$Y_{\mathrm{CTR}}(t) = R^*_{ip,\mathrm{CTR}}(t) + R^*_{ic,\mathrm{CTR}}(t), \tag{6.44}$$

where $R^*_{ip,\mathrm{CTR}}(t)$ and $R^*_{ic,\mathrm{CTR}}(t)$ have the following form

$$R^*_{ip,\mathrm{CTR}}(t) = C_1 e^{\lambda_{1,\mathrm{CTR}} t} + C_2 e^{\lambda_{2,\mathrm{CTR}} t}, \tag{6.45}$$

$$R^*_{ic,\mathrm{CTR}}(t) = C_1 \frac{k_{ii} + \lambda_{1,\mathrm{CTR}}}{k_{ir}} e^{\lambda_{1,\mathrm{CTR}} t} + C_2 \frac{k_{ii} + \lambda_{2,\mathrm{CTR}}}{k_{ir}} e^{\lambda_{2,\mathrm{CTR}} t} \tag{6.46}$$

where

$$\lambda_{\mathsf{CTR},1} = \frac{1}{2}\left[-(k_{ii} + k_{ir} + \delta_{ic}) - \sqrt{(k_{ii} + k_{ir} + \delta_{ic})^2 - 4k_{ii}\delta_{ic}}\right], \tag{6.47}$$

$$\lambda_{\mathsf{CTR},2} = \frac{1}{2}\left[-(k_{ii} + k_{ir} + \delta_{ic}) + \sqrt{(k_{ii} + k_{ir} + \delta_{ic})^2 - 4k_{ii}\delta_{ic}}\right] \tag{6.48}$$

are the eigenvalues of the model with $\delta_{ic} = \delta_{il} + \delta_{in}$ and

$$C_1 = -R^*_{ic,0} \frac{k_{ir}}{\lambda_{\mathsf{CTR},2} - \lambda_{\mathsf{CTR},1}} + R^*_{ip,0} \frac{k_{ii} + \lambda_{\mathsf{CTR},2}}{\lambda_{\mathsf{CTR},2} - \lambda_{\mathsf{CTR},1}}, \tag{6.49}$$

$$C_2 = R^*_{ic,0} \frac{k_{ir}}{\lambda_{\mathsf{CTR},2} - \lambda_{\mathsf{CTR},1}} - R^*_{ip,0} \frac{k_{ii} + \lambda_{\mathsf{CTR},1}}{\lambda_{\mathsf{CTR},2} - \lambda_{\mathsf{CTR},1}} \tag{6.50}$$

are the constant coefficients.

In another experiment, CHO cells were treated with or without NH_4Cl for 3 hours. Then, total cellular CTLA4 molecules were quantified by flow cytometry using anti-CTLA4 PE, a fluorescently labeled antibody. Data of this experiment is shown in **Figure 6.8**. This experiment can be represented by the following model

$$\begin{pmatrix}\dot{R}_{ip}(t)\\ \dot{R}_{ic}(t)\end{pmatrix} = \begin{pmatrix}-k_{ii} & k_{ir}\\ k_{ii} & -(k_{ir}+\delta_{in})\end{pmatrix}\begin{pmatrix}R_{ip}(t)\\ R_{ic}(t)\end{pmatrix} + \begin{pmatrix}\sigma_i\\ 0\end{pmatrix} \tag{6.51}$$

where degradation in cytoplasm only includes non-lysosomal degradation pathway (with rate δ_{in}). Model (6.51) has the following initial conditions which is similar to steady state values of general model (6.1) given in (6.2) with $\delta_{ic} = \delta_{il} + \delta_{in}$

$$R_{ip,0} = \frac{\sigma_i(k_{ir}+\delta_{il}+\delta_{in})}{k_{ii}(\delta_{il}+\delta_{in})}, \tag{6.52}$$

$$R_{ic,0} = \frac{\sigma_i}{\delta_{il}+\delta_{in}}. \tag{6.53}$$

Note that the total cellular CTLA4 before adding NH_4Cl is equal to:

$$R_{ip,0} + R_{ic,0} = \frac{\sigma_i(k_{ii}+k_{ir}+\delta_{il}+\delta_{in})}{k_{ii}(\delta_{il}+\delta_{in})}. \tag{6.54}$$

The exact solution of the model is as follows (see **Appendix B.4.1**)

$$R_{ip}(t) = -\frac{\sigma_i(\lambda_1+\lambda_2+k_{ii})}{\lambda_1\lambda_2} + C_1e^{\lambda_1 t} + C_2e^{\lambda_2 t}, \tag{6.55}$$

$$R_{ic}(t) = -\frac{\sigma_i}{k_{ir}}\frac{(k_{ii}+\lambda_1)(k_{ii}+\lambda 2)}{\lambda_1\lambda_2} + C_1\frac{k_{ii}+\lambda_1}{k_{ir}}e^{\lambda_1 t} + C_2\frac{k_{ii}+\lambda_2}{k_{ir}}e^{\lambda_2 t} \tag{6.56}$$

where

$$\lambda_1 = \frac{1}{2}\left[-(k_{ii}+k_{ir}+\delta_{in}) - \sqrt{(k_{ii}+k_{ir}+\delta_{in})^2 - 4k_{ii}\delta_{in}}\right], \tag{6.57}$$

$$\lambda_2 = \frac{1}{2}\left[-(k_{ii}+k_{ir}+\delta_{in}) + \sqrt{(k_{ii}+k_{ir}+\delta_{in})^2 - 4k_{ii}\delta_{in}}\right], \tag{6.58}$$

$$C_1 = -R_{ic,0}\frac{k_{ir}}{\lambda_2-\lambda_1} + R_{ip,0}\frac{k_{ii}+\lambda_2}{\lambda_2-\lambda_1} + \frac{\sigma_i(k_{ii}+\lambda_2)}{\lambda_1(\lambda_2-\lambda_1)}, \tag{6.59}$$

$$C_2 = R_{ic,0}\frac{k_{ir}}{\lambda_2-\lambda_1} - R_{ip,0}\frac{k_{ii}+\lambda_1}{\lambda_2-\lambda_1} - \frac{\sigma_i(k_{ii}+\lambda_1)}{\lambda_2(\lambda_2-\lambda_1)}. \tag{6.60}$$

$\lambda_{1,2}$ are the eigenvalues of the model (6.51). During parameter estimation by differential evolution, random generation of parameters may set extremely low values for δ_{in}, which results in one approximately zero eigenvalue in the model. In the special case of $\delta_{in} = 0$, the solution of the model is as follows (see **Appendix B.4.2**)

$$R_{ip}(t) = \frac{\sigma_i}{\lambda_2}\left[(k_{ii}+\lambda_2)t + \frac{k_{ii}}{\lambda_2}\right] + C_1 + C_2e^{\lambda_2 t}, \tag{6.61}$$

$$R_{ic}(t) = \frac{\sigma_i k_{ii}(k_{ii}+\lambda_2)}{k_{ir}\lambda_2}\left[t + \frac{1}{\lambda_2}\right] + C_1\frac{k_{ii}}{k_{ir}} + C_2\frac{k_{ii}+\lambda_2}{k_{ir}}e^{\lambda_2 t} \tag{6.62}$$

where

$$\lambda_1 = -(k_{ii}+k_{ir}), \tag{6.63}$$

$$\lambda_2 = 0 \tag{6.64}$$

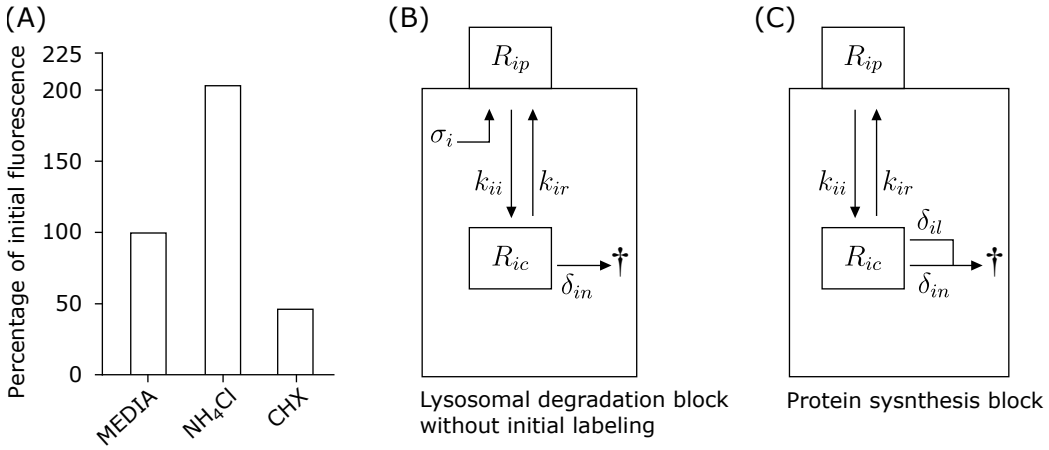

Figure 6.8: CTLA4 degradation and synthesis block. (A) CHO cells expressing CTLA4 were treated as shown for 3 hours followed by fixation and staining for total cellular CTLA4 using anti-CTLA4 PE. Cells were analyzed by flow cytometry, and the relative fluorescence was plotted. Data are reported in [212]. (B) Schematic of the model for NH_4Cl-dependent block of lysosomal degradation, given in (6.51). In this experiment $\delta_{il} = 0$. All CTLA4 molecules could be observed in this experiment, in contrast to model (6.36) where only an initially labeled subset of CTLA4 molecules were observed. (C) Schematic of the model for CHX-dependent CTLA4 synthesis block, given in (6.68). In this model, $\sigma_i = 0$, and total CTLA4 molecules were counted experimentally.

are the eigenvalues of the model and

$$C_1 = \left(1 + \frac{k_{ii}}{\lambda_2}\right) R_{ip,0} - \frac{k_{ir}}{\lambda_2} R_{ic,0}, \tag{6.65}$$

$$C_2 = \frac{k_{ir}}{\lambda_2} R_{ic,0} - \frac{k_{ii}}{\lambda_2} R_{ip,0} - \frac{\sigma_i k_{ii}}{\lambda_2^2} \tag{6.66}$$

are the constant coefficients. The quantified value shown in **Figure 6.8** is

$$Y_{\mathrm{NH_4Cl},2}(t) = \frac{R_{ip}(t) + R_{ic}(t)}{R_{ip,0} + R_{ic,0}} \tag{6.67}$$

where $R_{ip,0} + R_{ic,0}$ is given in (6.54). Note that in observer (6.67), the rate of protein synthesis (σ_i) cannot be observed.

6.2.5 Model 5: blocking receptor synthesis

To observe the contribution of CTLA4 synthesis in CTLA4 homeostatic numbers, CTLA4-expressing CHO cells were treated with Cycloheximide (CHX) which is known to block protein synthesis. The data in **Figure 6.8** indicates 3 hours of CTLA4 trafficking without protein synthesis ($\sigma_i = 0$). This experiment can be modeled by the following equations (shown schematically in **Figure 6.8C**), with initial CTLA4 values obtained from steady state values of the general model (6.1), which has the protein synthesis

$$\begin{pmatrix} \dot{R}_{ip}(t) \\ \dot{R}_{ic}(t) \end{pmatrix} = \begin{pmatrix} -k_{ii} & k_{ir} \\ k_{ii} & -(k_{ir} + \delta_{ic}) \end{pmatrix} \begin{pmatrix} R_{ip}(t) \\ R_{ic}(t) \end{pmatrix}. \tag{6.68}$$

At $t = 0$ the CTLA4 values are as follows (which indicates the CTLA4 values before adding CHX)

$$R_{ip,0} = \frac{\sigma_i(k_{ir} + \delta_{ic})}{k_{ii}\delta_{ic}},$$
$$R_{ic,0} = \frac{\sigma_i}{\delta_{ic}}. \tag{6.69}$$

Total number of cellular CTLA4 molecules before adding CHX is

$$R_{ip,0} + R_{ic,0} = \frac{\sigma_i(k_{ii} + k_{ir} + \delta_{ic})}{k_{ii}\delta_{ic}} = \frac{-\sigma_i(\lambda_1 + \lambda_2)}{\lambda_1\lambda_2} \tag{6.70}$$

where λ_1 and λ_2 are the eigenvalues of the model (6.68):

$$\lambda_1 = \frac{1}{2}\left[-(k_{ii} + k_{ir} + \delta_{ic}) - \sqrt{(k_{ii} + k_{ir} + \delta_{ic})^2 - 4k_{ii}\delta_{ic}}\right], \tag{6.71}$$
$$\lambda_2 = \frac{1}{2}\left[-(k_{ii} + k_{ir} + \delta_{ic}) + \sqrt{(k_{ii} + k_{ir} + \delta_{ic})^2 - 4k_{ii}\delta_{ic}}\right]. \tag{6.72}$$

The CTLA4 levels in CHO cells by treating with CHX are varying according to the following functions (see **Appendix B.5**):

$$R_{ip}(t) = C_1 e^{\lambda_1 t} + C_2 e^{\lambda_2 t}, \tag{6.73}$$
$$R_{ic}(t) = C_1\frac{k_{ii} + \lambda_1}{k_{ir}} e^{\lambda_1 t} + C_2\frac{k_{ii} + \lambda_2}{k_{ir}} e^{\lambda_2 t} \tag{6.74}$$

where

$$C_1 = \frac{\sigma_i[\lambda_1\lambda_2 + (k_{ir} + \delta_{ic})\lambda_2]}{\lambda_1\lambda_2(\lambda_2 - \lambda_1)}, \tag{6.75}$$
$$C_2 = -\frac{\sigma_i[\lambda_1\lambda_2 + (k_{ir} + \delta_{ic})\lambda_1]}{\lambda_1\lambda_2(\lambda_2 - \lambda_1)} \tag{6.76}$$

are the constant coefficients. The data in **Figure 6.8** indicates the ratio of the number of CTLA4 molecules at $t = 180$ minutes without protein synthesis and the control. The number of CTLA4 molecules in control cells is equal to the initial values. Control and synthesis-blocked cells are equivalent at $t = 0$. The observer of this experiment is as follows

$$Y_{\mathrm{CHX}}(t) = \frac{R_{ip}(t) + R_{ic}(t)}{R_{ip,0} + R_{ic,0}}. \tag{6.77}$$

Note that in (6.77), the rate of protein synthesis (σ_i) cannot be observed.

6.2.6 Model 6: receptor recycling

Kinetics of CTLA4 recycling was carried out by confocal microscopy. CTLA4-expressing CHO cells were incubated with Alexa488-conjugated anti-CTLA4 (a green antibody) for 60 min at $37\,^{\circ}\mathrm{C}$. During this step, a subset of CTLA4 molecules were labeled via cell surface and subsequently internalized or further recycled to the plasma membrane. Assume that the labeled CTLA4 on the plasma membrane and in cytoplasm are represented by R^g_{ip} and R^g_{ic}, respectively. Schematic of a model that can represent this labeling step is shown in **Figure 6.9A**. This model has the following form

$$\begin{pmatrix}\dot{R}_{ic}(t)\\ \dot{R}^g_{ip}(t)\\ \dot{R}^g_{ic}(t)\end{pmatrix} = \begin{pmatrix}-(k_{ir} + \delta_{ic}) & 0 & 0\\ k_{ir} & -k_{ii} & k_{ir}\\ 0 & k_{ii} & -(k_{ir} + \delta_{ic})\end{pmatrix}\begin{pmatrix}R_{ic}(t)\\ R^g_{ip}(t)\\ R^g_{ic}(t)\end{pmatrix} + \begin{pmatrix}0\\ \sigma_i\\ 0\end{pmatrix} \tag{6.78}$$

with the following initial conditions

$$R^g_{ip,0} = \frac{\sigma_i(k_{ir}+\delta_{ic})}{k_{ii}\delta_{ic}} \tag{6.79}$$

$$R_{ic,0} = \frac{\sigma_i}{\delta_{ic}} \tag{6.80}$$

$$R^g_{ic,0} = 0 \tag{6.81}$$

Model (6.78) is equivalent to model (6.16) representing the labeling process. Therefore, according to solutions given in (6.20), the following amount of CTLA4 are greed-labeled after $t_0 = 60$ minutes:

$$R_{ic,t_0} = \frac{\sigma_i}{\delta_{ic}} e^{-(k_{ir}+\delta_{ic})t_0} \tag{6.82}$$

$$R^g_{ip,t_0} = R^g_{ip,0} = \frac{\sigma_i(k_{ir}+\delta_{ic})}{k_{ii}\delta_{ic}} \tag{6.83}$$

$$R^g_{ic,t_0} = \frac{\sigma_i}{\delta_{ic}}\left(1 - e^{-(k_{ir}+\delta_{ic})t_0}\right) \tag{6.84}$$

Cells were then washed, and surface CTLA4 molecules were blocked on ice with unconjugated anti-human IgG, an antibody without color. Let's assume that this blocking antibody bound to all green-labeled CTLA4 molecules on plasma membrane (represented by R^{gB}_{ip}). Once the trafficking is allowed, these green and blocked CTLA4 molecules can be internalized to the cytoplasm (represented by R^{gB}_{ic}). Since the blocking process was on ice, no green and blocked CTLA4 molecules was internalized. Therefore, the values of of green-blocked CTLA molecules on plasma mebrane and in cytoplasm are:

$$R^{gB}_{ip,t_0} = R^g_{ip,t_0} = \frac{\sigma_i(k_{ir}+\delta_{ic})}{k_{ii}\delta_{ic}} \tag{6.85}$$

$$R^{gB}_{ic,t_0} = 0 \tag{6.86}$$

Next, cells were washed (no further CTLA4 blocking was possible) and incubated with Alexa555-conjugated anti-human IgG (a red antibody) at $37\,^{\circ}\mathrm{C}$. This antibody is able to bind to green-labeled CTLA4 molecules that are not blocked. Therefore, this allows to detect green-labeled CTLA4 molecules that are recycling to plasma membrane from cytoplasm. The red labeled CTLA4 molecules on plasma membrane and cytoplasm are represented by R^{gr}_{ip} and R^{gr}_{ic}, respectively. During the second labeling process states of the model follow equations below:

$$\begin{pmatrix} \dot{R}^{gB}_{ip}(t) \\ \dot{R}^{gB}_{ic}(t) \end{pmatrix} = \begin{pmatrix} -k_{ii} & k_{ir} \\ k_{ii} & -(k_{ir}+\delta_{ic}) \end{pmatrix} \begin{pmatrix} R^{gB}_{ip}(t) \\ R^{gB}_{ic}(t) \end{pmatrix} \tag{6.87}$$

$$\begin{pmatrix} \dot{R}^{g}_{ic}(t) \\ \dot{R}^{gr}_{ip}(t) \\ \dot{R}^{gr}_{ic}(t) \end{pmatrix} = \begin{pmatrix} -(k_{ir}+\delta_{ic}) & 0 & 0 \\ k_{ir} & -k_{ii} & k_{ir} \\ 0 & k_{ii} & -(k_{ir}+\delta_{ic}) \end{pmatrix} \begin{pmatrix} R^{g}_{ic}(t) \\ R^{gr}_{ip}(t) \\ R^{gr}_{ic}(t) \end{pmatrix} \tag{6.88}$$

with the initial conditions given in (6.84), (6.85), (6.86) and the followings:

$$R^{gr}_{ip,t_0} = 0 \tag{6.89}$$

$$R^{gr}_{ic,t_0} = 0 \tag{6.90}$$

Submodel (6.87) is equivalent to internalization model (6.26), and submodel (6.88) is equivalent to

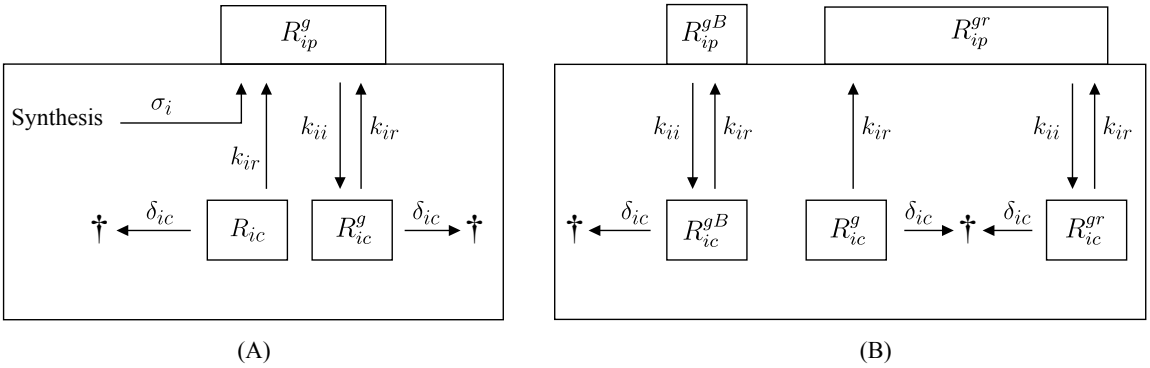

Figure 6.9: CTLA4 recycling model. Similar to PM/I experiment (Figure 6.4), nonlinear labeling model can be simplified to a linear ODE model. Only the simplified models are shown here. Recycling model is developed for two experimental steps: submodel (A) corresponds to first labeling process with Alexa488-conjugated anti-CTLA4 (green) and submodel (B) corresponds to second labeling step with Alexa555-conjugated anti-human IgG (red), during which the recycling of green-labeled CTLA4 molecules occurs after initially blocking the green-labeled CTLA4 molecules on plasma membrane (on ice). Note that the number of green-labeled CTLA4 molecules after 1 hour in submodel (A) is used as initial conditions for submodel (B).

homogeneous version of labeling model in (6.16). The following solutions can be obtained (see **Appendix B.6**):

$$R^{gB}_{ip}(t) = -\frac{k_{ii}+\lambda_3}{\lambda_2-\lambda_3}R^{gB}_{ip,0}e^{\lambda_2 t} + \frac{k_{ii}+\lambda_2}{\lambda_2-\lambda_3}R^{gB}_{ip,0}e^{\lambda_3 t}, \tag{6.91}$$

$$R^{gB}_{ic}(t) = \frac{k_{ii}}{\lambda_2-\lambda_3}R^{gB}_{ip,0}e^{\lambda_2 t} - \frac{k_{ii}}{\lambda_2-\lambda_3}R^{gB}_{ip,0}e^{\lambda_3 t}, \tag{6.92}$$

$$R^{g}_{ic}(t) = R^{g}_{ic,t_0}e^{\lambda_1 t}, \tag{6.93}$$

$$R^{gr}_{ip}(t) = -R^{g}_{ic,t_0}\frac{k_{ir}}{\lambda_3-\lambda_2}e^{\lambda_2 t} + R^{g}_{ic,t_0}\frac{k_{ir}}{\lambda_3-\lambda_2}e^{\lambda_3 t}, \tag{6.94}$$

$$R^{gr}_{ip}(t) = -R^{g}_{ic,t_0}e^{\lambda_1 t} - R^{g}_{ic,t_0}\frac{k_{ii}+\lambda_2}{\lambda_3-\lambda_2}e^{\lambda_2 t} + R^{g}_{ic,t_0}\frac{k_{ii}+\lambda_3}{\lambda_3-\lambda_2}e^{\lambda_3 t}, \tag{6.95}$$

where

$$\lambda_1 = -(k_{ir}+\delta_{ic}), \tag{6.96}$$

$$\lambda_2 = \frac{1}{2}\left[-(k_{ii}+k_{ir}+\delta_{ic}) - \sqrt{(k_{ii}+k_{ir}+\delta_{ic})^2 - 4k_{ii}\delta_{ic}}\right], \tag{6.97}$$

$$\lambda_3 = \frac{1}{2}\left[-(k_{ii}+k_{ir}+\delta_{ic}) + \sqrt{(k_{ii}+k_{ir}+\delta_{ic})^2 - 4k_{ii}\delta_{ic}}\right] \tag{6.98}$$

are the eigenvalues of the model, R^g_{ic,t_0} and $R^{gB}_{ip,0}$ are given in (6.84) and (6.85), respectively. In notation of variables, the superscript gr is taken from "green-red" which means that these molecules is labeled with both labeling antibody, gB is taken from "green-blocked" and g is taken from "green".

All the green and red labeled CTLA4 molecules were quantified by confocal microscopy. Experimental data are shown in **Figure 6.10**. Green and red fluorescent intensities are assumed to be proportional to the theoretical values, $\mathrm{G}(t)$ and $\mathrm{R}(t)$, respectively. Note that experimental values were measured by confocal microscopy, and therefore, only fractions of CTLA4 molecules on plasma membrane and in cytoplasm were

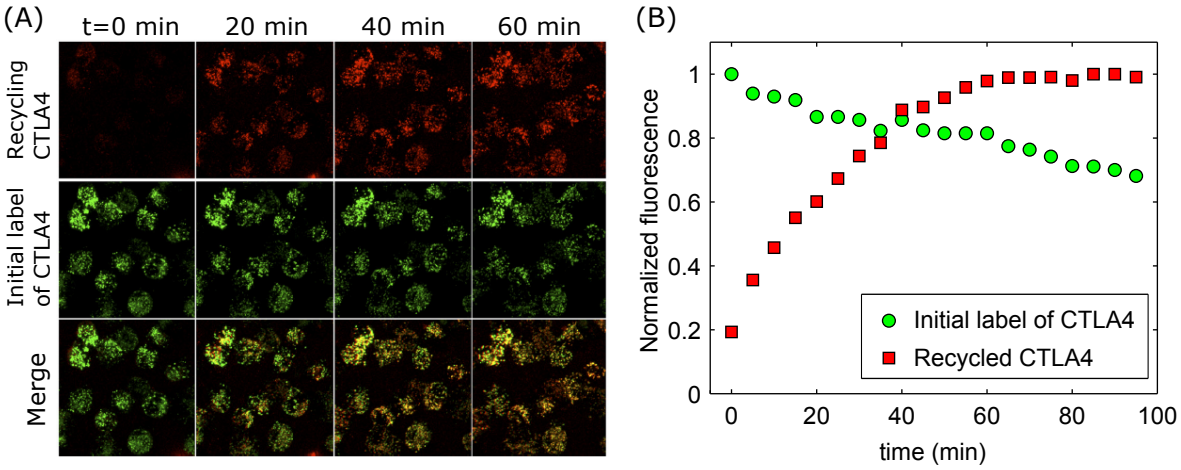

Figure 6.10: CTLA4 recycling data [212]. (A) Live-cell confocal imaging of recycling receptors was carried out using CTLA4-expressing CHO cells. Cells were incubated with Alexa488-conjugated anti-CTLA4 (green antibody) for 60 minutes at $37\,^{\circ}\mathrm{C}$. Cells were then washed, and surface CTLA4 receptors were blocked with unconjugated anti-human IgG at $4\,^{\circ}\mathrm{C}$ (secondary antibody without any color). Cells were then incubated with Alexa555-conjugated anti-human IgG (secondary antibody with red color) to detect recycling receptors. Confocal Z-stacks were then acquired at the time points shown. Panel (B) shows quantification of mean fluorescent intensities from (A).

observed (see equation (6.24) and **Figure 6.5**). These values are

$$\mathrm{G}(t) = \frac{V_{\mathrm{vis}}}{V}\left[R_{ic}^{gB}(t) + R_{ic}^{g}(t) + R_{ic}^{gr}(t)\right] + \frac{A_{\mathrm{vis}}}{A}\left[R_{ip}^{gB}(t) + R_{ip}^{gr}(t)\right] \tag{6.99}$$

$$\mathrm{R}(t) = \frac{V_{\mathrm{vis}}}{V}R_{ic}^{gr}(t) + \frac{A_{\mathrm{vis}}}{A}R_{ip}^{gr}(t) \tag{6.100}$$

from which the normalized values can be obtained:

$$\bar{\mathrm{G}}(t) = \frac{\mathrm{G}(t)}{\mathrm{G}(t=0)} \tag{6.101}$$

$$Y_{\mathrm{rc,R}}(t) = \bar{\mathrm{R}}(t) = \frac{\mathrm{R}(t)}{\max(\mathrm{R}(t))} \tag{6.102}$$

Note that in (6.101), the theoretical and experimental values for $t = 0$ are equal to 1. Therefore, normalization forces zero estimation error for first data point in green fluorescence. To avoid this, we define a scaling parameter S_{rc} which allows the identification procedure to estimate the initial data point as well. Further, nonzero value of red fluorescent intensity in **Figure 6.10A-B** at $t = 0$ indicates to a delay between the starting time of recycling process and measurement. We define a forward shifting time (Δt_{rc}) for experimental measurements as a parameter to take into account such delay. By this definition, we use the following modified theoretical value for green fluorescent measurement in parameter estimation:

$$Y_{\mathrm{rc,G}}(t) = \bar{\mathrm{G}}(t) = S_{\mathrm{rc}}\frac{\mathrm{G}(t)}{\mathrm{G}(\Delta t_{\mathrm{rc}})} \tag{6.103}$$

Note that since we considered the time shift in experimental values, and red fluorescent measurements are normalized to maximum value but not to initial data point, theoretical value (6.101) does not need any modification and is suitable for parameter estimation. From observers (6.103) and (6.102), the rate of protein synthesis (σ_i) cannot be observed.

6.2.7 Model 7: trans-endocytosis

It has been shown that CTLA4 can capture CD80/CD86 ligands from opposing cells by a process of trans-endocytosis [213]. This ligand capturing is followed by degradation inside CTLA4-expressing cells. Such an observation was performed in CHO-cell lines by live-cell imaging of CTLA4$^+$ CHO cells interacting with CHO cells expressing CD86 molecules. In this experiment, a CHO cell line used in which CD86 molecules tagged with green fluorescent protein (GFP). In a mixture sample of CD86- and CTLA4-expressing CHO cells, the kinetics of CD86 removal was observed by confocal microscopy (shown in **Figure 6.11**). Herein, the aim is to use such confocal microscopy data in order to estimated the rate of CD86 removal and its subsequent fates, such as degradation.

The trans-endocytosis model (depicted in **Figure 6.12**) is composed of essential CTLA4 trafficking sub-processes that considered in previous ligand-independent models (compare **Figure 6.12** with **Figure 6.2**), in addition to CD86-trafficking components in CD86-expressing cells and molecular reactions (CTLA4 + CD86 $\rightleftarrows$ CTLA4:CD86) in cells contact surface (A_{cs}). The underlying assumptions of trans-endocytosis model are the followings:

- Rates of CTLA4 molecule synthesis (σ_i), internalization (k_{ii}), recycling (k_{ir}), degradation (δ_{ic}, δ_{il} and δ_{in}) are identical to ligand-independent model (depicted in **Figure 6.2**).
- CD86 synthesis (with rate σ_{86}) results in the maintenance of a homeostatic number of CD86 molecules on the plasma membrane (L_{86p}) and subsequently in the cytoplasm (L_{86c}) after internalization (with k_{86i}). This assumes that newly synthesized CD86 molecules are not directly undergo the degradation pathway that exists in the cytoplasm, but only after exocytosis to plasma membrane and subsequent internalization to cytoplasm.
- The cytoplasmic CD86 molecules are degraded with a constant rate δ_{86c}.
- Exocytosis (recycling) of intracellular CD86 molecules (L_{86c}) is assumed to be negligible.
- Upon interaction with CTLA4$^+$ cells, CD86 molecules on the plasma membrane of CD86$^+$ cells (L_{86p}) bind to CTLA4 molecules on the plasma membrane of opposing cell (R_{ip}) with constant binding rate ($k_{i:86}$) and form CTLA4:CD86 complex ($R_{i:86p}$). This complex can unbind with a constant rate ($\widehat{k}_{i:86}$).
- CTLA4:CD86 complex on interaction surface ($R_{i:86p}$) can be internalized by CTLA4-expressing cell (with rate k_{t86}). These internalized complexes ($R_{i:86c}$) are directly degraded (with rate $\delta_{i:86c}$), or

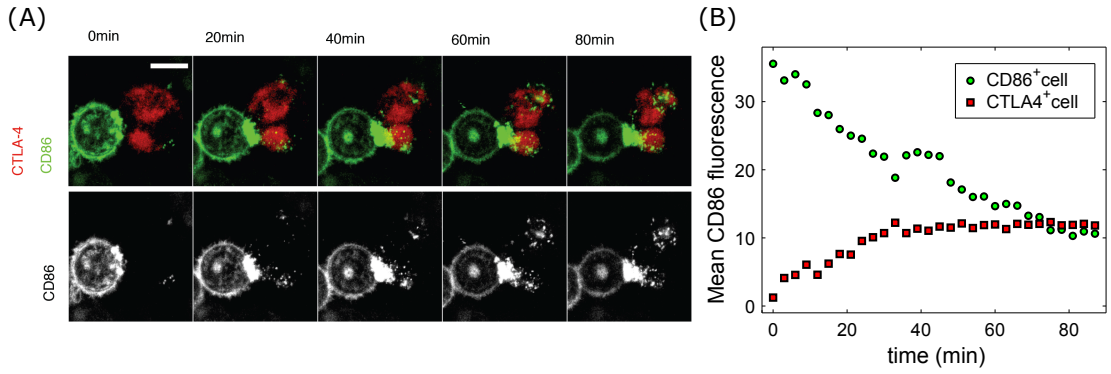

Figure 6.11: Trans-endocytosis data [213]. (A) Time-lapse (0-80 minutes) confocal micrographs of GFP-tagged CD86 (green) transfer into CTLA4 expressing cells which are stained red by pulsing anti-CTLA4 APC. White images show CD86 alone. (B) Quantitation of CD86 GFP mean fluorescence intensity of the cells shown in (A). Substantial depletion of GFP fluorescence from the plasma membrane of the CD86 donor cell and a corresponding increase in GFP inside the CTLA4$^+$ recipient cell is evident.

are dissociated (with rate k_{rc86}).

- CTLA4 molecules resulted from dissociation of CTLA4:CD86 complexes are recovered and added to cytoplasmic CTLA4 molecules (R_{ic}).
- Rate of CD86 degradation in CD86-expressing and CTLA4-expressing cells are identical.

Based on the above assumptions, trans-endocytosis model can be represented by the following nonlinear ODE-based model:

$$\dot{R}_{ic}(t) = k_{ii}R_{ip}(t) - (k_{ir} + \delta_{ic})R_{ic}(t) + k_{rc86}R_{i:86c}(t), \tag{6.104}$$

$$\dot{R}_{ip}(t) = \sigma_i + k_{ir}R_{ic}(t) - k_{ii}R_{ip}(t) - k_{i:86}\frac{R_{ip}(t)}{A}\frac{L_{86p}(t)}{A}A_{\text{cs}} + \widehat{k}_{i:86}R_{i:86p}(t), \tag{6.105}$$

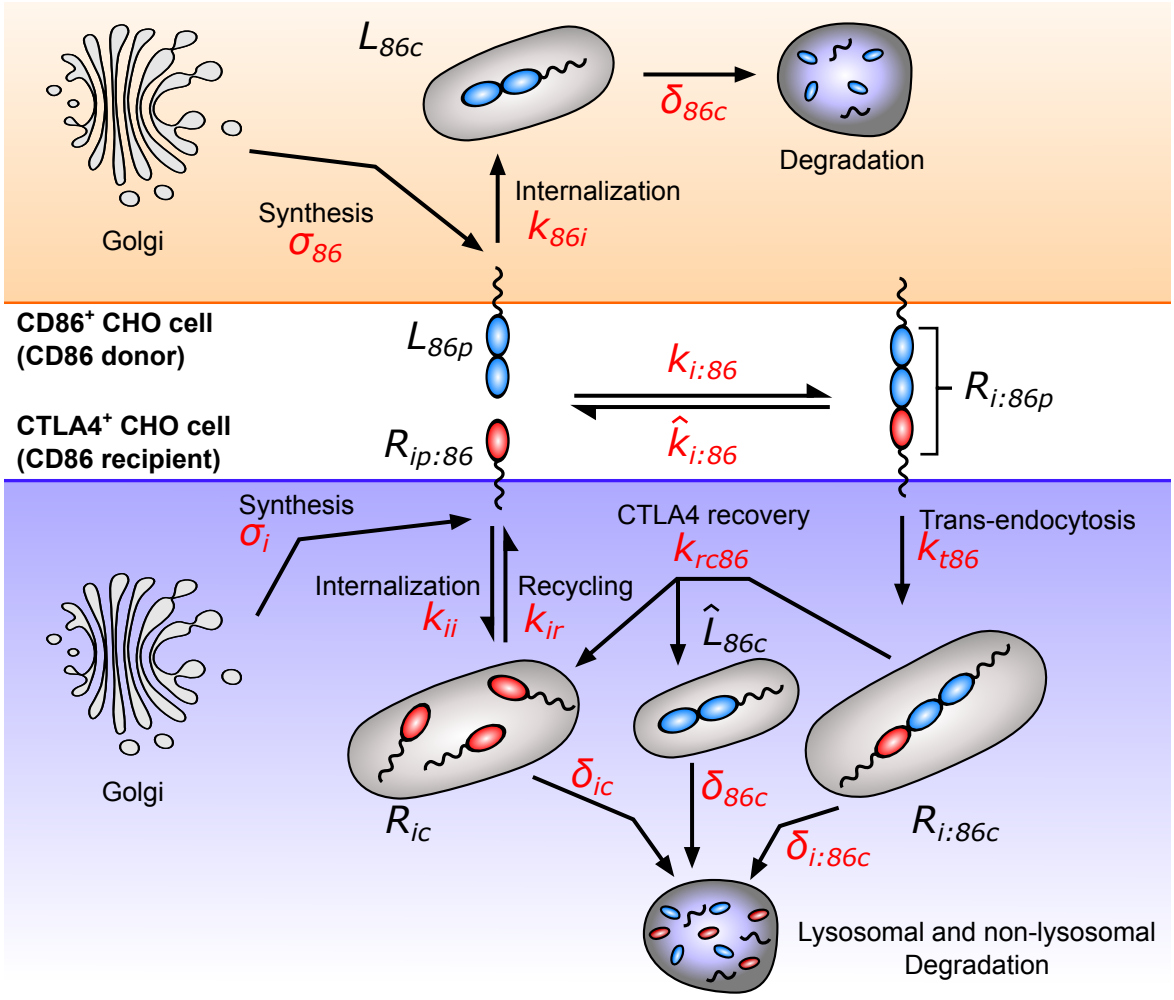

Figure 6.12: Schematic of trans-endocytosis model.

$$\dot{R}_{i:86p}(t) = k_{i:86}\frac{R_{ip}(t)}{A}\frac{L_{86p}(t)}{A}A_{\rm cs} - (k_{t86} + \widehat{k}_{i:86})R_{i:86p}(t), \tag{6.106}$$

$$\dot{R}_{i:86c}(t) = k_{t86}R_{i:86p}(t) - k_{rc86}R_{i:86c}(t) - \delta_{i:86c}R_{i:86c}(t), \tag{6.107}$$

$$\dot{\widehat{L}}_{86c}(t) = k_{rc86}R_{i:86c}(t) - \delta_{86c}\widehat{L}_{86c}(t), \tag{6.108}$$

$$\dot{L}_{86p}(t) = \sigma_{86} - k_{86i}L_{86p}(t) - k_{i:86}\frac{R_{ip}(t)}{A}\frac{L_{86p}(t)}{A}A_{\rm cs} + \widehat{k}_{i:86}R_{i:86p}(t), \tag{6.109}$$

$$\dot{L}_{86c}(t) = k_{86i}L_{86p}(t) - \delta_{86c}L_{86c}(t). \tag{6.110}$$

where $A_{\rm cs}$ is the total area of cell-cell contact surface with radius r and $A_{\rm cs,vis}$ is the visible area of contact surface in confocal microscopy (see **Figure 6.13**). Note that the nonlinearity of the model arises from the forward reaction of receptor-ligand binding (CTLA4 + CD86 $\rightarrow$ CTLA4:CD86).

The observers in this experiment are the mean fluorescent intensities acquired from CD86 donor cell and recipient cell. It is assumed that these intensities are proportional to theoretical values $G_d(t)$ and $G_r(t)$ for donor and recipient cells respectively

$$G_d(t) = \frac{V_{\rm vis}}{V}L_{86c}(t) + \frac{A_{\rm vis}}{A}L_{86p}(t) + \frac{1}{2}\frac{A_{\rm cs,vis}}{A_{\rm cs}}R_{i:86p}(t) \tag{6.111}$$

$$G_r(t) = \frac{V_{\rm vis}}{V}R_{i:86c}(t) + \frac{V_{\rm vis}}{V}\widehat{L}_{86c}(t) + \frac{1}{2}\frac{A_{\rm cs,vis}}{A_{\rm cs}}R_{i:86p}(t) \tag{6.112}$$

It is assumed that 50% of intensity arising from total CTLA4:CD86 complexes in contact surface was counted for each interacting cell.

We normalize data in **Figure 6.11B** to initial data point of CD86$^+$ cell. To avoid zero error of estimation for this data point, we define a scaling factor $S_{\rm trans}$, in the same way it was defined in (6.34) and (6.103).

As it is evident from **Figure 6.11A-B**, CD86 removal started before observing the samples in confocal microscopy. In order to incorporate this delay, an unknown forward shift $\Delta t_{\rm trans}$ is considered in data which will be estimated by parameter estimation algorithm. Hence, the following observes are used for parameter

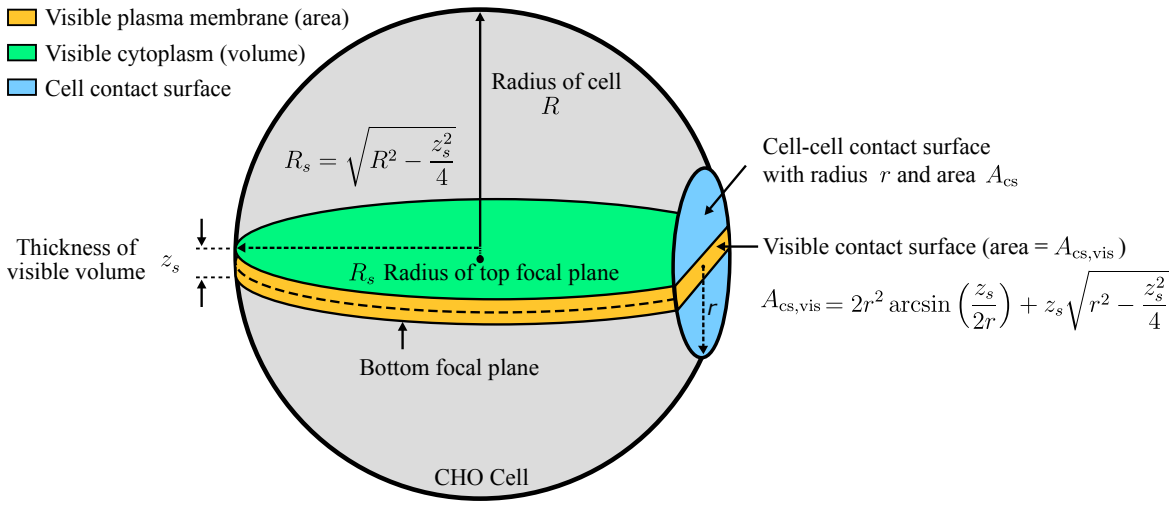

Figure 6.13: Visible area and volume of cell contacts in confocal microscopy.

estimation:

$$Y_{\mathrm{trans,d}}(t) = S_{\mathrm{trans}} \frac{G_d(t)}{G_d(\Delta t_{\mathrm{trans}})} \tag{6.113}$$

$$Y_{\mathrm{trans,r}}(t) = S_{\mathrm{trans}} \frac{G_r(t)}{G_d(\Delta t_{\mathrm{trans}})} \tag{6.114}$$

6.3 Results

The parameter estimation is divided into two steps. First, the parameters of ligand-independent model (shown in **Figure 6.2**) is acquired. Then, the parameters are used for ligand-dependent model in order to estimate remaining parameters.

6.3.1 Parameter estimation of ligand-independent model of CTLA4 trafficking

Summary of experimental and corresponding theoretical observations are given in **Table 6.1**.

Ligand-independent CTLA4 trafficking model in its simplest form (6.1) has 5 unknown parameters. There are 3 additional parameters that are concerned with the types of data reported in the literature and aimed to improve estimation quality. These parameters and associated dimensions are listed in **Table 6.2**. The following cost (objective) function $E(\theta)$ is minimized by differential evolution algorithm for parameter estimation:

$$E(\theta) = \frac{1}{\sum_{k=1}^{m} d_k} \sum_{k=1}^{m} \sum_{l=1}^{d_k} \left(\frac{\widehat{Y}_{kl} - Y_k(\theta, t_l)}{\widehat{Y}_{k,\max}} \right)^2 \tag{6.115}$$

where $\widehat{Y}_{kl}$ is observed value from k-th experiment at time $t = t_l$ and $Y_k(\theta, t_l)$ is corresponding theoretical value (observer) obtained from model with parameter set θ, d_k is the number of data points in k-th experiment, $\widehat{Y}_{k,\max}$ is the maximum observed experimental value in k-th experiment, and m is the number of independent experiments ($m \in \{1, \cdots, 7\}$). A differential evolution (DE) algorithm is performed, according to **pseudo-code 1** in chapter 3, with 1000 initial solutions with randomly generated parameters in range [0,5], $CR = 0.5$ and $F = 0.5$. Maximum number of generations $G_{\max} = 1000$ is considered as termination criterion of DE.

Table 6.1: Summary of ligand-independent experiments

Exp. No. (m)	Experiment description		Observer	Equation	# points	Max time
1	PM/I ratio		$Y_{\mathrm{PM/I}}$	(6.25)	1	30 min
2	Internalization		Y_{int}	(6.34)	5	30 min
3	Lysosomal degradation block of initially labeled CTLA4		$Y_{\mathrm{NH_4Cl,1}}$	(6.43)	3	360 min
4	Control experiment		Y_{CTR}	(6.44)	3	360 min
5	Lysosomal degradation block without initial labeling		$Y_{\mathrm{NH_4Cl,2}}$	(6.67)	1	180 min
6	Synthesis block		Y_{CHX}	(6.77)	1	180 min
7G	Recycling	Red fluorescent	$Y_{\mathrm{rc,R}}$	(6.102)	20	95 min
7R		Green fluorescent	$Y_{\mathrm{rc,G}}$	(6.103)	20	

First, an optimal parameter set (θ_t^*) is obtained by considering all the experiments. Next, improvement in the value of cost function with exclusion of each independent experiment, irrespective of obtained optimal parameter values, is evaluated by following formula

$$\Delta E_m = \frac{1}{d_m} \frac{E(\theta_t^*) - E(\theta_m^*)}{E(\theta_t^*)} \tag{6.116}$$

where $E(\theta_m^*)$ is the cost function evaluated by optimal parameter set θ_m^* obtained by exclusion of m-th experiment, d_m is the number of data points in experiment m and $m \in \{1, \cdots, 7\}$. ΔE_m is a measure for improvement in the value of cost function per excluded data point, and an index to show which experiment is the major impediment in decreasing the value of cost function. Experiment exclusion results are given in **Table 6.3**.

It turned out that exclusion of PM/I experiment, where the ratio of the number of CTLA4 molecules on the plasma membrane to internalized CTLA4 molecules was obtained after an initial labeling (see section 6.2.2), leads to a large improvement ($\approx 67\%$ decrease) in the value of cost function. The main uncertainty in PM/I experiment is the difference in fluorescent intensity of two different labeling antibodies that were employed. Another round of experiment exclusion by evaluating $\Delta E_{1,m}, m \in \{2, \cdots, 7\}$, which is the evaluation of (6.116) after excluding PM/I experiment ($m = 1$), reveals a decrease of $\approx 30\%$ in the value of cost function by removing data of lysosomal-degradation block (experiment $m = 5$), despite a minor change in obtained parameter values (not shown). In **Table 6.2**, the values of parameters are given with exclusion of experiments $m = 1$ and $m = 5$. The model simulations are shown in **Figure 6.14**.

Table 6.2: Ligand-independent CTLA4 trafficking parameters

Parameter	Description	Dimension	Estimated value
σ_i	CTLA4 synthesis rate	# min^{-1}	Not identified
k_{ii}	Internalization rate	min^{-1}	0.5192
k_{ir}	Recycling rate	min^{-1}	0.02
δ_{in}	non-lysosomal degradation	min^{-1}	0.0005
δ_{il}	Lysosomal degradation	min^{-1}	0.0036
δ_{ic}	Cytoplasmic degradation rate	min^{-1}	$\delta_{il} + \delta_{in}$
S_{int}	Scaling factor in internalization model; (6.34)	-	0.9641
S_{rc}	Scaling factor in recycling model; (6.103)	-	0.9819
Δt_{rc}	Shifting time in recycling data; (6.103)	min	6.77

Table 6.3: Experiment exclusion results

Exp. No. (m)	Experiment description		# points	ΔE_m	$\Delta E_{1,m}$
1	PM/I ratio		1	67.29	-
2	Internalization		5	15.08	-238.85
3	Lysosomal degradation block of initially labelled CTLA4		3	0.78	6.92
4	Control experiment		3	1.93	10.4
5	Lysosomal degradation block without initial labeling		1	8.66	30.09
6	Synthesis block		1	-0.08	4.28
7G	Recycling	Green fluorescent	20	-1.18	0.11
7R		Red fluorescent	20		

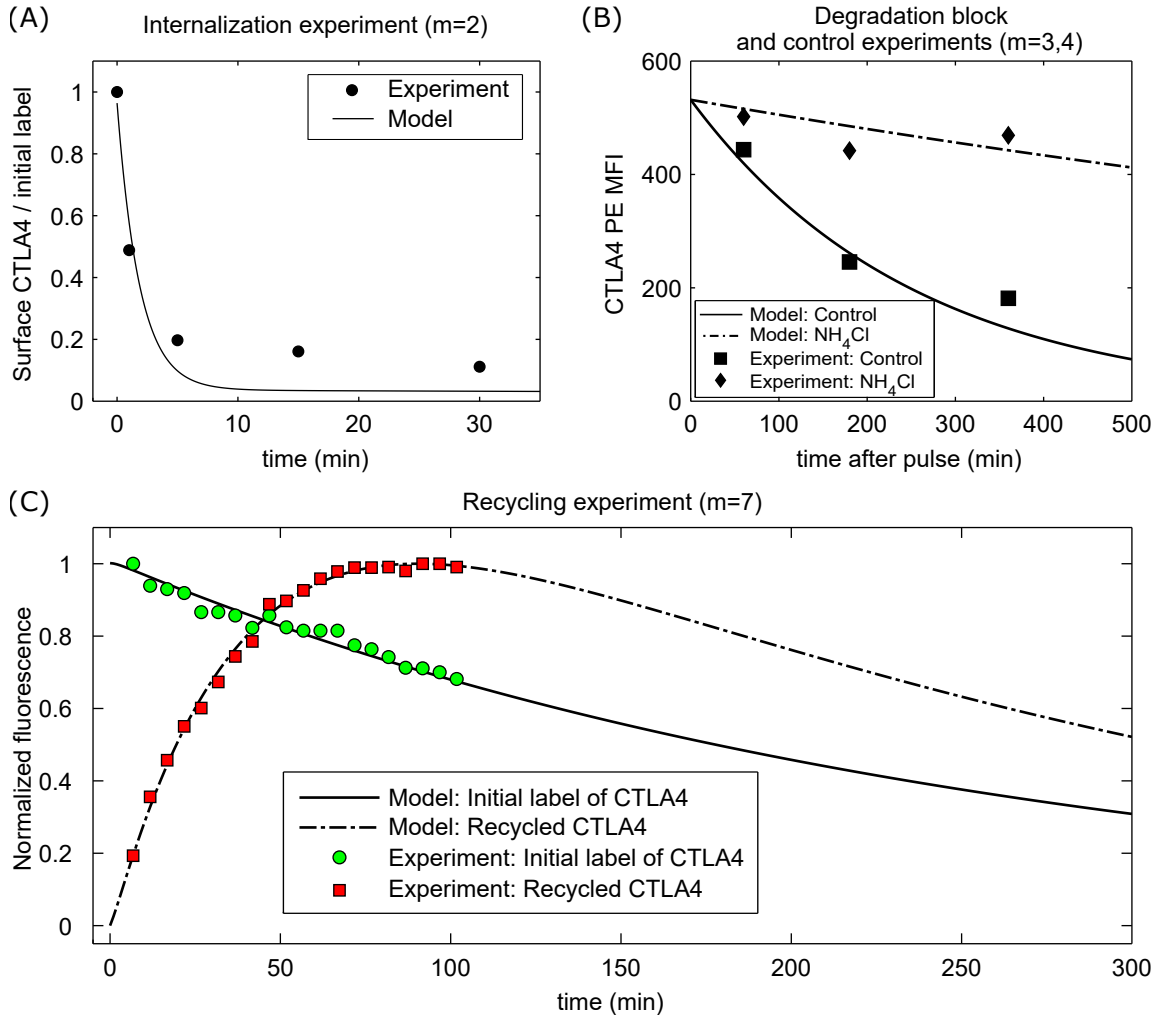

Figure 6.14: Parameter identification of ligand-independent model of CTLA4 trafficking. Parameters are given in Table 6.2. Experiments are summarized in Table 6.1. Rate of CTLA4 synthesis can only be estimated from degradation block and control experiments (m=3,4) shown in panel (B), where the absolute mean fluorescent intensities are provided ($\sigma_i = 2.69$ fluroscent intensity per minute). However, estimated rate has a dimension of fluorescent intensity per minute, but not the number of molecules ($\#$) per minute. Observed quantities in other ligand-independent experiments are independent of CTLA4 synthesis rate, as can be seen from theoretical values, mainly because of data normalization. Mean squared error of estimation for ligand-independent experiments m=1,$\cdots$,7 are $\mathrm{MSE}_1 = 0.738, \mathrm{MSE}_2 = 0.008, \mathrm{MSE}_3 = 0.0036, \mathrm{MSE}_4 = 0.006, \mathrm{MSE}_5 = 0.052, \mathrm{MSE}_6 = 0.008, \mathrm{MSE}_7 = 0.0003$. Note that experiments m=1,5 are not considered for parameter estimation.

6.3.2 Parameter estimation of trans-endocytosis

Trans-endocytosis model (**Figure 6.11**) has 14 parameters. 4 parameters ($k_{ii}, k_{ir}, \delta_{il}, \delta_{in}$) are estimated from ligand-independent models. Considering a CTLA4-independent model of CD86 trafficking (in the

absence of trans-endocytosis process):

$$\dot{L}_{86p}(t) = \sigma_{86} - k_{86i}L_{86p}(t), \tag{6.117}$$

$$\dot{L}_{86c}(t) = k_{86i}L_{86p}(t) - \delta_{86c}L_{86p}(t). \tag{6.118}$$

Equilibrium points for model above are the followings:

$$L_{86p} = \frac{\sigma_{86}}{k_{86i}}, \quad L_{86c} = \frac{\sigma_{86}}{\delta_{86c}}. \tag{6.119}$$

By considering that $X\%$ of total CD86 molecules are expressed on cell surface, we have:

$$\delta_{86c} = \frac{X}{1-X}k_{86i}. \tag{6.120}$$

The value of X is large since CD86 is mostly expressed on cell surface. We take $X = 98\%$ suggested by the authors of [213] (personal communication).

The affinity of reaction between CTLA4 and CD86 and formation of CTLA4:CD86 complex (CTLA4 + CD86 $\rightleftarrows$ CTLA4:CD86) is usually given in units of three-dimension, since they are obtained from soluble forms of reactants [14]. However, model contains a two-dimensional version of complex formation from membrane-bound reactants. Two-dimensional reactions have larger binding rates than three-dimensional reactions, since diffusion of membrane-bound reactants are more restricted. It is experimentally difficult to estimate two-dimensional binding rate, and therefore, commonly converted from three-dimensional rate constants by analytic approximations. We use approximated two-dimensional rate constants reported in [214]. Note that binding rate in the model has a dimension of $\#^{-1}\mu m^2 s^{-}1$, where $\#$ is the number of molecules. Experimental data shown in **Figure 6.11** report mean fluorescent intensity as an indicator of molecular number and consequently, binding rate should have a dimension of $[\text{Fluorescent Intensity}]^{-1}\mu m^2 s^{-1}$. Similar data normalization in both data and model, given in (6.113) and (6.114), allows to remove this discrepancy between dimensions. By using equation (6.120), and fixing binding constant rates ($k_{i:86}, \widehat{k}_{i:86}$), 7 unknown parameters remain unknown. We employ differential evolution algorithm to obtain optimal parameter set (θ^*), given observers in (6.113) and (6.114) and experimental data in **Figure 6.11**. The following cost function is minimized:

$$E(\theta) = \frac{1}{p}\left(\sum_{l=1}^{p_1}\left(\frac{\widehat{Y}_{d,l}}{\widehat{Y}_{d,1}} - Y_{\text{trans,d}}(\theta, t_l)\right)^2 + \omega^2 \sum_{l=1}^{p_2}\left(\frac{\widehat{Y}_{r,l}}{\widehat{Y}_{d,1}} - Y_{\text{trans,r}}(\theta, t_l)\right)^2\right) \tag{6.121}$$

where $\widehat{Y}_{d,l}$ is l-th experimental data point of CD86-donor cell (CD86-expressing cell), $\widehat{Y}_{r,l}$ is l-th experimental data of CD86-recipient cell (CTLA4-expressing cell), $p = 60$ is total number of data points, $p_1 = p_2 = 30$ is number of data points for each curve, and ω^2 is a weighting factor, defined as

$$\omega^2 = \left(\frac{\widehat{Y}_{d,1}}{\widehat{Y}_{r,\text{max}}}\right)^2 \tag{6.122}$$

Since the MFI curve for CD86-recipient cell ($\widehat{Y}_r$) has lower values than for CD86-donor cell ($\widehat{Y}_d$), the weighting factor ω^2 is introduced in order to increase the contribution of estimation error of the MFI curve for CD86-recipient cell. In general, one can normalize each curve, independent of other curves, to its maximum value; however, two curves in our experiment are dependent, and different data scale in these curves has an information that should not be neglected via data normalization. Instead, we use a weighting factor, rather than independent normalization, to make a fair contribution of the two curves in our cost function. This is the main reason why the cost function (6.121) differs from conventional cost functions in (6.115) or (3.39). Estimated parameters are reported in **Table 6.4**, and model prediction for the value of observers are shown in **Figure 6.15**.

Table 6.4: Parameters of trans-endocytosis model

Parameter	Description	Dimension	Value
σ_i	Rate of CTLA4 synthesis	$\#$ min^{-1}	875
σ_{86i}	Rate of CD86 synthesis	$\#$ min^{-1}	227
$k_{i:86}$	Two-dimensional binding rate of CTLA4 and CD86	$\#^{-1}$ μm^2 sec^{-1}	1.09; fixed
$\widehat{k}_{i:86}$	Unbinding rate of CTLA4:CD86 complex	sec^{-1}	5.1; fixed
k_{t86}	Trans-endocytosis rate of CTLA4:CD86 complex	min^{-1}	0.7341
k_{rc86}	Rate of CTLA4 recovery	min^{-1}	0.47307
$\delta_{i:86c}$	Rate of CTLA4:CD86 degradation	min^{-1}	0.0647148
k_{86i}	Rate of CD86 internalization	min^{-1}	0.0006
δ_{86c}	Rate of CD86 degradation	min^{-1}	$49k_{86i} = 0.0294$
S_{trans}	Scaling factor in trans-endocytosis model; (6.113) and (6.114)	-	0.957
Δt_{trans}	Shifting time in trans-endocytosis data; (6.113) and (6.114)	min	1.55

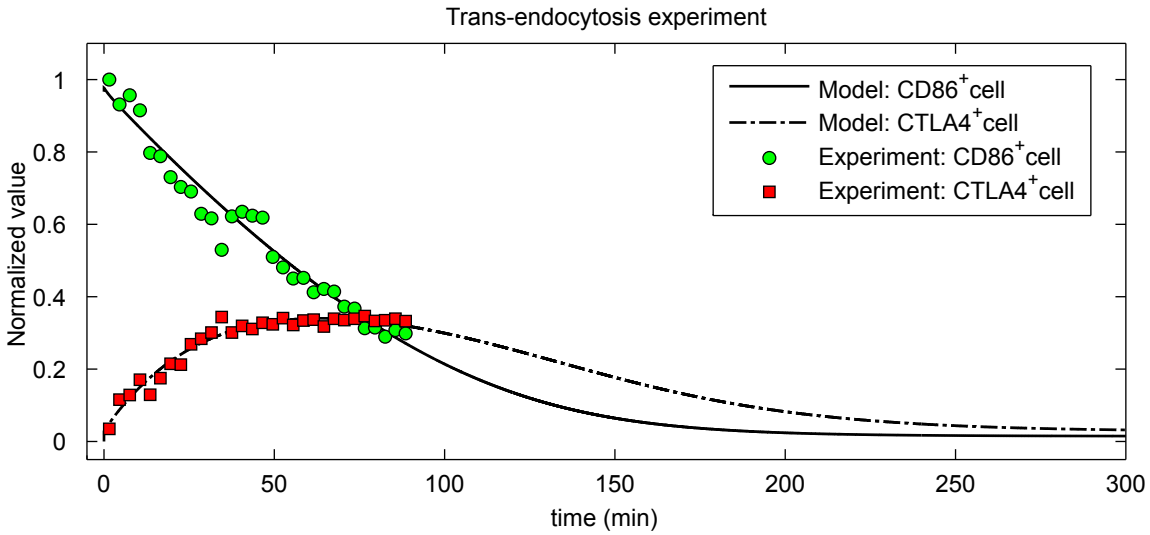

Figure 6.15: Parameter estimation of trans-endocytosis model. Parameters are given in Table 6.4. Mean squared error (MSE) of curves are $\text{MSE}_{\text{CTLA4}^+} = 0.0107, \text{MSE}_{\text{CD86}^+} = 0.0585$.

6.4 Summary

CTLA4 is an essential negative regulator of T cell immune responses and is a receptor that interacts with cell surface transmembrane ligands. Endocytosis of CTLA4 is continuous and rapid with subsequent recycling and degradation. Furthermore, upon ligation with co-stimulatory molecules, CTLA4 can remove the ligands from opposing cells by trans-endocytosis. In order to determine the impact of this cell-extrinsic mechanism of CTLA-4 in the regulation of T cell immune response, we proposed a CTLA4 trafficking model and quantify synthesis, internalization, recycling, and degradation rates of CTLA4. First, a general model is constructed by assuming all the basic mechanisms exist in CTLA-4 trafficking. Thereafter, according to the protocols used in the experiments, the general model is adapted in a way to capture the experiment-specific observations. These attempts lead to the identification of all CTLA4 trafficking parameters. The resulting and experimentally validated model can be used to develop new hypothesis of how the particular mechanism of ligands CD80/86 removal may impact onto the stimulatory potential of antigen presenting cells and, by this, onto the control of immune stimulation versus suppression.

Chapter 7

Summary, conclusions and outlook

In this thesis, a theoretical framework is presented for analysis of immunological processes involved in immune tolerance induction, maintenance and breaking in T cell repertoire. By using a simplistic view of immunological components and processes, a series of qualitative and quantitative mathematical models are constructed and analyzed to study one of the fundamental challenges of the field of immunology which is to explain how immune tolerance is induced or should be induced. Mathematical models of immune processes are constructed for three interdependent stages, with respect to location and time, which are summarized in the following sections.

7.1 Thymic selection

The construction phase of T cell repertoire in thymus is studied by agent-based modeling approach. The interest was to explain how regulatory (suppressor) T cells and conventional (effector) T cells are extracted from a pool of T precursor cells (thymocytes) with randomly generated antigen recognition receptor (T cell receptor, TCR). Agent-based modeling approach allows us to consider heterogeneity in generation of T cell receptor (TCR) sequences, and observe the consequences of such heterogeneity in thymic selection, which is not fully achievable in experiments. We are particularly able to track the signaling dynamics of each agent (cell) with changing the environmental factors (such as the number of peptides and antigen presenting cells), which is not fully achievable experimentally in single cell level. Different experimental protocols existing in the immunological literature are translated into different corresponding agent-based simulations. These simulations allowed the validation of the agent-based model with experimental evidences. Upon model validation, the presented agent-based model is used for predictions.

By using the agent-based model, a TCR-mediated signal integration hypothesis for thymic selection is studied. This hypothesis suggests a novel mechanism by which cells would be able to extract information about the specificity of their TCRs. By tracking the signaling behavior of cells, it is shown *in silico* that by relying on the strength and dynamics of integrated TCR signal, thymocytes are able to extract the affinity of their TCR to host's MHC molecules, the molecules that present antigens derived from both host's tissues and foreign microorganisms to T cells. This suggestion is based on correlation analysis between TCR signaling components and different affinity-based indices.

It is shown *in silico* that by selecting thymocytes that sustain their integrated TCR signal in a sufficiently high level, a T cell repertoire is constructed with cells that have sufficiently high MHC affinity. It is shown that high MHC affinity allows T cells to recognize a large subset of antigens, a property known as cross-reactivity. A T cell repertoire with cross-reactive T cells would cover antigenic space with a low and physiologically affordable number of T cells.

As the result of TCR signal-based selection, highly self-reactive thymocytes that differentiate to regulatory T cells are more cross-reactive than conventional T cells. This allows a low number of regulatory T cells to cover antigenic space, including both self and nonself. Self and nonself-specific regulatory T cells have been observed experimentally, but the extent of cross-reactivity in regulatory T cell repertoire has not been investigated experimentally.

According to the model, a thymic negative selection based on strong transient peaks of integrated TCR signal eliminates a large number of thymocytes with autoreactive TCRs. We found that the escaped autoreactive thymocytes express low MHC affinity TCRs. This property would restrict their activation in the periphery; they would require a high frequency of interaction with their specific self-antigens compared to high MHC affinity T cells. Additionally, modeling results show that some regulatory T cells are always activated along with conventional T cells in identical stimulatory condition. This would assure that upon activation of escaped self-reactive T cells, a suppressing immune response exists to regulate effector functions.

In this study, a binary representation of proteins are used as a simplification for protein structures. Theoretically, amino-acid sequences can be used to study thymic selection with a particular subset of self-antigens with known sequences. Further, affinity of protein interactions could be approximated by calculating their binding free energies. In practice, however, this demands a high computational power, even in the scale of a single interaction of proteins, and might not be applicable for simulating a large number of interactions.

Presented model is not a spatial model for thymic selection. Evidently, peptides are not distributed uniformly in thymic microenvironments [7]. Depending on the type of peptides, they are presented in different locations by different antigen presenting cells. It is of interest to investigate how adding space into thymic selection would limit positive and negative selections with respect to a particular self-peptide.

The proposed signal integration model is a proof of concept of how TCR-mediated integrated signal can be translated into fate decisions in thymus. A few biological data are used to fit parameters of the model, such as ratio of different repertoires or density of presentation for a particular peptide. Therefore, proposed model is a qualitative model of thymic selection. This model can be used for predicting the outcome of different manipulations in thymic selection; however, the predictions should be interpreted in a qualitative fashion, and no quantitative predication should be expected. Further investigations are required to identify biologically relevant TCR-mediated signals and required intracellular components that would allow translation of signaling dynamics into fate decisions.

7.2 Immune activation

After selection of T cell repertoire, activation and interplay of conventional T cells and regulatory T cells is studied by a series of models based on ODEs. In our study, autoimmunity is considered as a natural phenomenon, with autoimmune T cells being present in healthy individuals. Autoimmune responses are usually generated in the process of mounting an immune response to foreign antigens, but autoimmune disease may arise when autoimmunity is poorly regulated [215]. In this study, a parametric regime of the immune system is found such that a beneficial and tightly restricted autoimmune response is allowed.

Hierarchical models are constructed with considering essential components in immune activation and suppression. Complexities are added incrementally to an initially considered simple model, up to a degree that a qualitatively validated model for immune response is obtained. By taking hierarchical modeling approach, contribution of each added complexity is investigated, and the parametric regime of the model with biologically relevant behavior is extracted. In the presented models, no quantitative data is used; however, models are studied purely analytically, such that different behaviors of the model for different possible values of parameters are extracted. These are mainly achieved via parametric linear stability and bifurcation analysis.

By using the simplest model, it is shown that whether an immune response can be initiated is dependent on the quality of T cell clones (rate of cell proliferation and growth-factor secretion) that are stimulated by antigen. This criterion imposes a positive saddle equilibrium point in the model, which divides the space of initial conditions to sub- and super-thresholds, such that a minor and a major proliferative immune response can be obtained, respectively. The same saddle point results in a saddle-node bifurcation by increasing Ag-stimulation. The critical point where saddle-node bifurcation occurs defines a minimum requirement of Ag-stimulation for T cells in order to enter to the substantial proliferation phase of the immune response. In the most complex model, the minimum Ag-stimulation threshold depends on the absolute number and ratio of regulatory to conventional T cells, which is controlled by renewal rate of resting regulatory and naïve conventional T cells.

In the context of autoreactive T cells, renewal rate is tightly restricted by central tolerance in which thymocytes with high affinity TCRs to self-peptides are eliminated. This restriction does not largely affect thymic production of foreign-specific T cells. For natural regulatory T cells, renewal rate is tightly regulated by thymic selection of regulatory T cells, which dominantly induces peripheral tolerance. Other mechanisms in addition to thymic production contribute to the homeostatic number of regulatory and conventional T cells, which are not considered in the immune activation model presented here. A more complex ODE-based modeling of T cell homeostasis is proposed elsewhere [6] (model is introduced in section 3.1.2 and **Figure 3.3**), which relies on high resolution kinetic data of regulatory and conventional T cells population. This model considers other mechanisms, in addition to thymic export, for T cell homeostasis. In particular, conversion of conventional T cells to regulatory T cells is explicitly considered and quantified. As an extension, via coupling of the immune activation model and the homeostasis model given in [6], dependency of immune activation to T cell homeostatic mechanisms other than thymic export can be studied. However, the major obstacle of coupling these two models is that the immune activation model is a qualitative model of monoclonal T cell activation, whereas the model presented in [6] is a data-driven polyclonal model of T cell homeostasis. A scaling parameter would be needed to connect these two models.

Normally, immune response arises from activation and proliferation of multiple clones of regulatory and conventional T cells that cross-react to presented antigens. A possible modification for the model would be to consider polyclonal T cells that cross-react to identical antigen stimulation. Experimental mice models for immune responses against foreign and self antigens are well established. By employing experimental data to the immune activation model, the quantitative differences of parameters between self and nonself reactions can be revealed.

By using hierarchical models, it is shown that regulatory T cells are the necessary component for terminating the immune response after a major peak in population of effector T cells. Model suggests that a major immune response is only allowed for a limited time-window (depends on the parameters associated with regulatory T cells) after which the immune response is suppressed completely when antigen stimulation is resolved, or subsequently enter to oscillation phases when the antigen stimulation persists. Chronic state of the immune response which is arises from over activation of regulatory T cells is another interesting property that is observed from the immune activation model, and should be validated by experiments. An interplay between effector immune response and viral dynamics has not been considered, which is left for further investigations. Model suggests that low proliferating antigens (low rate of antigen stimulation) and highly proliferating antigens (high rate of antigen stimulation) are the challenging antigens for the immune system, since both of these two types of antigens cannot elicit a major immune response.

7.3 Regulation of immune stimulation

In addition to suppression of effector activities of conventional T cells, regulatory T cells control the stimulatory capacity of antigen presenting cells (APC). T cells require both antigen specific and non-specific stimulation by APCs. Antigen-nonspecific signal is induced via ligation of CD28 molecules expressed on

T cells with CD80/CD86 molecules expressed on APCs. In the immune activation model presented in chapter 5, only antigen-specific stimulation is considered. By augmenting antigen-nonspecific stimulation (costimulation) into the model, one has to take into account the negative feedback of regulatory T cells on APCs. This negative feedback is particularly resulted from newly discovered mechanism of CD80/CD86 removal (trans-endocytosis) by CTLA4 molecules expressed by regulatory T cells. As the first step to determine the contribution of trans-endocytosis mechanism in the immune suppression, one has to identify the unusual trafficking machinery of CTLA4 molecules that leads to efficient ligand removal.

In this study, a general trafficking model is constructed by taking into account the essential sub-processes involved in the trafficking of proteins. However, since different experimental protocols are used to observe kinetics of CTLA4 molecules, a modified version of the model is constructed for each experiment in order to use experimental data. These models are solved analytically. In each model, obtaining the analytic equivalent of observed variables revealed which parameters can or cannot be observed by corresponding experiment. It is shown that the rate of protein synthesis cannot be observed by most of experiments, due to data normalization. Further, obtaining the analytic solutions of presented models allows a low computational cost for parameter estimation. This is due to replacement of numerical integrations with algebraic equations. Optimal parameters set is obtained by differential evolution algorithm.

By estimation of parameters, it is shown that endocytosis of CTLA4 is rapid with subsequent recycling and degradation. A large ratio of internalization to recycling rates (≈ 26) explains the unusual distribution of CTLA4 molecules, with higher fraction of total CTLA4 molecules being located in cytoplasm. Furthermore, it is shown that upon ligation with costimulatory molecules, CTLA4 molecule can remove CD86 ligands from opposing cells by a rate in the order of CTLA4 internalization rate (≈ 1.4-fold). To the best of our knowledge, this is the first theoretical work for quantifying the rates of CTLA4 trafficking and associated trans-endocytosis.

In the presented model, only CD86 costimulatory molecules are considered. The same models can be applied with similar experimental protocols for CD80 molecules. Differences in removal rates of CD80 versus CD86 could be of interest as these two molecules are different in their expression regime in steady state and inflammation. CD80 expression is poor on professional APCs, but increases several days after interaction with T cells. In contrast, CD86 is constitutively expressed on professional APCs, which increases rapidly after antigen presentation to T cells [9]. It is not clear why two costimulatory molecules with identical functions but different expression regimes are used by the immune system.

Reaction between CD80/CD86 and CTLA4 molecules results in the formation of multivalent complexes, which is not considered in the trans-endocytosis model. As a modification, multivalent complex formation can be considered as sequential reactions on the cell-cell contact surface. However, it would be challenging to identify different ligand removal rates at different stages of sequential reactions. Such differences cannot be identified from the data given in [213].

The CTLA4-mediated regulation of T cell activation is the basis of some clinical therapies by using anti-CTLA4 antibodies or CTLA4 Immunoglobulin (Ig) fusion proteins. A strong CTLA4-mediated inhibition of T cell activation in cancer is treated with anti-CTLA4 molecules, which results in enhancement of effector functions of the immune system. In allergy or autoimmunity, CTLA4 Ig fusion proteins are used to block costimulatory molecules and inhibit costimulation via ligation of CD28 with CD80/CD86 molecules. These therapies are designed without considering special trafficking of CTLA4 molecules and associated trans-endocytosis mechanism. It would be of interest to investigate the efficiency, optimize, or even revise such therapies by considering the trans-endocytosis mechanism.

In summary, we presented mathematical models for three different stages of the immune system. These stages are interdependent, but they are usually studied experimentally as isolated components *in vitro*. For example, thymic selections that are studied *in vitro* in organ-cultured thymuses, are not affected by any feedback from peripheral cells or mechanisms. A recent study has shown that activated regulatory T cells recirculate to the thymus and suppress the selection of new regulatory T cells [216]. Further, immune activation is directly dependent on the type and properties of T cells that are daily exported by thymus

to periphery. Quantification of such feedback loops between different organs of the immune system is challenging, and cannot be investigated only by experiments. Mathematical modeling is a promising approach to investigate multi-stage mechanisms, such as immune tolerance presented in this study. The theoretical multi-stage studies are potentially able to use enormous but isolated experimental data to provide an overall picture of important mechanisms in the immune system, such as immune regulation.

Bibliography

[1] S. Khailaie, P. A. Robert, A. Toker, J. Huehn, and M. Meyer-Hermann, "A signal integration model of thymic selection and natural regulatory T cell commitment.," *J. Immunol.*, vol. 193, no. 12, pp. 5983–96, 2014.

[2] S. Khailaie, F. Bahrami, M. Janahmadi, P. Milanez-Almeida, J. Huehn, and M. Meyer-Hermann, "A mathematical model of immune activation with a unified self-nonself concept.," *Front. Immunol.*, vol. 4, p. 474, 2013.

[3] J. M. McCune, "The dynamics of CD4+ T-cell depletion in HIV disease," *Nature*, vol. 410, no. 6831, pp. 974–9, 2001.

[4] A. T. Haase, "Population biology of HIV-1 infection: viral and CD4+ T cell demographics and dynamics in lymphatic tissues," *Annu. Rev. Immunol.*, vol. 17, pp. 625–56, 1999.

[5] A. Corthay, "How do Regulatory T Cells Work?," *Scand. J. Immunol.*, vol. 70, no. 4, pp. 326–336, 2009.

[6] P. Milanez-Almeida, M. Meyer-Hermann, A. Toker, S. Khailaie, and J. Huehn, "Foxp3+ regulatory T-cell homeostasis quantitatively differs in murine peripheral lymph nodes and spleen," *Eur. J. Immunol.*, vol. 45, no. 1, p. 153âĂŞ166, 2015.

[7] L. Klein, B. Kyewski, P. M. Allen, and K. A. Hogquist, "Positive and negative selection of the T cell repertoire: what thymocytes see (and don't see)," *Nat. Rev. Immunol.*, vol. 14, no. 6, pp. 377–391, 2014.

[8] C. S. Hsieh, H. M. Lee, and C. W. Lio, "Selection of regulatory T cells in the thymus.," *Nat. Rev. Immunol.*, vol. 12, no. 3, pp. 157–67, 2012.

[9] D. J. Lenschow, G. H. Su, L. A. Zuckerman, N. Nabavi, C. L. Jellis, G. S. Gray, J. Miller, and J. A. Bluestone, "Expression and functional significance of an additional ligand for CTLA-4.," *Proc. Natl. Acad. Sci. USA*, vol. 90, no. 23, pp. 11054–8, 1993.

[10] J. A. Gross, E. Callas, and J. P. Allison, "Identification and distribution of the costimulatory receptor CD28 in the mouse.," *J. Immunol.*, vol. 149, no. 2, pp. 380–8, 1992.

[11] L. L. Lanier, S. O'Fallon, C. Somoza, J. H. Phillips, P. S. Linsley, K. Okumura, D. Ito, and M. Azuma, "CD80 (B7) and CD86 (B70) provide similar costimulatory signals for T cell proliferation, cytokine production, and generation of CTL.," *J. Immunol.*, vol. 154, no. 1, pp. 97–105, 1995.

[12] G. J. Freeman, D. B. Lombard, C. D. Gimmi, S. A. Brod, K. Lee, J. C. Laning, D. A. Hafler, M. E. Dorf, G. S. Gray, H. Reiser, C. H. June, C. B. Thompson, and L. M. Nadler, "CTLA-4 and CD28 mRNA are coexpressed in most T cells after activation. Expression of CTLA-4 and CD28 mRNA does not correlate with the pattern of lymphokine production.," *J. Immunol.*, vol. 149, no. 12, pp. 3795–801, 1992.

[13] L. S. Walker and D. M. Sansom, "The emerging role of CTLA4 as a cell-extrinsic regulator of T cell responses.," *Nat. Rev. Immunol.*, vol. 11, no. 12, pp. 852–63, 2011.

[14] A. V. Collins, D. W. Brodie, R. J. Gilbert, A. Iaboni, R. Manso-Sancho, B. Walse, D. I. Stuart, P. A. van der Merwe, and S. J. Davis, "The interaction properties of costimulatory molecules revisited.," *Immunity*, vol. 17, no. 2, pp. 201–10, 2002.

[15] A. Arazi, W. F. Pendergraft, R. M. Ribeiro, A. S. Perelson, and N. Hacohen, "Human systems immunology: hypothesis-based modeling and unbiased data-driven approaches," *Semin. Immunol.*, vol. 25, no. 3, pp. 193–200, 2013.

[16] A. Perelson and G. Oster, "Theoretical Studies of Clonal Selection: Minimal Antibody Repertoire Size and Reliability of Self-Non-Self Discrimination," *J. Theor. Biol.*, vol. 81, pp. 645–67, 1979.

[17] A. M. Bilate and J. J. Lafaille, "Induced CD4+Foxp3+ Regulatory T Cells in Immune Tolerance," *Annu. Rev. Immunol.*, vol. 30, pp. 733–58, 2012.

[18] X. Lin, M. Chen, Y. Liu, Z. Guo, X. He, D. Brand, and S. G. Zheng, "Advances in distinguishing natural from induced Foxp3(+) regulatory T cells," *Int. J. Clin. Exp. Pathol.*, vol. 6, no. 2, pp. 116–23, 2013.

[19] G. E. P. Box and N. R. Draper, *Empirical Model-Building and Response Surfaces*. Wiley Series in Probability and Statistics, Wiley, 1987.

[20] R. J. de Boer and P. Hogeweg, "Self-Nonself Discrimination due to Immunological Nonlinearities: the Analysis of a Series of Models by Numerical Methods," *Math. Med. Biol.*, vol. 4, no. 1, pp. 1–32, 1987.

[21] L. G. de Pillis, A. E. Radunskaya, and C. L. Wiseman, "A validated mathematical model of cell-mediated immune response to tumor growth.," *Cancer Res.*, vol. 65, no. 17, pp. 7950–7958, 2005.

[22] H. Moore and N. K. Li, "A mathematical model for chronic myelogenous leukemia (CML) and T cell interaction," *J. Theor. Biol.*, vol. 227, no. 4, pp. 513–23, 2004.

[23] R. Antia, C. T. Bergstrom, S. S. Pilyugin, S. M. Kaech, and R. Ahmed, "Models of CD8+ responses: 1. What is the antigen-independent proliferation program.," *J. Theor. Biol.*, vol. 221, no. 4, pp. 585–598, 2003.

[24] D. Wodarz and A. R. Thomsen, "Effect of the CTL proliferation program on virus dynamics.," *Int. Immunol.*, vol. 17, no. 9, pp. 1269–1276, 2005.

[25] N. J. Burroughs, B. Miguel Paz Mendes de Oliveira, and A. Adrego Pinto, "Regulatory T cell adjustment of quorum growth thresholds and the control of local immune responses.," *J. Theor. Biol.*, vol. 241, no. 1, pp. 134–141, 2006.

[26] J. Carneiro, K. León, I. Caramalho, C. Van Den Dool, R. Gardner, V. Oliveira, M. L. Bergman, N. Sepulveda, T. Paixão, J. Faro, and J. Demen-geot, "When three is not a crowd: a Crossregulation model of the dynamics and repertoire selection of regulatory CD4+ T cells," *Immunol. Rev.*, vol. 216, pp. 48–68, 2007.

[27] A. R. M. Almeida, I. F. Amado, J. Reynolds, J. Berges, G. Lythe, C. Molina-París, and A. a. Freitas, "Quorum-Sensing in CD4(+) T Cell Homeostasis: A Hypothesis and a Model.," *Front. immunol.*, vol. 3, no. 125, pp. 1–15, 2012.

[28] H. Y. Lee, D. J. Topham, S. Y. Park, J. Hollenbaugh, J. Treanor, T. R. Mosmann, X. Jin, B. M. Ward, H. Miao, J. Holden-Wiltse, A. S. Perelson, M. Zand, and H. Wu, "Simulation and prediction of the adaptive immune response to influenza A virus infection.," *J. Virol.*, vol. 83, no. 14, pp. 7151–7165, 2009.

[29] G. Shahaf, K. Johnson, and R. Mehr, "B cell development in aging mice: Lessons from mathematical modeling," *Int. Immunol.*, vol. 18, pp. 31–39, 2005.

[30] Y. Louzoun, S. Solomon, H. Atlan, and I. Cohen, "Proliferation and competition in discrete biological systems," *Bulletin math. biol.*, vol. 65, pp. 375–396, 2003.

[31] N. M. Shnerb, Y. Louzoun, E. Bettelheim, and S. Solomon, "The importance of being discrete: Life always wins on the surface," *Proc. Natl. Acad. Sci.*, vol. 97, no. 19, pp. 10322–10324, 2000.

[32] D. M. Catron, A. A. Itano, K. A. Pape, D. L. Mueller, and M. K. Jenkins, "Visualizing the first 50 hr of the primary immune response to a soluble antigen," *Immunity*, vol. 21, no. 3, pp. 341–7, 2004.

[33] A. Scherer, M. Salathe, and S. Bonhoeffer, "High epitope expression levels increase competition between T cells," *PLoS Comput. Biol.*, vol. 2, no. 8, p. e109, 2006.

[34] A. W. Goldrath and M. J. Bevan, "Selecting and maintaining a diverse T-cell repertoire," *Nature*, vol. 402, pp. 255–262, 1999.

[35] T. K. Starr, S. C. Jameson, and K. A. Hogquist, "Positive and negative selection of T cells.," *Annu. Rev. Immunol.*, vol. 21, pp. 139–76, 2003.

[36] J. Kappler, N. Roehm, and P. Marrack, "T cell tolerance by clonal elimination in the thymus.," *Cell*, vol. 49, pp. 273–280, 1987.

[37] D. H. Katz, T. Hamaoka, and B. Benacerraf, "Cell interactions between histoincompatible T and B lymphocytes. II. Failure of physiologic cooperative interactions between T and B lymphocytes from allogeneic donor strains in humoral response to hapten-protein conjugates.," *J. Exp. Med.*, vol. 137, no. 6, pp. 1405–1418, 1973.

[38] A. S. Rosenthal and E. M. Shevach, "Function of macrophages in antigen recognition by guinea pig T lymphocytes. I. Requirement for histocompatible macrophages and lymphocytes.," *J. Exp. Med.*, vol. 138, no. 5, pp. 1194–1212, 1973.

[39] R. M. Zinkernagel and P. C. Doherty, "Restriction of in vitro T cell-mediated cytotoxicity in lymphocytic choriomeningitis within a syngeneic or semiallogeneic system," *Nature*, vol. 248, pp. 701–702, 1974.

[40] M. J. Bevan, "In a radiation chimaera, host HâĂŞ2 antigens determine immune responsiveness of donor cytotoxic cells," *Nature*, vol. 269, pp. 417–418, 1977.

[41] R. M. Zinkernagel, G. N. Callahan, A. Althage, S. Cooper, P. A. Klein, and J. Klein, "On the thymus in the differentiation of "H-2 self-recognition" by T cells: evidence for dual recognition?," *J. Exp. Med.*, vol. 147, no. 3, pp. 882–896, 1978.

[42] J. Sprent, "Restricted helper function of F1 hybrid T cells positively selected to heterologous erythrocytes in irradiated parental strain mice. I. Failure to collaborate with B cells of the opposite parental strain not associated with active suppression," *J. Exp. Med.*, vol. 147, no. 4, pp. 1142–1158, 1978.

[43] J. W. Kappler and P. Marrack, "The role of H-2 linked genes in helper T-cell function. IV. Importance of T-cell genotype and host environment in I-region and Ir gene expression," *J. Exp. Med.*, vol. 148, no. 6, pp. 1510–1522, 1978.

[44] M. J. Bevan, "The major histocompatibility complex determines susceptibility to cytotoxic T cells directed against minor histocompatibility antigens," *J. Exp. Med.*, vol. 142, no. 6, pp. 1349–1364, 1975.

[45] H. S. Teh, J. Bennink, and H. Von Boehmer, "Selection of the T cell repertoire during ontogeny: limiting dilution analysis.," *Eur. J. Immunol.*, vol. 12, no. 10, pp. 887–892, 1982.

[46] K. A. Hogquist, M. A. Gavin, and B. M. J, "Positive selection of CD8+ T cells induced by major histocompatibility complex binding peptides in fetal thymic organ culture," *J. Exp. Med.*, vol. 177, no. 5, pp. 1469–1473, 1993.

[47] P. G. Ashton-Rickardt, L. Van Kaer, T. N. Schumacher, H. L. Ploegh, and S. Tonegawa, "Peptide contributes to the specificity of positive selection of CD8+ T cells in the thymus," *Cell*, vol. 73, no. 5, pp. 1041–1049, 1993.

[48] L. Ignatowicz, J. Kappler, and P. Marrack, "The Repertoire of T Cells Shaped by a Single MHC/Peptide Ligand," *Cell*, vol. 84, pp. 521–529, 1996.

[49] M. J. Bevan, "In thymic selection, peptide diversity gives and takes away.," *Immunity*, vol. 7, no. 2, pp. 175–8, 1997.

[50] M. J. Bevan, K. A. Hogquist, and S. C. Jameson, "Selecting the T cell receptor repertoire," *Science*, vol. 264, no. 5160, pp. 796–797, 1994.

[51] N. A. Danke, D. M. Koelle, C. Yee, S. Beheray, and W. W. Kwok, "Autoreactive T cells in healthy individuals.," *J. Immunol.*, vol. 172, no. 10, pp. 5967–5972, 2004.

[52] E. Suri-Payer, A. Z. Amar, A. M. Thornton, and E. M. Shevach, "CD4+CD25+ T cells inhibit both the induction and effector function of autoreactive T cells and represent a unique lineage of immunoregulatory cells.," *J. Immunol.*, vol. 160, no. 3, pp. 1212–8, 1998.

[53] A. E. Moran, K. L. Holzapfel, Y. Xing, N. R. Cunningham, J. S. Maltzman, J. Punt, and K. A. Hogquist, "T cell receptor signal strength in Treg and iNKT cell development demonstrated by a novel fluorescent reporter mouse," *J. Exp. Med.*, vol. 208, no. 6, pp. 1279–89, 2011.

[54] M. S. Jordan, A. Boesteanu, A. J. Reed, A. L. Petrone, A. E. Holenbeck, M. A. Lerman, A. Naji, and A. J. Caton, "Thymic selection of CD4+CD25+ regulatory T cells induced by an agonist self-peptide," *Nat. Immunol.*, vol. 2, no. 4, pp. 301–306, 2001.

[55] I. Apostolou, A. Sarukhan, L. Klein, and H. von Boehmer, "Origin of regulatory T cells with known specificity for antigen," *Nat. Immunol.*, vol. 3, no. 8, pp. 756–63, 2002.

[56] K. Kawahata, Y. Misaki, M. Yamauchi, S. Tsunekawa, K. Setoguchi, J. Miyazaki, and K. Yamamoto, "Generation of CD4+CD25+ regulatory T cells from autoreactive T cells simultaneously with their negative selection in the thymus and from nonautoreactive T cells by endogenous TCR expression," *J. Immunol.*, vol. 168, no. 9, pp. 4399–4405, 2002.

[57] B. A. Osborne, S. Smith, Z. Liu, K. McLaughlin, L. Grimm, and L. Schwartz, "Identification of genes induced during apoptosis in T lymphocytes.," *Immunol. Rev.*, vol. 142, pp. 301–320, 1994.

[58] C. S. Hsieh, Y. Liang, A. J. Tyznik, S. G. Self, D. Liggitt, and A. Y. Rudensky, "Recognition of the peripheral self by naturally arising CD25+ CD4+ T cell receptors," *Immunity*, vol. 21, pp. 267–277, 2004.

[59] C. S. Hsieh, Y. Zheng, Y. Liang, J. D. Fontenot, and A. Y. Rudensky, "An intersection between the self-reactive regulatory and nonregulatory T cell receptor repertoires," *Nat. Immunol.*, vol. 7, no. 4, pp. 401–410, 2006.

[60] R. Pacholczyk, H. Ignatowicz, P. Kraj, and L. Ignatowicz, "Origin and T cell receptor diversity of Foxp3+CD4+CD25+ T cells," *Immunity*, vol. 25, no. 2, pp. 249–259, 2006.

[61] J. Wong, R. Obst, M. Correia-Neves, G. Losyev, D. Mathis, and C. Benoist, "Adaptation of TCR repertoires to self-peptides in regulatory and nonregulatory CD4+ T cells," *J. Immunol.*, vol. 178, no. 11, pp. 7032–7041, 2007.

[62] P. Pacholczyk and J. Kern, "The T-cell receptor repertoire of regulatory T cells.," *Immunology*, vol. 125, no. 4, pp. 450–458, 2008.

[63] R. Pacholczyk, P. Kraj, and L. Ignatowicz, "Peptide specificity of thymic selection of CD4+CD25+ T cells.," *J. Immunol.*, vol. 168, no. 2, pp. 613–620, 2002.

[64] P. Romagnoli, D. Hudrisier, and J. P. van Meerwijk, "Preferential recognition of self antigens despite normal thymic deletion of CD4(+)CD25(+) regulatory T cells," *J. Immunol.*, vol. 168, no. 4, pp. 1644–1648, 2002.

[65] K. A. Kasow, X. Chen, J. Knowles, D. Wichlan, R. Handgretinger, and J. M. Riberdy, "Human CD4+CD25+ regulatory T cells share equally complex and comparable repertoires with CD4+CD25âĹŠ counterparts," *J. Immunol.*, vol. 172, no. 10, pp. 6123–6128, 2004.

[66] M. Fujishima, M. Hirokawa, N. Fujishima, and K. Sawada, "TCRalphabeta repertoire diversity of human naturally occurring CD4+CD25+ regulatory T cells," *Immunol. Lett.*, vol. 99, no. 2, pp. 193–197, 2005.

[67] T. Takahashi, Y. Kuniyasu, M. Toda, N. Sakaguchi, M. Itoh, M. Iwata, J. Shimizu, and S. Sakaguchi, "Immunologic self-tolerance maintained by CD25+CD4+ naturally anergic and suppressive T cells: induction of autoimmune disease by breaking their anergic/suppressive state," *Int. Immunol.*, vol. 10, no. 12, pp. 1969–80, 1998.

[68] D. Haribhai, W. Lin, L. M. Relland, N. Truong, C. B. Williams, and T. A. Chatila, "Regulatory T Cells Dynamically Control the Primary Immune Response to Foreign Antigen," *J. Immunol.*, vol. 178, no. 5, pp. 2961–2972, 2007.

[69] R. Pacholczyk, J. Kern, N. Singh, M. Iwashima, P. Kraj, and L. Ignatowicz, "Nonself-antigens are the cognate specificities of Foxp3+ regulatory T cells.," *Immunity*, vol. 27, no. 3, pp. 493–504, 2007.

[70] Y. Belkaid, C. A. Piccirillo, S. Mendez, E. M. Shevach, and D. L. Sacks, "CD4+CD25+ regulatory T cells control Leishmania major persistence and immunity.," *Nature*, vol. 420, pp. 502–7, 2002.

[71] S. Suvas, U. Kumaraguru, C. D. Pack, S. Lee, and B. T. Rouse, "CD4+CD25+ T cells regulate virus-specific primary and memory CD8+ T cell responses," *J. Exp. Med.*, vol. 198, pp. 889–901, 2003.

[72] P. Kisielow and A. Miazek, "Positive selection of T cells: rescue from programmed cell death and differentiation require continual engagement of the T cell receptor.," *J. Exp. Med.*, vol. 181, no. 6, pp. 1975–84, 1995.

[73] R. W. Wilkinson, G. Anderson, J. J. Owen, and E. J. Jenkinson, "Positive selection of thymocytes involves sustained interactions with the thymic microenvironment," *J. Immunol.*, vol. 155, no. 11, pp. 5234–5240, 1995.

[74] L. K. McNeil, T. K. Starr, and K. A. Hogquist, "A requirement for sustained ERK signaling during thymocyte positive selection in vivo.," *P. Natl. Acad. Sci. USA.*, vol. 102, no. 38, pp. 13574–9, 2005.

[75] B. B. Au-Yeung, H. J. Melichar, J. O. Ross, D. A. Cheng, J. Zikherman, K. M. Shokat, E. A. Robey, and A. Weiss, "Quantitative and temporal requirements revealed for Zap70 catalytic activity during T cell development," *Nat. Immunol.*, vol. 15, no. 7, pp. 687–694, 2014.

[76] S. Mariathasan, A. Zakarian, D. Bouchard, A. M. Michie, J. C. ZÃžÃśiga-PflÃijcker, and P. S. Ohashi, "Duration and strength of extracellular signal-regulated kinase signals are altered during positive versus negative thymocyte selection.," *J. Immunol.*, vol. 167, no. 9, pp. 4966–73, 2001.

[77] S. Mariathasan, S. S. Ho, A. Zakarian, and P. S. Ohashi, "Degree of ERK activation influences both positive and negative thymocyte selection.," *Eur. J. Immunol.*, vol. 30, no. 4, pp. 1060–8, 2000.

[78] G. Werlen, B. Hausmann, and E. Palmer, "A motif in the alpha beta T-cell receptor controls positive selection by modulating ERK activity," *Nature*, vol. 406, no. 6794, pp. 422–426, 2000.

[79] H. Tsukamoto, A. Irie, Y. Z. Chen, K. Takeshita, J. R. Kim, and Y. Nishimura, "TCR ligand avidity determines the mode of B-Raf/Raf-1/ERK activation leading to the activation of human CD4+ T cell clone.," *Eur. J. Immunol.*, vol. 36, no. 7, pp. 1926–37, 2006.

[80] M. A. Daniels, E. Teixeiro, J. Gill, B. Hausmann, D. Roubaty, K. Holmberg, G. Werlen, G. A. HollÃďnder, N. R. Gascoigne, and E. Palmer, "Thymic selection threshold defined by compartmentalization of Ras/MAPK signalling," *Nature*, vol. 444, no. 7120, pp. 724–9, 2006.

[81] G. P. Morris and P. M. Allen, "How the TCR balances sensitivity and specificity for the recognition of self and pathogens," *Nat. Immunol.*, vol. 13, no. 2, pp. 121–8, 2012.

[82] A. Košmrlj, A. K. Jha, E. S. Huseby, M. Kardar, and A. K. Chakraborty, "How the thymus designs antigen-specific and self-tolerant T cell receptor sequences," *P. Natl. Acad. Sci. USA.*, vol. 105, no. 43, pp. 16671–16676, 2008.

[83] D. L. Chao, M. P. Davenport, S. Forrest, and A. S. Perelson, "The effects of thymic selection on the range of T cell cross-reactivity," *Eur. J. Immunol.*, vol. 35, no. 12, pp. 3452–9, 2005.

[84] A. Scherer, A. Noest, and R. J. de Boer, "Activation-threshold tuning in an affinity model for the T-cell repertoire.," *P. Roy. Soc. B-Biol. Sci.*, vol. 271, no. 1539, pp. 609–16, 2004.

[85] V. Detours, R. Mehr, and A. S. Perelson, "A quantitative theory of affinity-driven T cell repertoire selection," *J. Theor. Biol.*, vol. 200, no. 4, pp. 389–403, 1999.

[86] V. Detours and A. S. Perelson, "Explaining high alloreactivity as a quantitative consequence of affinity-driven thymocyte selection," *P. Natl. Acad. Sci. USA.*, vol. 96, no. 9, pp. 5153–5158, 1999.

[87] I. Bains, H. M. van Santen, B. Seddon, and A. J. Yates, "Models of Self-Peptide Sampling by Developing T Cells Identify Candidate Mechanisms of Thymic Selection.," *PLoS Comput. Biol.*, vol. 9, no. 7, p. e1003102, 2013.

[88] H. M. Van Santen, C. Benoist, and D. Mathis, "Number of Treg cells that differentiate does not increase upon encounter of agonist ligand on thymic epithelial cells.," *J. Exp. Med.*, vol. 200, no. 10, pp. 1221–1230, 2004.

[89] Y. H. Ding, B. M. Baker, D. N. Garboczi, W. E. Biddison, and D. C. Wiley, "Four A6-TCR/peptide/HLA-A2 structures that generate very different T cell signals are nearly identical," *Immunity*, vol. 11, no. 1, pp. 45–56, 1999.

[90] A. J. Bankovich and K. C. Garcia, "Not Just Any T Cell Receptor Will Do," *Immunity*, vol. 18, no. 1, pp. 7–11, 2003.

[91] D. N. Garboczi, P. Ghosh, U. Utz, Q. R. Fan, W. E. Biddison, and D. C. Wiley, "Structure of the complex between human T-cell receptor, viral peptide and HLA-A2," *Nature*, vol. 384, no. 6605, pp. 134–141, 1996.

[92] K. C. Garcia, M. Degano, R. L. Stanfield, A. Brunmark, M. R. Jackson, P. A. Peterson, L. Teyton, and I. A. Wilson, "An alphabeta T cell receptor structure at 2.5 A and its orientation in the TCR-MHC complex," *Science*, vol. 274, no. 5285, pp. 209–219, 1996.

[93] J. P. Allison, B. W. McIntyre, and D. Bloch, "Tumor-specific antigen of murine T-lymphoma defined with monoclonal antibody.," *J. Immunol.*, vol. 129, no. 5, pp. 2293–2300, 1982.

[94] M. Gunzer, A. Schäfer, S. Borgmann, S. Grabbe, K. S. Zänker, E. B. Bröcker, E. Kämpgen, and P. Friedl, "Antigen presentation in extracellular matrix: interactions of T cells with dendritic cells are dynamic, short lived, and sequential.," *Immunity*, vol. 13, no. 3, pp. 323–32, 2000.

[95] C. Schmeitz, E. A. Hernandez-Vargas, R. Fliegert, A. H. Guse, and M. Meyer-Hermann, "A mathematical model of T lymphocyte calcium dynamics derived from single transmembrane protein properties.," *Front. Immunol.*, vol. 4, p. 277, 2013.

[96] A. Lanzavecchia, G. Lezzi, and A. Viola, "From TCR engagement to T cell activation: a kinetic view of T cell behavior.," *Cell*, vol. 96, no. 1, pp. 1–4, 1999.

[97] S. Valitutti, M. Dessing, K. Aktories, H. Gallati, and A. Lanzavecchia, "Sustained signaling leading to T cell activation results from prolonged T cell receptor occupancy. Role of T cell actin cytoskeleton," *J. Exp. Med.*, vol. 181, no. 2, pp. 577–584, 1995.

[98] C. Beeson, J. Rabinowitz, K. Tate, I. Guetgemann, Y. H. Chien, P. P. Jones, M. M. Davis, and H. M. McConnell, "Early Biochemical Signals Arise from Low Affinity TCR-Ligand Reactions at the Cell-Cell Interface," *J. Exp. Med.*, vol. 184, no. 2, pp. 777–82, 1996.

[99] D. Hudrisier, B. Kessler, S. Valitutti, C. Horvath, J. C. Cerottini, and I. F. Luescher, "The efficiency of antigen recognition by CD8+ CTL clones is determined by the frequency of serial TCR engagement.," *J. Immunol.*, vol. 161, no. 2, pp. 553–62, 1998.

[100] B. Ernst, D. S. Lee, J. M. Chang, J. Sprent, and C. D. Surh, "The peptide ligands mediating positive selection in the thymus control T cell survival and homeostatic proliferation in the periphery," *Immunity*, vol. 11, no. 2, pp. 173–81, 1999.

[101] C. Viret, F. S. Wong, and C. A. Janeway Jr, "Designing and maintaining the mature TCR repertoire: the continuum of self-peptide:self-MHC complex recognition," *Immunity*, vol. 10, no. 5, pp. 559–68, 1999.

[102] J. Kirberg, A. Berns, and H. von Boehmer, "Peripheral T cell survival requires continual ligation of the T cell receptor to major histocompatibility complex-encoded molecules," *J. Exp. Med.*, vol. 186, no. 8, pp. 1269–75, 1997.

[103] N. Garbi, G. J. HÃďmmerling, H. C. Probst, and M. van den Broek, "Tonic T cell signalling and T cell tolerance as opposite effects of self-recognition on dendritic cells.," *Curr. Opin. Immunol.*, vol. 22, no. 5, pp. 601–8, 2010.

[104] K. Hochweller, G. H. Wabnitz, Y. Samstag, J. Suffner, G. J. HÃďmmerling, and N. Garbi, "Dendritic cells control T cell tonic signaling required for responsiveness to foreign antigen.," *P. Natl. Acad. Sci. USA.*, vol. 107, no. 13, pp. 5931–6, 2010.

[105] G. M. Barton and A. Y. Rudensky, "Requirement for diverse, low-abundance peptides in positive selection of T cells," *Science*, vol. 283, no. 5398, pp. 67–70, 1999.

[106] B. Chmielowski, P. Muranski, P. Kisielow, and L. Ignatowicz, "On the role of high- and low-abundance class II MHC-peptide complexes in the thymic positive selection of CD4(+) T cells," *Int. Immunol.*, vol. 12, no. 1, pp. 67–72, 2000.

[107] D. F. Hunt, R. A. Henderson, J. Shabanowitz, K. Sakaguchi, H. Michel, N. Sevilir, A. L. Cox, E. Appella, and V. H. Engelhard, "Characterization of peptides bound to the class I MHC molecule HLA-A2.1 by mass spectrometry," *Science*, vol. 255, no. 5049, pp. 1261–1263, 1992.

[108] V. Müller and S. Bonhoeffer, "Quantitative constraints on the scope of negative selection," *Trends Immunol.*, vol. 24, no. 3, pp. 132–135, 2003.

[109] P. A. Reay, R. M. Kantor, and M. M. Davis, "Use of global amino acid replacements to define the requirements for MHC binding and T cell recognition of moth cytochrome c (93-103)," *J. Immunol.*, vol. 152, no. 8, pp. 3946–3957, 1994.

[110] H. von Boehmer, I. Aifantis, F. Gounari, O. Azogui, L. Haughn, I. Apostolou, E. Jaeckel, F. Grassi, and L. Klein, "Thymic selection revisited: how essential is it?," *Immunol. Rev.*, vol. 191, pp. 62–78, 2003.

[111] M. Merkenschlager, D. Graf, M. Lovatt, U. Bommhardt, R. Zamoyska, and A. G. Fisher, "How many thymocytes audition for selection?," *J. Exp. Med.*, vol. 186, no. 7, pp. 1149–1158, 1997.

[112] J. P. M. van Meerwijk, S. Marguerat, R. K. Lees, R. N. Germain, and B. J. Fowlkes, "Quantitative impact of thymic clonal deletion on the T cell repertoire," *J. Exp. Med.*, vol. 185, no. 3, pp. 377–83, 1997.

[113] S. J. Bensinger, A. Bandeira, M. S. Jordan, A. J. Caton, and T. M. Laufer, "Major histocompatibility complex class II-positive cortical epithelium mediates the selection of CD4(+)25(+) immunoregulatory T cells," *J. Exp. Med.*, vol. 194, no. 4, pp. 427–38, 2001.

[114] J. D. Fontenot, J. P. Rasmussen, L. M. Williams, J. L. Dooley, A. G. Farr, and A. Y. Rudensky, "Regulatory T cell lineage specification by the forkhead transcription factor Foxp3," *Immunity*, vol. 22, no. 3, pp. 329–41, 2005.

[115] J. Larkin 3rd, A. L. Rankin, C. C. Picca, M. P. Riley, S. A. Jenks, A. J. Sant, and A. J. Caton, "CD4+CD25+ regulatory T cell repertoire formation shaped by differential presentation of peptides from a self-antigen," *J. Immunol.*, vol. 180, no. 4, pp. 2149–57, 2008.

[116] G. L. Stritesky, S. C. Jameson, and K. A. Hogquist, "Selection of self-reactive T cells in the thymus," *Annu. Rev. Immunol.*, vol. 30, pp. 95–114, 2012.

[117] K. J. Maloy and F. Powrie, "Regulatory T cells in the control of immune pathology," *Nat. Immunol.*, vol. 2, no. 9, pp. 816–822, 2001.

[118] H. M. Lee, J. L. Bautista, J. Scott-Browne, J. F. Mohan, and C. S. Hsieh, "A broad range of self-reactivity drives thymic regulatory T cell selection to limit responses to self.," *Immunity*, vol. 37, no. 3, pp. 475–86, 2012.

[119] J. K. Kim, M. Klinger, J. Benjamin, Y. Xiao, D. J. Erle, D. R. Littman, and N. Killeen, "Impact of the TCR signal on regulatory T cell homeostasis, function, and trafficking," *PLoS One*, vol. 4, no. 8, p. e6580, 2009.

[120] K. W. Wucherpfennig, "T cell receptor crossreactivity as a general property of T cell recognition," *Mol. Immunol.*, vol. 40, no. 14-15, pp. 1009–17, 2004.

[121] D. B. Wilson, D. H. Wilson, K. Schroder, C. Pinilla, S. Blondelle, R. A. Houghten, and K. C. Garcia, "Specificity and degeneracy of T cells," *Mol. Immunol.*, vol. 40, no. 14-15, pp. 1047–55, 2004.

[122] C. D. Surh, D. S. Lee, W. P. Fung-Leung, L. Karlsson, and J. Sprent, "Thymic selection by a single MHC/peptide ligand produces a semidiverse repertoire of CD4+ T cells.," *Immunity*, vol. 7, no. 2, pp. 209–19, 1997.

[123] C. E. Grubin, S. Kovats, P. deRoos, and A. Y. Rudensky, "Deficient positive selection of CD4 T cells in mice displaying altered repertoires of MHC class II-bound self-peptides.," *Immunity*, vol. 7, pp. 197–208, 1997.

[124] S. Tourne, T. Miyazaki, A. Oxenius, L. Klein, T. Fehr, B. Kyewski, C. Benoist, and D. Mathis, "Selection of a broad repertoire of CD4+ T cells in H-2Ma0/0 mice.," *Immunity*, vol. 7, no. 2, pp. 187–195, 1997.

[125] H. von Boehmer, "Shaping the T Cell Repertoire," *J. Immunol.*, vol. 175, no. 11, pp. 7067–7068, 2005.

[126] E. S. Huseby, F. Crawford, J. White, J. Kappler, and P. Marrack, "Negative selection imparts peptide specificity to the mature T cell repertoire," *P. Natl. Acad. Sci. USA.*, vol. 100, no. 20, pp. 11565–11570, 2003.

[127] E. S. Huseby, J. White, F. Crawford, T. Vass, D. Becker, C. Pinilla, P. Marrack, and J. W. Kappler, "How the T cell repertoire becomes peptide and MHC specific.," *Cell*, vol. 122, no. 2, pp. 247–60, 2005.

[128] D. Mason, "A very high level of crossreactivity is an essential feature of the T-cell receptor," *Immunol. Today*, vol. 19, no. 9, pp. 395–404, 1998.

[129] J. A. M. Borghans and R. J. De Boer, "Crossreactivity of the T-cell receptor," *Immunol. Today*, vol. 19, pp. 428–429, 1998.

[130] N. K. Jerne, "The somatic generation of immune recognition," *Eur. J. Immunol.*, vol. 1, no. 1, pp. 1–9, 1971.

[131] S. Sakaguchi, N. Sakaguchi, J. Shimizu, S. Yamazaki, T. Sakihama, M. Itoh, Y. Kuniyasu, T. Nomura, M. Toda, and T. Takahashi, "Immunologic tolerance maintained by CD25+ CD4+ regulatory T cells: their common role in controlling autoimmunity, tumor immunity, and transplantation tolerance.," *Immunol. Rev.*, vol. 182, pp. 18–32, 2001.

[132] L. M. Relland, J. B. Williams, G. N. Relland, D. Haribhai, J. Ziegelbauer, M. Yassai, J. Gorski, and C. B. Williams, "The TCR repertoires of regulatory and conventional T cells specific for the same foreign antigen are distinct," *J. Immunol.*, vol. 189, no. 7, pp. 3566–3574, 2012.

[133] J. P. Hindley, C. Ferreira, E. Jones, S. N. Lauder, K. Ladell, K. K. Wynn, G. J. Betts, Y. Singh, D. A. Price, A. J. Godkin, J. Dyson, and A. Gallimore, "Analysis of the T-cell receptor repertoires of tumor-infiltrating conventional and regulatory T cells reveals no evidence for conversion in carcinogen-induced tumors," *Cancer Res.*, vol. 71, no. 3, pp. 736–746, 2011.

[134] A. M. Thornton and E. M. Shevach, "CD4+CD25+ immunoregulatory T cells suppress polyclonal T cell activation in vitro by inhibiting interleukin 2 production," *J. Exp. Med.*, vol. 188, no. 2, pp. 287–296, 1998.

[135] L. Klein, K. Khazaie, and H. von Boehmer, "In vivo dynamics of antigen-specific regulatory T cells not predicted from behavior in vitro," *P. Natl. Acad. Sci. USA.*, vol. 100, no. 15, pp. 8886–8891, 2003.

[136] K. V. Tarbell, S. Yamazaki, K. Olson, P. Toy, and R. M. Steinman, "CD25+ CD4+ T Cells, Expanded with Dendritic Cells Presenting a Single Autoantigenic Peptide, Suppress Autoimmune Diabetes," *J. Exp. Med.*, vol. 199, no. 11, pp. 1467–1477, 2004.

[137] D. Homann, A. Holz, A. Bot, B. Coon, T. Wolfe, J. Petersen, T. P. Dyrberg, M. J. Grusby, and M. G. von Herrath, "Autoreactive CD4+ T cells protect from autoimmune diabetes via bystander suppression using the IL-4/Stat6 pathway," *Immunity*, vol. 11, no. 4, pp. 463–472, 1999.

[138] P. Yu, R. K. Gregg, J. J. Bell, J. S. Ellis, R. Divekar, H. H. Lee, R. Jain, H. Waldner, J. C. Hardaway, M. Collins, V. K. Kuchroo, and H. Zaghouani, "Specific T regulatory cells display broad suppressive functions against experimental allergic encephalomyelitis upon activation with cognate antigen," *J. Immunol.*, vol. 174, no. 11, pp. 6772–6780, 2005.

[139] A. M. Thornton and E. M. Shevach, "Suppressor effector function of CD4+CD25+ immunoregulatory T cells is antigen nonspecific," *J. Immunol.*, vol. 164, no. 1, pp. 183–190, 2000.

[140] O. Acuto and F. Michel, "CD28-mediated co-stimulation: a quantitative support for TCR signalling," *Nat. Rev. Immunol.*, vol. 3, no. 12, pp. 939–51, 2003.

[141] B. P. Babbitt, P. M. Allen, G. Matsueda, E. Haber, and E. R. Unanue, "Binding of immunogenic peptides to Ia histocompatibility molecules," *Nature*, vol. 317, pp. 359–361, 1985.

[142] P. Guermonprez, J. Valladeau, L. Zitvogel, C. Théry, and S. Amigorena, "Antigen presentation and T cell stimulation by dendritic cells," *Annu. Rev. Immunol.*, vol. 20, pp. 621–667, 2002.

[143] J. W. Yewdell and S. M. Haeryfar, "Understanding presentation of viral antigens to CD8+ T cells in vivo: the key to rational vaccine design," *Annu. Rev. Immunol.*, vol. 23, pp. 651–682, 2005.

[144] D. Kanduc, A. Stufano, G. Lucchese, and A. Kusalik, "Massive peptide sharing between viral and human proteomes," *Peptides*, vol. 29, no. 10, pp. 1755–1766, 2008.

[145] B. Trost, A. Kusalik, G. Lucchese, and D. Kanduc, "Bacterial peptides are intensively present throughout the human proteome," *Self/nonself*, vol. 1, no. 1, pp. 71–74, 2010.

[146] M. Wolfl, A. Rutebemberwa, T. Mosbruger, Q. Mao, H. Li, D. Netski, S. C. Ray, D. Pardoll, J. Sidney, A. Sette, T. Kuntzen, D. G. Kavanagh, J. Kuball, P. D. Greenberg, and A. L. Cox, "Hepatitis C Virus Immune Escape via Exploitation of a Hole in the T cell repertoire," *J. Immunol.*, vol. 181, no. 9, pp. 6435–6446, 2008.

[147] T. McCaughtry and K. Hogquist, "Central tolerance: what have we learned from mice?," *Semin. Immunopathol.*, vol. 30, pp. 399–409, 2008.

[148] E. Palmer and D. Naeher, "Affinity threshold for thymic selection through a T-cell receptor-co-receptor zipper," *Nat. Rev. Immunol.*, vol. 9, pp. 207–213, 2009.

[149] M. Rolland, D. C. Nickle, W. Deng, N. Frahm, C. Brander, G. H. Learn, D. Heckerman, N. Jojic, V. Jojic, B. D. Walker, and J. I. Mullins, "Recognition of HIV-1 peptides by host CTL is related to HIV-1 similarity to human proteins.," *PloS one*, vol. 2, no. 9, p. e823, 2007.

[150] S. Frankild, R. J. D. Boer, O. Lund, M. Nielsen, and C. Kesmir, "Amino Acid Similarity Accounts for T Cell Cross- Reactivity and for Holes in the T Cell Repertoire," *PloS one*, vol. 3, no. 3, 2008.

[151] C. Bouneaud, P. Kourilsky, and P. Bousso, "Impact of negative selection on the T cell repertoire reactive to a self-peptide: a large fraction of T cell clones escapes clonal deletion," *Immunity*, vol. 13, pp. 829–840, 2000.

[152] D. Zehn and M. J. Bevan, "T cells with low avidity for a tissue-restricted antigen routinely evade central and peripheral tolerance and cause autoimmunity," *Immunity*, vol. 25, pp. 261–270, 2006.

[153] J. Derbinski and B. Kyewski, "How thymic antigen presenting cells sample the body's self-antigens.," *Curr. Opin. Immunol.*, vol. 22, no. 5, pp. 592–600, 2010.

[154] S. Enouz, L. Carrié, D. Merkler, M. J. Bevan, and D. Zehn, "Autoreactive T cells bypass negative selection and respond to self-antigen stimulation during infection.," *J. Exp. Med.*, vol. 209, no. 10, pp. 1769–79, 2012.

[155] A. M. Bulek, D. K. Cole, A. Skowera, G. Dolton, S. Gras, F. Madura, A. Fuller, J. J. Miles, E. Gostick, D. A. Price, J. W. Drijfhout, R. R. Knight, G. C. Huang, N. Lissin, P. E. Molloy, L. Wooldridge, B. K. Jakobsen, J. Rossjohn, M. Peakman, P. J. Rizkallah, and A. K. Sewell, "Structural basis for the killing of human beta cells by CD8(+) T cells in type 1 diabetes.," *Nat. Immunol.*, vol. 13, no. 3, pp. 283–289, 2012.

[156] D. L. Mueller, "Mechanisms maintaining peripheral tolerance," *Nat. Immunol.*, vol. 11, no. 12, pp. 21–27, 2010.

[157] J. R. Killebrew, N. Perdue, A. Kwan, A. M. Thornton, E. M. Shevach, and D. J. Campbell, "A self-reactive TCR drives the development of Foxp3+ regulatory T cells that prevent autoimmune disease," *J. Immunol.*, vol. 187, no. 2, pp. 861–869, 2011.

[158] J. M. Kim, J. P. Rasmussen, and A. Y. Rudensky, "Regulatory T cells prevent catastrophic autoimmunity throughout the lifespan of mice," *Nat. Immunol.*, vol. 8, pp. 191–197, 2006.

[159] K. Lahl, C. Loddenkemper, C. Drouin, J. Freyer, J. Arnason, G. Eberl, A. Hamann, H. Wagner, J. Huehn, and T. Sparwasser, "Selective depletion of Foxp3+ regulatory T cells induces a scurfy-like disease," *J. Exp. Med.*, vol. 204, no. 1, pp. 57–63, 2007.

[160] K. León, R. Peréz, A. Lage, and J. Carneiro, "Modelling T-cell-Mediated Suppression Dependent on Interactions in Multicellular Conjugates," *J. Theor. Biol.*, vol. 207, no. 2, pp. 231–254, 2000.

[161] J. Carneiro, T. Paixão, D. Milutinovic, J. Sousaa, K. León, R. Gardner, and J. Faro, "Immunological self-tolerance: Lessons from mathematical modeling," *J. Comp. Appl. Math.*, vol. 184, no. 1, pp. 77–100, 2005.

[162] P. S. Kim, P. P. Lee, and D. Levy, "Modeling regulation mechanisms in the immune system," *J. Theor. Biol.*, vol. 246, no. 1, pp. 33–69, 2007.

[163] N. J. Burroughs, M. F. Ferreira, B. Oliveira, and A. A. Pinto, "Autoimmunity arising from bystander proliferation of T cells in an immune response model," *Math. Comput. Model.*, vol. 53, no. 7, pp. 1389–1393, 2011.

[164] K. León, R. Peréz, A. Lage, and J. Carneiro, "Three-cell interactions in T cell-mediated suppression? A mathematical analysis of its quantitative implications," *J. Immunol.*, vol. 166, no. 9, pp. 5356–5365, 2001.

[165] D. Busse, M. de la Rosa, K. Hobiger, K. Thurley, M. Flossdorf, A. Scheffold, and T. Höfer, "Competing feedback loops shape IL-2 signaling between helper and regulatory T lymphocytes in cellular microenvironments," *P. Natl. Acad. Sci. USA.*, vol. 107, no. 7, 2010.

[166] A. Banz, C. Pontoux, and M. Papiernik, "Modulation of Fas-dependent apoptosis: a dynamic process controlling both the persistence and death of CD4 regulatory T cells and effector T cells," *J. Immunol.*, vol. 169, no. 2, pp. 750–757, 2002.

[167] S. P. Ellner and J. Guckenheimer, *Dynamic Models in Biology*. Princeton University Press, 2006.

[168] M. Hofmann, M. Radsak, G. Rechtsteiner, K. Wiemann, M. Günder, U. Bien-Gräter, R. Offringa, R. E. Toes, H. G. Rammensee, and H. Schild, "T cell avidity determines the level of CTL activation," *Eur. J. Immunol.*, vol. 34, no. 7, pp. 1798–1806, 2004.

[169] D. Zehn, S. Y. Lee, and M. J. Bevan, "Complete but curtailed T-cell response to very low-affinity antigen," *Nature*, vol. 458, no. 7235, pp. 211–214, 2009.

[170] M. Hebeisen, N. Rufer, S. G. Oberle, D. E. Speiser, and D. Zehn, "Signaling Mechanisms that Balance Anti-viral, Auto-reactive, and Antitumor Potential of Low Affinity T cells," *J. Clin. Cell. Immunol*, vol. S12, 2012.

[171] C. Bourgeois, Z. Hao, K. Rajewsky, A. J. Potocnik, and B. Stockinger, "Ablation of thymic export causes accelerated decay of naïve CD4 T cells in the periphery because of activation by environmental antigen," *P. Natl. Acad. Sci. USA.*, vol. 105, no. 25, pp. 8691–8696, 2008.

[172] K. Takada and S. C. Jameson, "Naive T cell homeostasis: from awareness of space to a sense of place.," *Nat. Rev. Immunol.*, vol. 9, no. 12, pp. 823–32, 2009.

[173] R. E. Callard, J. Stark, and A. J. Yates, "Fratricide: a mechanism for T memory-cell homeostasis," *Trends Immunol.*, vol. 24, no. 7, pp. 370–375, 2003.

[174] Y. Belkaid, "Regulatory T cells and infection: a dangerous necessity," *Nat. Rev. Immunol.*, vol. 7, pp. 875–888, 2007.

[175] Y. Zhou, "Regulatory T cells and viral infections," *Front. Biosci.*, vol. 13, pp. 1152–1170, 2008.

[176] K. Kretschmer, I. Apostolou, E. Jaeckel, K. Khazaie, and H. von Boehmer, "Making regulatory T cells with defined antigen specificity: role in autoimmunity and cancer," *Immunol. Rev*, vol. 212, pp. 163–169, 2006.

[177] K. Klages, C. T. Mayer, K. Lahl, C. Loddenkemper, M. W. Teng, S. F. Ngiow, M. J. Smyth, A. Hamann, J. Huehn, and T. Sparwasser, "Selective Depletion of Foxp3+ Regulatory T Cells Improves Effective Therapeutic Vaccination against Established Melanoma," *Cancer Res.*, vol. 70, no. 20, pp. 7788–7799, 2010.

[178] D. A. Vignali, L. W. Collison, and C. J. Workman, "How regulatory T cells work," *Nat. Rev. Immunol.*, vol. 8, no. 7, pp. 523–532, 2008.

[179] A. M. Thornton, P. E. Korty, D. Tran, E. A. Wohlfert, P. E. Murray, Y. Belkaid, and E. M. Shevach, "Expression of Helios, an Ikaros transcription factor family member, differentiates thymic-derived from peripherally induced Foxp3+ T regulatory cells," *J. Immunol.*, vol. 184, pp. 3433–3441, 2010.

[180] J. D. Fontenot, J. P. Rasmussen, M. A. Gavin, and A. Y. Rudensky, "A function for interleukin 2 in Foxp3-expressing regulatory T cells," *Nat. Immunol.*, vol. 6, pp. 1142–1151, 2005.

[181] T. Zou, A. J. Caton, G. a. Koretzky, and T. Kambayashi, "Dendritic cells induce regulatory T cell proliferation through antigen-dependent and -independent interactions.," *J. Immunol.*, vol. 185, no. 5, pp. 2790–9, 2010.

[182] S. Sakaguchi, "Naturally arising Foxp3-expressing CD25+CD4+ regulatory T cells in immunological tolerance to self and non-self," *Nat. Immunol.*, vol. 6, pp. 345–52, 2005.

[183] S. Li, E. J. Gowans, C. Chougnet, M. Plebanski, and U. Dittmer, "Natural regulatory T cells and persistent viral infection.," *J. Virol.*, vol. 82, no. 1, pp. 21–30, 2008.

[184] K. K. Dietze, G. Zelinskyy, K. Gibbert, S. Schimmer, S. Francois, L. Myers, T. Sparwasser, K. J. Hasenkrug, and U. Dittmer, "Transient depletion of regulatory T cells in transgenic mice reactivates virus-specific CD8 + T cells and reduces chronic retroviral set points," *P. Natl. Acad. Sci. USA.*, vol. 108, no. 6, pp. 2420–2425, 2011.

[185] Y. Keynan, C. M. Card, P. J. McLaren, M. R. Dawood, K. Kasper, and K. R. Fowke, "The role of regulatory T cells in chronic and acute viral infections.," *Clin. Infect. Dis.*, vol. 46, no. 7, pp. 1046–52, 2008.

[186] M. G. von Herrath, J. Dockter, and M. B. Oldstone, "How virus induces a rapid or slow onset insulin-dependent diabetes mellitus in a transgenic model," *Immunity*, vol. 1, pp. 231–242, 1994.

[187] M. J. Turner, E. R. Jellison, L. E. G., L. Puddington, and L. Lefrançois, "Avidity maturation of memory CD8 T cells is limited by self-antigen expression," *J. Exp. Med.*, vol. 205, no. 8, pp. 1859–1868, 2008.

[188] R. Barouch and M. Schwartz, "Autoreactive T cells induce neurotrophin production by immune and neural cells in injured rat optic nerve: implications for protective autoimmunity," *FASEB J.*, vol. 16, no. 10, pp. 1304–1306, 2002.

[189] H. H. Hofstetter, D. L. Sewell, F. Liu, M. Sandor, T. Forsthuber, P. V. Lehmann, and Z. Fabry, "Autoreactive T cells promote post-traumatic healing in the central nervous system," *J. Neuroimmunol.*, vol. 134, no. 1, pp. 25–34, 2003.

[190] H. Wekerle and R. Hohlfeld, "Beneficial brain autoimmunity?," *Brain*, vol. 133, no. 8, pp. 2182–2184, 2010.

[191] L. Baitsch, S. A. Fuertes-Marraco, A. Legat, C. Meyer, and D. E. Speiser, "The three main stumbling blocks for anticancer T cells," *Trends Immunol.*, vol. 33, no. 7, pp. 364–372, 2012.

[192] J. J. Goronzy and C. M. Weyand, "Understanding immunosenescence to improve responses to vaccines," *Nat. Immunol.*, vol. 14, pp. 428–436, 2013.

[193] Z. Vadasz, T. Haj, A. Kessel, and E. Toubi, "Age-related autoimmunity," *BMC Med.*, vol. 11, no. 94, 2013.

[194] E. J. Yager, M. Ahmed, K. Lanzer, T. D. Randall, D. L. Woodland, and M. A. Blackman, "Age-associated decline in T cell repertoire diversity leads to holes in the repertoire and impaired immunity to influenza virus," *J. Exp. Med.*, vol. 205, no. 3, pp. 711–723, 2008.

[195] S. Sakaguchi, M. Miyara, C. M. Costantino, and D. A. Hafler, "FOXP3+ regulatory T cells in the human immune system," *Nat. Rev. Immunol.*, vol. 10, pp. 490–500, 2010.

[196] J. Raynor, C. S. Lages, H. Shehata, D. A. Hildeman, and C. A. Chougnet, "Homeostasis and function of regulatory T cells in aging," *Curr. Opin. Immunol.*, vol. 24, no. 4, pp. 482–487, 2012.

[197] M. von Herrath, S. Sanda, and K. Herold, "Type 1 diabetes as a relapsing-remitting disease?," *Nat. Rev. Immunol.*, vol. 7, no. 12, pp. 988–94, 2007.

[198] A. Nylander and D. A. Hafler, "Multiple sclerosis," *J. Clin. Invest.*, vol. 122, no. 4, pp. 1180–1188, 2012.

[199] R. Lechler, J. G. Chai, F. Marelli-Berg, and G. Lombardi, "The contributions of T-cell anergy to peripheral T-cell tolerance.," *Immunology*, vol. 103, no. 3, pp. 262–9, 2001.

[200] Z. Grossman and A. Singer, "Tuning of activation thresholds explains flexibility in the selection and development of T cells in the thymus.," *P. Natl. Acad. Sci. USA.*, vol. 93, no. 25, pp. 14747–14752, 1996.

[201] A. Grakoui, S. K. Bromley, C. Sumen, M. M. Davis, A. S. Shaw, P. M. Allen, and M. L. Dustin, "The immunological synapse: a molecular machine controlling T cell activation," *Science*, vol. 285, no. 5425, pp. 221–7, 1999.

[202] C. R. Monks, B. A. Freiberg, H. Kupfer, N. Sciaky, and A. Kupfer, "Three-dimensional segregation of supramolecular activation clusters in T cells.," *Nature*, vol. 395, no. 6697, pp. 82–6, 1998.

[203] K. A. Frauwirth and C. B. Thompson, "Activation and inhibition of lymphocytes by costimulation," *J. Clin. Invest.*, vol. 109, no. 3, pp. 295–299, 2002.

[204] P. A. van der Merwe, D. L. Bodian, S. Daenke, P. Linsley, and S. J. Davis, "CD80 (B7-1) binds both CD28 and CTLA-4 with a low affinity and very fast kinetics," *J. Exp. Med.*, vol. 185, no. 3, pp. 393–403, 1997.

[205] T. L. Walunas, D. J. Lenschow, C. Y. Bakker, P. S. Linsley, G. J. Freeman, J. M. Green, C. B. Thompson, and J. A. Bluestone, "CTLA-4 can function as a negative regulator of T cell activation.," *Immunity*, vol. 1, no. 5, pp. 405–13, 1994.

[206] P. S. Linsley, J. L. Greene, P. Tan, J. Bradshaw, J. A. Ledbetter, C. Anasetti, and N. K. Damle, "Coexpression and functional cooperation of CTLA-4 and CD28 on activated T lymphocytes.," *J. Exp. Med.*, vol. 176, no. 6, pp. 1595–604, 1992.

[207] C. A. Chambers, T. J. Sullivan, and J. P. Allison, "Lymphoproliferation in CTLA-4-deficient mice is mediated by costimulation-dependent activation of CD4+ T cells," *Immunity*, vol. 7, no. 6, pp. 885–95, 1997.

[208] B. Metzler, C. Burkhart, and D. C. Wraith, "Phenotypic analysis of CTLA-4 and CD28 expression during transient peptide-induced T cell activation in vivo," *Int. Immunol.*, vol. 11, no. 5, pp. 667–75, 1999.

[209] S. Read, V. Malmström, and F. Powrie, "Cytotoxic T lymphocyte-associated antigen 4 plays an essential role in the function of CD25(+)CD4(+) regulatory cells that control intestinal inflammation," *J. Exp. Med.*, vol. 192, no. 2, pp. 295–302, 2000.

[210] T. Takahashi, T. Tagami, S. Yamazaki, T. Uede, J. Shimizu, N. Sakaguchi, T. W. Mak, and S. Sakaguchi, "Immunologic self-tolerance maintained by CD25(+)CD4(+) regulatory T cells constitutively expressing cytotoxic T lymphocyte-associated antigen 4.," *J. Exp. Med.*, vol. 192, no. 2, pp. 303–10, 2000.

[211] K. I. Mead, Y. Zheng, C. N. Manzotti, L. C. Perry, M. K. Liu, F. Burke, D. J. Powner, M. J. Wakelam, and D. M. Sansom, "Exocytosis of CTLA-4 is dependent on phospholipase D and ADP ribosylation factor-1 and stimulated during activation of regulatory T cells," *J. Immunol.*, vol. 174, no. 8, pp. 4803–11, 2005.

[212] O. S. Qureshi, S. Kaur, T. Z. Hou, L. E. Jeffery, N. S. Poulter, Z. Briggs, R. Kenefeck, A. K. Willox, S. J. Royle, J. Z. Rappoport, and D. M. Sansom, "Constitutive clathrin-mediated endocytosis of CTLA-4 persists during T cell activation.," *J. Biol. Chem.*, vol. 287, no. 12, pp. 9429–40, 2012.

[213] O. S. Qureshi, Y. Zheng, K. Nakamura, K. Attridge, C. Manzotti, E. M. Schmidt, J. Baker, L. E. Jeffery, S. Kaur, Z. Briggs, T. Z. Hou, C. E. Futter, G. Anderson, L. S. Walker, and D. M. Sansom, "Trans-endocytosis of CD80 and CD86: a molecular basis for the cell-extrinsic function of CTLA-4," *Science*, vol. 332, no. 6029, pp. 600–3, 2011.

[214] A. Jansson, E. Barnes, P. Klenerman, M. Harlen, P. Sorensen, S. J. Davis, and P. Nilsson, "A theoretical framework for quantitative analysis of the molecular basis of costimulation," *J. Immunol.*, vol. 175, no. 3, pp. 1575–85, 2005.

[215] D. Fairweather, *Autoimmune Disease: Mechanisms*. Encyclopedia of Life Sciences, John Wiley & Sons Ltd, 2007.

[216] N. Thiault, J. Darrigues, V. Adoue, M. Gros, B. Binet, C. Perals, B. Leobon, N. Fazilleau, O. P. Joffre, E. A. Robey, J. P. van Meerwijk, and P. Romagnoli, "Peripheral regulatory T lymphocytes recirculating to the thymus suppress the development of their precursors," *Nat. Immunol.*, vol. 16, no. 6, pp. 628–34, 2015.

Appendix A

Abbreviations

Ag	Antigen
APC	Antigen presenting cell
CHO	Chinese Hamster Ovary
CP	Cytoplasm
CTLA4	Cytotoxic T-lymphocyte-associated protein 4
IL-2	Interleukin-2
iTreg	Induced regulatory T cell
LN	Lymph node
MFI	Mean fluorescent intensity
nTreg	Natural regulatory T cell
ODE	Ordinary differential equation
PDE	Partial differential equation
PM	Plasma membrane
RHC	Routh-Hurwitz stability Criterion
Tconv	Conventional T cell
Treg	Regulatory T cell

Appendix B

Analytic solutions of CTLA4 trafficking models

B.1 Ratio of plasma membrane (PM) to internalized (I) CTLA4

Herein, the aim is to obtain solution of model (6.16), given the initial conditions (6.17). Model (6.16) can be considered in the form of $\dot{x}(t) = Ax(t) + g$, where $x(t)$ is an $n \times 1$ vector of CTLA4-associated functions and $\dot{x}(t)$ is the vector of first derivatives of these functions, and A is an $n \times n$ matrix, of which all elements are constants, and g is an $n \times 1$ vector with constant elements. The following characteristic equation can be obtained from squared matrix A:

$$\begin{aligned} Q(\lambda) &= \det(\lambda I_n - A) = \begin{vmatrix} \lambda + (k_{ir} + \delta_{ic}) & 0 & 0 \\ -k_{ir} & \lambda + k_{ii} & -k_{ir} \\ 0 & -k_{ii} & \lambda + (k_{ir} + \delta_{ic}) \end{vmatrix} \\ &= [\lambda + (k_{ir} + \delta_{ic})][\lambda^2 + (k_{ii} + k_{ir} + \delta_{ic})\lambda + k_{ii}\delta_{ic}] = 0. \end{aligned} \tag{B.1}$$

where I_n is the identity (unit) matrix of size n. Eigenvalues of the model are

$$\lambda_1 = -(k_{ir} + \delta_{ic}) \tag{B.2}$$

$$\lambda_2 = \frac{1}{2}\left[-(k_{ii} + k_{ir} + \delta_{ic}) - \sqrt{(k_{ii} + k_{ir} + \delta_{ic})^2 - 4k_{ii}\delta_{ic}}\right] \tag{B.3}$$

$$\lambda_3 = \frac{1}{2}\left[-(k_{ii} + k_{ir} + \delta_{ic}) + \sqrt{(k_{ii} + k_{ir} + \delta_{ic})^2 - 4k_{ii}\delta_{ic}}\right]. \tag{B.4}$$

Let v_i be an eigenvector of A associated to λ_i. We must have

$$Av_i = \lambda_i v_i \text{ or } (A - \lambda_i I_n)v_i = 0. \tag{B.5}$$

The following eigenvectors from associated eigenvalue can be constructed

$$v_1 = \begin{pmatrix} 1 \\ 0 \\ -1 \end{pmatrix}, v_2 = \begin{pmatrix} 0 \\ \frac{(k_{ir}+\delta_{ic})+\lambda_2}{k_{ii}} \\ 1 \end{pmatrix}, v_3 = \begin{pmatrix} 0 \\ \frac{(k_{ir}+\delta_{ic})+\lambda_3}{k_{ii}} \\ 1 \end{pmatrix}. \tag{B.6}$$

By using eigenvectors given above, fundamental matrix (defined in 3.4) can be obtained

$$\Phi(t) = \begin{pmatrix} e^{\lambda_1 t} & 0 & 0 \\ 0 & \frac{(k_{ir}+\delta_{ic})+\lambda_2}{k_{ii}} e^{\lambda_2 t} & \frac{(k_{ir}+\delta_{ic})+\lambda_3}{k_{ii}} e^{\lambda_3 t} \\ -e^{\lambda_1 t} & e^{\lambda_2 t} & e^{\lambda_3 t} \end{pmatrix}. \tag{B.7}$$

Next, we obtain the solution of the model by using the method of variation of parameters, presented in section (3.2.1.1.2). The solution of the nonhomogeneous linear system $\dot{x}(t) = Ax(t)+g$ is $x(t) = \Phi(t)u(t)$, where $\Phi(t)\dot{u}(t) = g$ is the following

$$\begin{pmatrix} e^{\lambda_1 t} & 0 & 0 \\ 0 & \frac{(k_{ir}+\delta_{ic})+\lambda_2}{k_{ii}} e^{\lambda_2 t} & \frac{(k_{ir}+\delta_{ic})+\lambda_3}{k_{ii}} e^{\lambda_3 t} \\ -e^{\lambda_1 t} & e^{\lambda_2 t} & e^{\lambda_3 t} \end{pmatrix} \begin{pmatrix} \dot{u}_1(t) \\ \dot{u}_2(t) \\ \dot{u}_3(t) \end{pmatrix} = \begin{pmatrix} 0 \\ \sigma_i \\ 0 \end{pmatrix} \tag{B.8}$$

Therefore, $u(t)$ can be obtained from the following differential equations.

$$e^{\lambda_1 t}\dot{u}_1(t) = 0 \Rightarrow \dot{u}_1(t) = 0 \Rightarrow u_1(t) = C_1, \tag{B.9}$$

$$\frac{(k_{ir}+\delta_{ic})+\lambda_2}{k_{ii}} e^{\lambda_2 t}\dot{u}_2(t) + \frac{(k_{ir}+\delta_{ic})+\lambda_3}{k_{ii}} e^{\lambda_3 t}\dot{u}_3(t) = \sigma_i, \tag{B.10}$$

$$-e^{\lambda_1 t}\dot{u}_1(t) + e^{\lambda_2 t}\dot{u}_2(t) + e^{\lambda_3 t}\dot{u}_3(t) = 0 \tag{B.11}$$

By using (B.9) in (B.11),

$$\dot{u}_2(t) = -e^{\lambda_3-\lambda_2}\dot{u}_3(t). \tag{B.12}$$

By employing (B.2) and (B.12) in (B.10), we obtain $\dot{u}_3(t)$ and subsequently, $u_3(t)$.

$$\frac{\lambda_2-\lambda_1}{k_{ii}} e^{\lambda_2 t}\dot{u}_2(t) + \frac{\lambda_3-\lambda_1}{k_{ii}} e^{\lambda_3 t}\dot{u}_3(t) = \sigma_i \Rightarrow \dot{u}_3(t) = \frac{\sigma_i k_{ii}}{\lambda_3-\lambda_2} e^{-\lambda_3 t}, \tag{B.13}$$

$$\Rightarrow u_3(t) = \frac{-\sigma_i k_{ii}}{\lambda_3(\lambda_3-\lambda_2)} e^{-\lambda_3 t} + C_3. \tag{B.14}$$

Next, $\dot{u}_2(t)$ and subsequently, $u_2(t)$ is obtained by using (B.13) in (B.12).

$$\dot{u}_2(t) = -e^{(\lambda_3-\lambda_2)t}\frac{\sigma_i k_{ii}}{\lambda_3-\lambda_2} e^{-\lambda_3 t} = -\frac{\sigma_i k_{ii}}{\lambda_3-\lambda_2} e^{-\lambda_2 t} \Rightarrow u_2(t) = \frac{\sigma_i k_{ii}}{\lambda_2(\lambda_3-\lambda_2)} e^{-\lambda_2 t} + C_2. \tag{B.15}$$

Next, by employing $u(t)$ in $x(t) = \Phi(t)u(t)$, solutions can be found.

$$x(t) = \begin{pmatrix} R_{ic}(t) \\ R^*_{ip}(t) \\ R^*_{ic}(t) \end{pmatrix} = \Phi(t)u(t) = \begin{pmatrix} e^{\lambda_1 t} & 0 & 0 \\ 0 & \frac{\lambda_2-\lambda_1}{k_{ii}} e^{\lambda_2 t} & \frac{\lambda_3-\lambda_1}{k_{ii}} e^{\lambda_3 t} \\ -e^{\lambda_1 t} & e^{\lambda_2 t} & e^{\lambda_3 t} \end{pmatrix} \begin{pmatrix} u_1(t) \\ u_2(t) \\ u_3(t) \end{pmatrix}, \tag{B.16}$$

$$R_{ic}(t) = C_1 e^{\lambda_1 t}, \tag{B.17}$$

$$R^*_{ip}(t) = \frac{\lambda_2-\lambda_1}{k_{ii}}e^{\lambda_2 t}\left[\frac{\sigma_i k_{ii}}{\lambda_2(\lambda_3-\lambda_2)}e^{-\lambda_2 t}+C_2\right]+\frac{\lambda_3-\lambda_1}{k_{ii}}e^{\lambda_3 t}\left[\frac{-\sigma_i k_{ii}}{\lambda_3(\lambda_3-\lambda_2)}e^{-\lambda_3 t}+C_3\right]$$
$$\Rightarrow R^*_{ip}(t) = \frac{\lambda_2-\lambda_1}{\lambda_2(\lambda_3-\lambda_2)}\sigma_i - \frac{\lambda_3-\lambda_1}{\lambda_3(\lambda_3-\lambda_2)}\sigma_i + \frac{C_2}{k_{ii}}(\lambda_2-\lambda_1)e^{\lambda_2 t}+\frac{C_3}{k_{ii}}(\lambda_3-\lambda_1)e^{\lambda_3 t}, \tag{B.18}$$

$$R^*_{ip}(t) = -\frac{\lambda_1}{\lambda_2\lambda_3}\sigma_i + \frac{C_2(\lambda_2-\lambda_1)}{k_{ii}}e^{\lambda_2 t}+\frac{C_3(\lambda_3-\lambda_1)}{k_{ii}}e^{\lambda_3 t}, \tag{B.19}$$

$$R^*_{ic}(t) = -C_1e^{\lambda_1 t}+e^{\lambda_2 t}\left[\frac{\sigma_i k_{ii}}{\lambda_2(\lambda_3-\lambda_2)}e^{-\lambda_2 t}+C_2\right]+e^{\lambda_3 t}\left[\frac{-\sigma_i k_{ii}}{\lambda_3(\lambda_3-\lambda_2)}e^{-\lambda_3 t}+C_3\right] \tag{B.20}$$
$$= -C_1e^{\lambda_1 t}+\frac{\sigma_i k_{ii}}{\lambda_2(\lambda_3-\lambda_2)}-\frac{\sigma_i k_{ii}}{\lambda_3(\lambda_3-\lambda_2)}+C_2e^{\lambda_2 t}+C_3e^{\lambda_3 t}, \tag{B.21}$$

$$R^*_{ic}(t) = \frac{\sigma_i k_{ii}}{\lambda_2\lambda_3}-C_1e^{\lambda_1 t}+C_2e^{\lambda_2 t}+C_3e^{\lambda_3 t}. \tag{B.22}$$

Model has the following initial conditions

$$R_{ic,0} = \frac{\sigma_i}{\delta_{ic}} \tag{B.23}$$
$$R^*_{ip,0} = \frac{\sigma_i(k_{ir}+\delta_{ic})}{k_{ii}\delta_{ic}} \tag{B.24}$$
$$R^*_{ic,0} = 0 \tag{B.25}$$

Constant coefficient vector C is determined by using the initial values of states. For obtaining C_1, we use (B.23) in (B.17) for $t = 0$,

$$R_{ic}(0) = C_1 = R_{ic,0}. \tag{B.26}$$

With using (B.24) in (B.19) for $t = 0$, we have

$$R^*_{ip}(0) = \frac{-\lambda_1}{\lambda_2\lambda_3}\sigma_i + \frac{C_2(\lambda_2-\lambda_1)}{k_{ii}}+\frac{C_3(\lambda_3-\lambda_1)}{k_{ii}} = \frac{\sigma_i(k_{ir}+\delta_{ic})}{k_{ii}\delta_{ic}}. \tag{B.27}$$

By knowing from (B.1) that $\lambda_2\lambda_3 = k_{ii}\delta_{ic}$, and by using (B.2) in (B.27), we obtain the following relation between C_2 and C_3

$$C_2 = \frac{\lambda_1-\lambda_3}{\lambda_2-\lambda_1}C_3. \tag{B.28}$$

By using (B.25) in (B.22) for $t = 0$,

$$R^*_{ic}(0) = \frac{\sigma_i k_{ii}}{\lambda_2\lambda_3}-C_1+C_2+C_3 = 0 \Rightarrow \frac{\lambda_2-\lambda_3}{\lambda_2-\lambda_1}C_3 = 0. \Rightarrow C_3 = 0 \tag{B.29}$$

By using (B.29) in (B.28), we have $C_2 = 0$. By substituting constant coefficient vector C, the following complete solutions can be obtained

$$R_{ic}(t) = \frac{\sigma_i}{\delta_{ic}}e^{\lambda_1 t}, \quad R^*_{ip}(t) = \frac{\sigma_i(k_{ir}+\delta_{ic})}{k_{ii}\delta_{ic}}, \quad R^*_{ic}(t) = \frac{\sigma_i}{\delta_{ic}}\left(1-e^{\lambda_1 t}\right) \tag{B.30}$$

B.2 Receptors internalization

Herein, the aim is to obtain solution of the internalization model (6.26), given the initial conditions (6.28). The following characteristic equation can be obtained from (6.26)

$$Q(\lambda) = \det \begin{pmatrix} \lambda + k_{ii} & -k_{ir} \\ -k_{ii} & \lambda + (k_{ir} + \delta_{ic}) \end{pmatrix} = \lambda^2 + (k_{ii} + k_{ir} + \delta_{ic})\lambda + k_{ii}\delta_{ic} = 0 \tag{B.31}$$

The eigenvalues of the model and associated eigenvectors are

$$\lambda_1 = \frac{1}{2}\left[-(k_{ii} + k_{ir} + \delta_{ic}) - \sqrt{(k_{ii} + k_{ir} + \delta_{ic})^2 - 4k_{ii}\delta_{ic}}\right], \quad v_1 = \begin{pmatrix} 1 \\ \frac{k_{ii}+\lambda_1}{k_{ir}} \end{pmatrix}, \tag{B.32}$$

$$\lambda_2 = \frac{1}{2}\left[-(k_{ii} + k_{ir} + \delta_{ic}) + \sqrt{(k_{ii} + k_{ir} + \delta_{ic})^2 - 4k_{ii}\delta_{ic}}\right], \quad v_2 = \begin{pmatrix} 1 \\ \frac{k_{ii}+\lambda_2}{k_{ir}} \end{pmatrix} \tag{B.33}$$

By using eigenvectors given above, fundamental matrix can be obtained

$$\Phi(t) = \begin{pmatrix} e^{\lambda_1 t} & e^{\lambda_2 t} \\ \frac{k_{ii}+\lambda_1}{k_{ir}} e^{\lambda_1 t} & \frac{k_{ii}+\lambda_2}{k_{ir}} e^{\lambda_2 t} \end{pmatrix}. \tag{B.34}$$

General solution is in the form of $x(t) = \Phi(t)C$

$$R^*_{ip}(t) = C_1 e^{\lambda_1 t} + C_2 e^{\lambda_2 t}, \tag{B.35}$$

$$R^*_{ic}(t) = C_1 \frac{k_{ii} + \lambda_1}{k_{ir}} e^{\lambda_1 t} + C_2 \frac{k_{ii} + \lambda_2}{k_{ir}} e^{\lambda_2 t}. \tag{B.36}$$

Initial conditions of the model are

$$R^*_{ip,0} = \frac{\sigma_i(k_{ir} + \delta_{ic})}{k_{ii}\delta_{ic}}, \tag{B.37}$$

$$R^*_{ic,0} = 0. \tag{B.38}$$

By using the initial condition, the constant coefficient C can be obtained. From (B.38) and (B.36) for $t = 0$, we have

$$R^*_{ic,0} = C_1 \frac{k_{ii} + \lambda_1}{k_{ir}} + C_2 \frac{k_{ii} + \lambda_2}{k_{ir}} = 0 \Rightarrow C_1 = -C_2 \frac{k_{ii} + \lambda_2}{k_{ii} + \lambda_1} \tag{B.39}$$

C_2 and subsequently $C1$ can be obtained from (B.37) and (B.35) for $t = 0$ and (B.39)

$$R^*_{ip,0} = C_1 + C_2 = -C_2 \frac{k_{ii} + \lambda_2}{k_{ii} + \lambda_1} + C_2 \Rightarrow C_2 = \frac{k_{ii} + \lambda_1}{\lambda_1 - \lambda_2} R^*_{ip,0} \tag{B.40}$$

$$\Rightarrow C_1 = -\frac{k_{ii} + \lambda_2}{\lambda_1 - \lambda_2} R^*_{ip,0}. \tag{B.41}$$

By substituting the constant coefficient vector C, the exact solution with given initial conditions is obtained

$$R^*_{ip}(t) = -\frac{k_{ii} + \lambda_2}{\lambda_1 - \lambda_2} R^*_{ip,0} e^{\lambda_1 t} + \frac{k_{ii} + \lambda_1}{\lambda_1 - \lambda_2} R^*_{ip,0} e^{\lambda_2 t}, \tag{B.42}$$

$$R^*_{ic}(t) = \frac{k_{ii}}{\lambda_1 - \lambda_2} R^*_{ip,0} e^{\lambda_1 t} - \frac{k_{ii}}{\lambda_1 - \lambda_2} R^*_{ip,0} e^{\lambda_2 t}. \tag{B.43}$$

B.3 Lysosomal degradation block of initially labeled CTLA4

Herein, the aim is to obtain solution of the model for degradation block experiment, given in (6.36), with initial conditions given in (6.35). Model (6.36) has the following characteristic equation

$$Q(\lambda) = \det \begin{pmatrix} \lambda + k_{ii} & -k_{ir} \\ -k_{ii} & \lambda + k_{ir} + \delta_{in} \end{pmatrix} = \lambda^2 + (k_{ii} + k_{ir} + \delta_{in})\lambda + k_{ii}\delta_{in} = 0. \tag{B.44}$$

The eigenvalues and associated eigenvectors are:

$$\lambda_1 = \frac{1}{2}\left[-(k_{ii} + k_{ir} + \delta_{in}) - \sqrt{(k_{ii} + k_{ir} + \delta_{in})^2 - 4k_{ii}\delta_{in}}\right], \quad v_1 = \begin{pmatrix} 1 \\ \frac{k_{ii}+\lambda_1}{k_{ir}} \end{pmatrix}, \tag{B.45}$$

$$\lambda_2 = \frac{1}{2}\left[-(k_{ii} + k_{ir} + \delta_{in}) + \sqrt{(k_{ii} + k_{ir} + \delta_{in})^2 - 4k_{ii}\delta_{in}}\right], \quad v_2 = \begin{pmatrix} 1 \\ \frac{k_{ii}+\lambda_2}{k_{ir}} \end{pmatrix}. \tag{B.46}$$

By using eigenvectors, we construct the following fundamental matrix

$$\Phi(t) = \begin{pmatrix} e^{\lambda_1 t} & e^{\lambda_2 t} \\ \frac{k_{ii}+\lambda_1}{k_{ir}} e^{\lambda_1 t} & \frac{k_{ii}+\lambda_2}{k_{ir}} e^{\lambda_2 t} \end{pmatrix} \tag{B.47}$$

from which, we can obtain the general solution

$$\begin{pmatrix} R^*_{ip}(t) \\ R^*_{ic}(t) \end{pmatrix} = \begin{pmatrix} e^{\lambda_1 t} & e^{\lambda_2 t} \\ \frac{k_{ii}+\lambda_1}{k_{ir}} e^{\lambda_1 t} & \frac{k_{ii}+\lambda_2}{k_{ir}} e^{\lambda_2 t} \end{pmatrix} \begin{pmatrix} C_1 \\ C_2 \end{pmatrix}. \tag{B.48}$$

The general solutions has the following form

$$R^*_{ip}(t) = C_1 e^{\lambda_1 t} + C_2 e^{\lambda_2 t}, \tag{B.49}$$

$$R^*_{ic}(t) = C_1 \frac{k_{ii} + \lambda_1}{k_{ir}} e^{\lambda_1 t} + C_2 \frac{k_{ii} + \lambda_2}{k_{ir}} e^{\lambda_2 t}. \tag{B.50}$$

Constant coefficient vector C can be obtain by using initial conditions $R^*_{ip,0}$ and $R^*_{ic,0}$. From (B.49) for $t = 0$, we have

$$R^*_{ip,0} = R_{ip}(0) = C_1 + C_2 \Rightarrow C_1 = R^*_{ip,0} - C_2. \tag{B.51}$$

By using (B.50) for $t = 0$ and (B.51), we have

$$R^*_{ic,0} = R_{ic}(0) = C_1 \frac{k_{ii} + \lambda_1}{k_{ir}} + C_2 \frac{k_{ii} + \lambda_2}{k_{ir}} = R^*_{ip,0} \frac{k_{ii} + \lambda_1}{k_{ir}} + C_2 \frac{\lambda_2 - \lambda_1}{k_{ir}} \tag{B.52}$$

$$\Rightarrow C_2 = \frac{k_{ir}}{\lambda_2 - \lambda_1}\left[R^*_{ic,0} - R^*_{ip,0} \frac{k_{ii} + \lambda_1}{k_{ir}}\right] \Rightarrow C_2 = R^*_{ic,0} \frac{k_{ir}}{\lambda_2 - \lambda_1} - R^*_{ip,0} \frac{k_{ii} + \lambda_1}{\lambda_2 - \lambda_1}. \tag{B.53}$$

By using (B.51) and (B.53), C_1 can be obtained

$$C_1 = -R^*_{ic,0} \frac{k_{ir}}{\lambda_2 - \lambda_1} + R^*_{ip,0} \frac{k_{ii} + \lambda_2}{\lambda_2 - \lambda_1}. \tag{B.54}$$

In the case of $\delta_{in} = 0$, the eigenvalues are simplified to

$$\lambda_1 = 0, \quad \lambda_2 = -(k_{ii} + k_{ir}). \tag{B.55}$$

Solutions can be obtained from the case where $\delta_{in} \neq 0$ by substituting $\lambda_1 = 0$.

B.4 Lysosomal degradation block without initial labeling

B.4.1 Case 1: $\delta_{in} \neq 0$

Herein, the aim is to obtain solution of the model for degradation block experiment without initial labeling, given in (6.51), with initial conditions given in (6.53). Characteristic equation of model (6.51) is the following

$$Q(\lambda) = \det \begin{pmatrix} \lambda + k_{ii} & -k_{ir} \\ -k_{ii} & \lambda + k_{ir} + \delta_{in} \end{pmatrix} = \lambda^2 + (k_{ii} + k_{ir} + \delta_{in})\lambda + k_{ii}\delta_{in} = 0. \tag{B.56}$$

Eigenvalues of the model and associated eigenvectors are

$$\lambda_1 = \frac{1}{2}\left[-(k_{ii} + k_{ir} + \delta_{in}) - \sqrt{(k_{ii} + k_{ir} + \delta_{in})^2 - 4k_{ii}\delta_{in}}\right], \quad v_1 = \begin{pmatrix} 1 \\ \frac{k_{ii}+\lambda_1}{k_{ir}} \end{pmatrix}, \tag{B.57}$$

$$\lambda_2 = \frac{1}{2}\left[-(k_{ii} + k_{ir} + \delta_{in}) + \sqrt{(k_{ii} + k_{ir} + \delta_{in})^2 - 4k_{ii}\delta_{in}}\right], \quad v_2 = \begin{pmatrix} 1 \\ \frac{k_{ii}+\lambda_2}{k_{ir}} \end{pmatrix}. \tag{B.58}$$

By using the above eigenvectors, we construct the following fundamental matrix

$$\Phi(t) = \begin{pmatrix} e^{\lambda_1 t} & e^{\lambda_2 t} \\ \frac{k_{ii}+\lambda_1}{k_{ir}} e^{\lambda_1 t} & \frac{k_{ii}+\lambda_2}{k_{ir}} e^{\lambda_2 t} \end{pmatrix}. \tag{B.59}$$

Next, we obtain the solution of the model by using variation of parameters method.

$$\Phi(t)\dot{u}(t) = \begin{pmatrix} \sigma_i \\ 0 \end{pmatrix} \Rightarrow \begin{pmatrix} e^{\lambda_1 t} & e^{\lambda_2 t} \\ \frac{k_{ii}+\lambda_1}{k_{ir}} e^{\lambda_1 t} & \frac{k_{ii}+\lambda_2}{k_{ir}} e^{\lambda_2 t} \end{pmatrix} \begin{pmatrix} \dot{u}_1(t) \\ \dot{u}_2(t) \end{pmatrix} = \begin{pmatrix} \sigma_i \\ 0 \end{pmatrix}. \tag{B.60}$$

$u(t)$ can be obtained from the following differential equations

$$e^{\lambda_1 t}\dot{u}_1(t) + e^{\lambda_2 t}\dot{u}_2(t) = \sigma_i \tag{B.61}$$

$$\frac{k_{ii} + \lambda_1}{k_{ir}} e^{\lambda_1 t}\dot{u}_1(t) + \frac{k_{ii} + \lambda_2}{k_{ir}} e^{\lambda_2 t}\dot{u}_2(t) = 0 \Rightarrow \dot{u}_1(t) = -\frac{k_{ii} + \lambda_2}{k_{ii} + \lambda_1} e^{(\lambda_2 - \lambda_1)t}\dot{u}_2(t) \tag{B.62}$$

By using (B.62) in (B.61), we have

$$e^{(\lambda_2-\lambda_1)t} e^{\lambda_1 t}\left(-\frac{k_{ii} + \lambda_2}{k_{ii} + \lambda_1}\right)\dot{u}_2(t) + e^{\lambda_2 t}\dot{u}_2(t) = \sigma_i \Rightarrow \dot{u}_2(t) = \frac{k_{ii} + \lambda_1}{\lambda_1 - \lambda_2}\sigma_i e^{-\lambda_2 t} \tag{B.63}$$

$$\Rightarrow u_2(t) = -\frac{\sigma_i(k_{ii} + \lambda_1)}{\lambda_2(\lambda_1 - \lambda_2)} e^{-\lambda_2 t} + C_2 \tag{B.64}$$

By using (B.63) in (B.62), we have:

$$\dot{u}_1(t) = -\frac{k_{ii} + \lambda_2}{\lambda_1 - \lambda_2}\sigma_i e^{-\lambda_1 t} \Rightarrow u_1(t) = \frac{\sigma_i(k_{ii} + \lambda_2)}{\lambda_1(\lambda_1 - \lambda_2)} e^{-\lambda_1 t} + C_1 \tag{B.65}$$

Next, we obtain general solution of the model

$$\begin{pmatrix} R_{ip}(t) \\ R_{ic}(t) \end{pmatrix} = \Phi(t)u(t) = \begin{pmatrix} e^{\lambda_1 t} & e^{\lambda_2 t} \\ \frac{k_{ii}+\lambda_1}{k_{ir}} e^{\lambda_1 t} & \frac{k_{ii}+\lambda_2}{k_{ir}} e^{\lambda_2 t} \end{pmatrix} \begin{pmatrix} \frac{\sigma_i(k_{ii}+\lambda_2)}{\lambda_1(\lambda_1-\lambda_2)} e^{-\lambda_1 t} + C_1 \\ -\frac{\sigma_i(k_{ii}+\lambda_1)}{\lambda_2(\lambda_1-\lambda_2)} e^{-\lambda_2 t} + C_2 \end{pmatrix} \tag{B.66}$$

From above, we expand general solutions

$$R_{ip}(t) = \frac{\sigma_i(k_{ii}+\lambda_2)}{\lambda_1(\lambda_1-\lambda_2)} + C_1 e^{\lambda_1 t} - \frac{\sigma_i(k_{ii}+\lambda_1)}{\lambda_2(\lambda_1-\lambda_2)} + C_2 e^{\lambda_2 t}$$
$$\Rightarrow R_{ip}(t) = -\frac{\sigma_i(\lambda_1+\lambda_2+k_{ii})}{\lambda_1\lambda_2} + C_1 e^{\lambda_1 t} + C_2 e^{\lambda_2 t} \tag{B.67}$$

$$R_{ic}(t) = \frac{k_{ii}+\lambda_1}{k_{ir}}\frac{\sigma_i(k_{ii}+\lambda_2)}{\lambda_1(\lambda_1-\lambda_2)} + C_1\frac{k_{ii}+\lambda_1}{k_{ir}}e^{\lambda_1 t} - \frac{k_{ii}+\lambda_2}{k_{ir}}\frac{\sigma_i(k_{ii}+\lambda_1)}{\lambda_2(\lambda_1-\lambda_2)} + C_2\frac{k_{ii}+\lambda_2}{k_{ir}}e^{\lambda_2 t}$$
$$\Rightarrow R_{ic}(t) = -\frac{\sigma_i}{k_{ir}}\frac{(k_{ii}+\lambda_1)(k_{ii}+\lambda 2)}{\lambda_1\lambda_2} + C_1\frac{k_{ii}+\lambda_1}{k_{ir}}e^{\lambda_1 t} + C_2\frac{k_{ii}+\lambda_2}{k_{ir}}e^{\lambda_2 t} \tag{B.68}$$

Let $R_{ip,0}$ and $R_{ic,0}$ be the initial conditions of model states. Next, we obtain constant coefficients C_1 and C_2. From (B.67) for $t = 0$, we have

$$R_{ip}(0) = \frac{\sigma_i(k_{ii}+\lambda_2)}{\lambda_1(\lambda_1-\lambda_2)} + C_1 - \frac{\sigma_i(k_{ii}+\lambda_1)}{\lambda_2(\lambda_1-\lambda_2)} + C_2 = \frac{\sigma_i\left[(k_{ii}+\lambda_2)\lambda_2 - (k_{ii}+\lambda_1)\lambda_1\right]}{\lambda_1\lambda_2(\lambda_1-\lambda_2)} + C_1 + C_2$$
$$= \frac{\sigma_i\left[k_{ii}(\lambda_2-\lambda_1) + (\lambda_2-\lambda_1)(\lambda_2+\lambda_1)\right]}{\lambda_1\lambda_2(\lambda_1-\lambda_2)} + C_1 + C_2 = -\frac{\sigma_i(\lambda_1+\lambda_2+k_{ii})}{\lambda_1\lambda_2} + C_1 + C_2 = R_{ip,0}$$
$$\Rightarrow C_1 = R_{ip,0} - C_2 + \frac{\sigma_i(\lambda_1+\lambda_2+k_{ii})}{\lambda_1\lambda_2} \tag{B.69}$$

From (B.68) for $t = 0$, we have

$$R_{ic}(0) = \frac{k_{ii}+\lambda_1}{k_{ir}}\frac{\sigma_i(k_{ii}+\lambda_2)}{\lambda_1(\lambda_1-\lambda_2)} + C_1\frac{k_{ii}+\lambda_1}{k_{ir}} - \frac{k_{ii}+\lambda_2}{k_{ir}}\frac{\sigma_i(k_{ii}+\lambda_1)}{\lambda_2(\lambda_1-\lambda_2)} + C_2\frac{k_{ii}+\lambda_2}{k_{ir}}$$
$$= \sigma_i\frac{\lambda_2(k_{ii}+\lambda_1)(k_{ii}+\lambda_2) - \lambda_1(k_{ii}+\lambda_1)(k_{ii}+\lambda_2)}{k_{ir}\lambda_1\lambda_2(\lambda_1-\lambda_2)} + C_1\frac{k_{ii}+\lambda_1}{k_{ir}} + C_2\frac{k_{ii}+\lambda_2}{k_{ir}}$$
$$= -\sigma_i\frac{(k_{ii}+\lambda_1)(k_{ii}+\lambda_2)}{k_{ir}\lambda_1\lambda_2} + C_1\frac{k_{ii}+\lambda_1}{k_{ir}} + C_2\frac{k_{ii}+\lambda_2}{k_{ir}} = R_{ic,0} \tag{B.70}$$

Next, by substituting C_1 from (B.69) in (B.70), we obtain C_2

$$R_{ic,0} = -\sigma_i\frac{(k_{ii}+\lambda_1)(k_{ii}+\lambda_2)}{k_{ir}\lambda_1\lambda_2} + \left[R_{ip,0} - C_2 + \frac{\sigma_i(\lambda_1+\lambda_2+k_{ii})}{\lambda_1\lambda_2}\right]\frac{k_{ii}+\lambda_1}{k_{ir}} + C_2\frac{k_{ii}+\lambda_2}{k_{ir}}$$
$$= R_{ip,0}\frac{k_{ii}+\lambda_1}{k_{ir}} + \frac{\lambda_2-\lambda_1}{k_{ir}}C_2 + \frac{\sigma_i(k_{ii}+\lambda_1)}{k_{ir}\lambda_2} = R_{ic,0}$$
$$\Rightarrow C_2 = R_{ic,0}\frac{k_{ir}}{\lambda_2-\lambda_1} - R_{ip,0}\frac{k_{ii}+\lambda_1}{\lambda_2-\lambda_1} - \frac{\sigma_i(k_{ii}+\lambda_1)}{\lambda_2(\lambda_2-\lambda_1)} \tag{B.71}$$

Next, by substituting C_2 from (B.71) in (B.69), C_1 can be obtained

$$C_1 = R_{ip,0} - \left[R_{ic,0}\frac{k_{ir}}{\lambda_2-\lambda_1} - R_{ip,0}\frac{k_{ii}+\lambda_1}{\lambda_2-\lambda_1} - \frac{\sigma_i(k_{ii}+\lambda_1)}{\lambda_2(\lambda_2-\lambda_1)}\right] + \frac{\sigma_i(\lambda_1+\lambda_2+k_{ii})}{\lambda_1\lambda_2}$$
$$= -R_{ic,0}\frac{k_{ir}}{\lambda_2-\lambda_1} + R_{ip,0}\frac{k_{ii}+\lambda_2}{\lambda_2-\lambda_1} + \frac{\sigma_i(k_{ii}+\lambda_1)}{\lambda_2(\lambda_2-\lambda_1)} + \frac{\sigma_i(\lambda_1+\lambda_2+k_{ii})}{\lambda_1\lambda_2}$$
$$\Rightarrow C_1 = -R_{ic,0}\frac{k_{ir}}{\lambda_2-\lambda_1} + R_{ip,0}\frac{k_{ii}+\lambda_2}{\lambda_2-\lambda_1} + \frac{\sigma_i(k_{ii}+\lambda_2)}{\lambda_1(\lambda_2-\lambda_1)} \tag{B.72}$$

B.4.2 Case 2: $\delta_{in} = 0$

Now, consider model (6.51) with $\delta_{in} = 0$ The characteristic equation in (B.56) is changed to the following

$$Q(\lambda) \ = \lambda^2 + (k_{ii} + k_{ir})\lambda = 0. \tag{B.73}$$

From above, the eigenvalues and associated eigenvectors can be obtained

$$\lambda_1 = 0, \quad v_1 = \begin{pmatrix} 1 \\ \frac{k_{ii}}{k_{ir}} \end{pmatrix}, \tag{B.74}$$

$$\lambda_2 = -(k_{ii} + k_{ir}), \quad v_2 = \begin{pmatrix} 1 \\ \frac{k_{ii}+\lambda_2}{k_{ir}} \end{pmatrix}. \tag{B.75}$$

By using eigenvectors $v_{1,2}$, the following fundamental matrix can be constructed

$$\Phi(t) = \begin{pmatrix} 1 & e^{\lambda_2 t} \\ \frac{k_{ii}}{k_{ir}} & \frac{k_{ii}+\lambda_2}{k_{ir}} e^{\lambda_2 t} \end{pmatrix}. \tag{B.76}$$

We obtain solutions of the system by using the method of variation of parameters. The aim is to find $u(t)$ from the following equation

$$\Phi(t)\dot{u}(t) = \begin{pmatrix} \sigma_i \\ 0 \end{pmatrix} \Rightarrow \begin{pmatrix} 1 & e^{\lambda_2 t} \\ \frac{k_{ii}}{k_{ir}} & \frac{k_{ii}+\lambda_2}{k_{ir}} e^{\lambda_2 t} \end{pmatrix} \begin{pmatrix} \dot{u}_1(t) \\ \dot{u}_2(t) \end{pmatrix} = \begin{pmatrix} \sigma_i \\ 0 \end{pmatrix}, \tag{B.77}$$

or equivalently, we want to obtain $u_{1,2}(t)$ from the following differential equations

$$\dot{u}_1(t) + e^{\lambda_2 t}\dot{u}_2(t) = \sigma_i \tag{B.78}$$

$$\frac{k_{ii}}{k_{ir}}\dot{u}_1(t) + \frac{k_{ii}+\lambda_2}{k_{ir}} e^{\lambda_2 t}\dot{u}_2(t) = 0 \Rightarrow \dot{u}_1(t) = -\frac{k_{ii}+\lambda_2}{k_{ii}} e^{\lambda_2 t}\dot{u}_2(t). \tag{B.79}$$

By using (B.79) in (B.78), we have

$$\left[1 - \frac{k_{ii}+\lambda_2}{k_{ii}}\right] e^{\lambda_2 t}\dot{u}_2(t) = \sigma_i \Rightarrow \dot{u}_2(t) = -\frac{\sigma_i k_{ii}}{\lambda_2} e^{-\lambda_2 t} \Rightarrow u_2(t) = \frac{\sigma_i k_{ii}}{\lambda_2^2} e^{-\lambda_2 t} + C_2. \tag{B.80}$$

Next, by substituting $\dot{u}_2$ from (B.80) in (B.78), we have

$$\dot{u}_1(t) = -\frac{k_{ii}+\lambda_2}{k_{ii}} e^{\lambda_2 t}\left[-\frac{\sigma_i k_{ii}}{\lambda_2} e^{-\lambda_2 t}\right] = \frac{\sigma_i(k_{ii}+\lambda_2)}{\lambda_2} \Rightarrow u_1(t) = \frac{\sigma_i(k_{ii}+\lambda_2)}{\lambda_2} t + C_1. \tag{B.81}$$

Next, we construct the general solutions

$$\begin{pmatrix} R_{ip}(t) \\ R_{ic}(t) \end{pmatrix} = \Phi(t)u(t) = \begin{pmatrix} 1 & e^{\lambda_2 t} \\ \frac{k_{ii}}{k_{ir}} & \frac{k_{ii}+\lambda_2}{k_{ir}} e^{\lambda_2 t} \end{pmatrix} \begin{pmatrix} \frac{\sigma_i(k_{ii}+\lambda_2)}{\lambda_2} t + C_1 \\ \frac{\sigma_i k_{ii}}{\lambda_2^2} e^{-\lambda_2 t} + C_2 \end{pmatrix}, \tag{B.82}$$

or equivalently,

$$R_{ip}(t) = \frac{\sigma_i}{\lambda_2}\left[(k_{ii}+\lambda_2)t + \frac{k_{ii}}{\lambda_2}\right] + C_1 + C_2 e^{\lambda_2 t}, \tag{B.83}$$

$$R_{ic}(t) = \frac{\sigma_i k_{ii}(k_{ii}+\lambda_2)}{k_{ir}\lambda_2}\left[t + \frac{1}{\lambda_2}\right] + C_1\frac{k_{ii}}{k_{ir}} + C_2\frac{k_{ii}+\lambda_2}{k_{ir}} e^{\lambda_2 t}. \tag{B.84}$$

We denote $R_{ip,0}$ and $R_{ic,0}$ as initial conditions of the model. We can obtain constant coefficients $C_{1,2}$ as functions of the initial conditions. From (B.83) for $t = 0$, we have

$$R_{ip,0} = R_{ip}(0) = \frac{\sigma_i k_{ii}}{\lambda_2^2} + C_1 + C_2 \Rightarrow C_1 = R_{ip,0} - \frac{\sigma_i k_{ii}}{\lambda_2^2} - C_2. \tag{B.85}$$

By using (B.85) in (B.84) for $t = 0$, C_2 can be obtained

$$\begin{aligned} R_{ic,0} &= R_{ic}(0) = C_1 \frac{k_{ii}}{k_{ir}} + \frac{\sigma_i k_{ii}(k_{ii}+\lambda_2)}{k_{ir}\lambda_2^2} + C_2 \frac{k_{ii}+\lambda_2}{k_{ir}} \\ &= \frac{k_{ii}}{k_{ir}} R_{ip,0} - \frac{\sigma_i k_{ii}^2}{k_{ir}\lambda_2^2} - \frac{k_{ii}}{k_{ir}} C_2 + \frac{\sigma_i k_{ii}(k_{ii}+\lambda_2)}{k_{ir}\lambda_2^2} + C_2 \frac{k_{ii}+\lambda_2}{k_{ir}} = \frac{k_{ii}}{k_{ir}} R_{ip,0} + C_2 \frac{\lambda_2}{k_{ir}} + \frac{\sigma_i k_{ii}}{k_{ir}\lambda_2} \\ &\Rightarrow C_2 = \frac{k_{ir}}{\lambda_2}\left[R_{ic,0} - \frac{k_{ii}}{k_{ir}} R_{ip,0} - \frac{\sigma_i k_{ii}}{k_{ir}\lambda_2}\right] \Rightarrow C_2 = \frac{k_{ir}}{\lambda_2} R_{ic,0} - \frac{k_{ii}}{\lambda_2} R_{ip,0} - \frac{\sigma_i k_{ii}}{\lambda_2^2}. \end{aligned} \tag{B.86}$$

C_1 can be found by using (B.86) in (B.85)

$$C_1 = R_{ip,0} - \frac{\sigma_i k_{ii}}{\lambda_2^2} - \frac{k_{ir}}{\lambda_2} R_{ic,0} + \frac{k_{ii}}{\lambda_2} R_{ip,0} + \frac{\sigma_i k_{ii}}{\lambda_2^2} \Rightarrow C_1 = \left(1 + \frac{k_{ii}}{\lambda_2}\right) R_{ip,0} - \frac{k_{ir}}{\lambda_2} R_{ic,0}. \tag{B.87}$$

B.5 Blocking protein synthesis

Herein, we obtain solution of model (6.68) for the experiment of blocking protein synthesis, with initial conditions given in (6.69). Characteristic equation of the model is the following

$$Q(\lambda) \ = \det \begin{bmatrix} \lambda + k_{ii} & -k_{ir} \\ -k_{ii} & \lambda + (k_{ir} + \delta_{ic}) \end{bmatrix} = \lambda^2 + (k_{ii} + k_{ir} + \delta_{ic})\lambda + k_{ii}\delta_{ic} = 0. \tag{B.88}$$

Eigenvalues of the model and associated eigenvectors are

$$\lambda_1 = \frac{1}{2}\left[-(k_{ii} + k_{ir} + \delta_{ic}) - \sqrt{(k_{ii} + k_{ir} + \delta_{ic})^2 - 4k_{ii}\delta_{ic}}\right], \quad v_1 = \begin{pmatrix} 1 \\ \frac{k_{ii}+\lambda_1}{k_{ir}} \end{pmatrix}, \tag{B.89}$$

$$\lambda_2 = \frac{1}{2}\left[-(k_{ii} + k_{ir} + \delta_{ic}) + \sqrt{(k_{ii} + k_{ir} + \delta_{ic})^2 - 4k_{ii}\delta_{ic}}\right], \quad v_2 = \begin{pmatrix} 1 \\ \frac{k_{ii}+\lambda_2}{k_{ir}} \end{pmatrix}. \tag{B.90}$$

By using eigenvectors $v_{1,2}$ given above, the following fundamental matrix can be constructed

$$\Phi(t) = \begin{pmatrix} e^{\lambda_1 t} & e^{\lambda_2 t} \\ \frac{k_{ii}+\lambda_1}{k_{ir}} e^{\lambda_1 t} & \frac{k_{ii}+\lambda_2}{k_{ir}} e^{\lambda_2 t} \end{pmatrix}. \tag{B.91}$$

By using the fundamental matrix, the following general solutions are obtained

$$\begin{pmatrix} R_{ip}(t) \\ R_{ic}(t) \end{pmatrix} = \Phi(t) C,$$

$$R_{ip}(t) = C_1 e^{\lambda_1 t} + C_2 e^{\lambda_2 t} \tag{B.92}$$

$$R_{ic}(t) = C_1 \frac{k_{ii} + \lambda_1}{k_{ir}} e^{\lambda_1 t} + C_2 \frac{k_{ii} + \lambda_2}{k_{ir}} e^{\lambda_2 t} \tag{B.93}$$

Model has the following initial conditions

$$R_{ip,0} = \frac{\sigma_i(k_{ir}+\delta_{ic})}{k_{ii}\delta_{ic}} = \frac{\sigma_i(k_{ir}+\delta_{ic})}{\lambda_1\lambda_2}, \tag{B.94}$$

$$R_{ic,0} = \frac{\sigma_i}{\delta_{ic}} = \frac{\sigma_i k_{ii}}{\lambda_1\lambda_2}. \tag{B.95}$$

To obtain constant coefficients $C_{1,2}$, we evaluate (B.92) and (B.93) at $t=0$ by using (B.94) and (B.95)

$$R_{ip,0} = R_{ip}(0) = C_1 + C_2 = \frac{\sigma_i(k_{ir}+\delta_{ic})}{\lambda_1\lambda_2} \Rightarrow C_1 = -C_2 + \frac{\sigma_i(k_{ir}+\delta_{ic})}{\lambda_1\lambda_2}. \tag{B.96}$$

By using (B.96) in (B.93) for $t=0$

$$\begin{aligned}
&R_{ic,0} = R_{ic}(0) = C_1\frac{k_{ii}+\lambda_1}{k_{ir}} + C_2\frac{k_{ii}+\lambda_2}{k_{ir}} = \frac{\sigma_i k_{ii}}{\lambda_1\lambda_2} \\
&\Rightarrow \left[-C_2 + \frac{\sigma_i(k_{ir}+\delta_{ic})}{\lambda_1\lambda_2}\right]\frac{k_{ii}+\lambda_1}{k_{ir}} + C_2\frac{k_{ii}+\lambda_2}{k_{ir}} \\
&= C_2\left[-\frac{k_{ii}+\lambda_1}{k_{ir}} + \frac{k_{ii}+\lambda_2}{k_{ir}}\right] + \frac{\sigma_i(k_{ir}+\delta_{ic})(k_{ii}+\lambda_1)}{\lambda_1\lambda_2 k_{ir}} \\
&= C_2\frac{\lambda_2-\lambda_1}{k_{ir}} + \frac{\sigma_i(k_{ir}+\delta_{ic})(k_{ii}+\lambda_1)}{\lambda_1\lambda_2 k_{ir}} = \frac{\sigma_i k_{ii}}{\lambda_1\lambda_2} \\
&\Rightarrow C_2(\lambda_2-\lambda_1) = \frac{\sigma_i k_{ii} k_{ir}}{\lambda_1\lambda_2} - \frac{\sigma_i(k_{ir}+\delta_{ic})(k_{ii}+\lambda_1)}{\lambda_1\lambda_2} = \frac{\sigma_i[-k_{ii}\delta_{ic} - (k_{ir}+\delta_{ic})\lambda_1]}{\lambda_1\lambda_2}
\end{aligned} \tag{B.97}$$

From quadratic equation (B.88) we extract $\lambda_1\lambda_2 = k_{ii}\delta_{ic}$ and use it in equation above to obtain simpler form of C_2

$$C_2 = -\frac{\sigma_i[\lambda_1\lambda_2 + (k_{ir}+\delta_{ic})\lambda_1]}{\lambda_1\lambda_2(\lambda_2-\lambda_1)}. \tag{B.98}$$

By using (B.98) in (B.96), C_1 can be obtained

$$C_1 = \frac{\sigma_i[\lambda_1\lambda_2 + (k_{ir}+\delta_{ic})\lambda_1]}{\lambda_1\lambda_2(\lambda_2-\lambda_1)} + \frac{\sigma_i(k_{ir}+\delta_{ic})}{\lambda_1\lambda_2} \Rightarrow C_1 = \frac{\sigma_i[\lambda_1\lambda_2 + (k_{ir}+\delta_{ic})\lambda_2]}{\lambda_1\lambda_2(\lambda_2-\lambda_1)} \tag{B.99}$$

B.6 Protein recycling

Herein, we obtain solution of recycling submodel (6.88). The following characteristic equation can be obtained from (6.88)

$$Q(\lambda) = \det\begin{pmatrix} \lambda+(k_{ir}+\delta_{ic}) & 0 & 0 \\ -k_{ir} & \lambda+k_{ii} & -k_{ir} \\ 0 & -k_{ii} & \lambda+(k_{ir}+\delta_{ic}) \end{pmatrix} \tag{B.100}$$

$$= [\lambda+(k_{ir}+\delta_{ic})][\lambda^2 + (k_{ii}+k_{ir}+\delta_{ic})\lambda + k_{ii}\delta_{ic}] = 0. \tag{B.101}$$

The eigenvalues of the model and associated eigenvectors are

$$\lambda_1 = -(k_{ir} + \delta_{ic}), \quad v_1 = \begin{pmatrix} 1 \\ 0 \\ -1 \end{pmatrix}, \tag{B.102}$$

$$\lambda_2 = \frac{1}{2}\left[-(k_{ii} + k_{ir} + \delta_{ic}) - \sqrt{(k_{ii} + k_{ir} + \delta_{ic})^2 - 4k_{ii}\delta_{ic}}\right], \quad v_2 = \begin{pmatrix} 0 \\ 1 \\ \frac{k_{ii}+\lambda_2}{k_{ir}} \end{pmatrix}, \tag{B.103}$$

$$\lambda_3 = \frac{1}{2}\left[-(k_{ii} + k_{ir} + \delta_{ic}) + \sqrt{(k_{ii} + k_{ir} + \delta_{ic})^2 - 4k_{ii}\delta_{ic}}\right], \quad v_3 = \begin{pmatrix} 0 \\ 1 \\ \frac{k_{ii}+\lambda_3}{k_{ir}} \end{pmatrix}. \tag{B.104}$$

By using the eigenvectors given above, the following fundamental matrix can be constructed

$$\Phi(t) = \begin{pmatrix} e^{\lambda_1 t} & 0 & 0 \\ 0 & e^{\lambda_2 t} & e^{\lambda_3 t} \\ -e^{\lambda_1 t} & \frac{k_{ii}+\lambda_2}{k_{ir}} e^{\lambda_2 t} & \frac{k_{ii}+\lambda_3}{k_{ir}} e^{\lambda_3 t} \end{pmatrix}. \tag{B.105}$$

from which the general solution can be obtained

$$R^g_{ic}(t) = C_1 e^{\lambda_1 t}, \tag{B.106}$$

$$R^{gr}_{ip}(t) = C_2 e^{\lambda_2 t} + C_3 e^{\lambda_3 t}, \tag{B.107}$$

$$R^{gr}_{ip}(t) = -C_1 e^{\lambda_1 t} + C_2 \frac{k_{ii} + \lambda_2}{k_{ir}} e^{\lambda_2 t} + C_3 \frac{k_{ii} + \lambda_3}{k_{ir}} e^{\lambda_3 t}. \tag{B.108}$$

Model has the following initial conditions

$$R^g_{ic}(0) = R^g_{ic,t_0}, \quad R^{gr}_{ip}(0) = 0, \quad R^{gr}_{ic}(0) = 0. \tag{B.109}$$

By using initial conditions above in general solutions for $t = 0$, constant coefficients $C_{1,2,3}$ can be obtained

$$C_1 = R^g_{ic,t_0}, \quad C_2 = -\frac{k_{ir}}{\lambda_3 - \lambda_2} C_1, \quad C_3 = \frac{k_{ir}}{\lambda_3 - \lambda_2} C_1. \tag{B.110}$$